STRATIGRAPHIC RECORD OF A DISTRIBUTARY FLUVIAL SYSTEM, PALEOSOLS, SOILS, AND THEIR PALEOCLIMATIC IMPLICATIONS DURING THE MIOCENE TO EARLY PLIOCENE, NORTHWESTERN ARGENTINA

A Dissertation

Presented to the Faculty of the Graduate School

of Cornell University

In Partial Fulfillment of the Requirements for the Degree of

Doctor of Philosophy in the Geological Sciences

by

José Juan Rosario

May 2017

STRATIGRAPHIC RECORD OF A DISTRIBUTARY FLUVIAL SYSTEM, PALEOSOLS, SOILS, AND THEIR PALEOCLIMATIC IMPLICATIONS DURING THE MIOCENE TO EARLY PLIOCENE, NORTHWESTERN ARGENTINA

José Juan Rosario, Ph. D.

Cornell University 2017

Abstract

The Andean topography influences regional climates on both sides of its physical structure. Sedimentary environments and climate might have evolved along the growth of the orographic barrier caused by the topographic uplift as the result of the interaction between the Nazca and South America tectonic plates. This study present evidence of the history of the sedimentary environments evolution and the paleoclimate response and sensitivity of the uplift of the Andes during the Miocene to Early Pliocene. To determine if environmental and climatic changes occurred during the geologic record three main subjects were studied: (1) The sedimentary record of three stratigraphic columns that produced a west-east profile; (2) Paleosols that were compared with the modern soils in order to establish correlations between past and modern sedimentary environment; (3) and the study of pedogenic calcium carbonates deposits through the analyses of Carbon and Oxygen stable isotope ratios. The sedimentary record exhibits an overall upward coarsening sequence that can be sub-divided in three main sedimentary cycles. These cycles are formed by alternations between sandstones and mudstones with the sandstones presenting different geometries. The paleosols identified

during the field work are present across the three stratigraphic columns. Most paleosols contain pedogenic calcium carbonate and were rich in clay, silt, amnd fine sand. The last set of analyses presented by carbon and oxygen resulted with isotopic values similar to today's rainfall values in the area for oxygen, and a consistent $\delta^{13}C$ values through time for carbon isotopes. The results from the sedimentary record represent a distributary fluvial system that has been progressing to the east that is correlated with tectonic events. The sub-cycles are representative of the lateral migration of the fluvial system. Paleosols present similar physical and mineralogical properties compared with modern soils. The range of values of stable isotopes suggest a climate history similar as todays. The sedimentary record presents a constant or a low variable climate of the Eastern Andean belt throughout the Miocene-Early Pliocene geologic time.

BIOGRAPHICAL SKETCH

I am the oldest son of a total of five siblings, a single mother and 2 grandparents that gave me love and most of the principles and values that I still hold until this day. We didn't have much, but what we had we valued, and I personally always have valued that that life has gave me for free. Since a child, my curiosity for nature and my enjoyment in school inspired me to be a scientist and my family always encourage us to pursue our dreams. Growing in a tropical island and be surrounded by so much vegetation and animals, I took the decision to study biological sciences to learn how are living things made, how living things interact with each other, and how we human being became humans. While finishing my undergraduate at the University of Puerto Rico at Cayey Campus, the field of ecology, physics, and organic chemistry made me want to pursue a scientific field that was integhrated at the same time that give me the opportunity to be in direct touch with nature besides the four walls of a laboratory. This is when I decided to answer the call to study geology. I was part of the graduate program of geology at the University of Puerto Rico at Mayaguez Campus, participate in teaching programs where I had the opportunity to instruct college students and school teachers in the fields of geology and ecology feeding my curiosity and inspiration to chase a carreer where I could acquire knowledge on a common base. Short after those experiences I applied to the Department of Earth & Atmospheric Sciences at Cornell University to start my training and career as a researcher. My studies at Cornell University open my life not only to a great academic experience but to have friends for all over the world including Russia, China, Chile, and so many other places where I have good and close friends. After several years at Cornell University and started to write my dissertations, I felt the urge to open my experiences outside the academia. One of the reasons for this was to test not neccesarily my knowledge in the field of geological sciences, but my new set of critical and creative thinking tools. I spent four years at the

US Geological Survey at Menlo Park in California. I applied my knowledge, promote research ideas in the field of paleoclimate and environmental sciences that I still working today as a member of a team of scientists that wake up everyday looking for new ways to learn the history of our planet and to live in harmony with nature. Once I came back to complete my degree at Cornell University, I never felt more happy about my decision to pursue a career as a researcher and be a geologist. I am in a stage where every btime that I look back to my life, I know that I have been heading in the right direction, including some bumps and stumbles along the way that now seem far away as lessons that help me to recognize not only what is the purpose of life, but that we as humans can create and give almost any purpose to our life as long as we are willing to step into the right road and start walking toward our destination.

DEDICATION

I dedicate my thesis to four outstanding human beings that have taught me three valuable life lessons, not with words, but by example. My mother Vilma Díaz Rodríguez that besides gave me the gift of life showed me what love and good will can accomplish. My grandparents Amelia Rodríguez and José Díaz for showed me that doesn't matter the circumstances I must always hold my dignity and integrity, never let the circumstances define me. Lastly but not less important, my advisor Professor Teresa E. Jordan for taught me that perseverance and good work ethics can take you anywhere. I am grateful for these magnificent beings been in my life and for always believe in me. It is up to me now to take these teachings forward.

ACKNOWLEDGMENTS

I would like to thank my thesis committee, Professors Teresa (Terry) E. Jordan, Louise A. Derry, and Johannes Lehmann for all the scientific and academic education that they had provided me during my studies and research at Cornell University. I would also like to show my appreciation to Professors Carmala N. Garzione and Pennilyn (Penny) Higgins at the University of Rochester for their immense collaboration in this project and the exciting scientific discussions that made possible the completion of this dissertation. I am also very thankful for our collaborators and friends in Salta, Argentina that are part of the XR-Geomap, especially to Roberto M. Hernández, Juan I. Hernández, Alejandra Dalenz Farjat, Luis A. Gonzalez, Andrés F. Alvararez, Edgar D. Gonzalez, Mario (Chopi) Aguilar, and Manolo. Their willingness to move forward the geological knowledge and education is one to be emulated. Finally, I would like to thank my colleagues and friends that not only gave me support, but share their scientific knowledge. This includes Dr. Greg Hoke, Dr. Peter Nester, and Dr. Cornelius Uba, all of which taught me a big deal about geology, critical thinking, and work ethics during our field trips in Chile and Argentina. Financial support provided it by National Science Foundation grant EAR 0635677 and Cornell University Fellowships.

TABLE OF CONTENTS

LIST OF FIGURES

CHAPTER 1

CHAPTER 2

LIST OF TABLES

Abstract

The Andean topography influences regional climates on both sides of its physical structure. Sedimentary environments and climate might have evolved along the growth of the orographic barrier caused by the topographic uplift as the result of the interaction between the Nazca and South America tectonic plates. This study present evidence of the history of the sedimentary environments evolution and the paleoclimate response and sensitivity of the uplift of the Andes during the Miocene to Early Pliocene. To determine if environmental and climatic changes occurred during the geologic record three main subjects were studied: (1) The sedimentary record of three stratigraphic columns that produced a west-east profile; (2) Paleosols that were compared with the modern soils in order to establish correlations between past and modern sedimentary environment; (3) and the study of pedogenic calcium carbonates deposits through the analyses of Carbon and Oxygen stable isotope ratios. The sedimentary record exhibits an overall upward coarsening sequence that can be sub-divided in three main sedimentary cycles. These cycles are formed by alternations between sandstones and mudstones with the sandstones presenting different geometries. The paleosols identified during the field work are present across the three stratigraphic columns. Most paleosols contain pedogenic calcium carbonate and were rich in clay, silt, amnd fine sand. The last set of analyses presented by carbon and oxygen resulted with isotopic values similar to today's rainfall values in the area for oxygen, and a consistent $\delta^{13}C$ values through time for carbon isotopes. The results from the sedimentary record represent a distributary fluvial system that has been progressing to the east that is correlated with tectonic events. The sub-cycles are

representative of the lateral migration of the fluvial system. Paleosols present similar physical and mineralogical properties compared with modern soils. The range of values of stable isotopes suggest a climate history similar as todays. The sedimentary record presents a constant or a low variable climate of the Eastern Andean belt throughout the Miocene-Early Pliocene geologic time.

CHAPTER 1

PALEOSOL CHARACTERISTICS AND VARIABILITY WITHIN THE MIDDLE AND LATE MIOCENE FORELAND BASIN LANDSCAPE EVOLUTION OF NORTHWESTERN ARGENTINA

Abstract

The evolution of climate within the South American continent over geologically long time spans may either have responded primarily to regional boundary conditions, like growth of the Andes Mountains, in contrast to physical forcing by the broader global climate as presented by the Atacama Desert. This opens the question about how the Central Andes Mountains have influenced the regional climate in the windward region in comparison with the leeward side of the Andes where the Atacama Desert is currently located. In other words, does the climatic development of these juxtaposed systems are synchronous? To answer this question for terrestrial paleo-environments, much of the information about environmental conditions is best recorded in paleosols that are preserved in sedimentary deposits. The interpretation of paleosols can be improved through the comparison with surrounding sediments, modern soils, and the landforms in which they are embedded.

This paper has the purpose to compare and contrast the environmental system that exists today in the low mountain ranges and neighboring plains of Salta and Jujuy Provinces, Argentina, to the environmental system that existed between 14.5 and 5 million years ago. This is the period of time when the Atacama Desert experience changes in aridity. This will establish the differences and similarities in their respective soil development to reveal the possible climatic scenarios at each period of time. The study analyzes paleosols in the Subandean foothills along the eastern flank of the Andes Mountains, throughout the characterization of soil profiles, microscopic analysis of soil textures, and their stratigraphic distribution.

Paleosols at Iruya, Peña Colorada, and La Porcelana Rivers present a west-east profile of soil development in the foreland basin adjacent the Andes throughout the Middle Miocene to Early Pliocene. These paleosols are formed mainly by AC, Bw, Bt, Bk, and BC horizons, in which illite, kaolinite, quartz, calcite, hematite and other iron-bearing minerals are present. Argillic calcisols are the most frequent paleosol type in the Subandean Belt with a fairly uniformly temporal distribution.

With reference to the modern landscape, the soils of analogous pedogenic development are alfisols and entisols; both the paleosols and these modern soils are characterized by clay illuviation and pedogenic carbonate precipitation. The paleosols in the Subandean Belt occur in sandstone and mudstone facies deposited by fluvial overbank sedimentation like that of the modern extensive Distributary Fluvial System. Both, modern and geologically preserved soils present significant pedogenic development. We conclude that this depositional system is the main control on the nature of the paleosols, whereas the vast accommodation space of the basin is the main control on the preservation of the ancient soils throughout the stratigraphic record. Hence, no evidence that corresponds to changes in climate were correlated with changes in the leeward side of the Andes, where the rain shadow effect is observed.

Introduction

The evolution of climate within the South American continent over geologically long spans of time may either have responded primarily to regional boundary conditions, like growth of the Andes Mountains, or to forcing by the broader global climate, or to both. Recent publications have proposed that major growth in elevation of the Andes Mountains during the Miocene and/or Pliocene disrupted the pattern and amount of precipitation in and adjacent to the Central Andes Mountains. We seek to test this hypothesis for the eastern flank of the Andes and adjacent lowlands.

For a terrestrial paleo-environment, the best source of the information about environmental conditions is paleosols, which are fossilized ancient soils that are preserved in sedimentary deposits. Among a long list of modern environmental properties that are tuned to climate state, few of the environmental properties are readily discernible in paleosols, limiting what can be measured of paleoclimate largely to rain fall and drainage. The interpretation of paleosols is not straightforward, and can be improved by comparing the ancient soils and surrounding sediments to modern soils and the landforms in which they are embedded. The stable isotopes of calcium carbonate preserved in paleosols offer information about air masses and vegetation in the ancient environment, and are treated in a companion paper (Rosario et al., 2017).

In this paper we compare and contrast the surface environmental system that exists today in the low mountain ranges and neighboring plains of Salta and Jujuy Provinces, Argentina, to the environmental system that existed between 14.5 and 5 million years ago (Figure 1). The major changes to boundary conditions on the regional environmental system have been caused by progressive tectonic deformation, by climate

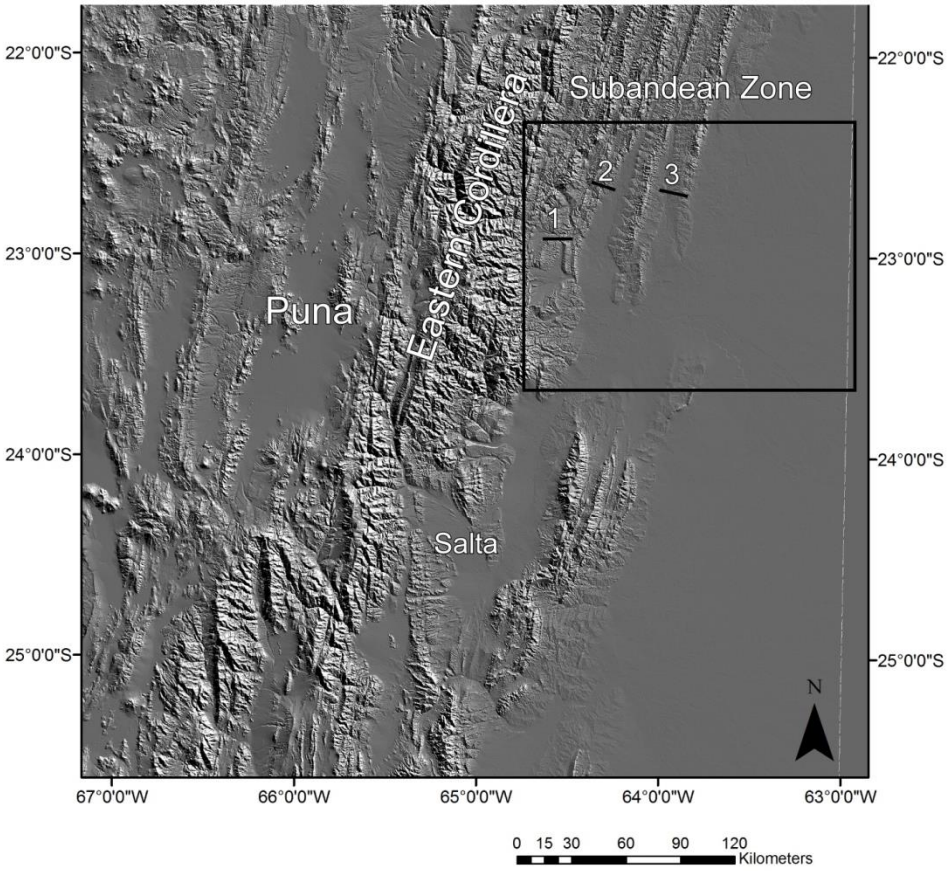
22°0'0"S
23°0'0"S
24°0'0"S
25°0'0"S
67°0'0"W
66°0'0"W
65°0'0"W
64°0'0"W
63°0'0"W
Subandean Zone
Eastern Cordillera
Puna
Salta
1
2
3
N
0 15 30 60 90 120
Kilometers

Figure 1: Area of Study Northwestern Argentina
This is the map of South America from latitudes 22 ^{o}S to 25^{o}S that shows the regional topography. Lines 1, 2, and 3 represent the stratigraphic sections for Iruya, Peña Colorada, and La Porcelana Rivers respectively.

change, by surface hydrology change, and by evolution of land plants. Two of these boundary conditions are dependent on the first one, as the progressive tectonic deformation created mountains where there had been previously a low lying depositional basin (Rosario et al., 2008). The climate as well as the surface hydrology changed because of the new topographic surface.

Due to the correlation between pedogenesis and regional climatic conditions, paleosols have been used as a proxy for climate state and paleoclimatic changes (Machette, 1985; Olson, 1989; Driese and Foreman., 1992; Kraus and Brown, 1993; Mack and James, 1994; Koch et al., 1995; Kraus, 1997; Deutz et al., 2001) including their profiles, mineralogy, geochemistry and stable isotopic signatures that response to average climatic conditions (Koch et al, 1995; Quade and Cerling, 1995; Behrensmeyer et al., 1995; Latorre et al., 1997; Zhou and Chafetz, 2010). Paleosols also serve as proxies for sediment accumulation rate (Birkeland, 1999) because they represent times of "landscape stability" during which sediment input was low to none, which in extreme cases are preserved in the stratigraphic record as surfaces of unconformity. They can be used as a proxy for weathering rate (Stern et al., 1997; Rech et al., 2001), by comparing the mineralogy of several paleosols formed at different times. In certain settings paleosols also reveal base level fluctuations (Zarate et al., 2009), because in coastal stratigraphic sections a soil developed under subaerial conditions during a sea level lowstand may be buried by aggrading sediment during the subsequent rise of sea level. Paleosols are also a tool for geomorphological interpretations (Ghosh, 1997; Birkeland, 1999; Rech et al., 2001), because soil properties are dependent on the slope gradient (erosion potential) and on hydrological variability across the landscape. For example, within some surface

depressions, soils display redox features that indicate moderate to poor drainage and temporary stagnant waters (Aslan and Autin., 1998; Hayes and Vepraskas, 2000; Jacobs et al., 2002; Vaughan et al., 2007).

This paper is focused on interpreting the spatial and temporal evolution of the geomorphology and bioclimatic changes in the foreland sedimentary basin of northwest Argentina (NWA) that formed in response to uplift of the Andes Mountains. The tectonic topography evolved due to the eastward structural displacement of the thrust-fold belt on the east flank of the Andes, known as the Subandean thrust belt (Echevarría et al. 2002; Kley et al., 2002; Husson and Moretti, 2002, Hulka et al., 2006). As the orogenic front moved eastward, the alluvial sedimentary system moved as well. The basic components of the paleo-environmental zones within the sedimentary basin have been characterized in published studies. For example, Hernández et al. (1996) identify the components of the depositional system to be alluvial fans, braided rivers, meandering rivers, and mud flats (Figures 2). The eastward shift of the positions of those environments through millions of years resulted in the vertical stacking of strata characteristic of each environment, which Disalvo and Stark (1983) described to be a vertical succession of three mega-progradational cycles. Also this eastward shift of the mountain front caused uplift and exposure of the foreland basin strata, which allows their study within the Subandean thrust belt.

We interpret the paleosols relative to the distributary fluvial system (i.e., mega-fan) geomorphological model described by Horton and DeCelles (1997, 2001), Shukla (2001), and Weissmann et al, (2010). Details of the stratigraphy and lithofacies of the NWA Miocene mega-fan will be published separately. DeCelles and Cavazza (1999)

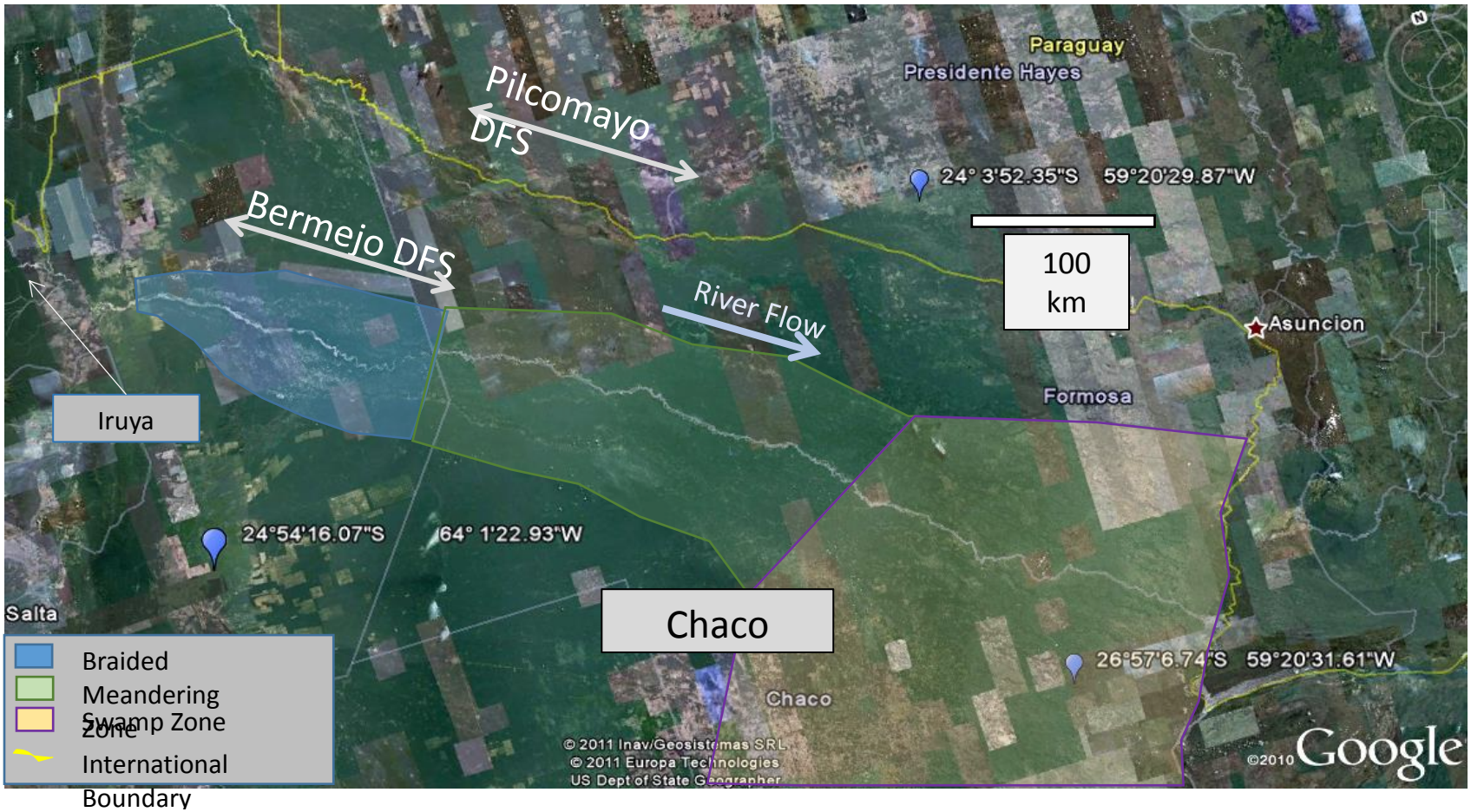
Pilcomayo DFS
Bermejo DFS
River Flow
Paraguay
Presidente Hayes
24° 3'52.35"S 59°20'29.87"W
100 km
Asuncion
Formosa
Iruya
24°54'16.07"S 64° 1'22.93"W
Salta
Chaco
26°57'6.74"S 59°20'31.61"W
Chaco
Braided
Meandering
Swamp Zone
International Boundary
© 2011 Inav/Geosistemas SRL
© 2011 Europa Technologies
US Dept of State Geographer
©2010 Google

Figure 2: Bermejo River and Distributary Fluvial System
The Distributary Fluvial System or megafan formed by the Bermejo River show three different areas formed by a braided zone, meandering zone, and a swamp zone. The Iruya River is located at the west of the Bermejo megafan.

show that a distributary depositional system is active today just a few kilometers north of our Argentine study area, in southern Bolivia. In a megafan alluvial system, two autogenic river controls on the deposition of sediment are expected: progressive lateral displacement that is perpendicular to downstream axis of the mega-fan, and episodic avulsion (Calvache and Viseras, 1997; Figure 2). In addition to those autogenic controls, one expects allogenic controls on the megafan in a setting in which a lowland sedimentary basin is fed water and detritus from an active mountain belt. The anticipated changes in the catchment that may impact the river in the lowland basin include: displacement of the boundary between the upland catchment and lowlands; climatic changes in response to either global change or the regional topographic evolution; and evolution of the catchment surface through processes that progress steadily, such as weathering and erosion, and processes that cause abrupt changes, such as stream piracy. Both autogenic and allogenic forcings on the Cenozoic rivers in the NWA sedimentary basin are likely to have affected soil development and paleosol preservation through time.

Describing and consequently categorizing the weathered profiles of the paleosols provides information with which to establish the stability of the sedimentary basin geomorphological system, and specifically to measure how dynamic (unstable) the floodplain might have been during the development of the Subandean thrust belt. Paleosols are commonly preserved in floodplains strata (Kraus, 1997; McCarthy et al., 1998; McCarthy and Plint, 2003), although paleosols can be found also over channel fill deposits and natural levees (Uba et al., 2005). However, paleosols developed in the latter settings are poorly preserved due to a high potential for erosion. Soil development over floodplains is not likely to be terminated by erosion of the soil layer, but the maturity of the soil is

limited in part by the repeated addition of sediment that settles from flood waters. The results of interspersing long intervals of soil development with brief intervals of sediment input are interbedded immature paleosols and lamina-sets of siltstone or sandstone. The event that deposits a sand-sheet commonly marks the "time-zero" for the development of a specific soil. Subsequently, burial of that soil by deposits of another flood allows the soil to be preserved, hence becoming a paleosol. The combined high rate of supply of sediments and of tectonic subsidence (Reynolds et al., 2000; Echevarría et al., 2003) are expected to enable a high rate of sediment accumulation and a high probability of preserving paleosols in NWA, and yet a low maturity of most of the soils. Floodplain deposits are one of the most frequent types of alluvial deposits throughout the Miocene stratigraphic units in the NWA Subandean belt (Hernández et al., 1996), therefore paleosols should be present in the stratigraphic record. In accord with the processes mentioned above, if the climate of the NWA has been affected from the Andean uplift during the Miocene, changes in paleosols should be present in the stratigraphic record. One possible scenario could be mineral and textural changes in paleosols as the result of an increase of rain fall trapped by the orographic barrier effect. If changes in the paleosols at the Atacama Desert were the hyper-aridification as the result of global climatic phenomena, such evidence should be found in the sedimentary record of the NWA due to the high sedimentation rate that characterize this basin. A third scenario could be the absence of any climatic signal observe through the paleosols representing either an asynchronous geologic record or that the climate from the windward and leeward of the Andeas involve more than one single climatic mechanism.

Background

Pedogenesis, Soils and Paleosols

Physical and biogeochemical processes of soil formation include additions and losses of sediment from topsoil and mineral transformation, lessivage, eluviation/ illuviation, and translocation (Birkeland, 1999; Brady and Weil, 2002; Andrews et al., 2004). These physical-biochemical processes are controlled by the climate, topography, biology, parent material, and time. These processes are compiled in the famous conceptual equation of Dokuchaev (1900) as, soil = f (climate, biota, parent material, topography, time). The identification and characterization of a paleosol can provide information about each of these controls. The soil features result from biogeochemical as well as physical processes that cause weathering on floodplains, which most commonly are translocation of clays and oxides, accumulation of clays, oxides, and salts, and transformation of minerals. We focus in this study on pedogenic $CaCO_3$ precipitated as a soil-respiration product, on clay mineralogy, and on oxides present in the paleosols. We choose these attributes because of the sensitivity of calcium carbonate, clays, and oxide minerals to environmental conditions, especially to the rain fall and drainage.

Paleosols are defined as ancient soils (Birkeland, 1999), which can be classified in 3 major categories: (1) Buried soils, (2) relict soils, and (3) exhumed soils. Buried soils are soils that were formed at earth's surface but were subsequently buried by overlying sediments. Relict soils are very old soils that have never been buried, but the conditions of formation (e.g. climate) differ from the present ones. Exhumed soils are soils that were buried and later were exposed to the surface by erosion. Catastrophic processes (storm, landslide, lava, etc.) that add new materials to the landscape surface make possible the

preservation of original soils, transforming them into paleosols and making them reliable for the study of past environmental and climatic conditions. However, most features that characterize fresh soils tend to be missing from paleosols, due to erosion, diagenesis, or overprint of pedological processes (Mack, 1993; Retallack, 1993). Hence, A horizons are rarely preserved, conserving B horizon at the top of the paleosol profile. Common features of paleosols tend to be rizoliths, bioturbarion, redox mottling, carbonate nodules, texture, and horizon boundaries, although the latter two features are likely to have been altered by compaction. Diagenesis is a common problem, which encompasses not only compression of soil texture by the overlying material, but the precipitation of diagenetic minerals by groundwater (e.g. calcium carbonate), and clay diagenesis caused by chemical exchange through time. These facts impact the suitability of modern soil classifications to the sedimentary rock record.

Soils are developed in the area of study on alluvial sediments. The degree of pedogenesis on floodplains depends on the distance from the channel in many cases, because the channel is the locus of erosion and flood waters that spread over soils (Kraus, 1997; Bridge, 2003). Erosion at channel margins by lateral channel migration is important because it destroys soil horizontal continuity. Flooding is important because it causes the superposition of sediment additions settled from flood waters on the top of the soil, to which pedogenesis must adapt or, if not, pedogenesis on the pre-existing surface terminates and it begins again on the new surface (Wilding et al., 1983; Birkeland, 1999). Over a long time interval, soils located on the floodplain will be eroded or buried as the alluvial topography evolves. The different stages of soil development in fluvial systems depend heavily on these factors, because the expansion and continuity of the soil sequence is

attached to its sedimentation processes over time. The various arrangements of soil succession over time are called chronosequences.

Chronosequences can be determined using the soil development distribution over an area for a given time framework. The soils in the Subandean Belt during the Middle Miocene through Early Pliocene are time-transgresive represented as a vertical chronosequence (Huggett, 1998). These are buried soils or paleosols (Retallack, 2001), which record pedogenic variability, spatially and through time.

One of the primary controls on the soil texture and mineral accumulation in soils is the climatic condition (Wilding et al., 1983; Brady and Weil, 2002). Clays and salts are indicative of climate conditions or low water availability as a dissolution or transportation agent. For example, soils formed under arid to semi-arid climates contain 2:1 clays such as smectite, illite, and chlorite. In contrast, soils developed under sub-humid to humid climates represent more developed weathering profiles, accumulating 1:1 clays such as kaolinite for example. Under extreme weathering conditions induced by high temperatures and high rainfall, oxide minerals commonly form (Brady and Weil, 2003; Andrews et al., 2004). Oxide minerals include goethite, gibbsite, and ferrihydrite. Soils with highly developed oxide minerals are known as lateritic soils, and are found in sub-tropical and tropical climate zones. The oxide mineral counterpart in semi-arid to arid soils is the accumulation of salts (Birkeland, 1999; Deutz et al., 2002), which accumulate where there is little precipitation or in regions with strong seasonality of rain fall. Salts include calcium carbonate, halite, anhydrite, gypsum, nitrates, and many others (Rech et al., 2003; Ewing et al., 2006).

In the area of study, soils form across the fluvial distributary system, or megafan (DeCelles, 2000; Horton and DeCelles, 2005). Megafans are low topographic gradient environments on which aggradation exceeds erosion. In the distal regions, fine sands and mud represent the majority of sediment deposited. In contrast, proximal zones accumulate coarser sediments represented by gravel bars and sand bars, and are strongly impacted by channel erosion (Shukla et al., 2001). On megafans, soil incidence is greatest at the distal part of the fluvial distributary system, perhaps as the result of a decrease in grain size and the decreased frequency of sediment discharge with increased distance from the megafan head (Shukla et al, 2001). The presence of soils in the proximal megafan is limited by the erosion produced by lateral movement of the river channel(s) or by avulsion.

Area of Study

The paleosols are located between the latitudes 22^{o}S and 23^{o}S near the geographical boundary of Argentina and Bolivia formed by the Bermejo and Grande de Tarija Rivers in the Andean foothills (Figure 1). Those rivers join and, as the Bermejo River, discharge into the Chaco Plain. The paleosols described in this paper correspond primarily to the Iruya River stratigraphic section (Figure 1). Paleosols from two additional locations, Peña Colorada and La Porcelana, are described briefly in order to illuminate the extent of the paleosols in NWA.

The composite Miocene to modern foreland sedimentary basin is regionally bounded on its west by the Central Andes Mountains (Eastern Cordillera) and on its east by the Paraguay River (Figures 1 and 2). The Miocene and Pliocene foreland basin strata are exposed in the Subandean mountain ranges. The modern basin is the broad Chaco Plain,

which spans over 600 km east-west width in eastern Argentina, eastern Bolivia, and Paraguay. The modern depositional environments and soils of the Chaco basin serve as analogues to the Miocene paleosols on which this paper focuses. The Bermejo River enters the Chaco Plain at an altitude a little less than 300 m above sea level, discharges through a distributive fluvial system with a SE-elongation, and ~700 km from the Andes it joins the south-flowing Paraguay River at an altitude of ~50 m above sea level. The mean gradient across the depositional basin is 0.02° (~34 cm/km, Figure 2).

The Subandean region geological setting is comprised of NNE-trending synclinal valleys and anticlinal ridges that expose Devonian and Silurian strata close to the axial planes of the anticlines. Such structures developed from the Late Miocene (~10 Ma) to the present, producing north-northeast-trending mountain ranges with elevations up to 1000 m. Stratigraphically overlying the Paleozoic strata are Miocene to Quaternary foreland basin strata, which are commonly exposed on the anticlinal limbs and form the floors of the synclinal valleys. The maximum thickness of the Miocene and Pliocene Subandean sedimentary deposits in NWA is up to ~5000 meters, topped by over 2000 meters of Quaternary deposits (Hernández et al, 1996; Echevarría et al., 2003). The progressive growth of new anticlinal ridges has been the single most important control on the sedimentary environments and thicknesses of foreland basin strata. First, the progressive, albeit probably episodic, eastward displacement of the thrust front has caused eastward displacement of the distributive fluvial system of the Chaco sedimentary basin (Horton and DeCelles, 2001). Second, the topography within the Subandean belt of synclines and anticlines controls the compartmentalization of small basins, so that deposits accumulate where synclines are subsiding (Echevarría et al., 2003).

To the west of the Subandean ranges is the Eastern Cordillera, with a topographic rise to ridgelines in excess of 4000 m elevation, and to its west is the Puna Plateau. The Eastern Cordillera is composed by Precambrian and Cambrian sedimentary and plutonic rocks, Paleozoic plutonic rocks, Ordovician sedimentary and volcanic rocks, and Permian-Carboniferous volcanic rocks (Reutter et al, 1984). Much of the drainage system that delivers sediments into the lowland basins of the Subandes and Chaco arises in catchments in the Eastern Cordillera (Figure 1). This implies that the parent materials of the paleosols and modern soils of the lowland basins are from weathering of siliciclastic rocks of the Eastern Cordillera as well as the Subandean ranges. It is expected that the details of the lithology of the paleosol parent material would have evolved through time, in response to the successive exposure of Paleozoic and Cenozoic formations along the axes of the anticlines.

The erosional force which acts upon the Eastern Cordillera is produced by an average annual precipitation between 300 to 800 mm that creates a sub-humid to subtropical region, while in the Puna rain fall does not exceed 300 mm/year (Figure 3). Mean annual precipitation in the Subandean belt is 800 mm/year, and it is monsoonal, with wet summers and dry winters. The precipitation in the proximal Chaco basin is 600-800 mm/yr, and more than 1000 mm/year in the distal part of the basin (Atlas de Suelos de Argentina, INTA, 1990). Between latitudes 10°S to 25°S, rainfall on the eastern Andes and the Chaco region is enhanced by two phenomena. First, generally easterly winds of the tropics carry water-vapor-laden air masses from the Amazon lowlands westward

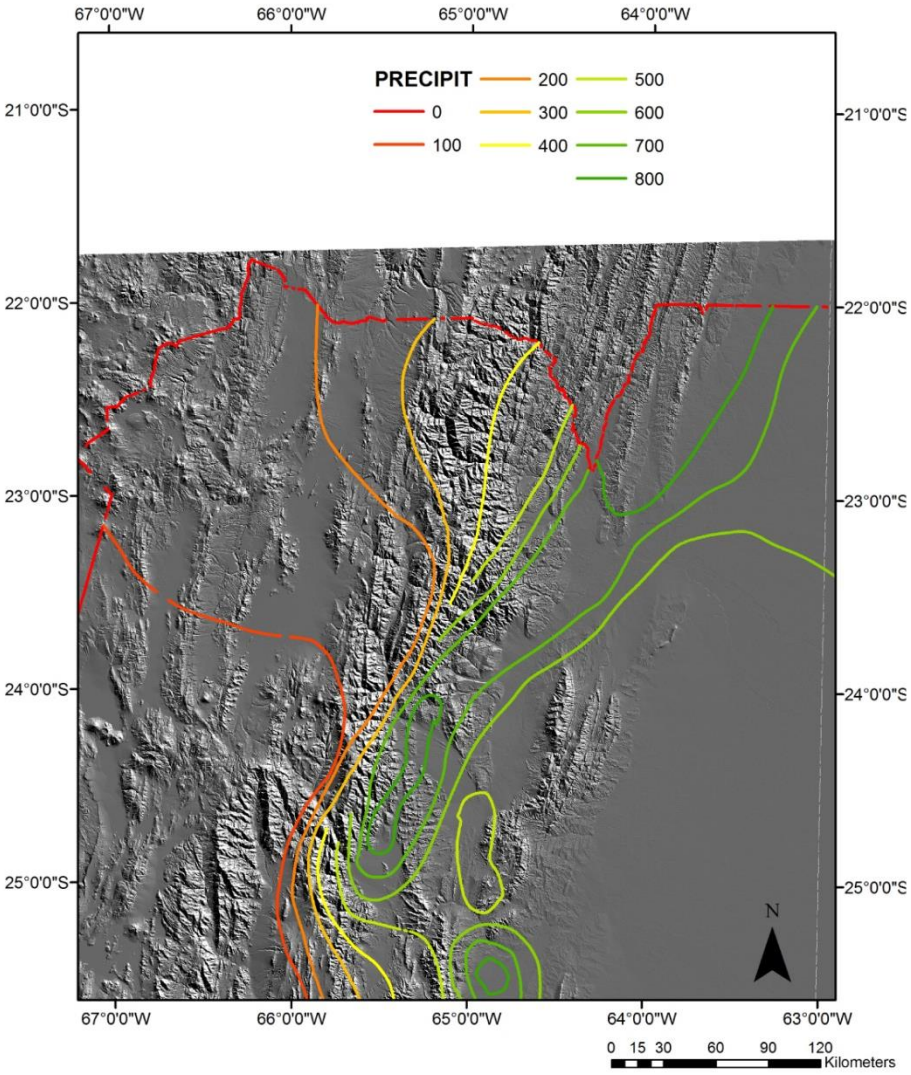
67°0'0"W
66°0'0"W
65°0'0"W
64°0'0"W
63°0'0"W
21°0'0"S
22°0'0"S
23°0'0"S
24°0'0"S
25°0'0"S
PRECIPIT
0
100
200
300
400
500
600
700
800
N
0 15 30 60 90 120
Kilometers

Figure 3: Precipitation Map of Northwestern Argentina
This is the precipitation of the area of study presented in mm presented in annual average values

toward the Andean orographic barrier, and rise of those air-masses over the mountains causes enhanced precipitation (Masek et al., 1994; Lenters and Cook, 1997). Second, an atmospheric phenomenon known as the Bolivian High causes a northeastward re-alignment of the prevailing winds (Lenters and Cook, 1997; Vizy and Cook, 2007), which brings Amazon basin moisture farther south along the Andean topographic front to the study area. Annual maximum and minimum temperatures of the Subandean ranges across these latitudes in Northwestern Argentina range from 45º C during the wet austral summer to about -5º C during the dry winter, with annual median temperatures of about 22º to 18º C (Figure 4). In response to the climate gradient, an east to west transect of the modern foreland basin encompasses vegetation changes from riparian shrubs (east) to sub-tropical forest (west) in the Chaco Basin.

Modern Soils

Modern soils are classified by the Food and Agriculture Organization (FAO) and Soil Taxonomy classification systems. For the purpose of this research, we will only use the Soil Taxonomy classification system. In Northwestern Argentina, soils located in the Subandean mountains and the Chaco Plain are dominated by four orders; Entisols, Inceptisols, Alfisols, and Mollisols (Figure 5). The distribution of the soil orders in this area is linked to the fluvial pattern and discharge (Figure 5).

The less developed soils in the Chaco Basin correspond to Entisols and Inceptisols. The reason for such low pedological development under a moderate annual precipitation regime is the high accumulation rate of river-derived sediments that predominates in the megafan lowlands (Figure 5). Sediment is distributed across the

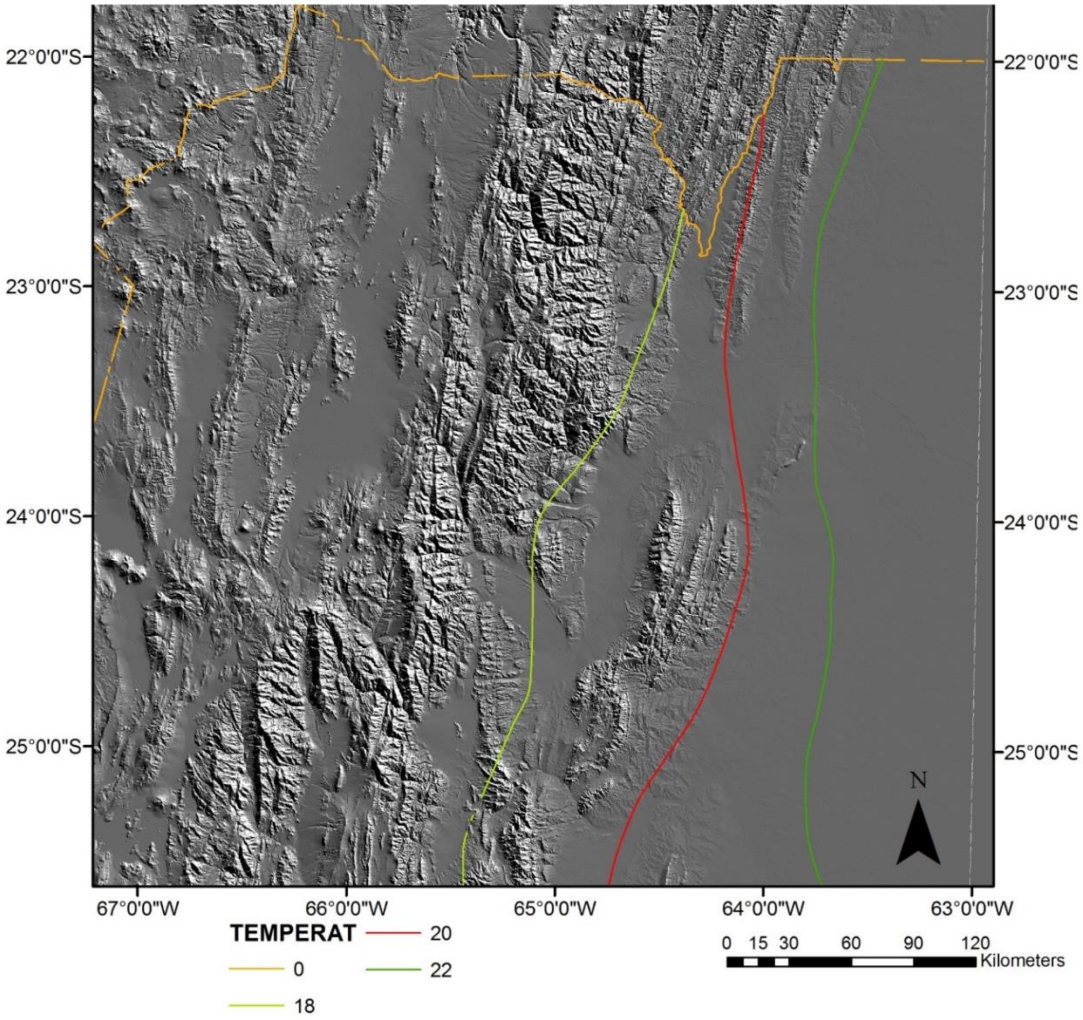
22°0'0"S
23°0'0"S
24°0'0"S
25°0'0"S
67°0'0"W
66°0'0"W
65°0'0"W
64°0'0"W
63°0'0"W
N
TEMPERAT
0
18
20
22
0 15 30 60 90 120
Kilometers

Figure 4: Average Annual Temperature for Nonwestern Argentina
Mean annual temperature values presented in °C. Stratigraphic sections are located between the 3 temperature contour lines at the upper right of this figure.

basin in a radial pattern, governed by the sediment discharge along the axis of the main river channel and the distributary or second-order channels (Figure 5). The development or maturity of the soils in the Chaco Basin depends on the intermittent sediment discharge pattern and on the proximity to the channel (Kraus, 1997; Bikerland, 1999).

A set of more mature soils is represented by mollisols and alfisols, which increase moving eastward from the proximal to distal parts of the Chaco sedimentary basin as well as the distance increases from the fluvial channels (Figure 6, GeoINTA). Mollisols are known as soils with a saturated base and high cation exchange capacity, which are the consequences of high calcium carbonate accumulation (mollic epipedon > 50% saturation in $CaCO_3$) in the B (buried) horizon. These soils cover about 66 % of the area in NWA.

Alfisols are soils with clay accumulation by illuviation and also a high base capacity ($\geq$ 35%), and cover about 33% of the area in the Bermejo megafan. Alfisols occur next to the stream channels where accumulation of pedogenic clays is preferred due to the high porosity and drainage of these areas. As in mollisols, the accumulation of calcium carbonate in the alfisols is a very important factor, due to the cation exchange capacity, soil pH (acidity buffer), and the plant nutrient cycle.

In order for calcium carbonate to precipitate in a soil several conditions need to be met. Because evaporation enhances calcium carbonate ($CaCO_3$) mineral precipitation, climate conditions are a key to $CaCO_3$ in soils (Suarez and Rhoades, 1982). In this case, the area of study experiences a high degree of seasonality, with a dry and cold austral winter and a humid and hot austral summer. Another possible condition is the availability of the mineral $CaCO_3$ itself that can be provided by the deposition of aerosols, by the weathering of igneous rocks (plagioclases), or by the combination of both present as mineral particles

(Suarez and Rhoades, 1982). However, no evidence of these processes was found in the soils. The coexistence of calcium carbonates and illuvial clay minerals also reflects a seasonal climate for the Subandean Belt.

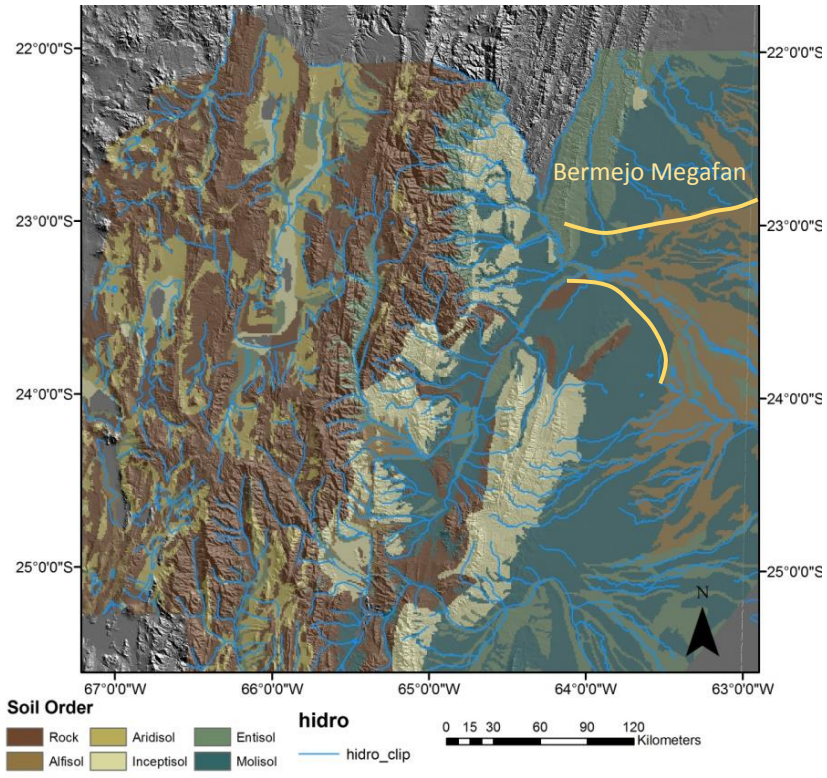
22°0'0"S
23°0'0"S
24°0'0"S
25°0'0"S
67°0'0"W
66°0'0"W
65°0'0"W
64°0'0"W
63°0'0"W
Bermejo Megafan
N
Soil Order
Rock
Aridisol
Entisol
Alfisol
Inceptisol
Molisol
hidro
hidro_clip
0 15 30 60 90 120
Kilometers

A

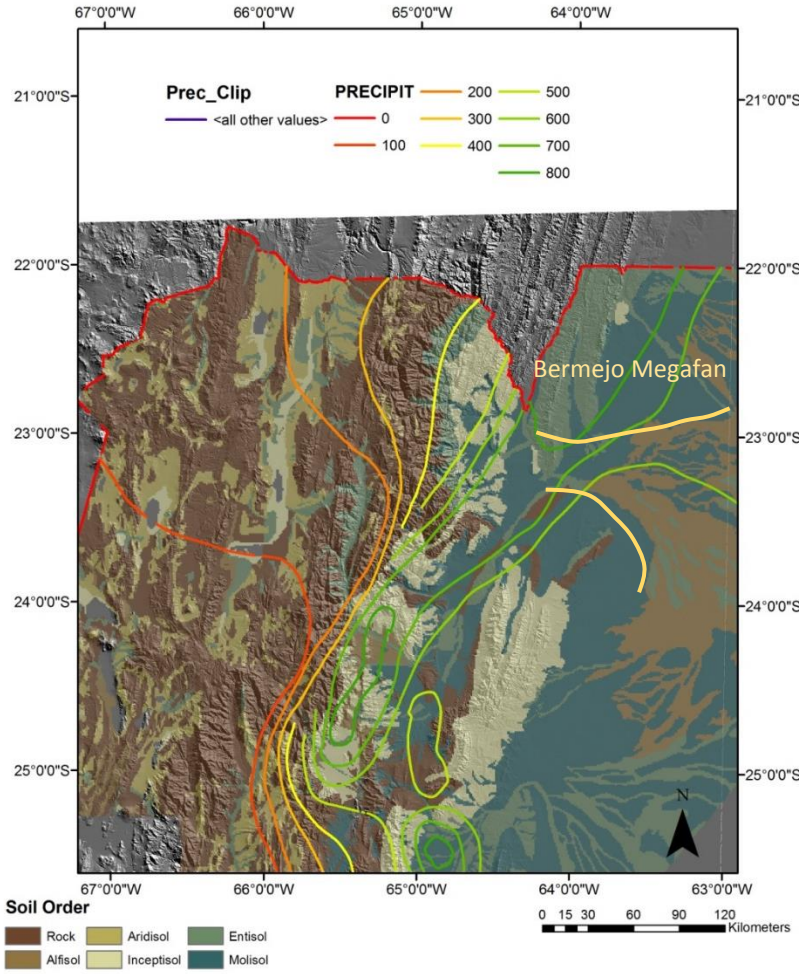
67°0'0"W
66°0'0"W
65°0'0"W
64°0'0"W
63°0'0"W
21°0'0"S
22°0'0"S
23°0'0"S
24°0'0"S
25°0'0"S
Prec_Clip
<all other values>
PRECIPIT
0
100
200
300
400
500
600
700
800
Bermejo Megafan
N
Soil Order
Rock
Aridisol
Entisol
Alfisol
Inceptisol
Molisol
0 15 30 60 90 120
Kilometers

B

Figure 5: Map of soil orders, major streams, and rain fall
A) Positions of major stream channels, B) and contours of mean annual precipitation in northwestern Argentina.

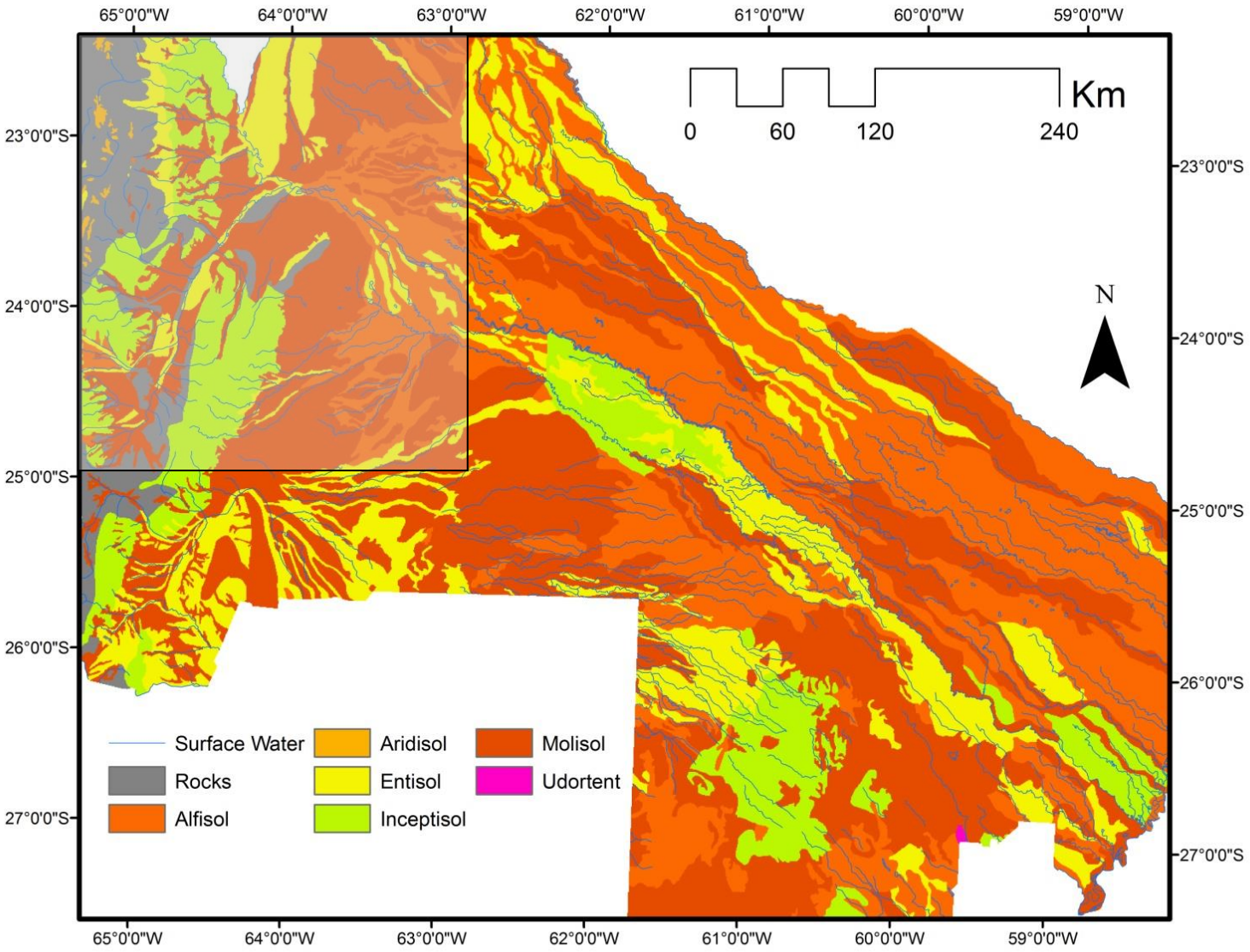
65°0'0"W
64°0'0"W
63°0'0"W
62°0'0"W
61°0'0"W
60°0'0"W
59°0'0"W
23°0'0"S
24°0'0"S
25°0'0"S
26°0'0"S
27°0'0"S
Km
0
60
120
240
N
Surface Water
Rocks
Alfisol
Aridisol
Entisol
Inceptisol
Molisol
Udortent

Figure 6: Soil Order Distribution in the Bermejo Distributary Fluvial System
This is a map of Bermejo Megafan and the distribution and arrangement of the soil and their order in the modern environment. The shaded area corresponds to the maps from Figure 5. Notice that once the Bermejo River start to move toward the lowlands, the soil order distribution is aligned with the river axis.

Paleosol Category	Pedological Profile	Weathering Profile	Structures	Pedoturbation
I	Non sedimentary structures (AC)	Rock structures visible	Massive	None
II	Low degree of horizonation (AC)	Rock structures visible with considerable mineralogical alteration (saprolite)	Massive	None
III	Moderate degree of horizonation (A,Bw,C)	Mineralogy altered, low Illuviation	Massive, granular	Low
IV	Moderate degree of horizonation (A,Bw, Bt, Bk,C)	Mineralogy altered, considerable Illuviation	Granular, blocky primatic	Moderate
V	Horizons easily visible	Mineralogy altered, Illuviation, translocation, accumulation	Granular, blocky primatic	High

Table 1.

Table 1: Paleosol Categories

Methodology

This study was placed in a known geologic time framework by building the field observation and sampling program upon published studies of three exposed stratigraphic sections located within the Subandean Ranges. The principal focus is the stratigraphic section exposed over the distance of approximately 15 km along the Iruya River, for which Hernández et al. (1996) measured, described, and dated about 7000 meters thickness of siliciclastic sediments. We rely on the results of the Hernández et al (1996) study, a related study (Echavarría et al., 2003), and new U-Pb geochronology (Chapter 2) to place the paleosols into a magnetostratigraphic- and tephrachronology-based time and tectonic framework.

We tied our observations both to geographic position, by recording the locations of all the paleosols using Global Position System (GPS) instrumentation, and to depositional age, by recording the stratigraphic horizon of each paleosol sample in the original measured section of Hernández et al. (1996). For this project, samples of paleosols were collected from the lower 4400 meters of the Río Iruya section, which encompass the Middle Miocene to Early Pliocene. The stratigraphic spacing between each sample collection site depended on the frequency of the spatial distribution of the paleosols. To characterize spatial variations in the paleosol-forming system, two more stratigraphic sections were studied which earlier had been measured, described, dated,

and interpreted by Echevarría and others (2003). For those sections, description and sampling campaigns followed the published sections exposed along banks of the Peña Colorada River and the La Porcelana River. These stratigraphic sections are approximately 2500 meters and 1900 meters thick, respectively.

Physical properties of the soils were examined, described, and then classified using the Mack (1993) paleosol classification. The colors and textures of each paleosol were described using the Munsell Chart and Udden-Wentworth classification charts, respectively. Two stages of paleosol classification were used, the first based on field observations and the second based on laboratory analyses. Field classification (Table1) takes into account the observable textures, color, pedogenic structures, and the level of biological activity inferred from root casts and bioturbation in each individual solum body. Laboratory analyses provide added information about mineralogy and micromorphology that lead to modification of soil classification. Where the paleosols had readily recognizable pedogenic structures (such as soil horizons), a sample of each distinctive feature was collected and stored in a sealable bag.

Those samples were analyzed to determine mineralogy and to identify microstructures. The mineralogy of the paleosols was analyzed by x-ray diffraction (XRD), focused on the lower zeta angles (θ) for clay mineral identification (Moore and Reynolds, 1989). The XRD shows the mineralogy present in paleosols such as the type of clays, calcium carbonate, and oxides. The microstructures were analyzed visually using petrographic thin sections. For several samples, a pair of thin sections was examined; the section was chosen to reveal both the matrix and nodular structures. Both sets of thin sections were analyzed on a microscope stage using both plane polarized and cross-polarized light conditions. Matrix thin sections include rizoliths, burrows, and mottling coloration, which provide the opportunity to look for evidence of pedogenesis and to deduce pedogenic processes. The thin section analysis shows the arrangement of the clays such as inter-granular coating or their flocculation, the existence of micro vein fills, the mineral arrangement within nodules,

etc. These data were used in the determination of physical processes like clay illuviation, grain overprint, mineral distribution, and microbiological activity.

Although every single feature gives us a clue with which to understand the level of soil maturity, the most important clues for this study are the biological activity (bioturbation and root casts) and the pedogenic development (horizons, and carbonate nodule presence). The degree of horizonation can reveal the stage of the paleosol maturity at the time of soil formation (Mack et al., 1993).

The paleosols are classified using the Mack et al, (1993) classification system, which takes into account what is really preserved, rather than being based on what could be the soil profile, which leads to an interpretation. Mack et al. (1993) identify nine possible paleosol classes that can be identified in the field based on their pedogenesis or weathering features. Although Mack et al (1993) do not use bioturbation or root fossils among the main criteria, these induce horizonation (e.g.: O, Bw, Bs), translocation, and accumulation of soluble minerals ($CaCO_3$). For this reason, these are an implicit part of the paleosol characteristics to be considered.

Results

Paleosol Profiles and Composition

Paleosols in the Iruya river section are the main focus of this paper. In accord with the results from single crystal zircon laser ablation, the time period represented by the strata is from 14 Ma to approximately 5 Ma, and the section containing paleosols is approximately 11 Ma to 5 Ma. In addition, the Peña Colorada (13.6 Ma to 5 Ma) and La

Porcelana (14.3 Ma to 5 Ma) sections augment the descriptions of the paleosols for the NWA.

The sedimentary characteristics observed during the fieldwork in the Iruya River section match the properties of fluvial system deposits, which include the paleosols interbedded within the strata. The dominant texture of the paleosols corresponds to a blocky structure. Nevertheless, paleosols with nodular and granular texture are also present in this sedimentary record. The chroma and hue range for these paleosols go from 5 yr 4/3 (yellowish) to 10 yr 5/3 (reddish).

Paleosols in the Miocene-Pliocene strata at Iruya River are mainly represented by B and C horizons with almost no A horizons. The texture of the matrix of the paleosols is composed of very fine grained sandy-silt, clayey-silt, or a sandy-silt and clay. In other words, from a soil scientist's perspective, these will fall into the categories of clay loam, loam, or silty clay loam.

Calcium carbonate nodules are a common pedogenic feature found in the Iruya River stratigraphic section. These nodules are present along each paleosol profile, but the frequency of nodules is higher at the upper and lower part of the horizons containing calcium carbonate (Bk; Figure 7, Figure 7C-F). The paleosol C horizon (partially

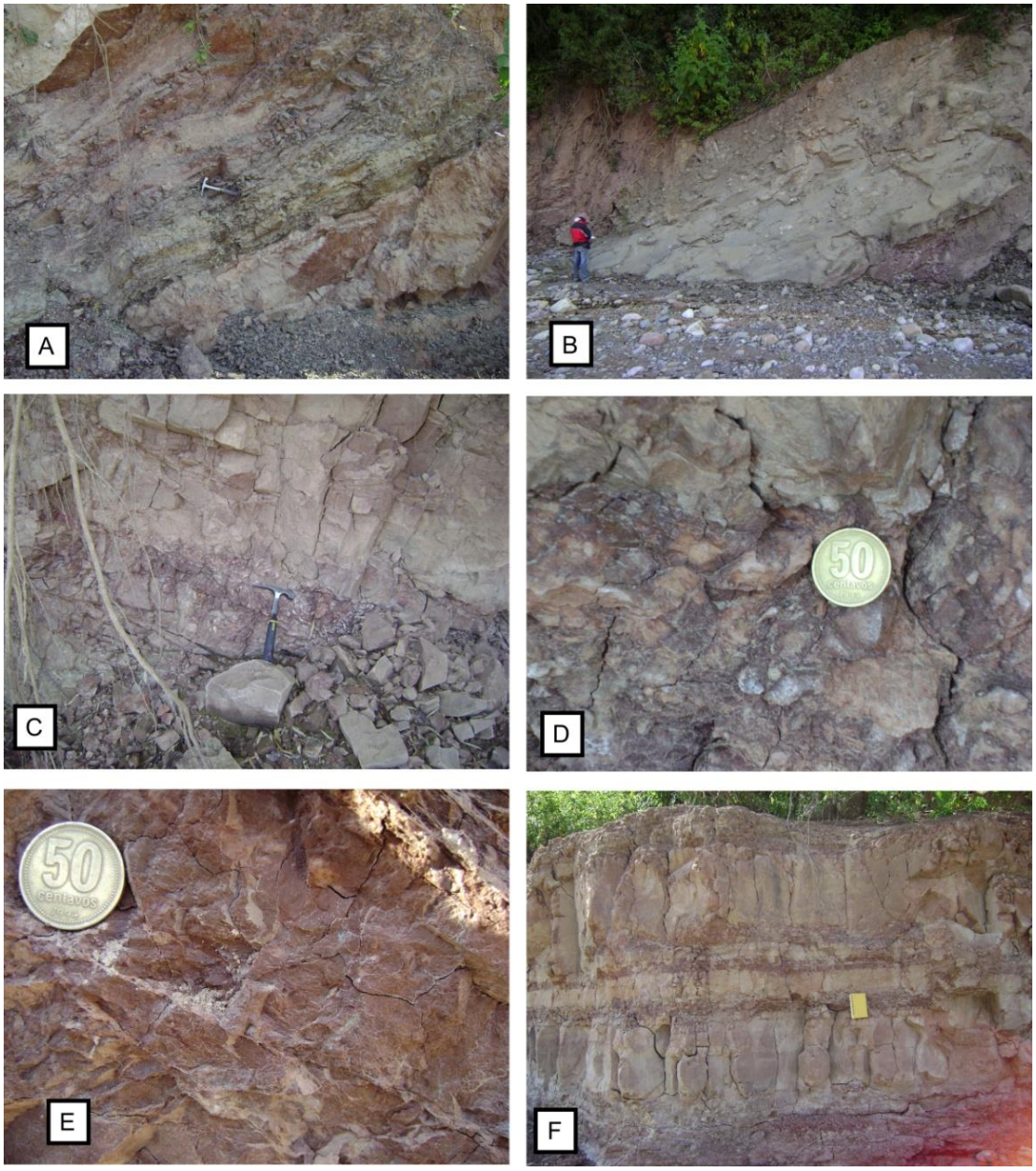
A
B
C
D
E
F

Figure 7: Paleosols in Northwestern Argentina
Figure A present a poorly developed soil at Iruya River, B present a sandstone with calcium carbonate nodules; C is a paleosols with calcium carbonate nodules behind the hammer, and D is a close up of the same soil; E is a picture where nodules and bioturbation can be observed at the center of the photo; F is a sequence of stack paleosols.

weathered parent material, regolith) is composed of a medium grained sand whereas the material above (paleosolum) is composed of finer material including mud and sandy mud (Figures 7C and 7F).

The color of the matrix of the paleosols is described as 10R 3/2 with a contrast in the sandstone color, which is 7.5 YR 7/2. Even though calcium carbonate nodules (magnified areas shown in black squares in Figures 8A and 8B) are present in the B horizons, the accumulation of oxidized clays is also evident giving the reddish coloration. The original continuity of the paleosol horizons cannot be fully evaluated, because of the limited extent of the outcrop exposure. But it is possible to observe the relationship between sandstone and mudstone deposits, where the sandstones are truncated by mudstones at the top and the bottom of each sedimentary fluvial sequence. Another common feature of these soils is the presence of rhizoliths or root casts (Figure 9). The root cast length varies from about 5 cm to approximately 25 cm long (Figure 9B).

The stratigraphy is displayed and the green bars next to it are the paleosol locations along the column (Figure 10). The grain size distribution increases upward from mud to conglomerate. Over 60 paleosol profiles were examined. Paleosols are more frequent in deposits younger than 7.5 Ma (Figure 10 and Figure 11). However, the floodplain texture changes upward in the stratigraphic column (Figure 10a). From 5.8 Ma to the top of the column, paleosol profiles are massive Bt horizons with thin Bk horizons covered by thick sandstones. This paleosols mark a different stage of development (Category V). Nevertheless, these paleosols are rich in clay and calcium carbonate, yet the thickness of the horizons and the more localized nodule areas in the profile suggest more stable or less transitional floodplain areas.

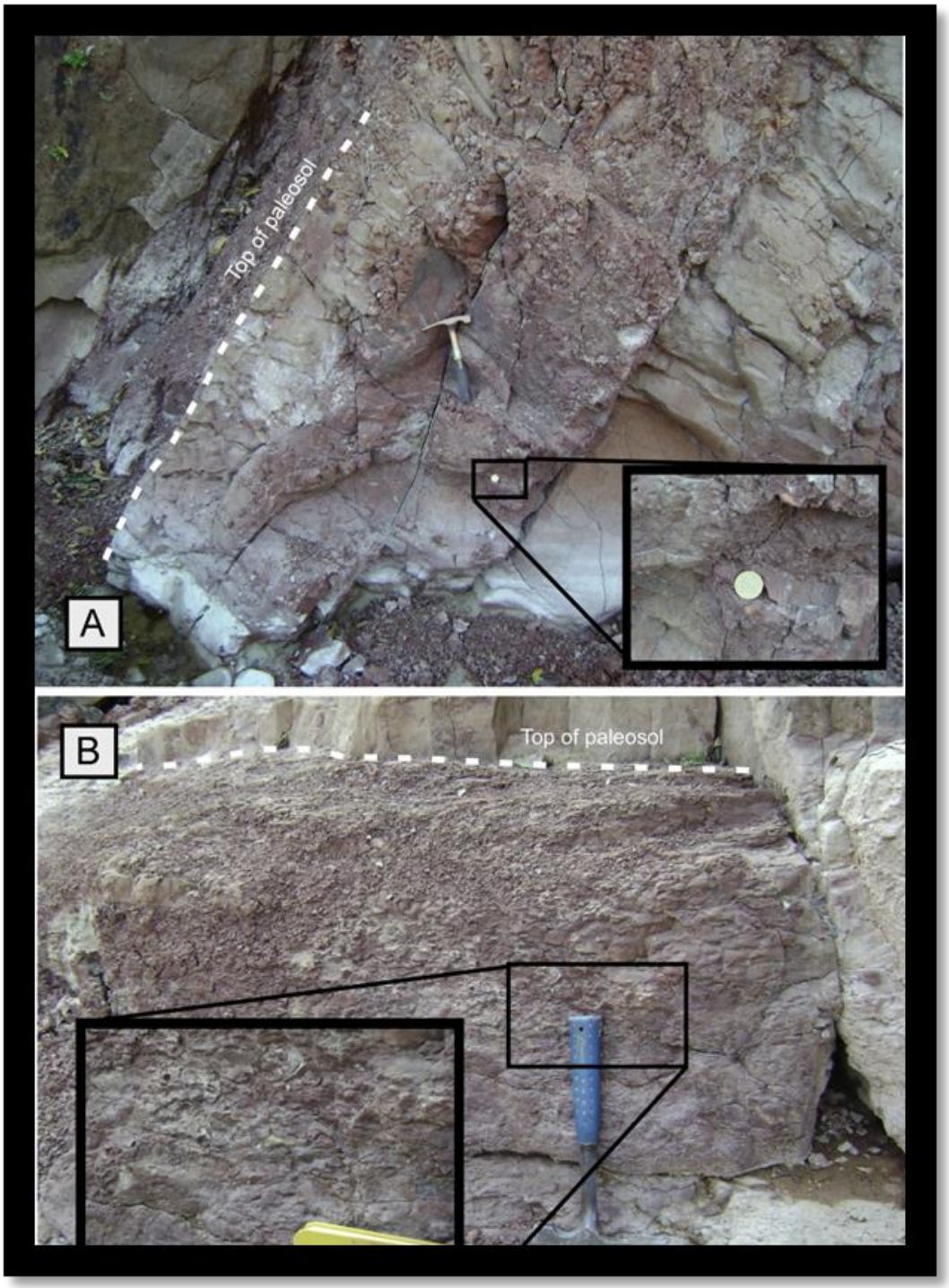
Top of paleosol
A
B
Top of paleosol

Figure 8: Iruya River Paleosols with two types of Sandstone Boundaries
Figure 8A represent a paleosol with a highly weathered boundary between mudstone and sandstone where the first sandstone addition must be slower compared with 8B. B is a paleosols bounded at the top by a sharp contact with a sandstone strata, probably the result of a single sedimentary event.

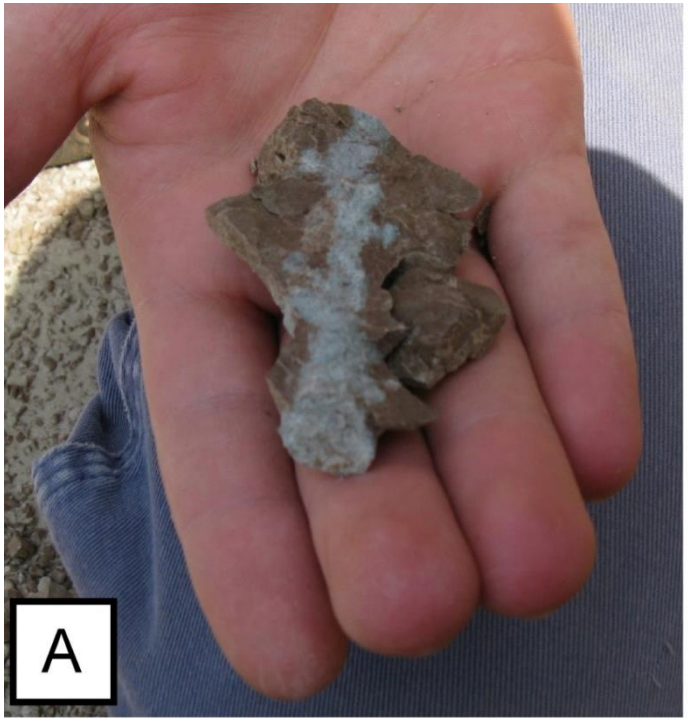
A

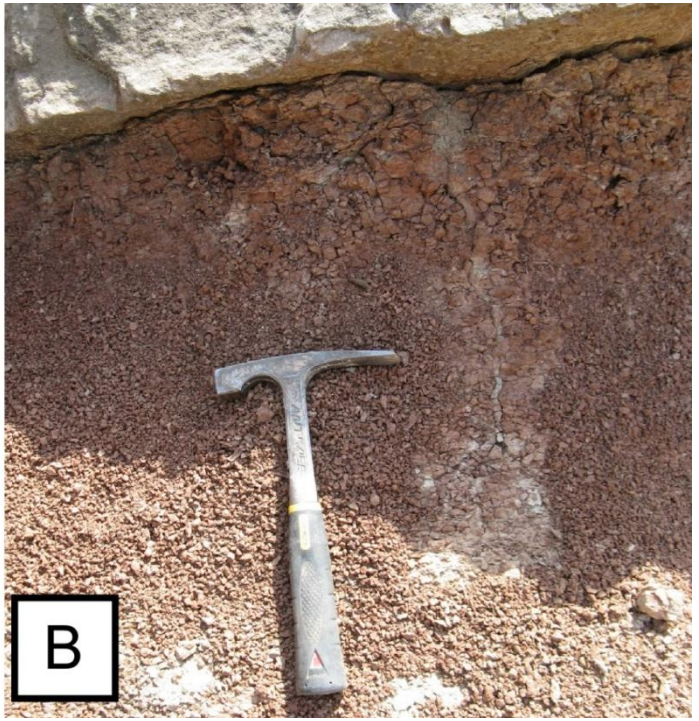
B

Figure 9: Rhizolith and Redox Paleosol Features
Figure 9A) This is a close up of a fragment of the rizolith in Figure 9B. It is possible to notice the mineral deposition as the result of a redox reaction inside the root system

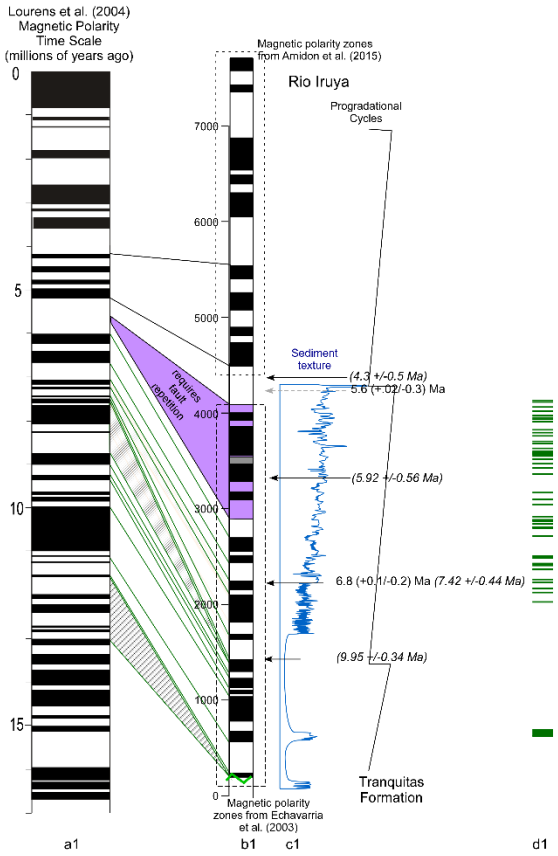
Lourens et al. (2004)
Magnetic Polarity
Time Scale
(millions of years ago)
Magnetic polarity zones
from Amidon et al. (2015)
Rio Iruya
Progradational
Cycles
Sediment
texture
requires
fault
repetition
(4.3 +/-0.5 Ma)
5.6 (+.02/-0.3) Ma
(5.92 +/-0.56 Ma)
6.8 (+0.1/-0.2) Ma (7.42 +/-0.44 Ma)
(9.95 +/-0.34 Ma)
Tranquitas
Formation
Magnetic polarity
zones from Echavarria
et al. (2003)
a1
b1
c1
d1

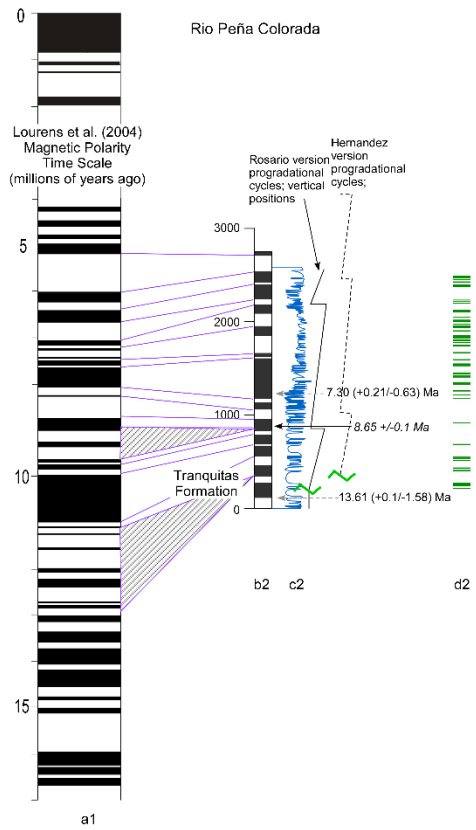
Rio Peña Colorada
Lourens et al. (2004)
Magnetic Polarity
Time Scale
(millions of years ago)
Rosario version
progradational
cycles; vertical
positions
Hernandez
version
progradational
cycles;
7.30 (+0.21/-0.63) Ma
8.65 +/-0.1 Ma
13.61 (+0.1/-1.58) Ma
Tranquitas
Formation
a1
b2
c2
d2

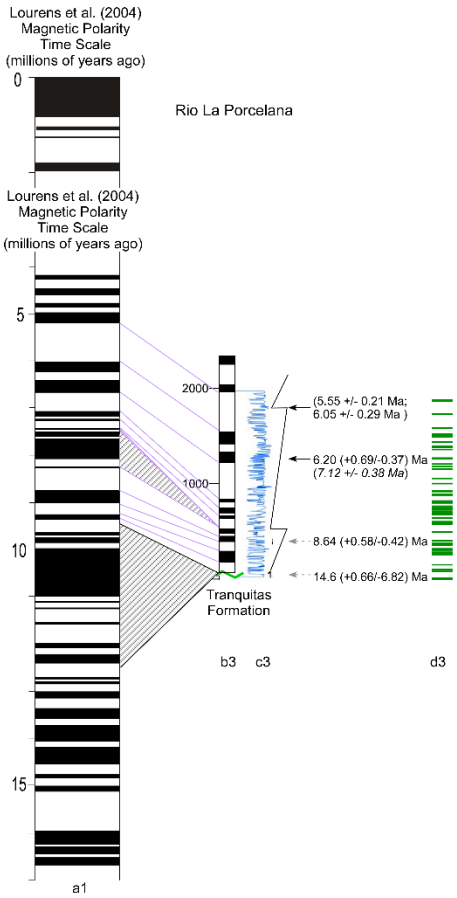
Lourens et al. (2004)
Magnetic Polarity
Time Scale
(millions of years ago)
Rio La Porcelana
Lourens et al. (2004)
Magnetic Polarity
Time Scale
(millions of years ago)
(5.55 +/- 0.21 Ma;
6.05 +/- 0.29 Ma)
6.20 (+0.69/-0.37) Ma
(7.12 +/- 0.38 Ma)
8.64 (+0.58/-0.42) Ma
14.6 (+0.66/-6.82) Ma
Tranquitas
Formation
a1
b3
c3
d3

Figure 10: Stratigraphy of the River Sections and the Paleosols Position for this study
This figure shows the global magnetostratigraphic data with the paleomagnetic data from Hernandez et al. (1996), the radiometric data from the analysis of zircons, and the paleosol position in every location. Sections a, b, and c corresponds to Iruya, La Porcelana, and Peña Colorada respectively.

Paleosols in NWA are also found in locations that are east of the Iruya River, at Peña Colorada and La Porcelana Rivers (Figure 1). The parent material is sandstone and mudstone that gradually increases up-section in grain size as well as in the thickness of the strata (Figure 10 b and c), without reaching conglomerate facies like those of in the upper part of the Iruya River column. The development stages of these paleosols fall into categories II, III, and IV, with an even frequency distributed along the stratigraphic columns. These paleosols are rich in clay and calcium carbonate as well. However, there is a difference in the calcium carbonate content for Peña Colorada and La Porcelana in that the clay percentage is higher than the calcium carbonate amount, unlike in the Iruya River section. The clay content is 20 % more and the calcium carbonate is < 10% in most of the section, in particular in the Peña Colorada paleosols. Paleosols in Peña Colorada exhibit high oxidation conditions, including horizons cemented by goethite and clay minerals. This variability in texture in particular, implies a different paleosol geomorphology suggesting a more restricted and poorly drained setting compared with Iruya River for example.

Mineralogy and Microstructures

The dominant paleosol minerals are illite, kaolinite, and calcium carbonate (calcite; Figure 12). The red and yellow colorations are the result of hematite (oxide) with kaolinite and illite (clays). The Iruya River section displays a calcium carbonate content ranging between 5 to 15% when measured in the lab for geochemical analyses of stable isotopes. The paleosols in the Peña Colorada section contain much less calcium carbonate (<10%). However, the paleosols in Peña Colorada exhibit minerals with a

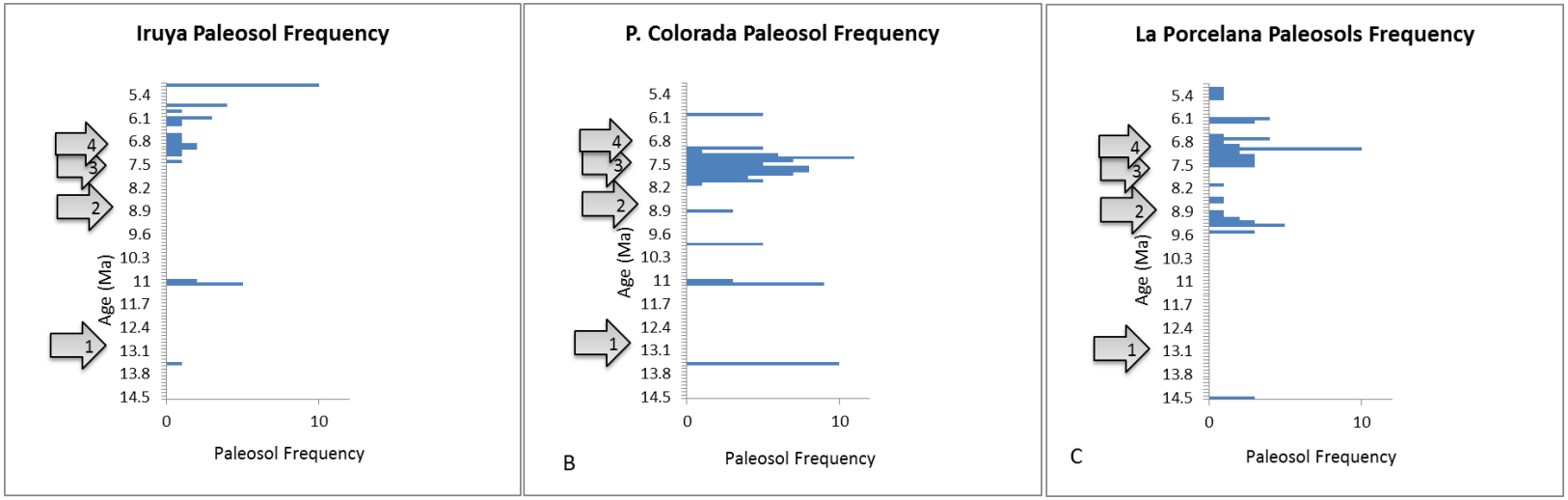
Iruya Paleosol Frequency
5.4
6.1
6.8
7.5
8.2
8.9
9.6
10.3
11
11.7
12.4
13.1
13.8
14.5
Age (Ma)
4
3
2
1
0
10
Paleosol Frequency
P. Colorada Paleosol Frequency
B
La Porcelana Paleosols Frequency
C

Figure 11: Paleosols Distribution for the Stratigraphic Sections Over Time
A represents the Iruya River soil distribution over time with the different thrust-fold belt events presented in Echevarría et al (2003); B and C are the paleosols distribution over time for Peña Colorada and La Porcelana stratigraphic sections respectively. Arrows represent the 4 times of thrust movement during the time span of this study: (1) Eastern Cordillera, estimated at 12 Ma; (2) Pescado range, 8.5 Ma; (3) Pintascayo Range, 7.5; and (4) Oran Range, 6.9 Ma.

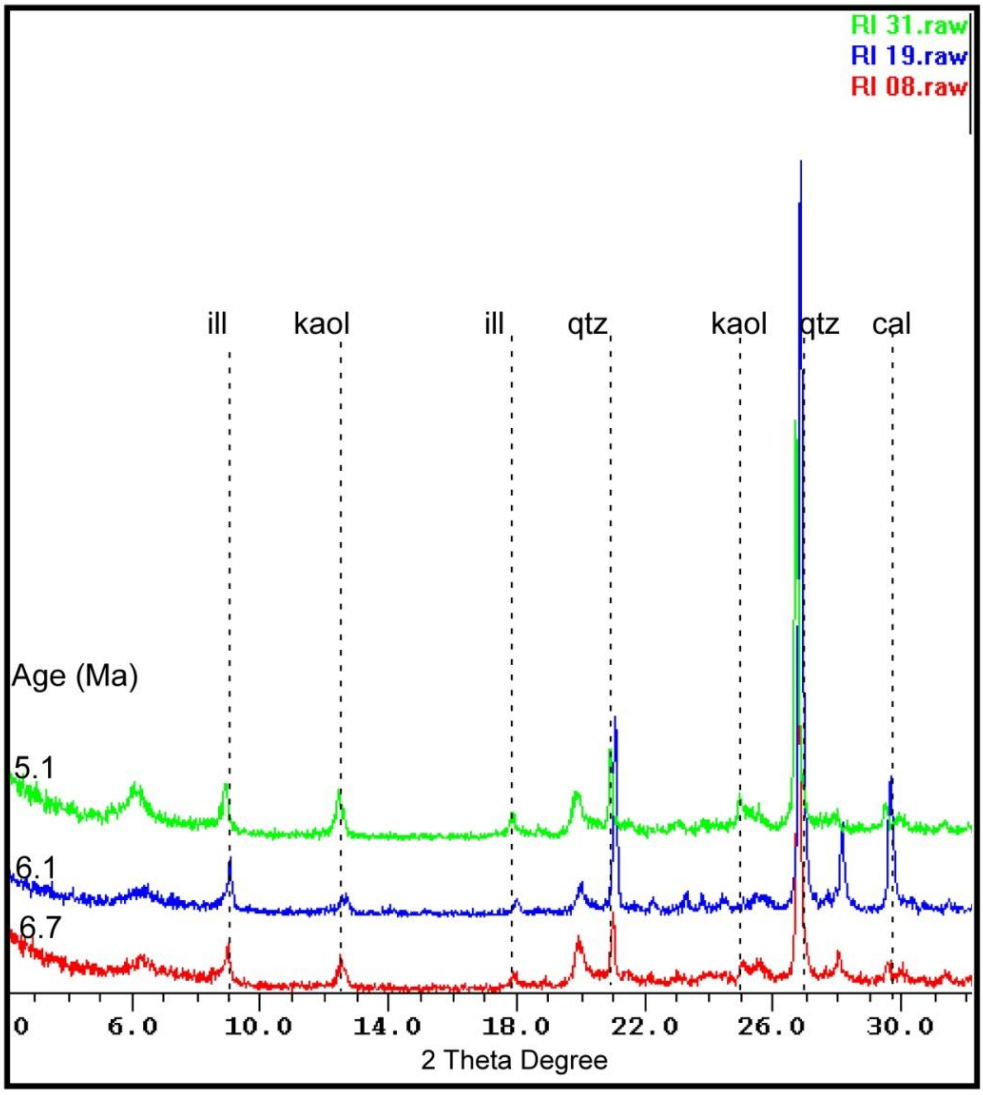
RI 31.raw
RI 19.raw
RI 08.raw
ill
kaol
ill
qtz
kaol
qtz
cal
Age (Ma)
5.1
6.1
6.7
0
6.0
10.0
14.0
18.0
22.0
26.0
30.0
2 Theta Degree

Figure 12: Iruya River XRD for representative Paleosols in the Stratigraphic Column
This is the XRD for three paleosols at Iruya River section that represent the constant mineralogy through the Late Miocene.

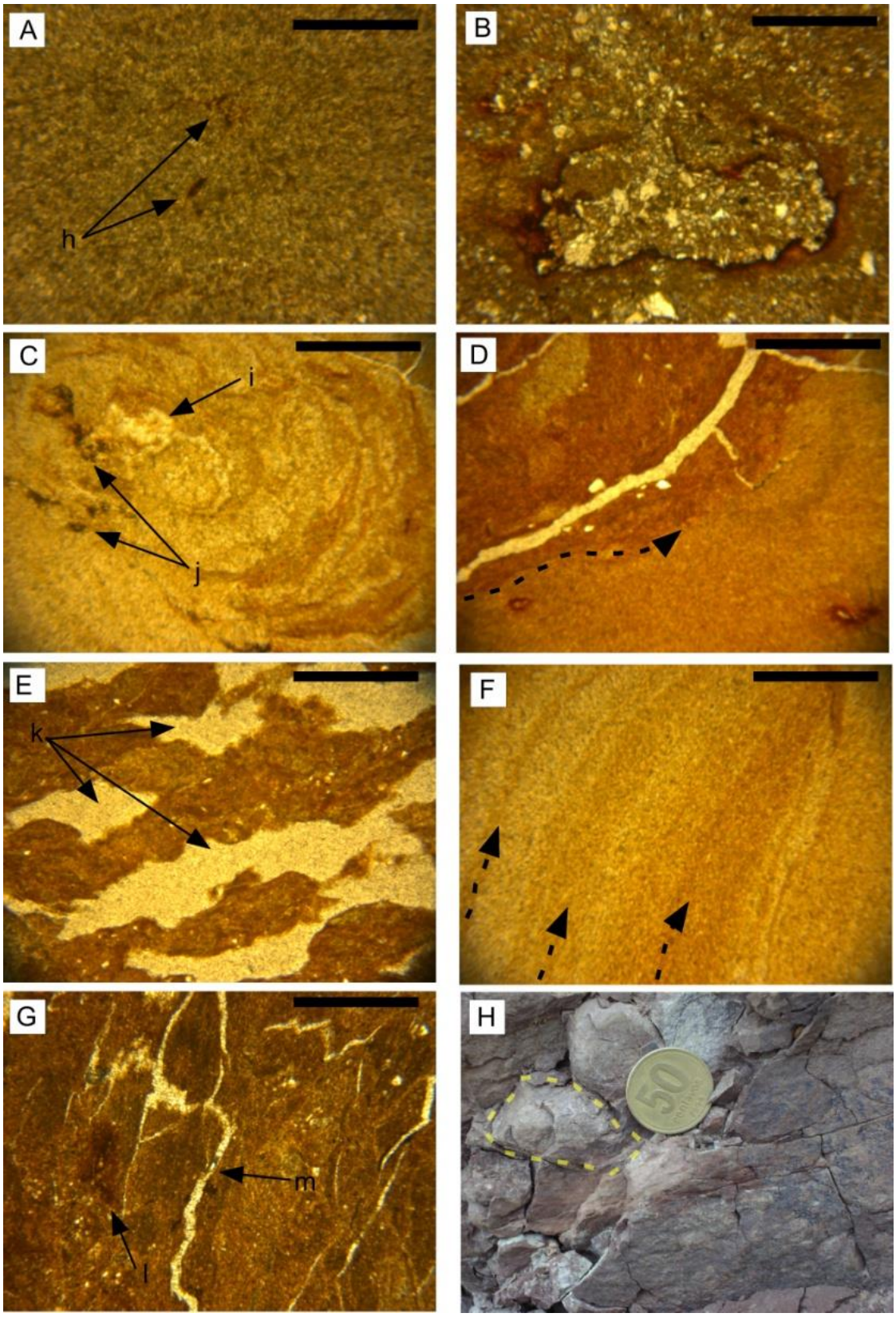
A
h
B
C
i
j
D
E
k
F
G
m
l
H

Figure 13: Micromorphology of Paleosols for the Iruya River Stratigraphic Section
A) Oxidation micro-mottling; B) Oxide coating around calcium carbonate micro-concretion; C) Calcium carbonate nodule core (i) and oxidation mottling (j) at different position in the calcium carbonate nodule; D) Clay coating around calcium carbonate nodule. It is possible to see that the calcium carbonate vein is post-depositional in relation with the argillic coating; E) Calcium carbonate mineral precipitation (k) inside a rhizolith observed in a cross section view; F) Calcium carbonate and argillic coating succession; G) Oxidation mottling (l) and calcium carbonate veins (m) in the paleosol matrix; H) Peds of paleosol showing soil development record.

greater degree of oxidation. La Porcelana paleosol mineralogy is identical to the Iruya River, with the difference that calcium carbonate nodules are more abundant in the Iruya section. Most of the calcium carbonate occurs dispersed within the matrix for samples from the Peña Colorada and La Porcelana river sections, with the exception of the root casts found in both places. However, clay minerals are deposited in the three sections, with kaolinite and illite as the dominant clays.

Pedogenic micro-features are subdivided in two groups; the analysis of the matrix and a second group that relies in the analysis of macrostructures like roots, tubules, and nodules. Oxidation and reduction features are common in the matrix (Figure 13 A and B), and coating of clay and oxides are a frequent feature found in the Iruya section paleosols (Figure 13 B and C). As observed in Figure 13D darker area, a nodule deposited in the upper section of a paleosol profile contains ped-relicts as evidence of the cohesion of the material produced by the cementation of clays.

Biological macrostructures are present in the forms of root-casts, burrows, or traces (Figures 9 and Figure 13). Figure 13E is a cross section of a rhizolith in the Iruya River section. The fossilized root (dark coloration) shows the porous structure that was replaced by calcium carbonate (arrows). However, paleosol matrix also has calcium carbonate in the fissures formed within the paleosol profile (Figure 13G), showing that the precipitation of the mineral is a common process in these paleosols.

Overall, the calcium carbonate is observed in nodular structures and peds (Figure 13H), whereas the paleososol matrix is clay-dominated with oxide micro-nodules and oxide-clay coatings around the solum voids.

Paleosol Frequency

In addition to the characteristics of the paleosols in Iruya River, their frequency along the stratigraphic section also provides evidence of the climatic and environmental setting present at the time of soil development (Figure 10). Paleosol frequency was quantified as the number of paleosols over an interval of 100 meters (Figure 11). As paleosols are restricted to the mudstone deposits, the resolution in the distribution of paleosols over time using magnetostratigraphy is limited by the number of samples taken in every sample interval where mudstones were present.

The Iruya River stratigraphic section presents the greatest frequency of paleosol between 7.5 Ma and 5 Ma, but paleosols are present from 13.5 Ma to approximately 5.1 Ma (Figure 11A). No data were obtained from the age range between 13.5 Ma to 11 Ma due to lack of exposure. The distribution of paleosols in this section can be described as skewed to the right, but the missing part of the stratigraphic section may influence this result. Nevertheless, analyzing just the measured section from 7.5 Ma to 5.1 Ma, the paleosol distribution forms a normal bell shape (Figure 11). Paleosol frequency in Peña Colorada River section exhibits a different arrangement (Figure 11B). The paleosol ages range from 13.5 Ma to 5.5 Ma, with the greatest presence of paleosols between 8.2 Ma to 6.9 Ma in the studied section. However, no paleosols were obtained during 13 Ma to 11 Ma because no outcrop was exposed at the Peña Colorada River for this time. The mode for the paleosol distribution is about 7.5 Ma and a tendency to be a left skewed paleosol histogram. La Porcelana River section presents paleosol distributed from approximately 14 Ma to 5 Ma, with the greatest frequency between 8 Ma to 7 Ma (Figure 11C). The mode

for this section is at 7.0 Ma, and exhibit a close to normal distribution when compared with the previous stratigraphic sections studied here.

Discussion

Environmental Processes Involved in Paleosol Development

Field characteristics in the Iruya River section match the properties of fluvial system deposits along a tectonic front that were described by Disalvo and Stark (1983) during the Miocene-Pliocene Andean orogenic displacement. However, we depart from Disalvo and Starks (1983) in recognizing for the Cenozoic strata in the Iruya River section three progradational cycles, which can be described as sub-cycles of a single coarsening upward progradational sequence.

The parent material of the paleosols is interpreted as floodplain deposits that were fed periodically by flood waters that rose over the channel margins to flood the overbank region. This means that the development of the soil in the ancient environment depended greatly on the stability of the fluvial system or periodicity of the storm events. Taking the modern environment for comparison, we can observe in Figure 6 how the inceptisols and entisols are juxtapose to alfisols and mollisols as evidence of more mature soils further away from the main channel. These present the disposition for the further areas to exhibit more mature soils that will be affected by the addition of sediments from storm waters. Common paleosols developed over floodplain deposits are shown in Figure 7. These paleosols, with poor to medium development and essentially no sedimentary structures, have a blocky texture. Blocky texture tends to vary from soil to soil in modern

environments, but the ratio between clay and sand is sometimes referred to as the main control of this soil texture (Makabe et al., 2009; He et al., 2009).

The sedimentological arrangement suggests that the sandstone represents a channel sand deposit or crevasse-splay sand deposit, which was covered by flood-borne mud deposits. Pedogenesis started to develop after each flood event. Once this process is repeated over time, the outcome will be the paleosol shown in Figure 7F, a stack of paleosols separated by thin sandstone strata (< 20 cm) capped at the top and bottom with a thick layer of sandstone. These paleosols are formed by AC horizons.

The most common well-developed Iruya River paleosols are classified as argillic-calcisols (Figure 8). These paleosol profiles are normally about 1-meter-thick, with a 20 to 40 cm Bk, Bt, Bkt, or Bw horizon, and fall into categories III and IV of table 1. The top of the paleosol (B horizon) represents an erosional surface, which is a planar contact in most of the cases.

The presence of longer roots tends to be a sign of vegetation adapted to a setting of limited water supply or nutrients, because plants tend to develop longer roots as well as low canopy density when nutrients and water are scarce or not easily reachable (Lima et al., 2010). The color of the rhizoliths implies redox reaction (Figure 9A) possibly when water is uptake by roots from deep soil horizons and then released from superficial roots into upper soil layers.

The micro-scale features visible in thin sections reveal the micro-textural arrangement and the distribution of minerals in the paleosol matrix and calcium carbonate nodules. Microstructures can help to define the environmental and climatic conditions under which paleosols developed (Brewer, 1976; Douglas and Thompsom, 1985;

McCarthy et al., 1998; McCarthy and Plint, 2005). Paleosol features such as diagnostic horizons are lost commonly by erosion, diagenesis, or pedogenic overprint. Nevertheless, much evidence of pedogenesis can be recovered from analysis of microstructures within soil profiles, such as evidence of clay translocation and illuviation, nodular growth, recrystallization, and diagenesis (McCarthy et al., 1998; Figure 13).

In order to form clay coatings like those of the Iruya section (Figure 13 B and C), suspension and re-flocculation of clays must occur once translocation took place (Brady and Weil, 2001). The presence of clay-coating layers suggests illuviation processes as the mechanism of deposition (Ringrose-Voase and Humphreys, 1994). The alternation between clay and carbonate coating also suggests repeated changes between dry and wet season conditions. One plausible interpretation is that calcium carbonate percolated and precipitated during dry periods, and then clay illuviated from overlying horizons during rainy seasons. Such illuviation is consistent with the observation that the top-most material of most paleosols has been eroded, using the reasoning that, once illuviation of clay occurred, the cohesion between particles decreased as the result of the residual poor interaction of the coarser material that was left behind in the top horizon.

The micro-oxide nodules are formed by the moisture content in the pores of the soil profile. Once good aeration is established when the soil permeability is connected to the surface, this allows the oxidation of iron. However, if reduced iron is contained in the root channel, this suggests a downward movement of the water in the root system. On the other hand, calcium carbonate nodules are deposited if illuviation occurs and moisture is subsequently evaporated and lead to crystallization of carbonates. However, in addition a

second process is required for the precipitation of the mineral ($CaCO_3$), which combines soil CO_2 respiration (microbial/plant) and Ca that is present in the solum.

As described by McCarthy et al. (1998), pedo-relicts are detritus formed by previous paleosols that have been transported a short distance, deposited, and "trapped", where they become parent material to a different soil profile. This suggests two processes; the recycling of paleosol material, and the erosion of paleosol upper horizons.

In soils, the co-occurrence of 2:1 and 1:1 clays require seasonal changes in precipitation between dry and wet periods (Schaetzl and Anderson, 2005). 2:1 clays such as illite and chlorite are mainly the product of a detrital deposit, in contrast to kaolinite that is commonly founds as the result of weathering. In modern soils, the precipitation and preservation of calcite is also favored in areas with wet and dry seasonal changes (Brady and Weil, 2002). In Iruya River section paleosol textures are highly influenced by the presence of calcium carbonate in the form of nodules and cement. Nevertheless, the interpretation in seasonality does not comes from the presence of clays and carbonates, but rather the interlayering arrangement between these minerals present in the calcium carbonate nodules.

Temporal Characteristics of Paleosol Development and Preservation

The span of time for the stratigraphic sections in the Iruya River, Peña Colorada River, and at La Porcelana was obtained from previous work (Hernández et al., 1996; Echevarría et al., 2002; Amidon et al., 2015) through paleomagnetic studies tied to volcanic ash chronology (Hernández et al, 1996; Galli and Hernández, 1999; Reynolds et al., 2001; Echevarría et al., 2003; Amidon et al. 2015). To increase the number of horizons of known

numerical age, to resolve some conflicting information for horizons studied previously, and to reduce the uncertainties of interpretations caused by mixing various dating methods, we applied the single crystal laser ablation U-Pb isotopic dating method to zircons from several volcanic ashes and to detrital zircons from several sandstones (Chapter 2 p. 16).

The combined constraints from magnetic polarity stratigraphy and zircon age spectra are best interpreted to show that the part of the Iruya River section in which we analyzed paleosols accumulated between about 14 Ma to 5.1 Ma. We analyzed the magnetostratigraphic profile to estimate the completeness of the preservation of strata (McRae, 1990). The Iruya River stratigraphic section from the first 4,500 meters and using the Tranquitas Formation as the base of this unit, was divided into age subsets of 100,000 years over a span of time of one million years using Cande and Kent's (1992) Global Magnetic Polarity Scale. The result reveals that up to 60% of the sedimentary history at a 100,000 year scale is preserved.

The magnetostratigraphic column (Figure 10) indicates sediment accumulation at the high rate of about 0.8 km/Myr for the Iruya River area through the time interval from about 7.5 to 5.1 Ma It is within this period of time that paleosols are best preserved as a consequence of the dominance of burial processes over erosion. Consequently, paleosol properties of the foreland basin landscape are well preserved in a vertical sequence.

Tranquitas paleosol characteristics, when present, tend to represent highly developed and oxidic paleosol conditions, whereas the paleosols in strata overlying the Tranquitas Formation at Iruya River, Peña Colorada, and La Porcelana River stratigraphic sections are represented by argillic-calcisols. The record of paleosols depends on the history of the rate of accumulation of sediment, because landscape evolution and soil

formation are directly linked (Birkeland, 1999). The sequence of structurally generated topographic subsidence at the site of the Iruya River section provides a soil vertical chronosequence, a manifestation of the sequential phenomena of sediment deposition and subsequent soil formation explained by Birkeland (1999). Evidence of the oldest pedogenic development in the three sections is found in this formation, within sandstones sheets that vary from 2 to 5 meters thick, sometimes with intercalated thinner sandstone sheets from 10 cm to 40 cm thick. These paleosols contain calcium carbonate nodules, and low clay or silt content (< 10%) in the matrix.

Even though paleosol development might occur over abandoned channel deposits (Uba et al., 2005), this case was not observed for the paleosols in the NWA area. However, with an increase upward in the section in sand material in the paleosols, there was a resultant increase in pore permeability. This resulted in better soil drainage in the younger paleosols.

The arrangement of the frequency in time of the paleosols shows similarities and differences that might be correlated with the DFS environmental setting. For the Iruya River, 3 to 10 paleosols occur each million-year interval (Figure 10), and each paleosol represents a time intervals of 10,000 to 50,000 years. The Iruya River section forms a bell-shape paleosol distribution, whereas Peña Colorada and La Porcelana present a left-skewed paleosol distribution. Iruya River represents the proximal stratigraphic section of the orographic front, compared with the more distal depositional environments of the other two sections. The Iruya River section suggests that it might have experienced more erosion from the main channel due to the fact that channel deposits are thicker, composed of coarser sand, and with scours at the bases of the beds, which are interpreted as evidence of a closer

proximity to the main river trunk. On the other hand, rivers fed the Peña Colorada and La Porcelana sections sand deposits not only less frequently, but with less erosive impact, suggesting a possible greater distance from the main river channel. Curiously, the age at which the paleosol frequency was maximum is approximately equal for the Iruya, Peña Colorada, and La Porcelana locations. One might expect the frequency of paleosols to be controlled by the lateral displacement of the DFS axis (e.g., a shift to North or South). The fan shape of many of these systems (Weissmann et al., 2010; Hartley et al., 2010) may affect the paleosol development. Whereas the radial angle of migration is fixed, the absolute distance of migration increases from proximal to distal location on a fan. Thus migration of the main channel causes the axis to move away faster next to the most distal sections of the system in contrast with the proximal zone, which might cause less frequent but more mature paleosols in the La Porcelana site relative to the other two locations. Such interpretation is inferred when the megafan geometry and the sedimentary facies are taking into account for the NWA.

Individual paleosols that contribute to the high frequency part of the column tend to be poorly developed (Figure 7F) with a repeated set of thin paleosol solum horizons (20 cm to 40 cm thick). For Iruya River this occurs from 2500 to 3700 meters position in the stratigraphic column (Figure 10). On the other hand, the examples of more mature paleosols do not occur in this time interval, but instead in horizons that represents palesols further away from the main fluvial channel (Kraus and Brown, 1993; Kraus, 1997).

Modern Depositional Setting as an Analogue for the Ancient Deposits and Paleosols

A modern distributive fluvial system is developed to the east of the Subandean foothills (Figure 2). This paper draws on the studies of distributive fluvial systems (DFS) by Weissmann et al. (2010) and Hartley et al. (2010), to describe the modern and geological sedimentary systems. The Bermejo Megafan (or DFS, Figure 2) is analogous to the northern mega-fans in Bolivia described by Horton and DeCelles (2001), with a zonation of the depositional environments comparable to the Mega-fan described by Shukla et al (2001).

East of the modern deformation front, the Bermejo DFS stretches nearly 700 km distance along an ESE-trending axis, though it is only 130 km wide in the widest region. This DFS is formed in the Andean Foreland along the Bermejo River, which flows from the Andes Mountains into the Chaco basin. According to Hartley et al. (2010), the Bermejo River system falls into the braided to meandering DFS category. A series of depositional settings occur in succession with increasing distance from the point of emergence from the highlands. We identify three distinctive zones, based on the geomorphology of the river and floodplains. In the proximal region, next to the mountain front, water and sediment are carried in dominantly braided channels, and this facies is designated as the braided-sand facies as observed in the field (Figure 2). This facies is the most proximal part of the DFS or megafan; it is fan-shaped, with the narrow fan apex located where the Bermejo River emerges from an incised channel across the San Antonio Range. A prominent feature of the braided channel pattern is longitudinal sand bars, where a high density of smaller stream channels within the river can be observed (Figure 2 and 19). It can be observed that floodplain areas are covered by sand deposits produced during the intermittent discharge

of river waters during the wet summers. Soils developed in this proximal area of braided-sand facies are dominantly Entisols, Inceptisols, and Alfisols (Figure 6). Figure 14 shows that Entisols occur on sand bars deposits. Sand bars are areas of constant sediment discharge and erosion, which is one reason for soils to display low maturity. Another reason for low soil maturity could be the lateral migration of the river bank, which erodes soils. Floodplain areas are characterized by Fluvents, where the accumulation of fine sediments (silt and clay) is observed. Floodplain areas next to the river channel also experience sediment discharge, but to a lesser degree than the river sand bars.

At a greater distance from the mega-fan apex (>150 km), a second river morphometry occurs in the Chaco basin, characterized by its meandering channel system (Figures 2, 8, & 16). Several stream remnants can be observed that run parallel to the main sinuous pathway. These probably carry water and sediment during storm events. A higher density of streams is present at the northwest zone of this intermediate meandering stream system, where abandoned or ephemeral stream channels feed small oxbow lakes. The NW zone is also dominated by Entisols and Alfisols. However, Mollisols are also present as part of the areas surrounding the river channel and floodplain, developed on fluvial terraces. The Entisols are correlated with sand bar deposits, as in the most proximal section from the DFS apex. But in this intermediate geomorphic zone, Alfisol coverage is more widespread compared with the proximal DFS section. This probably occurs as the result of the river meandering pathway, because here the sediment discharge is more restricted or less widespread in comparison to the braided area.

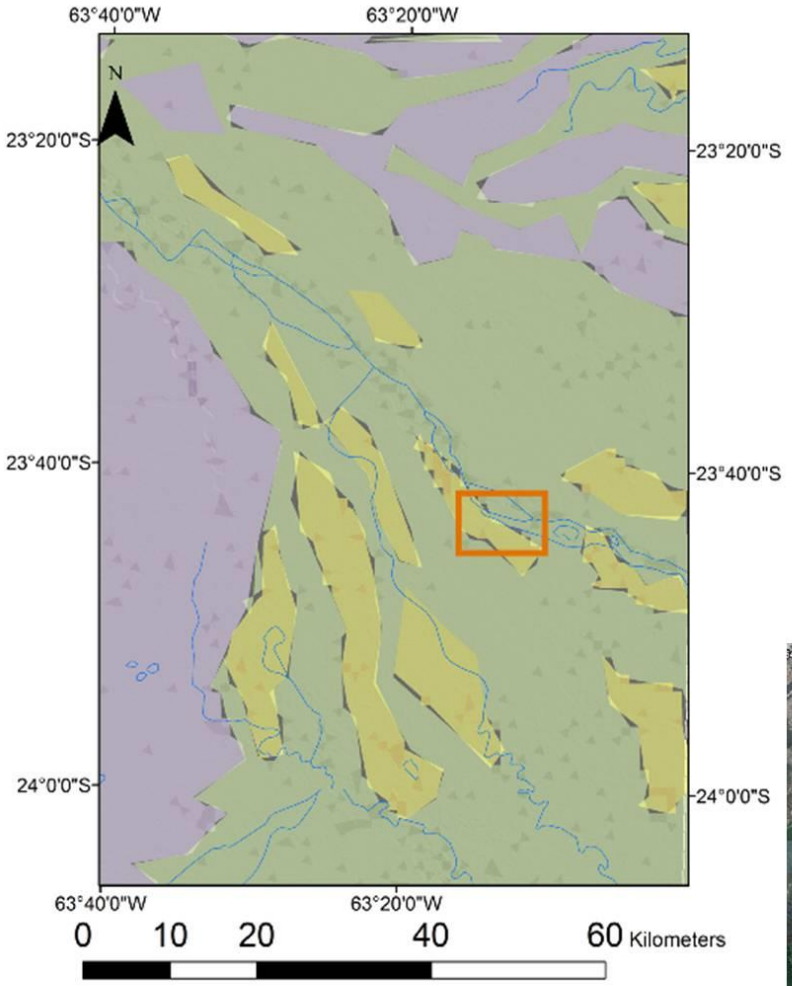

Surface Hydro	Alfisols	Molisols
Entisols		
0	0	0
1 - 3	1 - 3	1 - 3
4 - 6	4 - 6	4 - 6
7 - 9	7 - 9	7 - 9
10 - 12	10 - 12	10 - 12
13 - 15	13 - 15	13 - 15
16 - 18	16 - 18	16 - 18
19 - 21	19 - 21	19 - 21
22 - 24	22 - 24	22 - 24
	25 - 27	25 - 27

Braided River Section Showed Below

Figure 14: Modern Soil Order Distribution and Slope in the Bermejo Distributary Fluvial System

Shades of each color indicate slope of the land surface. The orange square represents the same area in both pictures. The soils presented in this map present constant and low slope across the DFS near the studied area.

The third geomorphic pattern appears around 500 km from the DFS apex, in the most distal section of the system (Figure 2). It is the lowland depositional system, which exhibits a high density of flooded areas or stagnant waters. Here, oxbow lakes are prominent, sometimes overlapping with one another to produce extensive swamp areas. Soils are developed under a variety of orders, from Entisols to Mollisols for example (Figures 5, 8, and 15).

It is very important to point out that across the 700 km distance from the apex to the toe of the DFS, landscape and hydrological conditions change. The zones are changing from sub-tropical to tropical around longitude 61º, 00, 00 W (Figure 6), as the result of the rain-fall pattern distribution and basin accommodation space arrangement. The rain fall decreases toward the west until the topographic front of the Andes, where precipitation increases as the result of the orographic effect. On the other hand, the landscape decreases in slope to the east, which decreases the water surface gradient, hence stagnant waters and swamp areas are more common relative to the areas next to the DFS apex.

Because a proximal to distal variation in the facies of the modern distributive fluvial system is well developed in the NWA modern depositional basin as well as other basins, a spatial displacement of the Miocene and Pliocene depositional environments is an expected consequence of eastward migration of the tectonic uplift (Horton and DeCelles, 2001; DeCelles and Cavazza, 1999). The spatial arrangement of the soils in the mega-fan varies along two axes, both with increasing distance from the apex to toe along a NW-SE trend, and with increasing distance from the channel into the floodplain areas, along a variable but dominantly NE-SW axis. More mature soils are developed moving

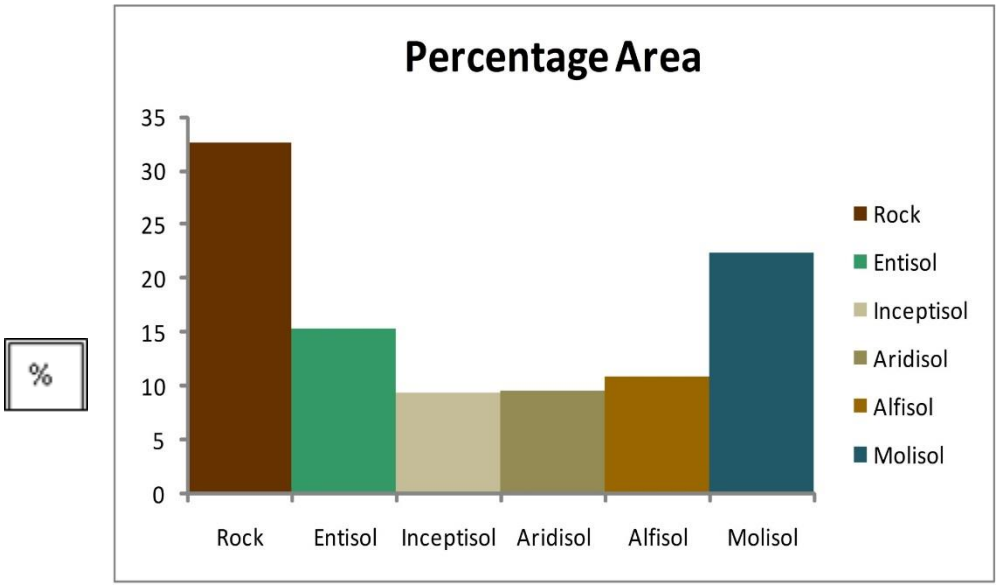
Percentage Area
%
35
30
25
20
15
10
5
0
Rock
Entisol
Inceptisol
Aridisol
Alfisol
Molisol
Rock
Entisol
Inceptisol
Aridisol
Alfisol
Molisol

Figure 15: Area of Modern Soils in the Northwestern Argentina
This is the distribution by percentage of the soil orders as presented in Figure 5. The highest percentage corresponds to the rock surface area that is part of the Bermejo catchment area. However, once into the lowland, Entisols and Alfisols are the most dominant soils next to the main river channel leaving the more mature soils (Mollisols) in areas further away from the channel.

toward the toe as well as toward the floodplain areas away from the river channel(s). Soils near the apex of the Bermejo DFS go from poorly developed entisols to well-developed mollisols with increasing distance from the main channel. The youngest or the most incipient soil order in Bermejo DFS is represented by Entisols, and the most mature one by Mollisols (Figures 5, 16, and 17). Alfisols represent the intermediate developed soils for this region, because these are correlated with fluvial deposits as well as Entisols. Looking at Figure 14, Mollisols are basically developed over fluvial terraces where the process of continuous sediment deposition is less frequent compared to the areas adjacent to the main river channel.

Relationships of Paleosols to Thrust Belt Activity

As previously justified by Mingramm et al. (1979), Starck and Schulz (1996), Hernández et al. (1996), and Echavarría et al. (2003), the time encompassed by deposition of these foreland basin strata spans the crustal shortening caused by the Subandean thrust-fold belt (Echavarría et al., 2003). The thrust-fold belt propagation produced syn-deformational strata within both a broad foredeep basin and within the synclines between each anticlinal range (DeCelles and Giles, 1996), thus recording the landscape deformation history. Hernández et al. (1996) suggests that the Subandean thrust-fold belt propagation started with the end of the uplift of Eastern Cordillera front at about 12.8 Ma. Our corroboration of the Hernández et al. (1996) Iruya River section ages also clarifies that the section accumulated prior to as well as during the several-kilometer-scale Andean surface uplift that was suggested by Gosh et al (2006) and Garzione et al. (2006). The new data

also gives us the opportunity to look at Peña Colorada paleosol development before the Pintascayo and Baja de Oran anticlinal ridges formed, as well as

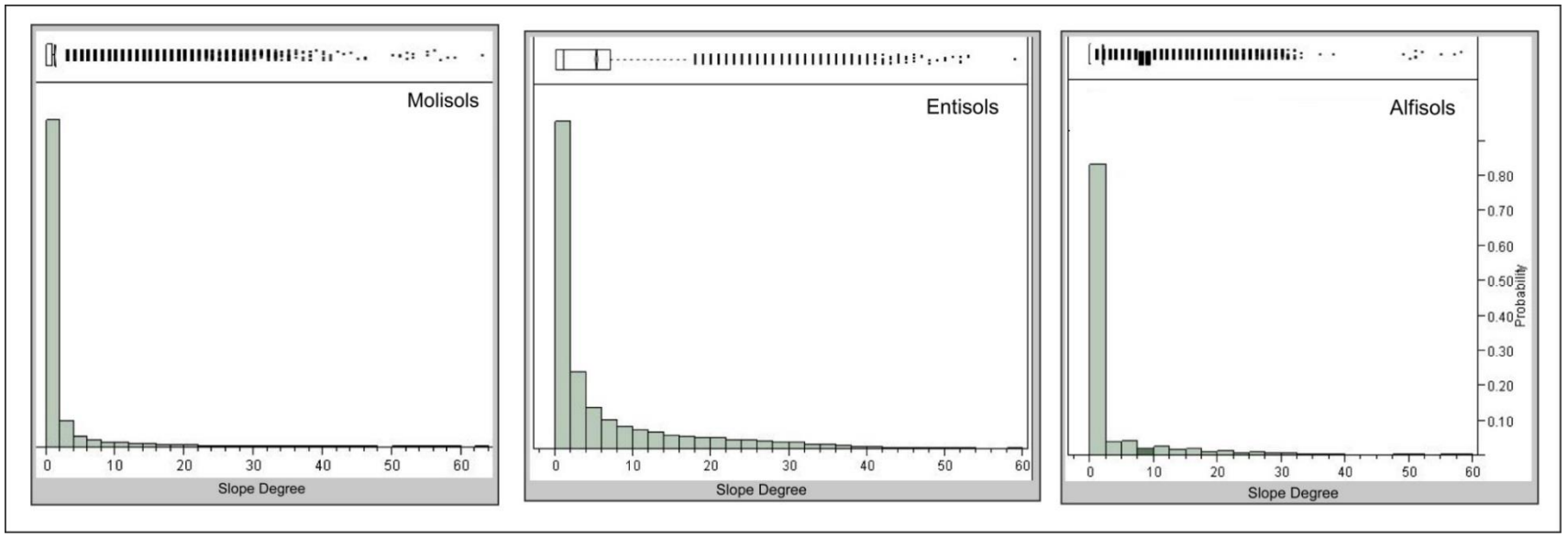
Molisols
Entisols
Alfisols
0
10
20
30
40
50
60
Slope Degree
0.80
0.70
0.60
0.50
0.40
0.30
0.20
0.10
Probability

Figure 16: Soil Order Distribution of the Main Soils in Northwestern Argentina vs Slope Incident

This Figure presents the probability distribution of modern soils in accord with the slope gradient in the Bermejo Megafan using the data from Figure 14. Entisols present the most probable soils in the systems followed by Alfisols due to a wider range of slope values. This presents that once the megafan reach the lowlands where the slope gradient is at their lowest values, Mollisols are the prefer soil to be developed in the DFS.

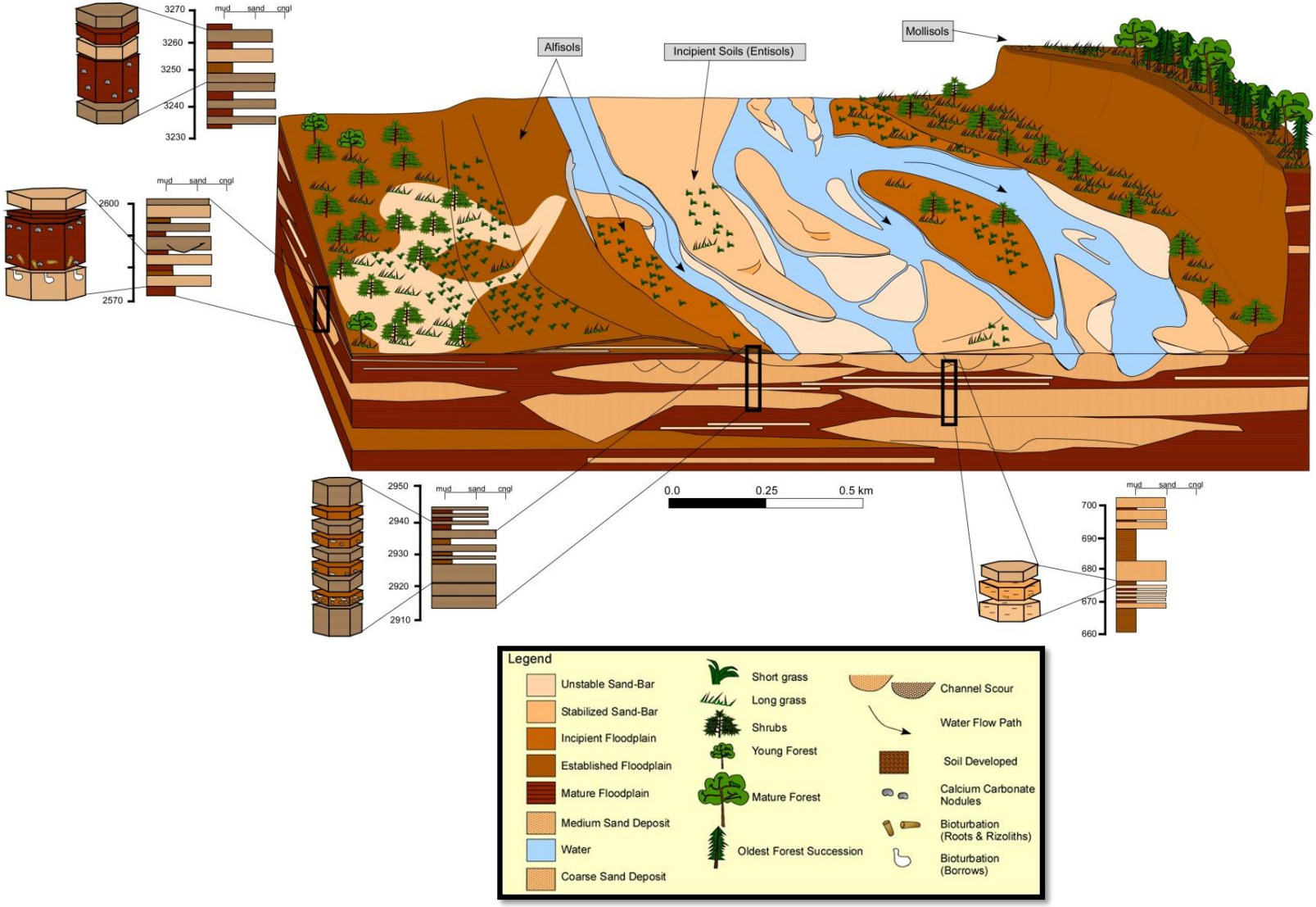
Alfisols
Incipient Soils (Entisols)
Mollisols
mud sand cngl
3270
3260
3250
3240
3230
2600
2570
2950
2940
2930
2920
2910
700
690
680
670
660
0.0 0.25 0.5 km
Legend
Unstable Sand-Bar
Stabilized Sand-Bar
Incipient Floodplain
Established Floodplain
Mature Floodplain
Medium Sand Deposit
Water
Coarse Sand Deposit
Short grass
Long grass
Shrubs
Young Forest
Mature Forest
Oldest Forest Succession
Channel Scour
Water Flow Path
Soil Developed
Calcium Carbonate Nodules
Bioturbation (Roots & Rizoliths)
Bioturbation (Borrows)

Figure 17: Interpretation of Paleosols in the Sedimentary Record and the Modern Distributary Fluvial System

This is the conceptual model of the paleosol development and preservation as the paleogeographical conclusion from the paleosol profiles and the digital data from the geographic information systems computed in this study. The distant from the main river channels determined the maturity of soils as well as their vertical arrangement.

La Porcelana paleosol development prior to formation of the Baja de Oran and San Antonio anticlinal ridges.

The eastward encroachment of the topographic range which controlled the position of the megafan apex into the foreland basin is registered by the vertical column at the Iruya River. The texture of the paleosols changes upward in the Iruya River section. Younger paleosols contain more sand in their matrix. This can be explained by the systematic changes within the fluvial sedimentary system as the proximal section of the DFS traversed the landscape. Compared to distal areas, the proximal zone incorporated coarser parent material, supplied from the channel discharge. However, the paleosols possess a high clay content (30 to 10%) even in the top of the stratigraphic column, in the youngest strata. A reason for the high clay content in paleosols in the Iruya River as well as Peña Colorada and La Porcelana sections is that all paleosols found and discussed here were developed in the floodplain areas. Nevertheless, mud content in Peña Colorada and La Porcelana paleosols is interpreted as the result of further distances of these areas from the megafan apex and the main channel.

In a foreland basin, one might question whether the migrating Subandean Belt influenced the paleosol development in terms of major soil properties, yet no significant change through time in the distribution of paleosols is observed to correlate with the development of the Subandean belts (Figure 11). For the deformation highlighted by Hernández et al (1996) and Echevarría et al. (2003) at about 12.5 Ma and 8.5 Ma, no significant changes in soil development were found in the proximal Iruya River section. This lack of consequence in the soil record is also true at the two eastern sites in relationship to the thrust activity that began by 7.5 Ma on a thrust east of the Iruya River section.

Nevertheless, the accumulated deformation on this thrust transformed the Iruya section from a foredeep position to hybrid marginal wedge-top/foredeep position, such that paleosol development after 6.9 Ma, the time of another deformation pulse nearby, corresponds to the maximum of the normal distribution bell shape, which represents the greatest paleosol incidence in the geologic record for the Iruya River section. During this time paleosols are highest in abundance and with intermediate maturity of the paleosol profiles. This is interpreted to have resulted from abundant accommodation space during this time, where the DFS sediment input was at its highest (1.01 m/ky) and the lateral displacement of the fluvial system produced the stacked paleosols pattern. Later, when thrusting of structures located close to and East of the Peña Colorada and La Porcelana sites began to increase the local subsidence rates, they also increased the frequency of paleosol burial preservation.

The intercalation of layers with thickness in the range of micrometers between calcium carbonates and clay minerals that form the carbonate nodules suggests seasonal climatic conditions. During the dry season, calcium carbonate tends to precipitate due to its solubility, where clay illuviation occurs during the wet season, because of translocation from the upper soil horizons into underlying horizons, such as B and lower ones. Few paleosols contain oxides minerals along with clay coating (Figure 13A, 13B, and 13G) that occurs between the pore spaces of the soils and the water trapped within those pores. However, the appearance of macro-oxide nodules in Peña Colorada indicates poor drainage conditions when compared with paleosols from Iruya or La Porcelana sections.

These Middle Miocene to Lower Pliocene NWA paleosols are dominantly argillic-calcisols, with the exception that at Peña Colorada section argillic-oxisols are also present. Argillic-calcisol morphological features are constant throughout the stratigraphic columns, changing only in their thickness as the megafan environment translated to the east through time. The lack of variability in soil morphological features as well as their mineral content suggests that a stable climate prevailed during 13 to 5 Ma. In other words, the variability of the climate produced by annual and inter-annual rain fall changes remained constant from the Middle Miocene to the Early Pliocene. Furthermore, the paleosol properties suggest that their climate was probably very similar to present climate in the Bermejo megafan area.

Conclusions

In light of the paleosol distribution, pedogenic profiles and mineralogical composition, the paleosols in NWA are described geologically as argillic-calcisols. The lack of difference in morphological and micromorphological features among the many paleosols that span 4000 meters and approximately 8 million years of history in the stratigraphic column of Iruya River, suggests a nearly constant climate during the Miocene to Pliocene period. This climate is interpreted to have been a wet-dry seasonal climate. Hence, no evidence was found to correspond to a change in climate forced by the uplift of the Andes during the Middle Miocene to early Pliocene.

Instead, the distribution and frequency of paleosol-bearing horizons within the stratigraphic columns reveal that there was a higher frequency of paleosol rejuvenation or burial during the time that deformation created a syncline at the location of the Iruya River

column. The high rate of paleosol preservation might be the result of the combined lateral migration of the main channel and the abundant accommodation space of the basin during this time. The possible depositional environmental setting is illustrated in Figure 17, which describe not only the environmental setting, but the possible set of vegetation using as a reference the modern environment. We suggest that the frequency of paleosols in NWA is attached to the position in the DFS, and its lateral migration, which depends on the sedimentary depositional rate and the accommodation space of the Foreland Basin.

This study demonstrates no changes in climate during the studied period of time. However, further analyses of stable isotopes of oxygen and carbon in the modern soils present variations along the megafan. This along with the study of the sedimentary facies, will provide a more comprehensive paleography of the megafan and sedimentary basin setting through time.

References

Aslan, A., and Autin, W. J., 1998, Holocene flood-plain soil formation in the southern lower Mississippi Valley: Implications for interpreting alluvial paleosols: Geological Society of America Bulletin, v. 110, no. 4, p. 433-449.

Brady, N.C., Weil, R.R., 2001, The Nature and Properties of Soils, 13th Ed.

Behrensmeyer, A. K., Willis, B. J., and Quade, J., 1995, Floodplains and Paleosols of Pakistan Neogene and Wyoming Paleogene Deposits - A Comparative-Study: Palaeogeography Palaeoclimatology Palaeoecology, v. 115, no. 1-4, p. 37-60.

Calvache, M. L., and Viseras, C., 1997, Long-term control mechanisms of stream piracy processes in southeast Spain: Earth Surface Processes and Landforms, v. 22, no. 2, p. 93-105.

DeCelles, P. G., and Cavazza, W., 1999, A comparison of fluvial megafans in the Cordilleran (Upper Cretaceous) and modern Himalayan foreland basin systems: Geological Society of America Bulletin, v. 111, no. 9, p. 1315-1334.

DeCelles, P. G., and Giles, K. A., 1996, Foreland basin systems: Basin Research, v. 8, no. 2, p. 105-123.

Driese, S. G., and Foreman, J. L., 1992, Paleopedology and Paleoclimatic Implications of Late Ordovician Vertic Paleosols, Juniata Formation, Southern Appalachians: Journal of Sedimentary Petrology, v. 62, no. 1, p. 71-83.

Echavarria, L., Hernandez, R., Allmendinger, R., and Reynolds, J., 2003, Subandean thrust and fold belt of northwestem Argentina: Geometry and timing of the Andean evolution: Aapg Bulletin, v. 87, no. 6, p. 965-985.

Ghosh, P., 1997, Geomorphology and palaeoclimatology of some Upper Cretaceous palaeosols in central India: Sedimentary Geology, v. 110, no. 1-2, p. 25-49.

Hartley, A. J., Weissmann, G. S., Nichols, G. J., and Warwick, G. L., 2010, Large Distributive Fluvial Systems: Characteristics, Distribution, and Controls on Development: Journal of Sedimentary Research, v. 80, no. 1-2, p. 167-183.

Haschenburger, J. K., and Cowie, M., 2009, Floodplain stages in the braided Ngarururoro River, New Zealand: Geomorphology, v. 103, no. 3, p. 466-475.

He, Y., Hu, K. L., Chen, D. L., Suter, H. C., Li, Y., Li, B. G., Yuan, X. Y., and Huang, Y. F., 2010, Three dimensional spatial distribution modeling of soil texture under agricultural systems using a sequence indicator simulation algorithm: Computers and Electronics in Agriculture, v. 71, p. S24-S31.

Hernández, R. M., J. Reynolds, and A. Di Salvo, 1996, Análisis tectosedimentario y ubicación geocronológica del Grupo Oraán en el río Iruya: Boletín de Informaciones Petroleras, Tercera Epoca, v. 45, p. 80–93.

Horton, B. K., and DeCelles, P. G., 1997, The modern foreland basin system adjacent to the Central Andes: Geology, v. 25, no. 10, p. 895-898.

-, 2001, Modern and ancient fluvial megafans in the foreland basin system of the central Andes, southern Bolivia: implications for drainage network evolution in fold-thrust belts: Basin Research, v. 13, no. 1, p. 43-63.

Huggett, R. J., 1998, Soil chronosequences, soil development, and soil evolution: a critical review: Catena, v. 32, no. 3-4, p. 155-172.

Hulka, C., Grafe, K. U., Sames, B., Uba, C. E., and Heubeck, C., 2006, Depositional setting of the middle to Late Miocene Yecua formation of the Chaco Foreland Basin, Southern

Bolivia: Journal of South American Earth Sciences, v. 21, no. 1-2, p. 135-150.
Husson, L., and Moretti, I., 2002, Thermal regime of fold and thrust belts - an application to the Bolivian sub Andean zone: Tectonophysics, v. 345, no. 1-4, p. 253-280.
Kraus, M.J., 1997. Lower Eocene alluvial Paleosols; pedogenic development, stratigraphic relationships, and Paleosolrlandscape associations. Palaeogeogr., Palaeoclimatol., Palaeoecol. 129, 387–406.
Kraus, M. J., and Aslan, A., 1993, Eocene Hydromorphic Paleosols - Significance For Interpreting Ancient Floodplain Processes: Journal of Sedimentary Petrology, v. 63, no. 3, p. 453-463.
Kraus, M.J., Bown, T.M., 1993. Short-term sediment accumulation rates determined from Eocene alluvial paleosols. Geology 21, 743–746.
Kraus, M. J., and Gwinn, B., 1997, Facies and facies architecture of Paleogene floodplain deposits, Willwood Formation, Bighorn Basin, Wyoming, USA: Sedimentary Geology, v. 114, no. 1-4, p. 33-54.
Latorre, C., Quade, J., and McIntosh, W. C., 1997, The expansion of C-4 grasses and global change in the late Miocene: Stable isotope evidence from the Americas: Earth and Planetary Science Letters, v. 146, no. 1-2, p. 83-96.
Lima, T. T. S., Miranda, I. S., and Vasconcelos, S. S., 2010, Effects of water and nutrient availability on fine root growth in eastern Amazonian forest regrowth, Brazil: New Phytologist, v. 187, no. 3, p. 622-630.
Mack, G.H., James, W.C., Monger, H.C., 1993. Classification of paleosols. Geol. Soc. Am. Bull. 105, 129–136.
Makabe, S., Kakuda, K., Sasaki, Y., Ando, T., Fujii, H., and Ando, H., 2009, Relationship between mineral composition or soil texture and available silicon in alluvial paddy soils on the Shounai Plain, Japan: Soil Science and Plant Nutrition, v. 55, no. 2, p. 300-308.
Masek, J. G., Isacks, B. L., Gubbels, T. L., and Fielding, E. J., 1994, Erosion and Tectonics at The Margins of Continental Plateaus: Journal of Geophysical Research-Solid Earth, v. 99, no. B7, p. 13941-13956.
McCarthy, P. J., Martini, I. P., and Leckie, D. A., 1998, Use of micromorphology for palaeoenvironmental interpretation of complex alluvial palaeosols: an example from the Mill Creek Formation (Albian), southwestern Alberta, Canada: Palaeogeography Palaeoclimatology Palaeoecology, v. 143, no. 1-3, p. 87-110.
McCarthy, P. J., and Plint, A. G., 1998, Recognition of interfluve sequence boundaries: Integrating paleopedology and sequence stratigraphy: Geology, v. 26, no. 5, p. 387-390.
Quade, J., and Cerling, T. E., 1995, Expansion of C-4 grasses in the late Miocene of northern pakistan - Evidence from stable isotopes in paleosols: Palaeogeography Palaeoclimatology Palaeoecology, v. 115, no. 1-4, p. 91-116.
Reynolds, J. H., Galli, C. I., Hernandez, R. M., Idleman, B. D., Kotila, J. M., Hilliard, R. V., and Naeser, C. W., 2000, Middle Miocene tectonic development of the Transition Zone, Salta Province, northwest Argentina: Magnetic stratigraphy from the Metan Subgroup, Sierra de Gonzalez: Geological Society of America Bulletin, v. 112, no. 11, p. 1736-1751.
Shukla, U. K., Singh, I. B., Sharma, M., and Sharma, S., 2001, A model of alluvial megafan sedimentation: Ganga Megafan: Sedimentary Geology, v. 144, no. 3-4, p. 243-262.
Srivastava, P., Parkash, B., and Pal, D. K., 1998, Clay minerals in soils as evidence of Holocene climatic change, central Indo-Gangetic Plains, north-central India: Quaternary Research, v. 50, no. 3, p. 230-239.

Stern, L. A., Chamberlain, C. P., Reynolds, R. C., and Johnson, G. D., 1997, Oxygen isotope evidence of climate change from pedogenic clay minerals in the Himalayan molasse: Geochimica Et Cosmochimica Acta, v. 61, no. 4, p. 731-744.

Suarez, D.L., and Rhoades, J.D., 1982, The apparent solubility of calcium carbonate in soils: Soil Sci. Soc. Am. J., v:46, p. 716-722.

Uba, C. E., Heubeck, C., and Hulka, C., 2005, Facies analysis and basin architecture of the Neogene Subandean synorogenic wedge, southern Bolivia: Sedimentary Geology, v. 180, no. 3-4, p. 91-123.

Weissmann, G. S., Hartley, A. J., Nichols, G. J., Scuderi, L. A., Olson, M., Buehler, H., and Banteah, R., 2010, Fluvial form in modern continental sedimentary basins: Distributive fluvial systems: Geology, v. 38, no. 1, p. 39-42.

Zarate, M., Kemp, R., and Toms, P., 2009, Late Quaternary landscape reconstruction and geochronology in the northern Pampas of Buenos Aires province, Argentina: Journal of South American Earth Sciences, v. 27, no. 1, p. 88-99.

Zhou, J., and Chafetz, H. S., 2010, Pedogenic Carbonates in Texas: Stable-Isotope Distributions and Their Implications for Reconstructing Region-Wide Paleoenvironments: Journal of Sedimentary Research, v. 80, no. 1-2, p. 137-150.

CHAPTER 2

THE FORELAND BASIN STRATIGRAPHIC RECORD OF MIO-PLIOCENE ENVIRONMENTAL CONDITIONS IN THE SUBANDEAN BELT, NORTHWESTERN ARGENTINA

Abstract

The Subandean thrust belt in NW Argentina has advanced eastward towards the Brazilian craton during the Miocene-Pliocene. The fluviatile environment developed in the Subandean foreland basin is controlled by topography and water availability, which are highly coupled with precipitation and tectonics. Hence, any climatic variability and major topographic changes likely affect sedimentation processes. The Miocene-Pliocene sedimentary record from outcrops along Iruya River, Peña Colorada River, and La Porcelana River shows a stratigraphic series that cycles between mudstones and sandstones. The stratigraphic thickness varies from west to east; the thickest section crops out along the Iruya River, ~4500 m, and at the eastern site, La Porcelana River, the thickness is ~1900 m. The stratigraphic thickness from these three sections corresponds the geologic time interval where the uplift of the Andes occurred in accord with the literature. However, the entire stratigraphic columns are registered from Miocene to the modern days giving a stratigraphic thickness of over 7000 meters at Iruya River section for example. Previous studies identified three progradational mega-cycles interpreted that reflect the evolution of the Subandean Belt.

Thirteen samples of zircons were separated and analyzed for single crystal laser ablation U-Pb dating. The new zircon U-Pb data show that the Tranquitas Formation spans at least 14.5–13.5 Ma. The youngest volcanic ash dated occurs in the Iruya River section, with an age of 5.1 Ma. These results allow improvement in the correlation of previous magnetic polarity stratigraphy data to the time scale. These new correlations better constrain the timing of changes in the depositional system.

Based on the observation that there are many more oscillations within the tectonic megacycles which may reflect climatic or hydrologic cyclicity, we searched for evidence that

would clarify how tectonics and climate control the cyclicity between mudstones, sandstones, and paleosols. In the Iruya River section, mudstone unit thickness varies from oldest (~14 Ma) to youngest (5 Ma) strata, between 5 m and 50 cm, respectively. However, in the uppermost 400 m of the studied section, near 5.6 Ma, the trend reversed, with mudstones exceeding 2 m thick, interbedded with sandstone. The mudstone color where paleosol development was identified ranges from red-yellowish to red-brown. Calcium carbonate is present in the matrix of these paleosols, sometimes in the form of nodules or root casts. Sandstones thicken over time towards the present, opposite to the trend of mudstones. These are quartz-rich sediments, light-grey and yellowish color in Iruya River basin, but brown-yellow, red-brown, and dark-gray in Peña Colorada and La Porcelana River basins. The difference in coloration in the sandstones is due to the change in texture as the result of mud incorporated in the red-brown sandstones and hydrocarbons in the dark-grey ones. Twelve sedimentary facies were identified that describe the sedimentary record between channels, overbank deposits, floodplains, and paleosols. Floodplain facies of the proximal Iruya River strata are characterized by recurrent paleosol development and the several categories of interbedded river channels facies. Homogeneous sandstones facies characterize the more distal Peña Colorada and La Porcelana River sections.

A seismic reflection profile that crosses the Iruya River section shows the depositional environment at a larger spatial scale and reveals the three major depositional sequences. Reflections corresponding to the Tranquitas Formation are of high amplitude. Although the seismic geometry appears conformable above those strong reflections, the top of Tranquitas is the only readily seen unconformity in field observations. The first progradational cycle is marked by a particularly non-reflective interval, corresponding to dominantly floodplain facies. The second progradational cycle is characterized by better reflectivity than in the first cycle, and by patches of

laterally discontinuous belts of strong reflection. I interpret that the stronger reflections correspond to channel-rich parts of the Distributary Fluvial System, and that the patchy distribution shows lateral migration of the DFS.

This set of analyses implies that the Distributary Fluvial System environment has dominated the foreland basin for at least 14 million years. The First and Second Progradational Cycles are interpreted to be tectonically driven by pulses of accommodation space and movement of the topographic front. The sub-cycles are interpreted to result from the lateral migration of the DFS. Neither tectonic activity nor climate change are needed to explain those lateral shifts. The facies of the first two progradational cycles are repetitive which implies that there was no major climate change between 12 Ma and 5 Ma.

Introduction

Sedimentary rocks preserved in foreland basins can elucidate the history of the evolution of continental environments, and the relationship of the environmental conditions to climate and to tectonic events (Galli and Hernandez, 1999; DeCelles and Cavazza, 1999; Horton et al., 2004; Bennet et al., 2006; Augustsson et al., 2008). Documentation of foreland basin development has contributed to understanding crustal shortening, subsidence, and topographic uplift (Flemings et al., 1986; Flemings and Jordan, 1990; Cardozo and Jordan, 2001; Jordan et al., 2001 Ruskin et al., 2011; Salvany-Josep et al., 2011). The objective of this paper is to demonstrate the response of features of the depositional environment to the evolution of South America's climate conditions and of the Subandean Thrust Belt between latitudes 22º05'S and 23º00' S, and longitudes 64 º07'W to 64 º36'W.

The foreland basin studied was located east of the Central Andes. The modern extent of this Miocene system includes the Subandean Belt and the Chaco Plains of northwestern Argentina (NWA) and southern Bolivia (Figure 1). The study area was selected due to the extensive prior knowledge of the crustal evolution since the Middle Miocene (Allmendinger and Gubbels, 1996; Hernández et al., 1996; Echevarría et al., 2003; Rosario et al., 2008; Mulch et al., 2010; Judge and Allmendinger, 2011; DeCelles et al, 2011), of the orographic barrier at the Eastern Cordillera that produces a rain shadow effect for air masses moving from the foreland westward across the Andes (Masek et al., 1994; Garreaud et al., 2003; Quade et al., 2007; Garreaud et al., 2009; Galewesky, 2009;Garreaud et al., 2010), and of the ages of the foreland basin strata, based on magnetostratigraphy as well as radiometric dating (Hernández et al., 1996; Reynolds et al., 1991; Reynolds et al., 2000; Echevarría et al., 2003). Also, this study of the Andean foreland basin of

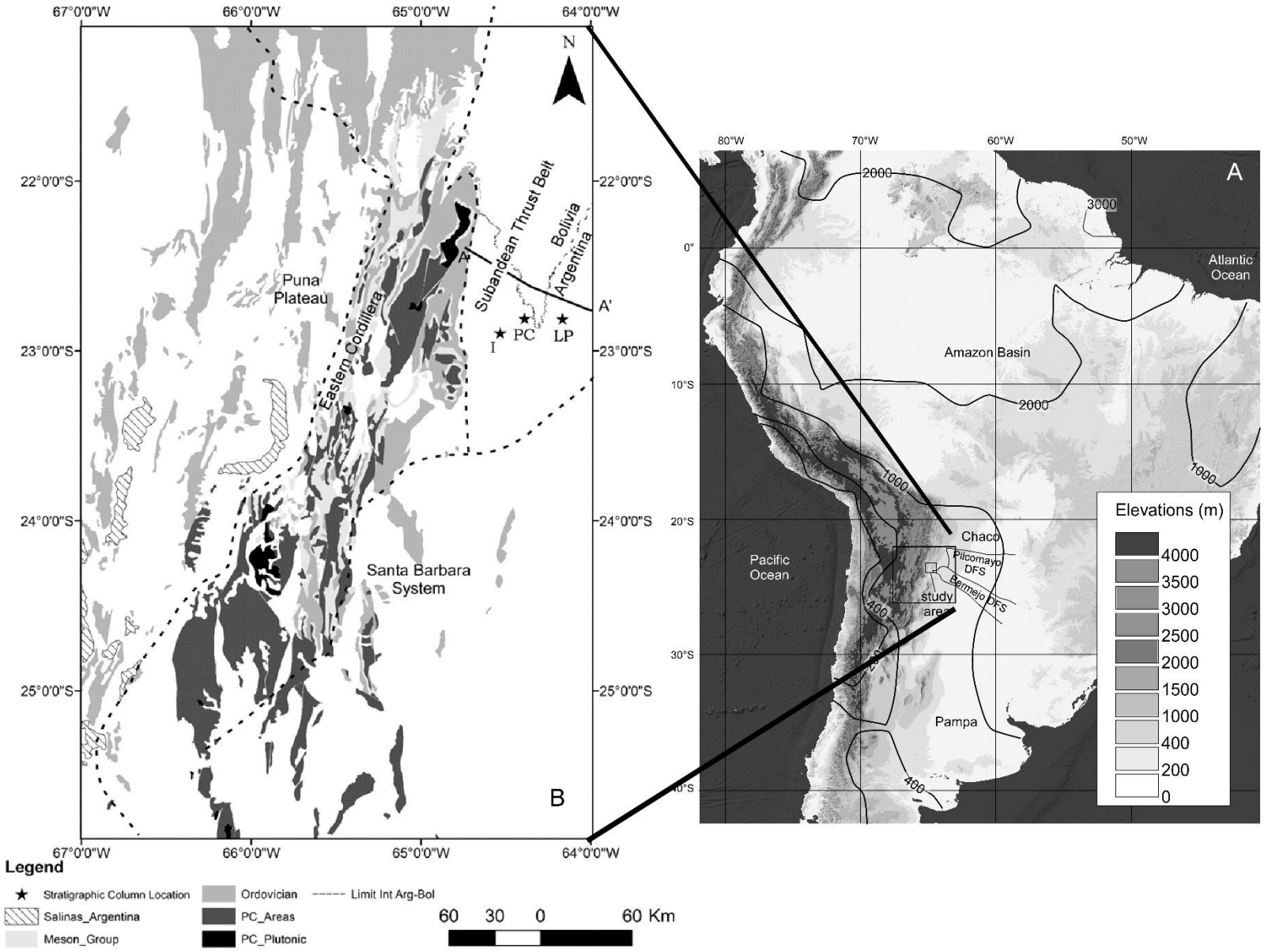
67°0'0"W
66°0'0"W
65°0'0"W
64°0'0"W
22°0'0"S
23°0'0"S
24°0'0"S
25°0'0"S
N
Puna Plateau
Eastern Cordillera
Subandean Thrust Belt
Bolivia
Argentina
A
A'
I
PC
LP
Santa Barbara System
B
Legend
Stratigraphic Column Location
Salinas_Argentina
Meson_Group
Ordovician
PC_Areas
PC_Plutonic
Limit Int Arg-Bol
60 30 0 60 Km
80°W
70°W
60°W
50°W
0°
10°S
20°S
30°S
40°S
2000
3000
1000
400
Atlantic Ocean
Amazon Basin
Pacific Ocean
Chaco
Pilcomayo DFS
Bermejo DFS
study area
Pampa
Elevations (m)
4000
3500
3000
2500
2000
1500
1000
400
200
0

Figure 1: Geologic map of the study area in the Central Andes of northwestern
This study focuses on the Subandean thrust belt and adjacent foreland basin on the eastern flank of the Andes in central South Amnerica (Figure 1A and B). The studied stratigraphic sections (Figure 1B) are exposed by erosion along the Iruya (I), Peña Colorada (PC), and La Porcelana (LP) Rivers (stars). A structural profile across the Subandean Ranges (A to A') is illustrated in Figure 2. The sediment supply for these modern rivers comes from the Eastern Cordillera where the Meson Group and Puncoviscana Formation are present (see legend).

NWA can be compared to studies in the southern Bolivian Chaco Basin (DeCelles et al., 2003 a,b; Uba et al., 2006; DeCelles et al., 2007; Uba et al., 2007; Uba et al., 2009; DeCelles et al., 2011).

The sedimentary record presented here, it's illustrated by three different stratigraphic sections exposed in the incised valleys of the Iruya River, Peña Colorada River, and La Porcelana River (Figure 1). These sections are located in NWA in the Subandean thrust belt ranges, where individual highlands are known as Pescado, Pintascayo, Baja de Oran, and San Antonio Ranges (Sierras) from west to east respectively (Hernández et al., 1996; Echevarría et al., 2003; Figure 2C). These mountain ranges represent anticlinal structures, with synclines expressed as valleys where small sedimentary basins were developed (Husson and Moretti, 2002). Crustal shortening is the mechanism that formed these anticlines and topographic highlands, as the result of eastward propagation of a thrust and fold system (Echevarría et al., 2003; Judge and Allmendinger, 2011). The development of the belts started over 8.5 to 9.0 Ma and is still progressing today (Hernández et al., 1996; Echevarría et al., 2003). For this study, the stratigraphic sections are the Cretaceous-Neogene rock formations composed by the Salta and Oran groups. These rock units represent the time of development of the Subandean belt, also the presumed period of time when the orographic barrier of the Andes reached its maximum (Isacks, 1988; Masek et al., 1994; Hernández et al., 1996; Allmendinger et al., 1997; Echevarría et al., 2003; Siks and Horton, 2011).

The Cenozoic foreland basin of the Andes in NWA has the thickest section in a sub-thrust position under the Eastern Cordillera with the basin filling strata gradually thinning to the east until the Brazilian craton. Foreland basin architecture consists of several zones: the wedge top, foredeep, fore-bulge, and back-bulge (Figure 2A; Jordan, 1995; Horton and DeCelles, 1997; McQuarrie and DeCelles, 2001; Horton et al., 2004; Leier et al., 2005; McQuarrie et al., 2005; Carrapa and DeCelles, 2008; DeCelles et al., 2011). The forebulge is the zone with the highest

probability to experience intense erosion, hence unconformities are commonly expected in the stratigraphic record. The forebulge was already farther east than the current eastern margin of the Subandean belt at the time of the initiation of thrust-fold development in the western Subandean belt (Baby et al., 1989; DeCelles et al., 2011). Therefore, to this study of rocks exposed within the Subandean belt, the foreland basin zones of interest are the foredeep and the wedge top. This is a reason to expect a well preserved fluvial sedimentary record during the Neogene for this area.

The environmental conditions of the modern Chaco Basin are considered to be a useful analogue to the depositional conditions during the Miocene and Pliocene (Uba et al, 2005). The modern rivers draining from the Eastern Cordillera and Subandean Ranges supply water and sediment to several alluvial fans in excess of 100 km long, referred to as mega-fans (Leier et al., 2005; Hartley et al., 2010). From a northern position in the basin and moving southward, these are at latitude 18^0 S the Grande River mega-fan, the Parapetí River, Pilcomayo River, and Bermejo River mega-fans, ending at latitude 23^0 S. Mega-fans as described by DeCelles and Cavazza (1999), Horton and DeCelles (2001), Shukla et al (2001), Leier et al (2005), Hartley et al (2010), Weissmann et al (2010) correspond to fluvial systems that can extend hundreds of kilometers parallel the direction of principal water flow, and tens of kilometers wide. Viewed from the perspective of depositional processes, Hartley et al (2010), and Weissmann et al (2010) have recommended that these large inland geomorphological features be referred to as Distributary Fluvial Systems, because the diagnostic features in the geological record will be those that are associated with fluvial processes of rivers that lose water in the down-dip direction. Hence, it is expected that the sedimentary facies change from the proximity of the mountain front towards the basin, as well as from the perpendicular distance from the main stream channel. For this study, the Bermejo Mega-fan or the Distributary Fluvial System (DFS) corresponding to the Bermejo River

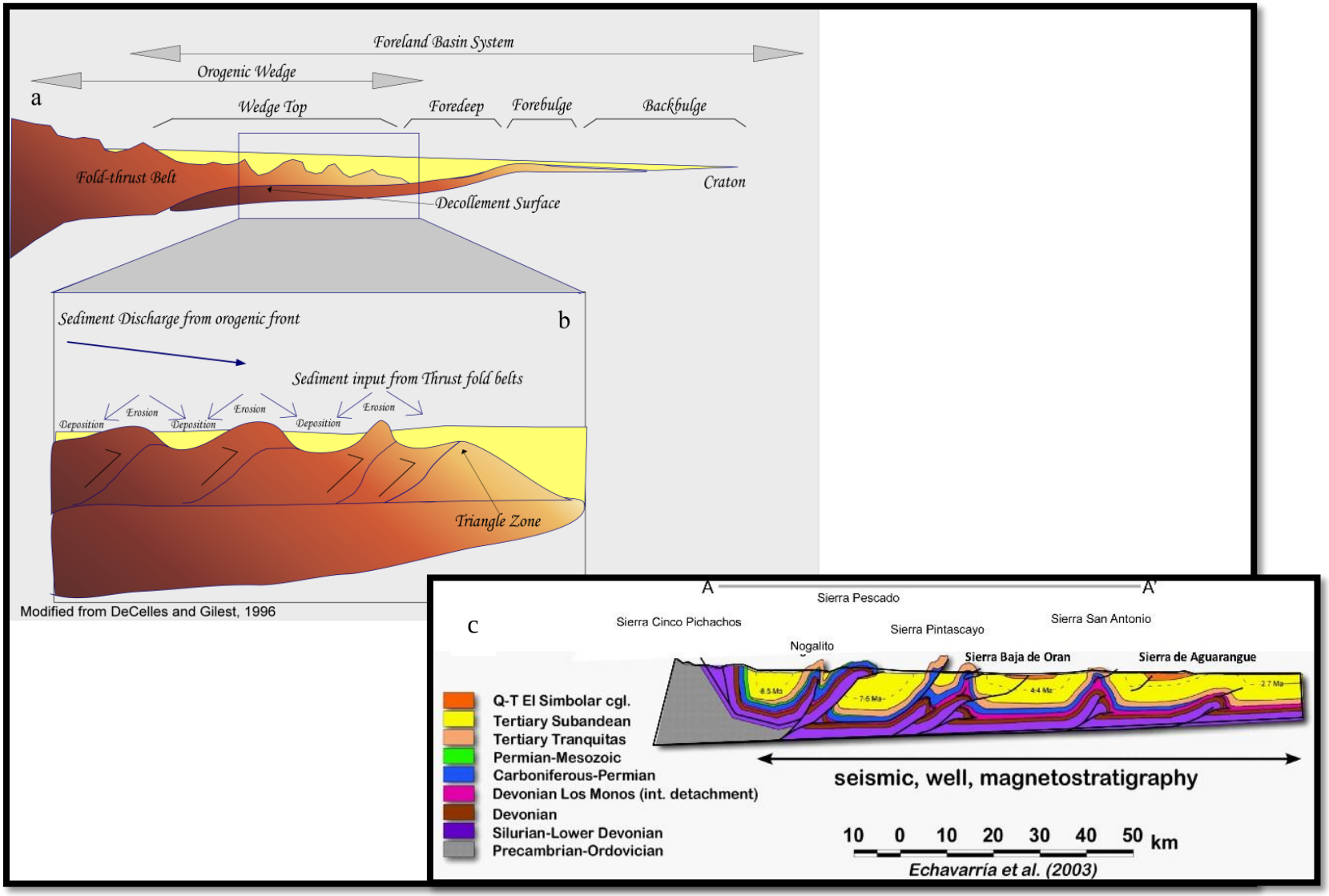
Foreland Basin System
Orogenic Wedge
a
Wedge Top
Foredeep
Forebulge
Backbulge
Fold-thrust Belt
Craton
Decollement Surface
Sediment Discharge from orogenic front
b
Sediment input from Thrust fold belts
Erosion
Deposition
Erosion
Deposition
Erosion
Deposition
Triangle Zone
Modified from DeCelles and Gilest, 1996
c
A
A'
Sierra Pescado
Sierra Cinco Pichachos
Sierra Pintascayo
Sierra San Antonio
Nogalito
Sierra Baja de Oran
Sierra de Aguarangue
8.5 Ma
7.5 Ma
4.4 Ma
2.7 Ma
Q-T El Simbolar cgl.
Tertiary Subandean
Tertiary Tranquitas
Permian-Mesozoic
Carboniferous-Permian
Devonian Los Monos (int. detachment)
Devonian
Silurian-Lower Devonian
Precambrian-Ordovician
seismic, well, magnetostratigraphy
10 0 10 20 30 40 50 km
Echavarría et al. (2003)

Figure 2: Foreland Basin Schematic Diagram Central Andes

Foreland basins are described by DeCelles and Giles (1996) as elongated regions (in map view) with a high accommodation space (in cross section, shown here). Figures (a) and (b) are schematic cross sections, while (c) is a detailed structural cross section from Echevarría et al. (2003) of the study area (see Figure 1 for location). In these three cross sections, yellow represents sediments deposited in the foreland basin; the rocks represented by brown (a, b) and multiple colors (c) were created prior to the development of a fold-thrust belt. The generic foreland basin system (a) is formed by four main zones known as the (1) wedge top, (2) foredeep, (3) forebulge, and (4) the backbulge. In the wedge top (b), once deformation produces a topographic expression, intrabasinal erosion results from a change of the slope gradient. (C) In the case of the Andes the Eastern Cordillera (western boundary of system) is the main sediment source for the foreland basin. For the study area, intrabasinal sediment sources developed progressively as thrust faults and associated anticlines progressed toward the east (right).

is the closest fluvial depositional system to the area of study (Figure 1). One major focus of this study is to document the depositional environment during the fill of the Chaco basin in order to learn when the Bermejo DFS originated, and what was its sedimentary response to the Neogene crustal shortening.

As part of this study the zircons in several volcanic ashes and sandstones were analyzed by U-Pb dating technique, to improve the age control for the published magnetostratigraphy. This improvement is valuable to better understand the three-dimensional distribution of lithofacies.

This paper will present the development of the sedimentary record through three different sets of data. The first section is formed by the geochronology results obtained from zircons. The second section is composed by the description of the sedimentary record. Here, lithology, facies, and sedimentary sequences are presented. Finally, reflection seismic data are presented and interpreted in terms of sedimentary architecture. This integrated set of data presents the characteristics of the environment of deposition at different spatial-scales of observations.

Area of Study

The area of study is located within the low ranges along the eastern flank of the Andes, to the east of the Puna Plateau and Eastern Cordillera in Jujuy and Salta provinces of northwestern Argentina (NWA). The studied stratigraphic sections are between latitudes $22^{0}30'$S to $23^{0}00'$S, and longitudes $64^{0}00'$W to $64^{0}40'$W, with the Iruya River exposing the westernmost and La Porcelana River exposing the easternmost sections for this study. The Peña Colorada stratigraphic column was studied at an intermediate location.

The Eastern Cordillera and anticlines of the Subandean belt expose rocks as old as, in the west, Pre-Cambrian rocks, and as young as Tertiary strata and Quaternary deposits; the Quaternary

deposits reach eastward into the Chaco basin (Figure 1). Pre-Cambrian and Cambrian rocks units are exposed by anticlinal structures. The U-Pb ages of zircons of the Pre-Cambrian and Cambrian Puncoviscana and El Meson Formations have been determined (Figure 1; Adams and Bhattacharya, 2005; Adams, 2008; Collo et al., 2009; Augustsson et al., 2011), which makes those formations especially useful for studies of possible sedimentary sources for Miocene and Quaternary sedimentary deposits.

Northwestern Argentina is an area known for the hydrocarbon production (Echevarría et al., 1996). The Monos Formation, Carboniferous in age, forms the main source of gas and oil production. This has been the main reason for the collection of numerous seismic reflection profiles and efforts to study the surface geology of the Subandean Belt.

The synclines within the Subandean belt developed intra-mountain belt small basins that encompass with distinctive sedimentary and age patterns (Figure 2 A-C). Rivers flowing through anticlines, where the older rocks are eroded at the summit, produce local source areas for sediment delivery into the synclines. However, sediments carried by rivers from the Eastern Cordillera province at the west side of the Subandean Belt are the main source for the sediments deposited into the synclines.

The sedimentary record in the area of study is formed by Tertiary and Quaternary deposits. These deposits were created largely from detritus eroded from exposed rocks of the Eastern Cordillera and the tops of the anticlines, and secondarily from volcanic ashes that are key for the radiometric analyses of this study. Miocene deposits are formed mainly by sandstones and mudstones, with increasing abundance of conglomerates in upper levels of the basin fill that corresponds to Pliocene deposits.

The rivers that drain the Eastern Cordillera and Subandean Ranges of the Andes produce a range of hydrological, sedimentological, vegetation, and soil development features within the modern Chaco foreland basin. At the present time, sediments are distributed into the Chaco basin as fluvial deposits transported by several rivers, including the Pilcomayo and the Bermejo Rivers. The Bermejo River enters the Chaco Plain at an altitude a little less than 300 m above sea level, where it discharges through a distributive fluvial system with a NW-SE elongation. The Bermejo River produced an irregular water discharge between 20 m^3/s and 14000 m^3/s depending on the annual season. At approximately 700 km from the Andes, it joins the south-flowing Paraguay River at an altitude about 50 m above sea level. The mean gradient across the depositional basin is 0.02° or 34 cm/km (Leier et al., 2005; Hartley et al., 2010).

The area is densely vegetated, which is the reason that field work for this study was carried out within the small canyons of the Iruya, Peña Colorada, and La Porcelana Rivers. For moisture-laden air masses moving from the tropical center of South America southward and westward across the Andean topography, the orographic effect begins at the Subandean Ranges and continues across the Eastern Cordillera. This produces an average annual precipitation within the study area between 600 to 800 mm (Chapter 1, Figure 3) that creates a sub-humid to subtropical region, while at the top of the Andes, the Puna Plateau rain fall does not exceed the 200 mm/year. The climate is monsoonal, with wet summers and dry winters. The precipitation in the proximal Chaco basin is 600-800 mm/yr, and over 1000 mm/year in the distal part of the basin (*Atlas de Suelos de Argentina*, INTA).

Soils are coupled to the geomorphology of the area, and reflect the combination of the climate and the depositional setting where they are formed. Entisols are dominant in the mountainous regions of the Subandean belt, whereas Alfisols, Inceptisols, and Mollisols are

common in the proximal regions of the Chaco basin, with variations that are dependent on their proximity to the rivers (see chapter 1 for details). The vegetation and soils change eastward across the surface of the Bermejo DFS.

Stratigraphy of the Foreland Basin

The Subandean Belt of folds and thrust faults has been developing in a foreland basin located on the eastern flank of the central Andes. The basin-filling strata are represented by Cenozoic deposits (Hernández et al., 1996; Echevarría et al, 2003; Uba et al., 2005; Uba et al., 2007; DeCelles et al., 2011).

The foreland deposits to the north of the area of study, between latitudes 19ºS and 22ºS, are formed by a series of fluvial and marine facies (Figure 3, left column). The oldest strata correspond to the Petaca Formation with an age approximately 27 Ma (Gubbels et al., 1993; Husson and Moretti, 2002; Uba et al., 2005; Uba et al., 2007) overlying an unconformity against Cretaceous strata (Figure 3). The Petaca Formation consists, from oldest to youngest, of a series of paleosols, a reworked pedogenic conglomerate, sandstones, and mudstones, and it reaches up to 250 m thick (Uba et al., 2005). The Yecua Formation corresponds to the subsequent deposits with a basal age around 14 Ma, also overlying an unconformity. Uba et al. (2005) describe these deposits as a short lived marine incursion, probably produced during the transgression of the Paranense Sea (Hernández et al., 2005). It is composed mainly by calcareous sandstone, fossiliferous limestone, and varicolored mudstone. This formation has a thickness of approximately 350 meters. This is overlain by the Tariquia Formation with a basal age of approximately 7 Ma and an age for its upper contact of 6 Ma. Though short-lived, the Taraquia Formation represents the major thickness of strata in southern Bolivia, of approximately 4500 m.

These deposits are formed by a series of interbedded mudstones and sandstones. The upper contact of the Tariquia Formation with the Guandacay Formation is conformable. The Guandacay Formation consists predominantly of pebble conglomerates and coarse grained sandstone with minor mudstones, and is up to 1500 m thick. Overlying the Guandacay Formation across a regional unconformity is the Emborozu. Formation, whose base is approximately 3.3 Ma. The Emborozu Formation consists of a coarsening-upward sequence of cobble-boulder conglomerate, with interbedded red sandstone and mudstones as described by Uba et al. (2005). The formations discussed above follow from oldest to youngest a west-east trend from the Eastern Cordillera into the Chaco Plain. The southeastern Bolivian strata represent the same age range of sedimentary deposits and analogous relations to deformation in their neighboring part of the Subandean belt as do the foreland basin strata within the study area in Argentina.

The foreland basin deposits to the south of the study region, in Salta province between latitudes 24°S and 25°S, are described as the Orán Group (Galli and Hernández, 1999) (Figure 3, right column). The Orán Group overlies the Cretaceous-Eocene Salta Group strata across an unconformity. The base of the Orán Group has an estimated age of approximately 40 Ma, based on stratigraphic correlation (Galli and Hernández, 1999). In accord with Reynolds et al. (2000), the Oran Group reaches 5000 m thickness at the Arroyo Gonzalez section. The Oran group is divided into two sub-groups: the lower is the Metán, which is characterized by interbedded sandstone and mudstone; the upper is the Jujuy which is formed by a sequence of conglomerates (Russo, 1972; Galli and Hernández, 1999; DeCelles et al., 2011). The western part of the foreland basin system (Figure 3, right column, west) includes a series of proximal facies accumulated initially in the proximal foredeep and subsequently in the wedge-top region, described and dated by DeCelles et al. (2011) and Carrapa et al., (2012). The more analogous part of the basin for the

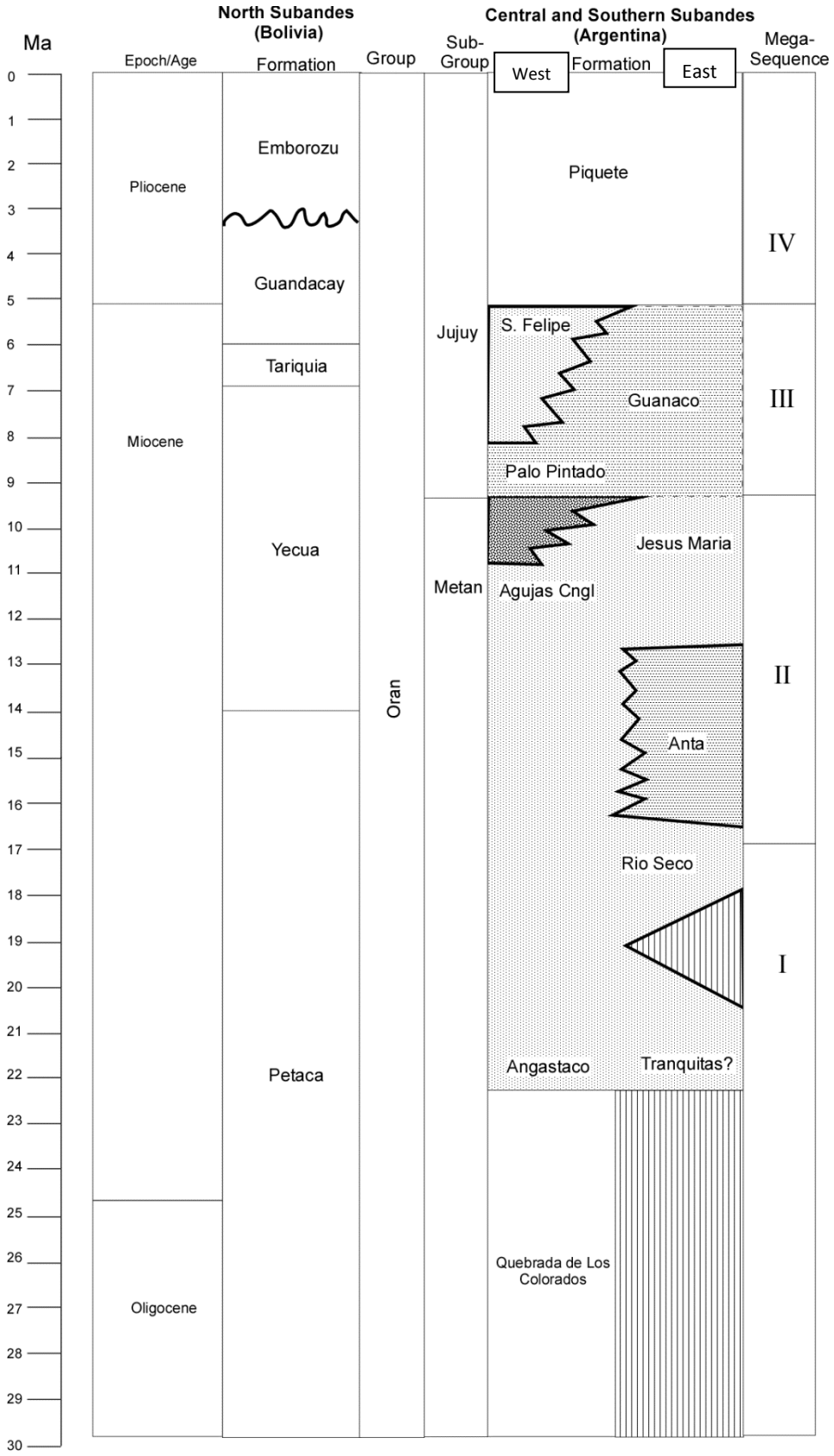
Ma
North Subandes (Bolivia)
Central and Southern Subandes (Argentina)
Epoch/Age
Formation
Group
Sub-Group
West
Formation
East
Mega-Sequence
0
1
2
3
4
5
6
7
8
9
10
11
12
13
14
15
16
17
18
19
20
21
22
23
24
25
26
27
28
29
30
Pliocene
Miocene
Oligocene
Emborozu
Guandacay
Tariquia
Yecua
Petaca
Oran
Jujuy
Metan
Piquete
S. Felipe
Guanaco
Palo Pintado
Jesus Maria
Agujas Cngl
Anta
Rio Seco
Angastaco
Tranquitas?
Quebrada de Los Colorados
IV
III
II
I

Figure 3: Stratigraphic Summary NWA

Stratigraphy of foreland basin fill of northwestern Argentina (right-hand column meta-sequences) compared to stratigraphic units in the same basin to the north (Bolivia; Gubbels et al., 1993; Husson and Moretti, 2002; Uba et al., 2005; Uba et al., 2007) and south (Santa Barbara System; Russo, 1972; Galli and Hernández, 1999; DeCelles et al., 2011). The North Subandes refers to the area in Bolivia relative to the study area for this study, as well as the Central and Southern Subandes. These sedimentary records give us a reference of how the adjacent sedimentary basins compare to the NWA basins that are part of the Chaco Plain. Lines that appear jagged such as the one between Guandacay and Emborozu, or San Felipe and Guanaco, represents unconformities.

purposes of this study is the eastern sector (Figure 3, right column, east), whose units are summarized here.

The Metán Group is formed by Río Seco Formation at the base, followed by Anta Formation, and Jesus María Formation at the top (Figure 3). Río Seco, with an average thickness of 110 meters, and Jesus María with a thickness up to 1120 meters, are characterized by brown and red-brown sandstones and siltstones with a lack of mudstones. The age of Jesus María Formation still is in debate, as the result of dating by lithostratigraphy correlation analysis. Different groups assigned different ages in accord with their stratigraphic interpretation: Early Eocene (Gebhard et al., 1974), Eocene to Oligocene (Mingramm and Russo, 1972), and Oligocene to Miocene (Russo and Serraiotto, 1978). However, Reynolds et al (2000) presents an age of about 15.1 Ma for an Early Miocene Metán Group deposits. The Anta Formation at Río Piedras locality is characterized by red mudstones with interlayered green mudstones, gypsum, and oolitic limestone, and exhibits a thickness up to 720 m. Nevertheless, the same formation is described as a predominantly red, very fine grained sandstones, siltstones, and mudstones, including the above description as well at the Río Gonzalez locality (Reynolds et al., 2000). The age obtained for this formation shows the oldest age of 15.2 Ma by magnetic stratigraphy at Río Piedras. Jesus María Formation is described by Reynolds et al. (2000) as red and gray interbedded siltstones, sandstones, and intra-formational conglomerates, with two coarsening-upward cycles observed at different locations. This formation presents a thickness up to 1120 meters, and an age between 15.2 Ma to 13.0 Ma in accord with its paleomagnetic data (Reynolds et al., 2000). To the west during deposition of the Jesus Maria Formation, DeCelles et al. (2011) describe the Agujas Conglomerate as syndepositional deposits. This formation represents the proximal sedimentation in the basin within the Eastern Cordillera.

The Jujuy Subgroup is divided into the Guanaco Formation at the base and Piquete Formation at the top. The Guanaco Formation is formed by medium to coarse grained grayish-red sandstones and conglomerates with interbedded red to orange siltstones. The thickness of the Guanaco is approximately 2150 meters (Reynolds et al., 2000). The Piquete Formation consists of dark red to pinkish beds of polymictic cobble to boulder conglomerate, coarse to fine sandstones, and siltstones (Reynolds et al., 2000). The estimated thickness of the Piquete Formation is about 830 m (Gebhard, 1974).

Starck and Vergani (1996) described the development of three mega-sequences (Figure 3, Roman Numerals on right margin) as the eastward propagation of the foreland basin system during the Eocene to the present. For the study area, Hernández et al (1996) and Echevarría et al (2003) presented the aggradational sequences in the foreland basin that they interpret to have accompanied early to middle Miocene stages of Andean crustal deformation. This study presents, for the Miocene and Pliocene Subandean-Chaco Basin, new time constraints, new insights into how the sedimentary environments behaved during foreland basin evolution, and the information regarding the depositional geometry.

Methods

For the radiometric dating analyses, U-Pb mass spectrometry analyses were carried out Arizona LaserChron Center, University of Arizona during July 2009. The method used was single-crystal laser ablation-multicollector-inductively couple plasma-mass spectrometry (LA-MC-ICP-MS). The first mineral separation was conducted at the Laboratorio de Geoquímica, Universidad de Salta, Argentina, where the samples were crushed, pulverized, and separated from magnetic minerals. A second mineral separation was done using heavy liquids at the Arizona LaserChron

Center. Once the zircons were separated and mounted in glass plates, analyses were executed as described in Gehrels et al. (2006), Johnston et al. (2009), and Barbeau et al. (2009). For most samples, about 100 zircon grains were analyzed using laser-ablation. For the other samples, whose initial results displayed a close and consistent cluster of ages of the first ~25 grains, a smaller set of grains were analyzed. The ages from detrital zircons were visualized and manipulated using the Isoplot software created by Ludwig (2003). Age estimates and distributions were calculated using Probability Density Plots (PDP) and Weighted Density Plots (WDP).

Four samples collected specifically for detrital zircons were collected from Peña Colorada River section, three volcanic ashes from Iruya River, and three volcanic or reworked tephra samples from La Porcelana. The results were compared with previous dates obtained from the literature. During interpretation of the age distributions, consideration was given to the fact that the age distribution of zircons might not represent differences in the zircon primary sources, because the population distributions are influenced by grain size, sorting, and abrasion of the zircon by erosion and hydraulic fractionation (see Lawrence et al., 2011). Nevertheless, zircons acquired from volcanic ashes for this study present euhedral geometries that were interpreted as short or non-hydraulic transportation, in contrast with the detrital zircons. We analyzed the resulting zircon age populations using methods that are suited for constraining depositional ages and not the methods of provenance analysis. To place maximum constraints on the depositional ages, this study uses the weighted mean age of the ages of the peaks in the range of 2σ for one mode (Gehrels et al., 2006; Barbeau et al., 2009). However, this study also uses as a criteria for age that at least 3 grains from the same sample with ages no more than 1 Myr have to be present in the sample in order to determine that this specific age is a valid indication of the youngest age.

Over seven thousand meters of stratigraphic section were studied for the analyses of the sedimentary environment. This included field description and measurement of the units, besides the collection of five volcanic ashes and three samples detrital for zircons. The sedimentary deposits were described using the Miall (1996) standards for fluvial deposits, and the Mack et al. (1993) categories for the over hundred paleosols found. A Munsell color-chart was used for the rock as well as paleosols descriptions. The collection of the data obtained from field observations were going to be described to synthesis of sedimentary facies that were going to be presented in tables with detailed description throughout this publication.

Field observations were integrated with seismic data to enable observation of the lateral continuity of the strata and for regional analysis of the basin. The seismic data were facilitated by XR-Geomap, Salta, Argentina. Seismic profile of 27202 was analyzed. This profile was provided as a time section in the SEGY file format, and it was processed using Vista Seismic Data Processing Software to create a depth section. The first phase of the analysis corresponded to a seismic sequence analysis, in which lateral terminations of reflections was mapped. The second analysis phase was to characterize the seismic facies (d). Last, a stratigraphic column with corresponding facies information derived from surface studies was correlated to the seismic reflection depth profile, to extrapolate the chronological information and depositional environment data into the seismic facies and reflection geometry data. For the analysis of this profile and characterization of the seismic reflections, the Atlas of Seismic Stratigraphy by A.W. Bally 1987 was used as the main reference.

Chronostratigraphy

U-Pb Ages of Zircons

Context and Approach

The ages of the Subandean Tertiary strata have been studied using several radiometric methods and fossil record (Reynolds et al., 2000; Echevarría et al., 2003; Uba et al, 2005, DeCelles et al, 2011). Even though several groups had worked very hard on the age constraints of the Subandean Belts and adjacent basins, this study provide independent geochonological results to be attached to the space-time development of the evolution of the tectonic events involved in the foreland basin during the Middle Miocene and Early Pliocene.

The chronology of the Subandean-Chaco sections of northernmost Argentina was analyzed by Hernández et al. (1996) and Echevarría et al. (2003) using various methods, including tephra chronology (fission track for zircons; 40Ar/39Ar in biotites) and paleomagnetic analyses. A significant result of these studies was to develop a chronology of thrust fault formation which documents the eastward propagation of crustal deformation of the Subandean fold and thrust belt. Nevertheless, a comparison of the results in the Subandean Belt region by different studies who used differing dating techniques reveals several ambiguities (Amidon et al., 2015).

From the aforementioned studies, it was apparent that volcanic ashes were available and provided an opportunity to implement new tephra-chronology analysis throughout the basin fill of the Subandean Belt, and hence an opportunity for consistency of the dating method. Geochronological analyses in zircons have gained popularity during the last decades (Augustsson, C. & Bahlburg, H., 2003; Augustsson et al., 2006; Davila et al., 2007; DeCelles et; al., 2007; Collo et al., 2009; Gehrels et al., 2011; Amidon et al., 2015). Zircons are resistant to both physical abrasion and chemical weathering, providing an excellent candidate for the measurements of the

isotopic chemical composition (in this case U-Pb) of the parent igneous rocks. Therefore, for consistency in the methodology, we implemented the analysis of U-Pb ages of zircons from volcanic ashes and from detrital deposits for all our samples.

General Overview of Results

From the Iruya River section, three volcanic ash samples were analyzed (Figure 4). For each sample, a detrital zircon population is evident, but also there is a cluster of Neogene zircon U-Pb ages which meet the criteria to be considered as evidence of the depositional age of the stratum. The oldest depositional age corresponds to a sample collected about 2200 m above the base of the stratigraphic section, which is a highly weathered volcanic ash. This is sample Iruya T0, which yielded an age of 6.8 +0.1/-0.2 Ma (Figure 5A). The youngest age found for the Iruya section is 5.1 +0.3/-0.2 Ma (sample Iruya T4A, Figure 5B). The third analyzed volcanic ash, located right beneath the preceding one, gave an age of 5.6 +0.2/-0.3 Ma (Iruya T4). These zircon ages set up the age constraints to be combined with the magnetostratigraphy from Hernández et al (1996) and Echevarría et al (2003). However, this study found no volcanic tephra near the base of the Iruya River. Four sandstones from the Peña Colorada section were analyzed. Two of them (P. Colorada S1; P. Colorada S4) have populations of detrital zircons that are consistent with their deposition during the Late Miocene, and thus those two contribute to constraining their depositional age. The other two samples are of value for provenance studies but not for chronostratigraphy. For the easternmost section, La Porcelana, three reworked volcanic ashes (Porce T1; Porce T2; La Procelana Bentonite) contain zircon populations consistent with Late Miocene and Pliocene deposition.

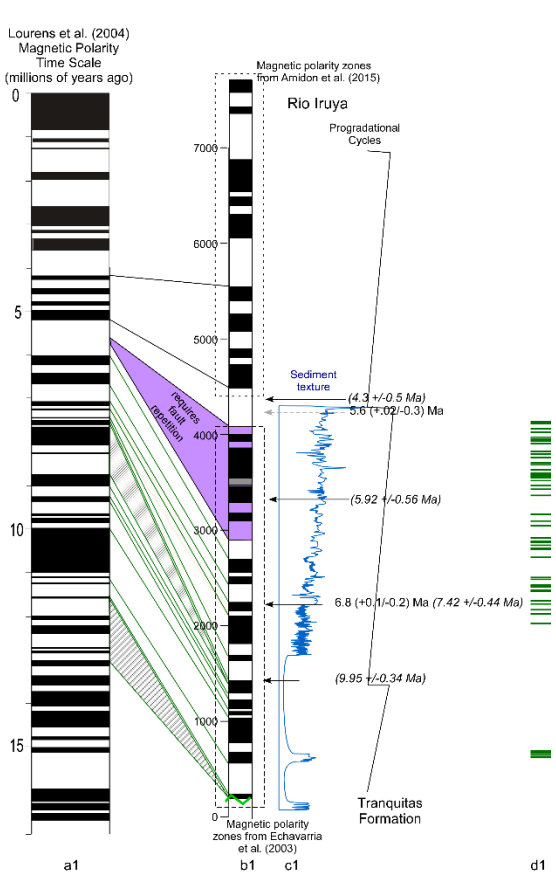
Lourens et al. (2004)
Magnetic Polarity
Time Scale
(millions of years ago)
Magnetic polarity zones
from Amidon et al. (2015)
Rio Iruya
Progradational
Cycles
Sediment
texture
requires
fault
repetition
(4.3 +/-0.5 Ma)
5.6 (+.02/-0.3) Ma
(5.92 +/-0.56 Ma)
6.8 (+0.1/-0.2) Ma (7.42 +/-0.44 Ma)
(9.95 +/-0.34 Ma)
Tranquitas
Formation
Magnetic polarity
zones from Echavarria
et al. (2003)
a1
b1
c1
d1

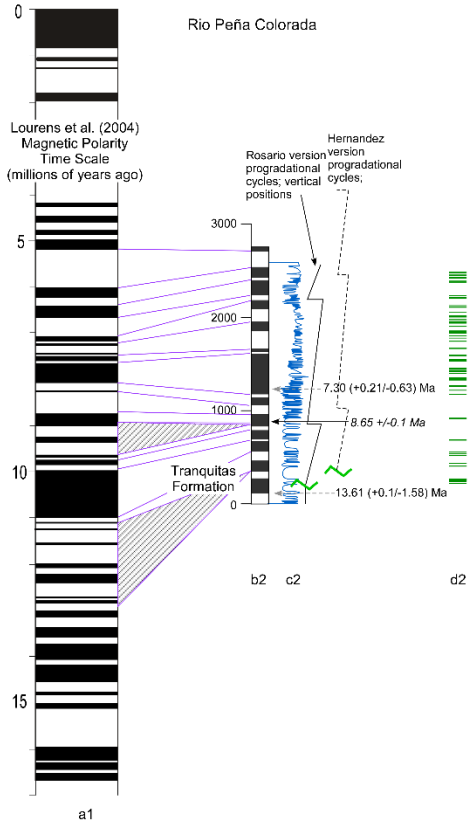
Rio Peña Colorada
Lourens et al. (2004)
Magnetic Polarity
Time Scale
(millions of years ago)
Rosario version
progradational
cycles; vertical
positions
Hernandez
version
progradational
cycles;
7.30 (+0.21/-0.63) Ma
8.65 +/-0.1 Ma
13.61 (+0.1/-1.58) Ma
Tranquitas
Formation
a1
b2
c2
d2

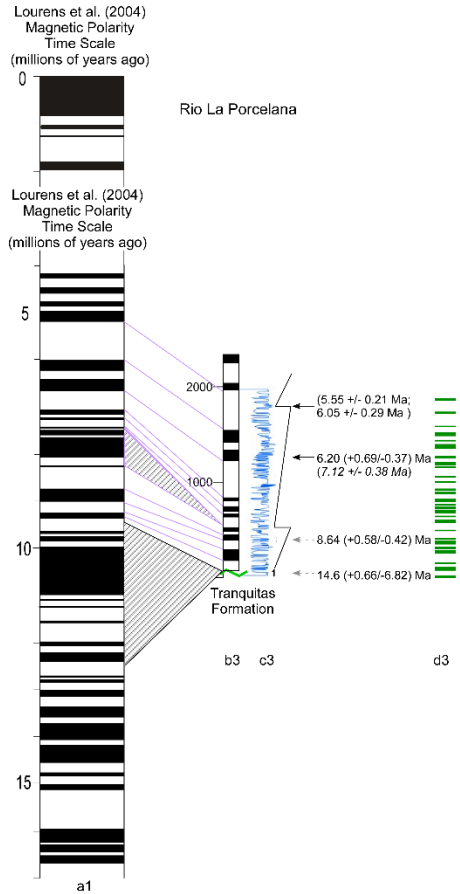
Rio La Porcelana
Lourens et al. (2004)
Magnetic Polarity
Time Scale
(millions of years ago)
(5.55 +/- 0.21 Ma;
6.05 +/- 0.29 Ma)
6.20 (+0.69/-0.37) Ma
(7.12 +/- 0.38 Ma)
8.64 (+0.58/-0.42) Ma
14.6 (+0.66/-6.82) Ma
Tranquitas
Formation
a1
b3
c3
d3

Figure 4: Magnetostratigraphy, Lithostratigraphy, Paleosol Stratigraphic Position, and Radiometric Dates

This figure presents the geochronolgical data for each of three stratigraphic columns, and the revised correlation of each local column to the Global Magnetic Time Scale. The left column for each place a1, is the global magnetic polarity time scale (Loures et al., 2004). The columns labeled as b1, b2, and b3, correspond to the local magnetic polarity column for Iruya, Peña Colorada, and La Porcelana, respectively (Echavarría et al., 2003; Amidon et al., 2015). The columns c1,c2,and c3 correspond to the summary of grain size distribution in each column. Columns d1, d2, and d3, are the horizons containing paleosols in each stratigraphic column. Noted are the stratigraphic levels of each dated volcanic deposit, with the best interpreted age with one standartd deviation.

Iruya River Details

Two of the three Iruya section analyzed volcanic ashes reveal populations of zircon ages that indicate little reworking between their parent volcanic eruption and their deposition, but one of the volcanic ashes reveals a combination of multiply recycled detrital materials mixed with new eruptive material (Figure 5.) The zircon single-crystal age distribution of volcanic ash Iruya T0 ranges from approximately from 4.8 to 7.6 Ma with the highest probability density about 6.8 Ma. This set of ages are obtained from the age range of 35 grain analyzed, which are the values used for the weighted density plot (Fig. 5A). Even though the three youngest values correspond to approximately 4.8, 5.4, and 5.4 Ma, there is sufficient continuity of the age values of the other grains that the weighted density analysis is a better approach to calculate the age of the deposit, rather than reliance on the three youngest grains. The probability density plot (PDP; Fig. 5A, lower plot) displays a bell shaped distribution of the 35 zircons. Both the weighted density and the PDP analysis coincide in yielding an average age of about 6.8 Ma with a 95% confidence from this coherent group of zircons (Figure 5A).

The stratigraphically intermediate volcanic ash sample, Iruya T4, exhibits three zircon age populations, with at least two of them easily divisible and a polymodal age distribution (Figure 5C). The oldest age population family spans from 1078 to 2394 Ma. The middle age peak values range from 463 to 594 Ma. The youngest age population family for this volcanic ash runs from 3.6 to 11.4 Ma. In total, these represent two old and one young population of zircon ages. The maximum depositional age is given by the youngest zircon population with a weighted density and PDP of 5.6 +0.02/-0.3 Ma.

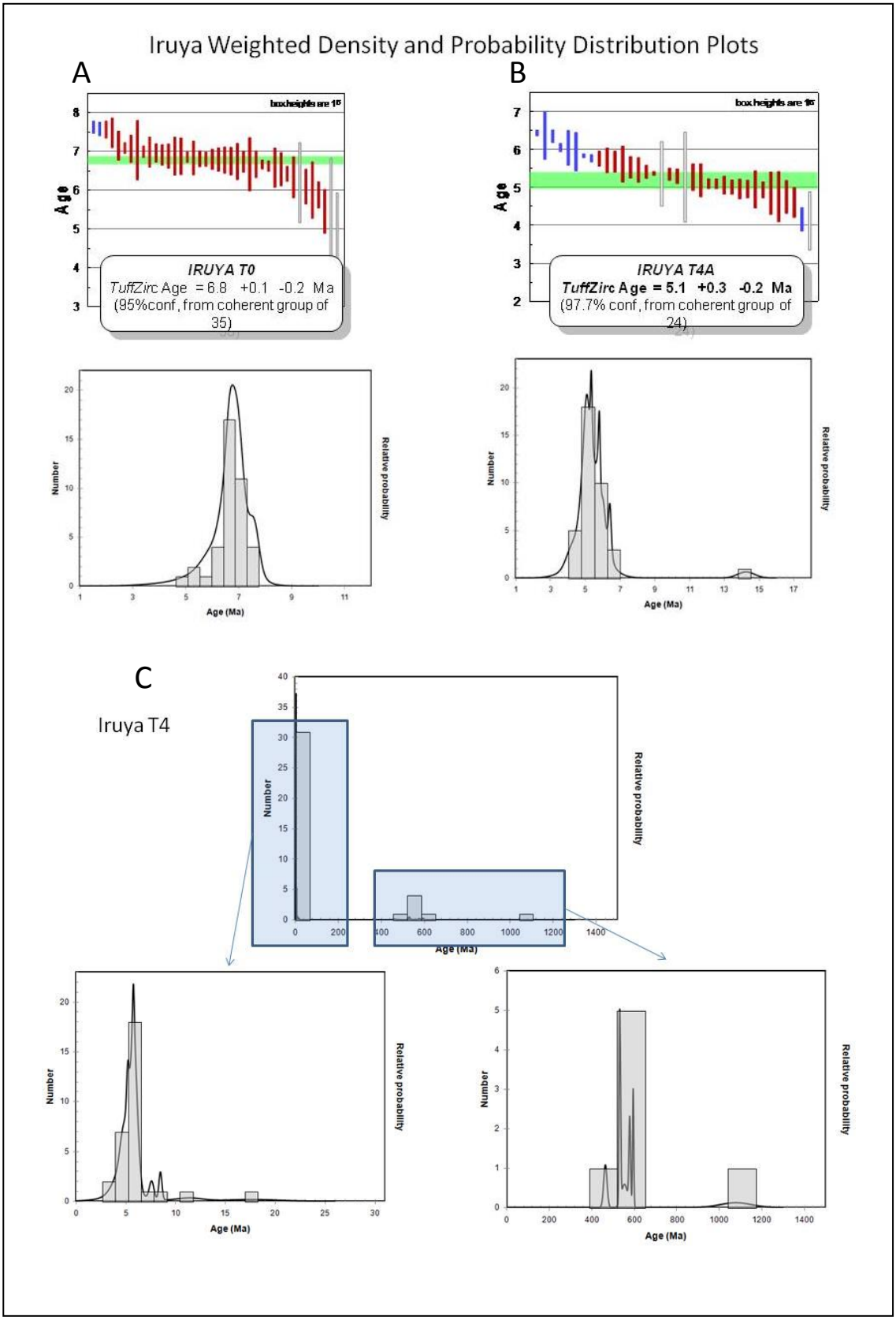
Iruya Weighted Density and Probability Distribution Plots
A
B
box heights are 1σ
Age
IRUYA T0
TuffZirc Age = 6.8 +0.1 -0.2 Ma
(95%conf, from coherent group of 35)
IRUYA T4A
TuffZirc Age = 5.1 +0.3 -0.2 Ma
(97.7% conf, from coherent group of 24)
Number
Relative probability
Age (Ma)
C
Iruya T4

Figure 5: U-Pb results from zircon grains for three volcanic ashes sampled along the Iruya River

For the stratigraphically lowest (T0) and and highest ashes (T4A), both a weighted density age graph (A, B: top) and a probability density plot (A, B: lower part) are shown. C) Illustrates a probability density plot for the third ash (T4) that is immediately beneath T4A. This shows that the zircons are multi-modal, and the content of each mode is clarified by dividing the probability density graph into two parts with a high degree of age resolution for time younger than 30 Ma (left) and a low degree of age resolution (right).

The stratigraphically highest volcanic ash, Iruya T4A, yielded the youngest zircon ages, with an age of approximately 5.1 Ma. The ages of zircons from T4A span from 4.1 to 14.3 Ma, with the highest percentage of the distribution of the ages (97.7%) at 5.1 Ma (Figure 5B). Even though the PDP shows a bimodal distribution of ages, the older peak is formed by only one grain with an age of 14.3 Ma. This is an example of a case in which it is appropriate to exclude an outlier data point from the statistical analysis of the age, based on the lack of values to support a second population among the 36 zircon grain analyzed. Excluding that outlier, the range of values is from 4.1 to 6.4 Ma.

Peña Colorada River Details

In Peña Colorada River section, four samples of sandstone were analyzed in order to obtain the ages of the detrital zircons. The distribution of ages for this site is presented in Figures 6–9. It is very noticeable that the zircon ages families differ among the four samples, and only two of them include young zircon populations.

Peña Colorada Sandstone 1 (P. Colorada S1) sampled the lowest stratigraphic position, and yields a polymodal distribution (Figure 6). The main peak of the age distribution given by the PDP is around 560 Ma (Figure 6B). Another noteworthy peak for zircon ages is at 1100 Ma, which is an older set of zircons that were not well represented in the Iruya River volcanic deposits. Figures 6A and 6C focus on the youngest peak. These seven Miocene and Pliocene zircons define the maximum depositional age for this sample, but examination of the dispersion of those data suggest four of the zircon ages should be excluded due to lack of coherence. A depositional age of about 13.6 Ma was calculated using the three coherent zircon ages, with a resultant 75% confidence for the age of the deposit (Figure 6A, C).

Peña Colorada Sandstone 2 (P. Colorada S2) contains zircon grains that span from 6.6 to 2726 Ma. The dominant population has a weighted mean age of about 523 Ma (Figure 7). The higher density of ages for this sample is around 523 Ma with a skewed to the right distribution. Even though three more clusters of ages can be identified, no other peak stands out. P. Colorada S2 proved to not be useful for constraining the age of deposition.

Peña Colorada Sandstone 3 (P. Colorada S3) revealed a single Late Miocene zircon, with an age of 7.4 Ma (Figure 8). But this is only one grain, which is not enough to provide a statistically valid age. The oldest age for this sample is 1931 Ma, with the most reliable youngest age of 243 Ma. The weighted age distribution produces a calculated age of 483.5 +15.64/-19.05 Ma. The most prominent peak density for this sample is around 500 Ma whereas a secondary peak yields an age of 574 Ma. These age values are similar to those of P. Colorada S2. While valuable as an indication of provenance, this sample provides no valid stratigraphic ages constraints.

The last sandstone sample for this section is Peña Colorada Sandstone 4 (P. Colorada S4) (Figure 9). The age range for zircons in this sample spans 5.6 to 2917 Ma. The PDP presents five clusters of ages (Figure 9B) with the youngest cluster spanning values of 5.6 to 7.7 Ma (Figure 9A). An age gap exists between the youngest and second-youngest clusters, with the youngest value for the second cluster of 309 Ma (Figure 9B), and the most prominent cluster yields an age value of 553 Ma. If the youngest cluster is used to calculate the maximum depositional age of the sandstone horizon, the weighted average age is 7.70 +0.21/-0.63 Ma (Figure 9A). All but the youngest cluster represent Paleozoic and Precambrian zircon grains which would be useful for provenance study, but these do not to constrain the depositional age of this horizon.

La Porcelana River Details

La Porcelana river section is represented by two volcanic ash samples identified as Porce T1 and Porce T2. A third sample, a mudstone about 0.5 thick, was identified tentatively in the field as a bentonite (La Porcelana Bentonite). However, the mixed particle sizes within the bed led to the alternative hypothesis that this deposit was a reworked rather than primary volcanic ash fall, a premise that is supported by the zircon age spectrum.

La Porcelana Bentonite (Figure 10) is the stratigraphically lowest sample in the La Porcelana section, from the Tranquitas Formation. Only 28 zircon grains adequate to yield U-Pb ages were obtained from this mudstone-textured rock. The zircon grains range between 7.3 Ma and 1764 Ma, with clusters of ages in the Middle Miocene, around 497, and around 1273 Ma (Figure 10B). Inclusive of all grains younger than 300 Ma (Figure 10B and C), analysis of uncertainty of individual zircons (those exceeding 2-sigma are excluded) and of variance from the

A

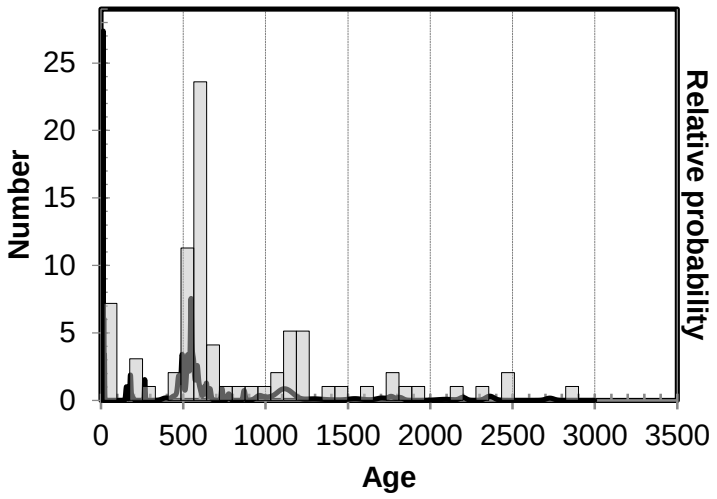
Number
Relative probability
25
20
15
10
5
0
0
500
1000
1500
2000
2500
3000
3500
Age

B

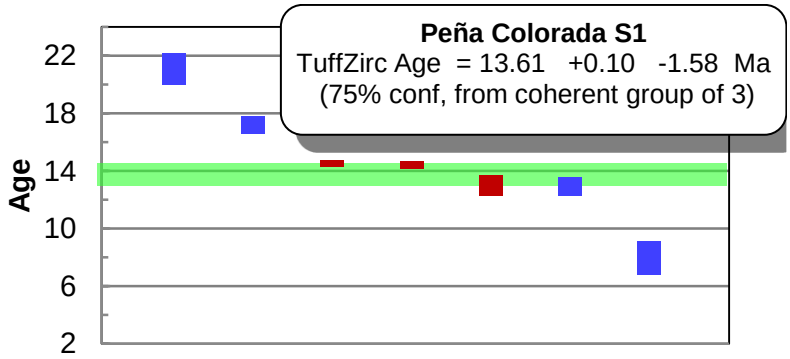
Peña Colorada S1
TuffZirc Age = 13.61 +0.10 -1.58 Ma
(75% conf, from coherent group of 3)
Age
22
18
14
10
6
2

C

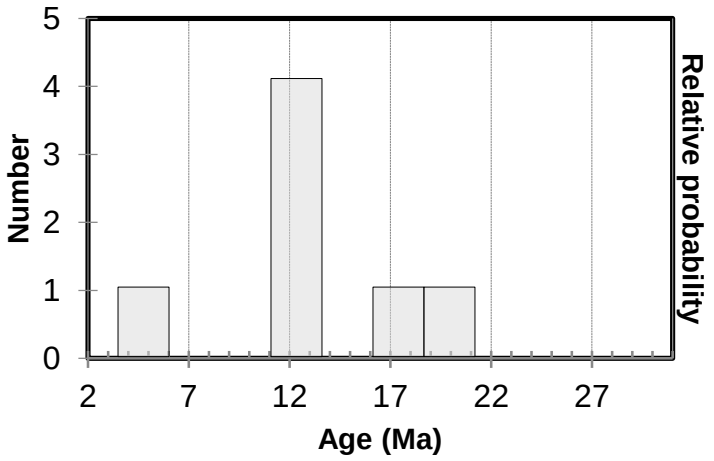
Number
Relative probability
5
4
3
2
1
0
2
7
12
17
22
27
Age (Ma)

Figure 6: Peña Colorada S1 U-Pb dating Results
The ages represented here were obtained from the analysis of detrital zircons in a sandstone sample (A). The weighted average (B) shows a maximum depositional age of 13.6 Ma, which can be observed that the density probability plot (A) shows the youngest population of zircons ages around 13.6 with a subsequent population with a peak around 547 Ma. Figure 6C illustrates the abundance of the youngest zircons.

A

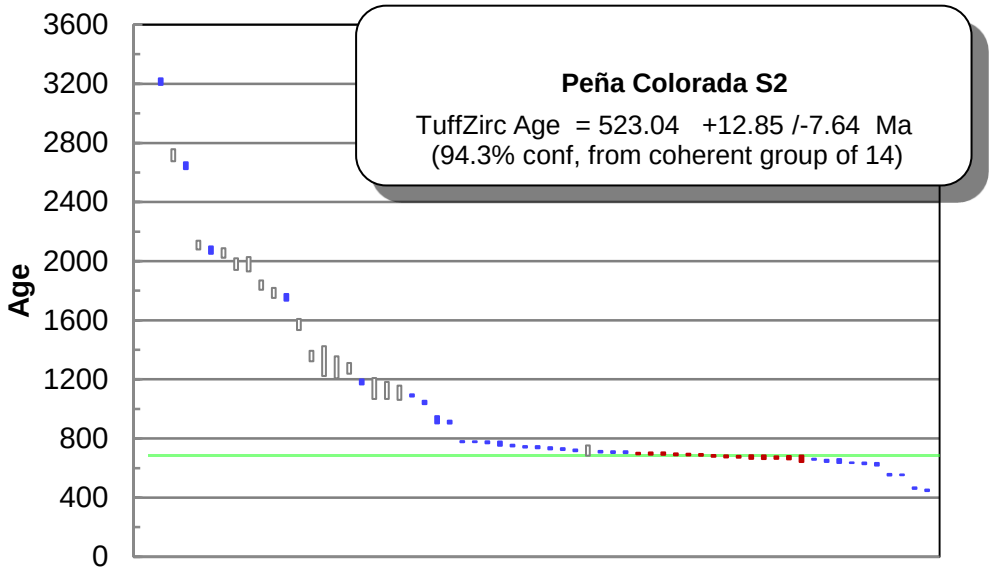
Peña Colorada S2
TuffZirc Age = 523.04 +12.85 /-7.64 Ma
(94.3% conf, from coherent group of 14)
Age
3600
3200
2800
2400
2000
1600
1200
800
400
0

B

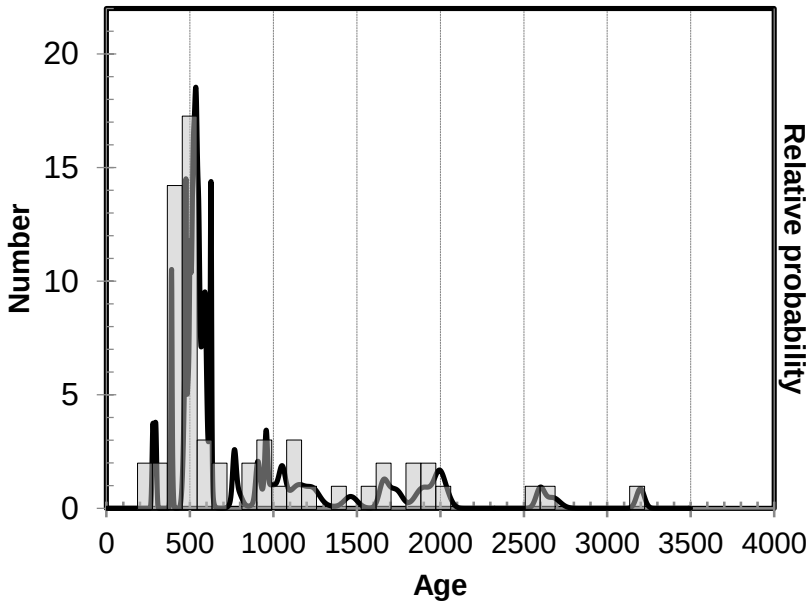
Number
Relative probability
Age
20
15
10
5
0
0
500
1000
1500
2000
2500
3000
3500
4000

Figure 7: Peña Colorada S2 Dating Results

The ages represented here were obtained from the analysis of detrital zircons in sandstone. This sample has a weighted average value of 523 Ma (A). The main cluster of ages is around this value. The full population of ages includes values close to 3300 Ma.

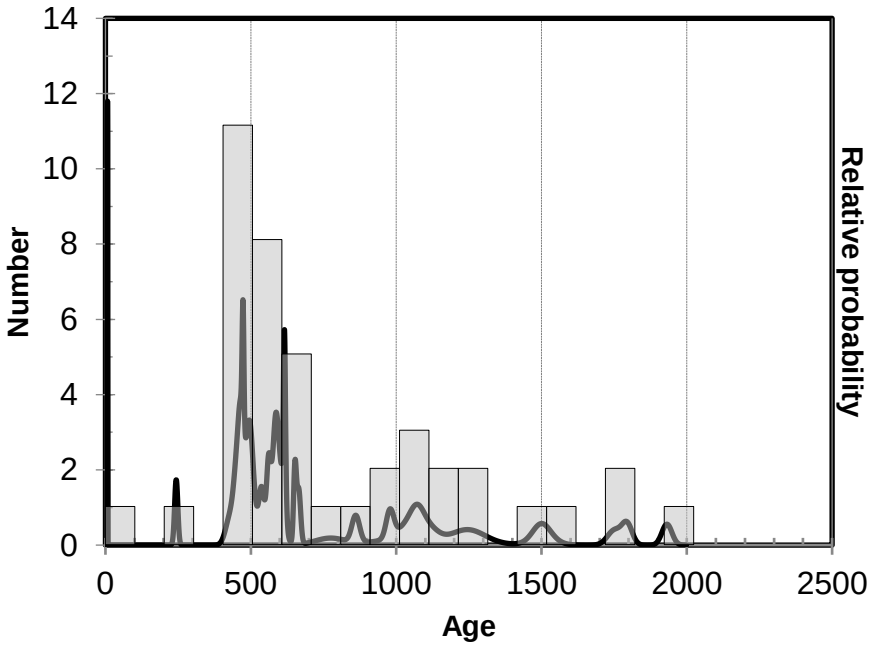
14
12
10
8
6
4
2
0
Number
Relative probability
0
500
1000
1500
2000
2500
Age

Figure 8: Peña Colorada S3 Dating Results
The ages represented here were obtained from the analysis of detrital zircons in sandstone. The density probability plot shows the main peak at 483 Ma. However, calculating the weighted density for the sample, the age results is 574 Ma. That weighted average is understandable given the two visible clusters near 400 Ma and 600 Ma.

A

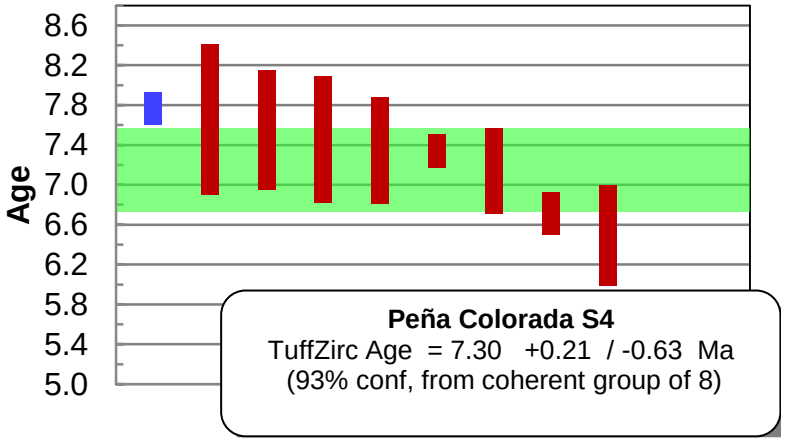
8.6
8.2
7.8
7.4
7.0
6.6
6.2
5.8
5.4
5.0
Age
Peña Colorada S4
TuffZirc Age = 7.30 +0.21 / -0.63 Ma
(93% conf, from coherent group of 8)

B

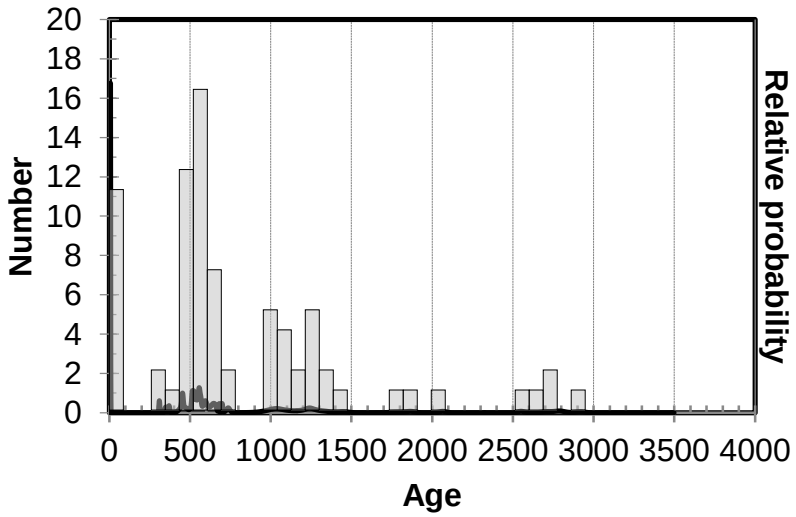
20
18
16
14
12
10
8
6
4
2
0
Number
Relative probability
0 500 1000 1500 2000 2500 3000 3500 4000
Age

C

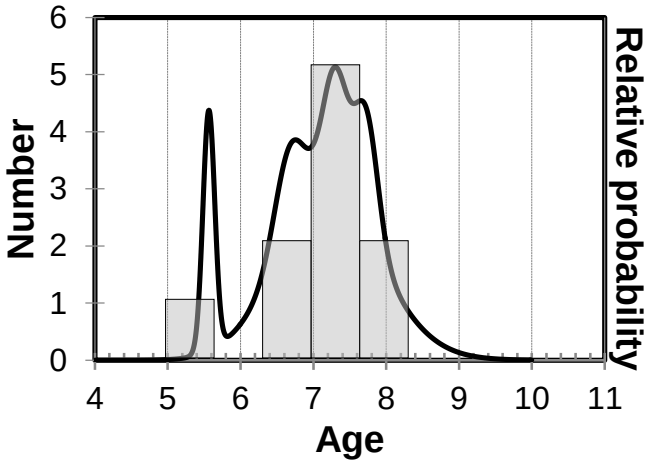
6
5
4
3
2
1
0
Number
Relative probability
4 5 6 7 8 9 10 11
Age

Figure 9: Peña Colorada S4 Dating Results
The ages represented here were obtained from the analysis of detrital zircons in sandstone. (A) Shows the weighted age calculated by isoplot. (B) This is the Probability Density Plot for the whole population of zircon grains. (C) This is an enlargement of the youngest values.

A

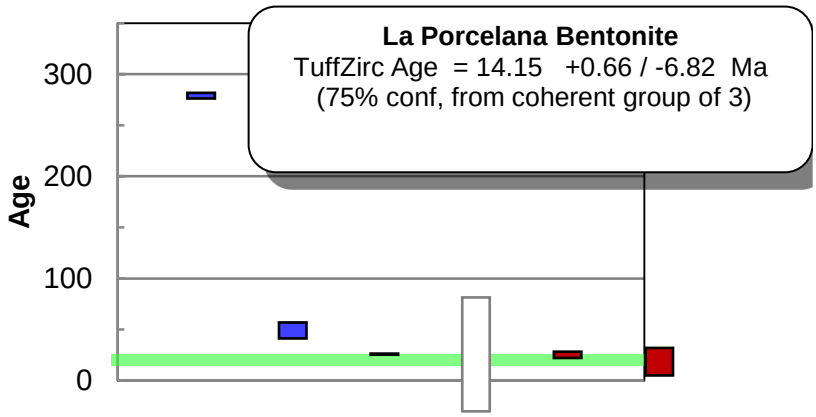
La Porcelana Bentonite
TuffZirc Age = 14.15 +0.66 / -6.82 Ma
(75% conf, from coherent group of 3)
Age
300
200
100
0

B

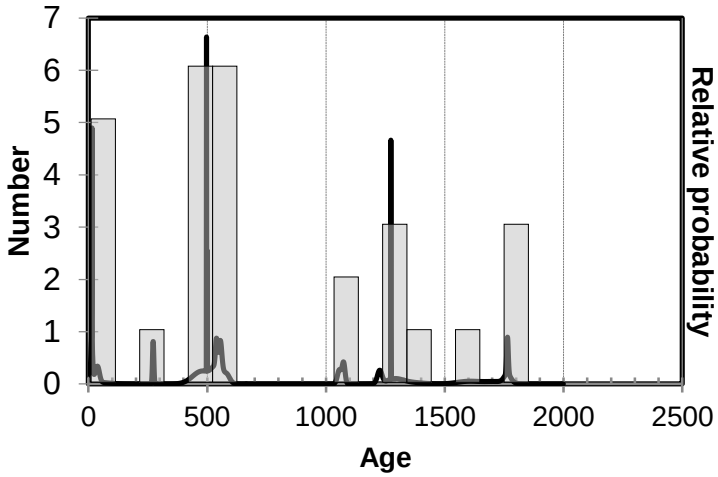
Number
Relative probability
Age
0
1
2
3
4
5
6
7
0
500
1000
1500
2000
2500

C

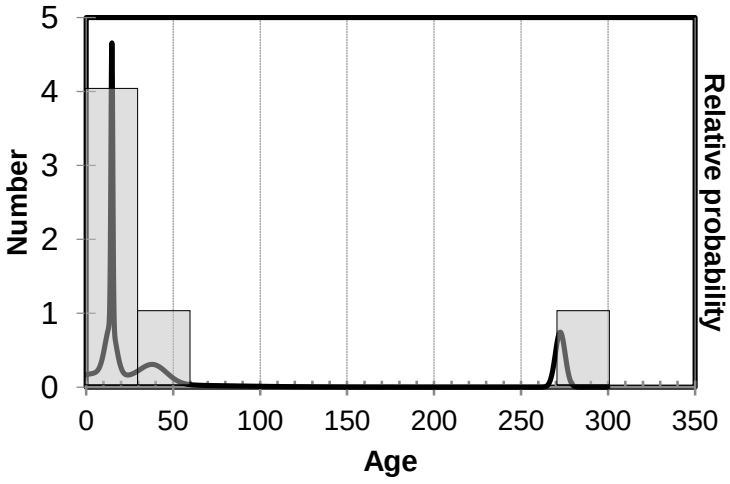
Number
Relative probability
Age
0
1
2
3
4
5
0
50
100
150
200
250
300
350

Figure 10: La Porcelana Bentonite Zircon Ages
(A) This shows the weighted age calculated by isotplot. (B) shows the Probability Density Plot for the whole population of zircon grains, and (C) shows an enlargement for the youngest values.

mean, lead to inclusion of 3 zircons in calculation of the median age value (calculated using TuffZirc), which suggests a maximum depositional age of 14.2 Ma. The values for the older clusters are not important for constraining the age of the Tranquitas Formation, but they demonstrate that the mudstone is a reworked volcanic deposit rather than a primary air-fall bentonite.

Of the other two samples of volcanic origin, the stratigraphically lower example is La Porcelana volcanic ash T1 (Porce T1). The zircons range in age from 6.2 to 2940 Ma. This sample has several zircon family age groups, but the most prominent one is around 10 Ma and the second most prominent population is around 500 Ma (Figure 11 A and B). Focusing only on the youngest age cluster with 9 coherent grains, the weighted mean depositional age of this volcanic ash is 8.6 Ma. The age distribution of La Porcelana volcanic ash T2 displays several age-families (Figure 11B), with the most conspicuous ones at 6 and 500 Ma. Considering only the 13 zircons with coherent ages (Figure 11A), the weighted average depositional age is about 6.2 Ma. The pre-Miocene zircon ages distributions of Porce T1 and Porce T2 are similar (Figure 11B).

Interpretation of U-Pb Chronostratigraphic Constraints

Among the samples collected because field criteria suggested that they were near-primary volcanic deposits, there are a range of zircon population styles. Within individual samples, the dispersion of ages of young zircons may contribute to understanding of their reworking by surface processes after their primary deposition as a volcanic ash. Several opportunities to modify the zircon age population exist during reworking of a volcanic ash. First, volcanic ashes are easily weathered, and the transportation of the detrital particles over long distances will result in the disaggregation of rock fragments by the congruent dissolution of the minerals (Soman et al.,

2010.). Transport of the original volcanic zircons by water or wind will cause sorting by particle size (Lawrence et al., 2011). Also, Lawrence et al. (2011) demonstrated that as zircon grains are transported by fluvial or aeolian processes, the abrasion of the external layers in each grain exposes successively older zones in the grain. In total, one would expect that narrow clusters of zircon age values in tephras suggest that the deposit suffered only a short transportation distance from its first location of deposition. Alternatively, a volcanic ash that has been significantly reworked may have a broader age spectrum or a somewhat shifted spectrum compared to the parent volcanic ash.

Using that reasoning, the unimodal distribution of ages in Iruya TO (Figure 5) may indicate that there was little abrasion, and therefore it may represent a short transportation distance from a location where the primary volcanic ash fell to the sedimentary resting place at which it was sampled. For these examples with a narrow distribution of ages (e.g., Figure 5A and 5B; Porce T1 and T2, Figure 11), the results are similar to what one would expect based on their stratigraphic position and on prior chronostratigraphic studies (e.g., Figure 4).

A contrasting situation is displayed by Iruya T4A (Figure 5C), which has a set of Miocene-Pliocene zircons but is polymodal. Such results might be representative of several processes, inclusive of grain abrasion by transportation (Lawrence et al., 2011), mixing of sediment sources, or recycling of the source at successive time steps.

Many of the samples were intentionally collected to analyze detrital populations, and these have populations that differ from the volcanic ashes. For example, sample P. Colorado S2 (Figure 7) has a wide range of values (6.6 to 2726 Ma) and no significant peak in the Miocene-Pliocene age range. That populations is interpreted to show that the provenance(s) for the zircon, and by inference the sand grains in general, must be a recycled one. Nevertheless, some of the sandstone samples contain a sufficient number of young zircons to confirm a Mio-Pliocene volcanic

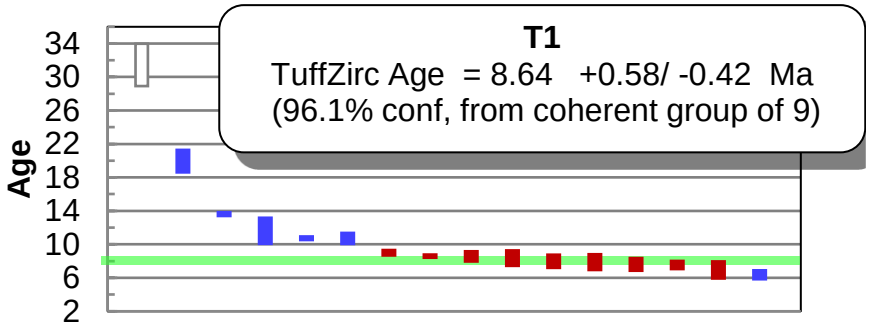
T1
TuffZirc Age = 8.64 +0.58/ -0.42 Ma
(96.1% conf, from coherent group of 9)
Age
34
30
26
22
18
14
10
6
2

A

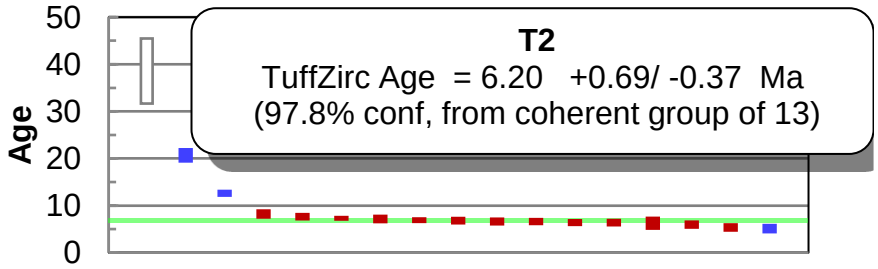
T2
TuffZirc Age = 6.20 +0.69/ -0.37 Ma
(97.8% conf, from coherent group of 13)
Age
50
40
30
20
10
0

B

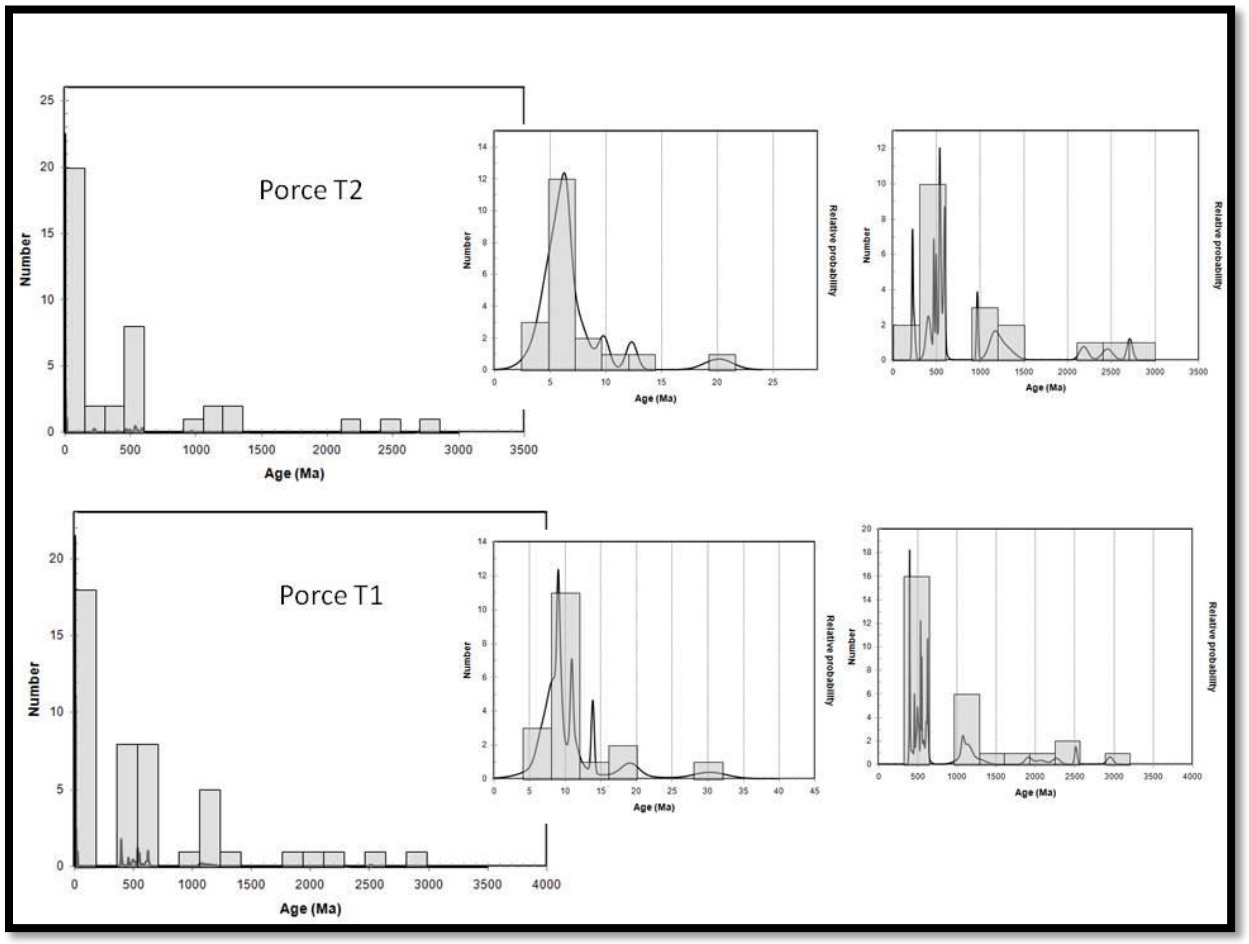
Porce T2
Number
Age (Ma)
Relative probability
Porce T1
Number
Age (Ma)
Relative probability

Figure 11: La Porcelana T1 and T2 Zircon U-Pb Dating Results
(A) Volcanic ashes T1 and T2 from La Porcelana River section are presented with their ages as weighted average plots. (B) These are the Probability Density Plots for both deposits including a subset of graphs presenting the clusters of ages enlarged to illustrate the youngest and older populations of zircon grains. Sample T1 exhibits a major peak in the value of 9.0 Ma, but weighted average calculation suggests that it has an age of 8.6 Ma. Sample T2 presents an age of 6.2 Ma with a maximum age peak at 7 Ma.

contribution. Examples include P. Colorada S1 (Figure 6) and S4 (Figure 9), which provide valuable constraints on maximum ages of deposition of the corresponding stratum.

The P. Colorada S1 (Figure 6) and La Porcelana Bentonite (Figure 10) grain populations both point toward a starting time of sedimentation within the Subandean-Chaco Basin during the Middle Miocene, approximately 13–14 Ma. For the La Porcelana River section, this result suggests a time of initiation that is about 3 million years older than the correlations proposed earlier by Echevarría et al (2003). For the Peña Colorada River section, the new age constraints suggests that deposition began 3 million years earlier than the correlations by Hernández et al (1996) and Echevarría et al. (2003).

U/Pb detrital zircon geochronology results increased the accuracy of time constraints for the Subandean-Chaco Basin sedimentary record. The mean and median dates calculated from the zircons in volcanic ashes do not violate the stratigraphic order of the deposits (Figure 4), and these are consistent with the ages presented by Hernández et al. (1996), and Echevarría et al (2003). Nevertheless, if the error bars on the U-Pb ages interpreted to be depositional ages (Figure 4) are considered, there is some overlap of apparent depositional ages.

The clusters of ages around 500 to 600 Ma fall within the zircon populations described by Augustsson et al. (2011) and Adams et al. (2008; 2011), who studied the Precambrian, Cambrian and Ordovician rocks of northwestern Argentina. The formations that are deduced to be the sand grain sources, based on the zircon age populations reported in the literature, are the Meson Group and the Puncoviscana Formations (Figure 1; Collo et al., 2009; Augustsson et al., 2006, 2008).

Correlation of the Magnetic Polarity Zones to the Time Scale with new U-Pb Constraints

Correlations of the three stratigraphic columns to the magnetic polarity time scale and to other sections in the basin can be improved, utilizing the new U-Pb results. The new depositional age constraints from three horizons in the Iruya stratigraphic section, two horizons in the Peña Colorada section, and three horizons from La Porcelana stratigraphic section are combined with tephra ages reported in the literature and with magnetic polarity zones (Figure 4). This re-analysis allows re-evaluation of the chronosequences proposed by Echevarría et al. (2003). Furthermore, the inclusion of information about the variation of the proportions of mudstone, sandstone, and conglomerates permits scrutiny of the relationships between changes in the depositional environment system and external factors whose ages are known in other locations.

One of the most important results of this chronological study is the improved definition of the age of the Tranquitas Formation (Figure 4) which was described previously in the study area by Hernández et al. (1996) and Echevarría et al. (2003). Although the Tranquitas Formation crops out in the Iruya River section as a set of sandstones and paleosols similar to those in the other two sections, no U-Pb zircon data could be extracted at this location. In contrast, the zircon analyses for the Tranquitas Formation at Peña Colorada and La Porcelana Rivers are the first dates reported for this formation (Figures 4; 12). Samples of horizons near the top of the Tranquitas Formation suggest deposition approximately 13.6 Ma and 14.2 Ma at Peña Colorada and La Porcelana, respectively. The Tranquitas Formation was considered by Hernández et al. (1996), Echevarría et al. (2003) and Rosario et al. (2008) to pre-date the beginning of Subandean fold and thrust deformation. DeCelles et al. (2011) demonstrate that during the time of deposition of the Tranquitas Formation, confirmed in this thesis to be the Middle Miocene, the locus of foreland deformation was in the Eastern Cordillera.

That age calibration of the base of the magnetostratigraphic column and addition of new age constraints in overlying horizons requires a re-evaluation of the ages. There is little impact caused by confirmation of the middle Miocene age for the Tranquitas Formation, in that there is a regional unconformity above that formation. For example, in a correlation of the Iruya River magnetic stratigraphy, Hernández et al. (1996) considered the Tranquitas Formation age to be of about 16 Ma, whereas Echevarría et al. (2003) correlated the Tranquitas Formation at Peña Colorada River as if its top were 12–13 Ma.

The new ages at higher stratigraphic positions have more potential to change the perceived correlations and to impact the interpreted ages of Subandean thrust belt deformation (e.g., Echevarría et al., 2003). These new ages could potentially shift thrust ages to earlier parts of the time scale than indicated by earlier correlations, and therefore may move to an earlier time the start of the deformation of the Subandean Belt, as reported by Hernández et al. (1996) with an starting age of approximately 10 Ma. Echevarría et al. (2003) estimated an age of 13.5 Ma by stratigraphic correlation at Iruya River section, but made no attempt to estimate a thrust initiation age based on the other stratigraphic sections.

The new U-Pb age constraints on the magnetostratigraphic correlation increase the difficulty of correlation of the Iruya River column. Amidon et al. (2015; Figure 4) reconfirmed the polarity zone pattern for the Iruya column above the interval on which this study focuses. The base of their column near 4500 m above the section base correlates to approximately 5.5 Ma. The new U-Pb dates confirm that polarity zones approximately 2200 m above the base of the section can be no older than 6.8 Ma (uncertainty of +0.1 and -0.2 Ma). Between the base of the Amidon et al. (2015) section and the newly dated volcanic ash near 2200 m the local magnetic polarity column contains 12 polarity reversals, yet the Global Magnetic Polarity Time Scale contains only 4

reversals between 5.5 Ma and 6.8 Ma. This means that about 500 m of strata might be repeated by faulting (Figure 4).

The deposits known as the Oran group or as the Subandean Tertiary Sequences could be over represented in thickness. This result signifies an over estimation in sedimentation rate, an erroneous time span for the deposition of sedimentary environments, and as mentioned above a repetition of magnetic reversals. All of these consequences can be summarized and an erroneous history interpretation of the sedimentary basin and its subsidence development.

Following the sedimentary patterns in combination with the zircon ages and the paleomagnetic data, four main stratigraphic units can be observed. From the top of Tranquitas Fm. to about 7.5 Ma a set of fine grain stratigraphic beds are observed, to fall into a coarser or sandy set of strata. At Iruya River, the strata tend to follow an upward coarsening sequence, until 400 meters of sediments before reach the end of the stratigraphic column. It is a similar sediment pattern observed at Peña Colorada that end at about 5.6 Ma when a correlated age is integrated from Las Manzanas Stratigraphic section from Echevarría et al (2003). This sediment sequence started later at La Porcelana section, presenting an age of 7.12 Ma. The last sedimentary pattern is exhibited as an Increase in sediment grain size on all the stratigraphic sections.

The new correlations confirm patterns of thickness change indicated by prior studies: twice as much sediment was deposited and preserved at the Iruya section compared to at Peña Colorada and La Porcelana. La Porcelana represents the thinnest sedimentary column preserved over the approximately 8 My time span, demonstrating a decrease of sediment thickness from the west to the east. These large-scale basin architecture characteristics set the stage for a description of the sedimentary deposits, and to better understand the sedimentary environments that accompanied this basin geometry.

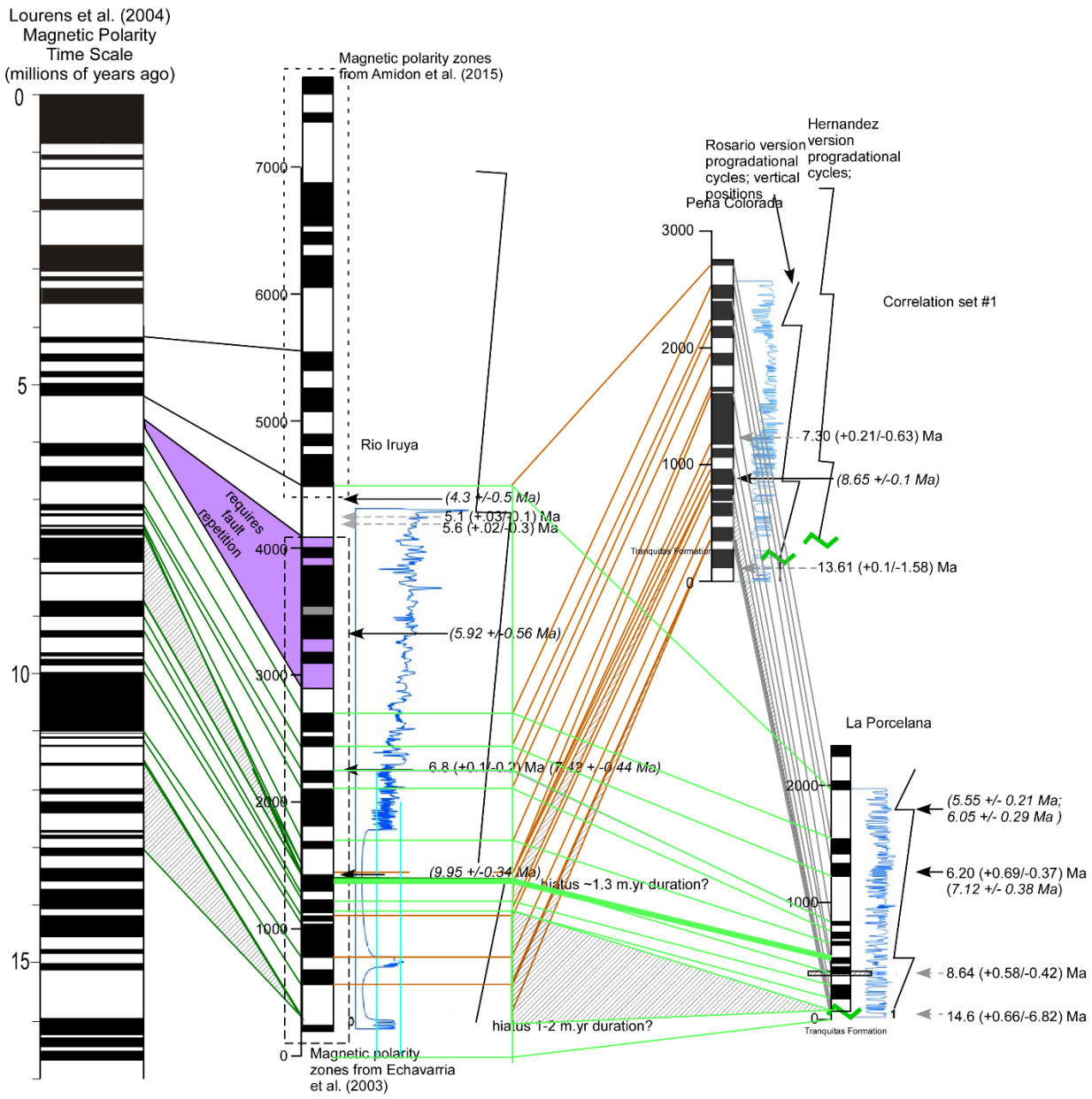
Lourens et al. (2004)
Magnetic Polarity
Time Scale
(millions of years ago)
Magnetic polarity zones
from Amidon et al. (2015)
Rosario version
progradational
cycles; vertical
positions
Hernandez
version
progradational
cycles;
Peña Colorada
Correlation set #1
Rio Iruya
requires
fault
repetition
(4.3 +/-0.5 Ma)
5.1 (+.03/-0.1) Ma
5.6 (+.02/-0.3) Ma
7.30 (+0.21/-0.63) Ma
(8.65 +/-0.1 Ma)
13.61 (+0.1/-1.58) Ma
Tranquitas Formation
(5.92 +/-0.56 Ma)
6.8 (+0.1/-0.2) Ma (7.42 +/-0.44 Ma)
(9.95 +/-0.34 Ma)
hiatus ~1.3 m.yr duration?
hiatus 1-2 m.yr duration?
La Porcelana
(5.55 +/- 0.21 Ma;
6.05 +/- 0.29 Ma)
6.20 (+0.69/-0.37) Ma
(7.12 +/- 0.38 Ma)
8.64 (+0.58/-0.42) Ma
14.6 (+0.66/-6.82) Ma
Tranquitas Formation
Magnetic polarity
zones from Echavarria
et al. (2003)

Figure 12: Chronostratigraphic Correlation
This correlation among the three spatially separated columns is an interpretation based in the location-specific correlations presented in Figure 4. The locations presented by the non-linear arrangement of the columns corresponds to the spatial relations in the field (see Figure 25 for more details).

Stratigraphy

Sedimentary Basin Setting

The strata of the NWA during the Tertiary to Pliocene age are formed of continental deposits represented by sets of mudstones, sandstones, and conglomerates (Hernández et al., 1996; Hernández et al., 2002; Echevarría et al., 2003; Uba et al., 2005, 2006, 2007, 2009). These deposits formed in a foreland basin. Tectonic activity between the South America and Nazca plates that caused the uplift of the Andes (Allmendinger et al., 1997), the shortening of the hinterland, and the potential incremental increases in sediment discharge are all anticipated to have influenced the foreland basins of the eastern Andes.

Subsidence is an important process that accounts for the large scale facets of the stratigraphic architecture (Kraus, 1992; Cardozo and Jordan, 2001). Subsidence is one of the main stratigraphic controls in foreland basins (Jordan et al., 1988; Cardozo and Jordan, 2001; Martinod et al, 2016), accompanied by the lithology of the sediment source area, the climate, and eustatic or regional base level (Kraus, 1992; Folguera et al, 2015). Both the uplift of the Eastern Cordillera and the progressive development of the Subandean Thrust Belt would have significant effects on the basin subsidence, mechanically caused by the isostatic response to thickening of the crust, and amplified by sediment loading (Flemings and Jordan, 1989, 1990; Ingersoll and Busby, 1998). In greater detail, the Subandean Thrust Belt contributes additional characteristics to the geometry of the basin and sedimentary architecture due to segmentation of the foreland by anticlines and synclines, which results in the compartmentalization of smaller basins (Laffa et al., 2011; Mortimer et al., 2016). The greatest thickness of basin fill is in what is today the wedge-top position (Jordan et al., 1995), thinning toward the Brazilian Craton until the fore-bulge is reached (Horton, 1998; DeCelles et al., 2011) about 300 km east of the present Andean mountain front.

The time interval studied, 14-5 Ma, Middle Miocene to Early Pliocene, corresponds to the time reported for abrupt uplift of the Andes (~3000 m), which has been interpreted to have changed not only the topography but also the regional climate (Garzione et al., 2014). To establish how the foreland sedimentary environment responded during this important tectonic time period, I observed the sedimentary lithology, facies, and architecture of these Neogene sediments.

During the time interval studied, the Iruya River section (4420 m reported thickness) forms the thickest sedimentary column, compared to Peña Colorada (2560 m) and La Porcelana (1960 m). The environment of deposition is described in the following sections for each of the studied locations, organized by formation (Tranquitas) and by progradation cycles, and in succession by location (Iruya, Peña Colorada, and La Porcelana).

Iruya River

Lithology

The first area studied is located at the Iruya River, which represents the western stratigraphic column and the one most proximal to the Eastern Cordillera (Figure 1, 2, 4, and 13). The entire column is formed by over 7400 meters of conglomerates, sandstones and mudstones interbeds in a coarsening-upward sequence. However, this study described and analyzed only the lower 4420 meters in thickness.

Tranquitas Formation

The stratigraphy of the Iruya River starts with a set of coarse sandstones that are arranged in several sand packages bounded and subdivided by erosional surfaces. These erosional surfaces reveal scours following deposition of each sandstone bed. All that is preserved of the depositional setting is sandstone, with no pebbles or coarser sediments (Fig 13 and 14). The amalgamated set

of sandstones contains calcium carbonate concretions probably formed as the result of pore fluids during the depositional event. Each sandstone stratum is about 1 to 10 meters in thickness. The sandstones have a characteristic reddish to yellowish color (2.5 YR ¾, 5 YR 5/6 Munsell Chart). These are often followed by a mudstone bed of about 1 meter in thickness. This pattern between sandstone packages and mudstones is observed for about 70 meters thickness in the stratigraphic section, followed by about 520 meters of a covered stratigraphic section. The first 80 meters described in the Iruya River section are known as part of the Tranquitas Formation (Hernández et al., 1996, 2002; Echevarría et al., 2003) which is the basal unit in the Orán Group (Hernández et al., 1996). Hernández et al. (1996, 2005) mentioned that this formation is mainly formed by sandstones and varies in thickness from approximately 350 to 650 meters in the Chaco Basin.

The sandstone strata with grain size from medium to coarse sand with concave and scoured boundaries between sandstones and mudstones strata form the facies Sch (see Table 1). These sandstone packages are interrupted by the mudstone strata followed by another set of sandstones. The finer strata formed by mud deposits with fine sand, silt, and clays, with laminations as its internal structure, are described as facies Fll. Many of the mudstone strata tend to present highly intense weathered features in the form of peds or muds-sand aggregates. The overall arrangement between sandstones and mudstones, Sch and Fll, in which the mudstones present pedogenic features is described as the sedimentary facies Tq.

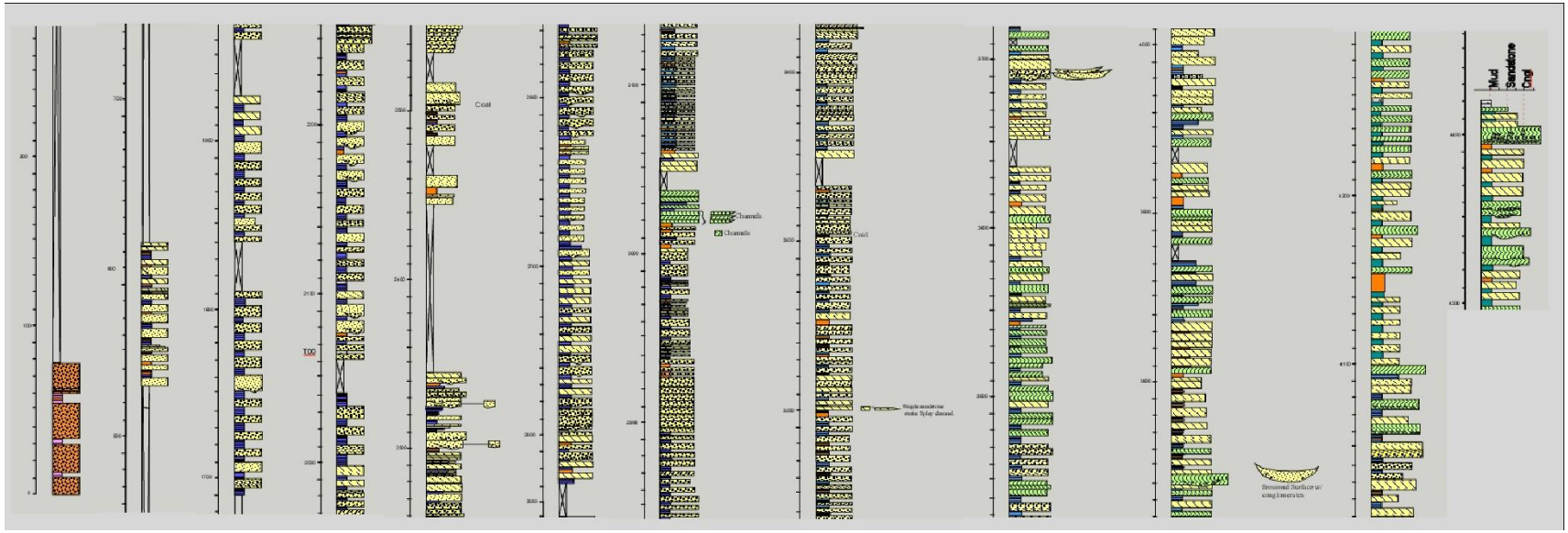
Coal
Channels
Channels
Coal
Mud
Sandstone
Cngl

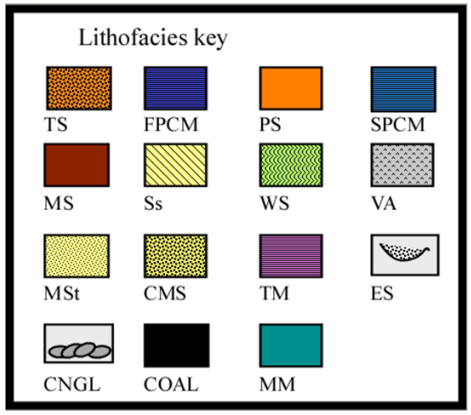
Lithofacies key
TS
FPCM
PS
SPCM
MS
Ss
WS
VA
MSt
CMS
TM
ES
CNGL
COAL
MM

Figure 13: Iruya River stratigraphic column

Grain size is indicated by the width of the column (maximum particle size corresponds to greatest width) and symbols illustrate the sedimentary structures. Key Lithofacies: TS: Tranquitas Sandstones; FPCM: First Progradational Cycle Mudstones; PS: Paleosols; SPCM: Second Progradational Cycle Mudstones; MS: Mud Strata; Ss: Laminated/Stratified Sandstone; WS: Wedge Sandstone (Sch, Scch); VA: Volcanic Ash; MSt: Massive Sandstone Package (one or several facies); CMS: Coarse Massive Sandstone (one or several facies); TM: Tranquitas Mudstones; ES: Erosional Surface; CNGL: Conglomerate; MM: Massive Mudstone

First Progradational Cycle (Echevarría et al. 2003)

On top of the Tranquitas Formation, 80 meters of sandstones and mudstones alternations (Figure 15) differ from those in the Tranquitas Formation. Here, sandstones form strata of 2 to 5 meters thickness; mudstones interbeds are an almost homogenous in their strata thickness. Sandstones beds that are arranged as tabular sand sheets of light-yellowish (7.5 YR 5/4) color are bounded by mudstones (clay and silt particles) colored yellowish red (5 YR 4/4). This combination is described as ST sedimentary facies (Table 1). The mudstones contain yellow-greenish (2.5 GY 5/2) mottles and small cracks (2 to 5 mm wide and up to 20 cm long in the vertical stratigraphic direction). These are interpreted to form under reduced conditions. The sandstones are composed of fine sand, and are laminated at a millimeters scale. The mudstones are subdivided by thin sandstone layers of about 2 to 10 cm thick. This set of ST sandstones and mudstones occurs repeatedly. The architecture of this set of sandstones and mudstones differs from those in the Tranquitas Formation. The sedimentary facies Sch are followed by Fll facies followed by ST facies (Sch →Fll →ST→Fll). That 80-m-thick section is followed by almost 1000 meters of no-data in the stratigraphic column. This is because of the limited continuity of outcrop along the banks of the Iruya River.

Second Progradational Cycle (Echevarría et al. 2003)

The next strata exposed occur almost 1700 meters above the base of the stratigraphic column. The entire First Progradational Cycle of previous workers is covered. Between 1700 m to almost 2240 meters, sandstones with well pronounced scour surfaces and sandstones with geometries of lens-shape are arranged in packages similar to the Tranquitas Formation (TF). The lowest volcanic ash sampled for U-Pb radiometric analysis, located at 2160 meters in the

stratigraphic column (Figure 4), corresponds to this facies group. The whole section is an interlayering between sandstones and mudstones, with a dominant sheet-like structure in the sandstones, going from fine to medium sand grains, laminated sandstones, and mudstones with 2-5 cm interbedded sand laminations (Figure 16). The thickness of sandstones relative to interlayered mudstones-thin-sandstone strata remains constant with an average ratio of approximately 1:1, with an average thickness of 4 meters for each bed. However, the sandstone laminations within the mudstones presents thickness from 10 to 25 cm. The sandstones in this section are formed by thick-to-massive, fine to coarse tabular strata (ST), often overlain by a sandstone deposit of about 0.5 meters in thickness with a concave geometry that pinches-out against the interlayered mudstone-thin-sandstone strata. The color of the sandstones, including the thin-sandstone layers within mudstones is 10YR 5/3, and mudstones values are in the color spectrum of 5YR 4/3 Hue. These sandstones interbedded with the above mudstones correspond to facies Scch, and these are covered by a ST or Fll sedimentary facies. The sequence at this section in the stratigraphic column follows a facies order Fll→ST→Scch→ST/Fll, with an upward coarsening in the grain size in the sandstone beds. Several mudstone deposits, composed of clay, silt, and sand, exhibit bioturbation including the presence of roots, and in many cases these deposits contain calcium carbonate nodules. These deposits are described as Paleosols or facies PS, and these are present in several horizons through the stratigraphic column.

Subsequently right after the 2400 m, a sequence of massive sandstones is deposited, each with a basal erosional contact above the underlying interlayered mudstone. The sandstone versus mudstone ratio becomes 3:1, with sandstone dominance. Above the 2500 meters level in the stratigraphic column, coarse grained sandstones delimit by texture the new arrangement of

Facies Code	Lithology	Sedimentary Structure	Interpretation
Fln	Mud, Silt, Fine Sand	Massive, no laminations, clay rich mudstone	Floodplain with no coarse sediment deposits, distal position from stream channel
Fll	Mud, Silt, fine to coarse Sand	Sand and Mud laminations, often carbonate nodules present	Floodplain with frequent sediment discharge from the nearby channels, close proximity to the main channel
Flc	Mud, Silt, Fine to Coarse Sand	Massive, Calcium Carbonate Sand lamination	Floodplain with a sandstone layer with cemented calcium carbonate
ST	Fine to Coarse Sand, frequent bioturbation	Tabular, sometimes linguoid sandstones bounded by mudstones, ripples	Crevasse splays
Sch	Medium to Coarse sandstone	Scours, concave internal boundaries	Sandstone Channel deposits, sand bars
Scch	Fine to Coarse Sand	Scours, concave internal boundaries	Crevasse splay channel
CNGL	Sand, Pebbles, Boulders	Massive Gravel Supported conglomerate	Gravel Channel deposits, gravel-bar
Ss	Sand medium to Coarse	Laminated sand sheet	Flash Flood Deposits, crevasse splay
SCGL	Sand, Pebbles	Stratified Sand supported Conglomerate	Channel deposits, gravelly sand bars
PS	Mud, Silt, Sand, Bio-turbation, Roots, Carbonate Nodules	Pedogenic features: Peds, nodules, horizonation	Soils with Chemical precipitation
C	Coal, Coarse Sand	Plant Residues, Mud films	Vegetated swamp deposits
Tq	Sand, mud, silt	Alternation of sandstones and mudstones with pedogenic features	Channel and floodplain deposits with soil development

Table 1: Sedimentary Facies Northwestern Argentina (Adapted facies designation scheme of Miall 1996)

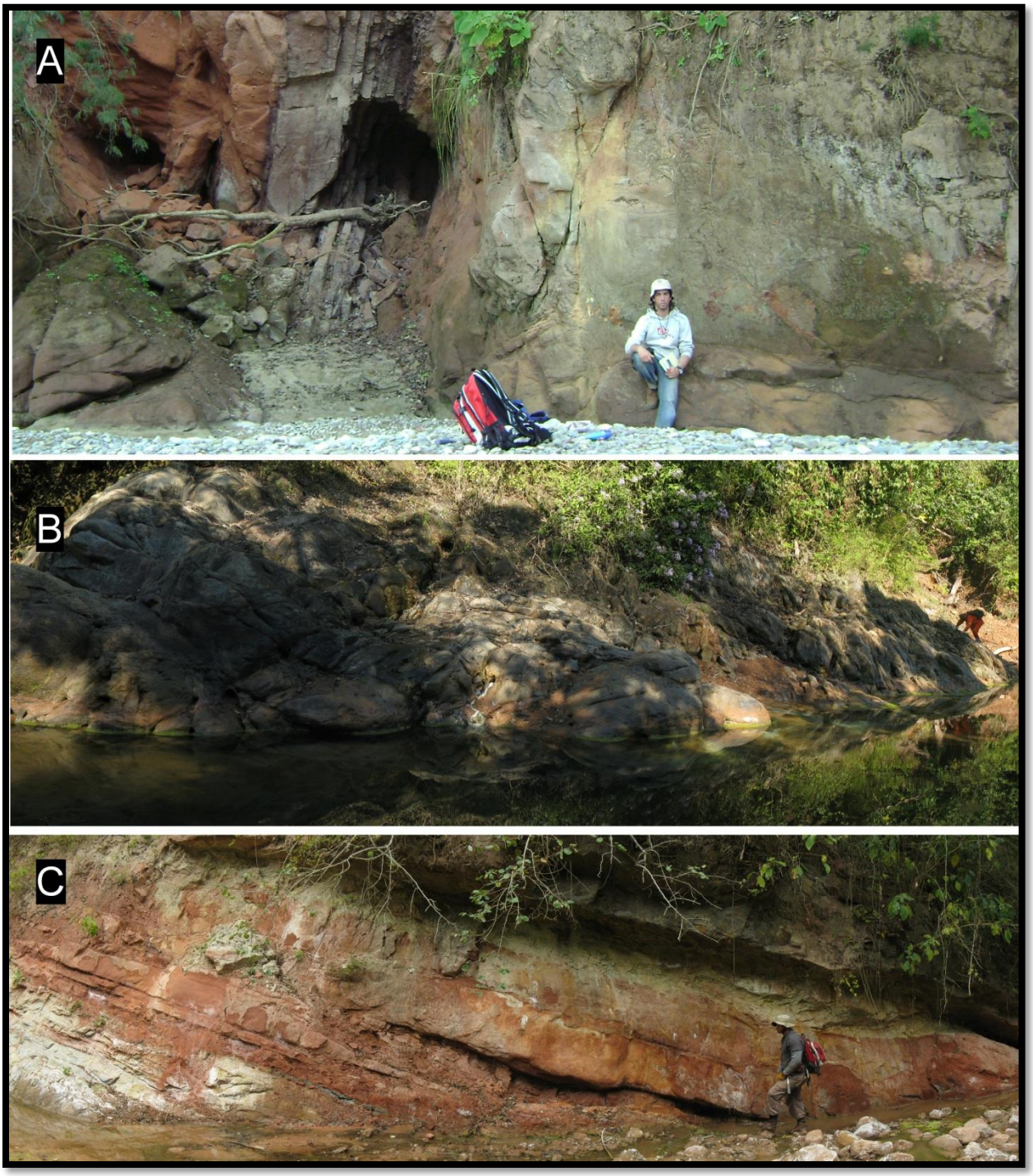
A
B
C

Figure 14: Tranquitas Formation in Three Locations
(A) Iruya, (B) Peña Colorada), and (C) La Porcelana. Tranquitas Formation is formed by amalgamated sandstones at Iruya and Peña Colorada versus La Porcelana where this formation besides sandstones also contain mudstones and paleosols.

sandstones and mudstone bed packages. A charcoal deposit of less than 0.5 meters is located between two sandstones, with the underlying sandstone presenting facies ST, and the above sandstone presenting Sch facies. The grain size of sandstones starts to decrease gradually to fine sand until reach the stratigraphic position of about 2800 meters. This section of over 400 meters in thickness composed by fine grained massive laminated sandstones is described as facies Ss, coarse grained sandstones with concave geometries bounded in amalgamated tabular strata. This sequence stops at the 2900 meters stratigraphic level, where there is a sandstone bed of about 30 meters thickness (Figure 13). This thick sandstone bed divides the progradational cycle into two 2 stratigraphic packages of bedsets. These two sedimentary packages formed by sandstone and mudstone are basically identical coloration and internal structure with the exception of the occurrence of intrabeded sandstone concave geometries around the 2800 meters. The repeated and almost homogeneous sequence of sandstones (Ss) and mudstones (Fll) of no more than a meter in thickness intercalate between tabular strata of sandstones (ST) with internal structures that appear to be erosional surfaces (Sch) that were buried by a secondary sandstone (ST) deposit. However, this second series of mudstones that separate the sandstones are mainly identical to the first package of sandstones and mudstones bedsets with the only difference of input of a coarser sand into the mudstone matrix as well as into the thin sandstone layers that are within these mudstones (Figure 16). The 30 meters of sandstone bed that bound at the top of this second package (Figure 13) forms a multistorey set of sandstones easily observable by what apparently looks like erosional surfaces within the sandstone bed. Some of the tabular sandstone strata in the second package can be observed to exhibit a lenticular shape (Figure 13 & 16), but this feature might be often present in other sandstone beds that are just covered by soil or vegetation and are not visible.

On top of the 30 meters sandstone bed is almost 100 meters of sandstones and mudstones arranged in a different pattern, which is formed by bed sets of sandstone of about 5 meters thickness followed by almost 15 meters of sandstones of 1 meter thickness and mudstones of 0.5 meters thickness, the latter two types in aggregated to reach a 5 meters thick sandstone. The sequence stops at 3060 meters in the stratigraphic column until a different arrangement in the sedimentary record start. At the top of this bed set, a coarse sandstone stratum with easily recognizable erosional surfaces covered by another sandstone stratum formed the limit of the sequence. This sedimentary interval is described here as the boundary between the second and third package of bed sets. The main sedimentological feature is the sandstone texture with an upward coarsening gradation, with sandstones presenting pebble layers and the multistorey channels formed by lenticular geometries (Figure 17). This sediment arrangement is described as facies SCGL, or conglomeratic sandstones with a wedge geometry.

Beginning at 3060 m above the base of the section, the subsequent package of strata of almost 400 meters in thickness corresponds to an analogous sandstone and mudstone arrangement of sediments as those between 2600-3000 m. Here, the main difference is that this sequence starts with interlayering between sandstones and mudstones of almost 1:1 ratio with thickness of no more than 0.5 meters, and ends up with a ratio of 3:1 meters in thickness with a dominance of sandstones over the mudstones. At about 3300 meters in the stratigraphic column, a second charcoal bed is interbedded between two sandstone beds. Between 3300 and 3490 meters in the column, sandstones become dominant in thickness over the mudstones (3:1 ratio in meters) until the 4050 meters stratigraphic level. This interval in the stratigraphic column exhibits fluctuation in grain size of the sandstones between fine to coarse sand. Fluctuation between the sandstone spacing, separated by the mudstones, is also observed. This package of sediments of about 600 meters


A
B
C
D

Figure 15: Sedimentary facies of the First Progradational cycle at the Iruya River section (A) Sandstone representative of the Sch Facies. (B and D) Floodplain deposits. (C) Sandstone deposit. One of the scientists from this expedition is standing at the left close to the center of this picture for scale.

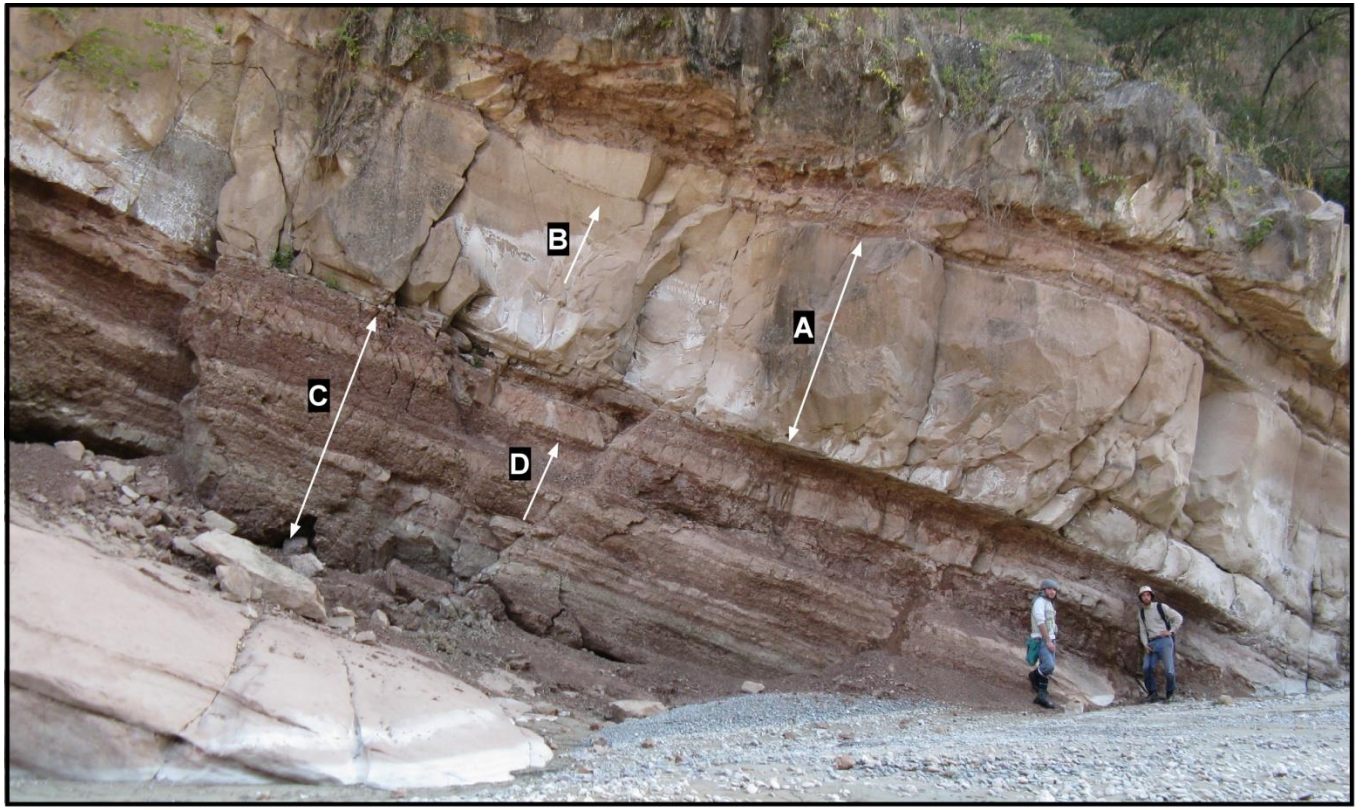
B
A
C
D


E
F

Figure 16: Facies of the Second Progradational Cycle
(A) Tabular sandstone. (B) Scour surface. (C) Mudstone interlayered with thin sandstone strata. (D) Thin sandstone strata. (E) Massive non-stratified mudstone overlain by a (F) sandstone.

thickness it is the least homogeneous due to the variability of the sandstone and mudstone frequency, the very thin clay rich mudstone layers on top of most of the mudstones (facies Md), and the variability of the grain size in the sandstones and mudstones. Sedimentary facies SCGL become prominent within this section up to about the 4100 meters stratigraphic level.

Third Progradational Cycle (Echevarría et al. 2003)

The uppermost 350 meters of strata studied in the Iruya River are formed by thick sandstones. Unlike in underlying parts of the section, the intervening thick mudstones contain almost no interbedded thin sandstone layers. The thickness of the sandstone strata can be as much as almost 10 meters at their maximum and 3 meters for the minimum stratum thickness. Mudstones are an almost constant thickness of 5 meters on average (Figure 18), and are frequently formed by mud, silt, fine to coarse sand, with pebble-size calcium carbonate sand layers. This sediment arrangement is described as facies Flc. This arrangement of mudstones defines the third progradational cycle described by Echevarría et al. (2003) and Hernández et al. (1996). It is within this package of bed sets that the first paraconglomerates and conglomerates appeared at the 4350 meters stratigraphic level. Above that first conglomerate are another 50 meters thickness of thick sandstones and mudstones, followed upward by another conglomerate of a little more than 10 meters thickness. The conglomerate at this level, formed by sand, pebbles, and boulders, is gravel supported and forms the sedimentary facies GCGL (Figure 18). The top of the stratigraphic column is capped by 2 volcanic ashes that were analyzed for tephra-radiometric dating.

A

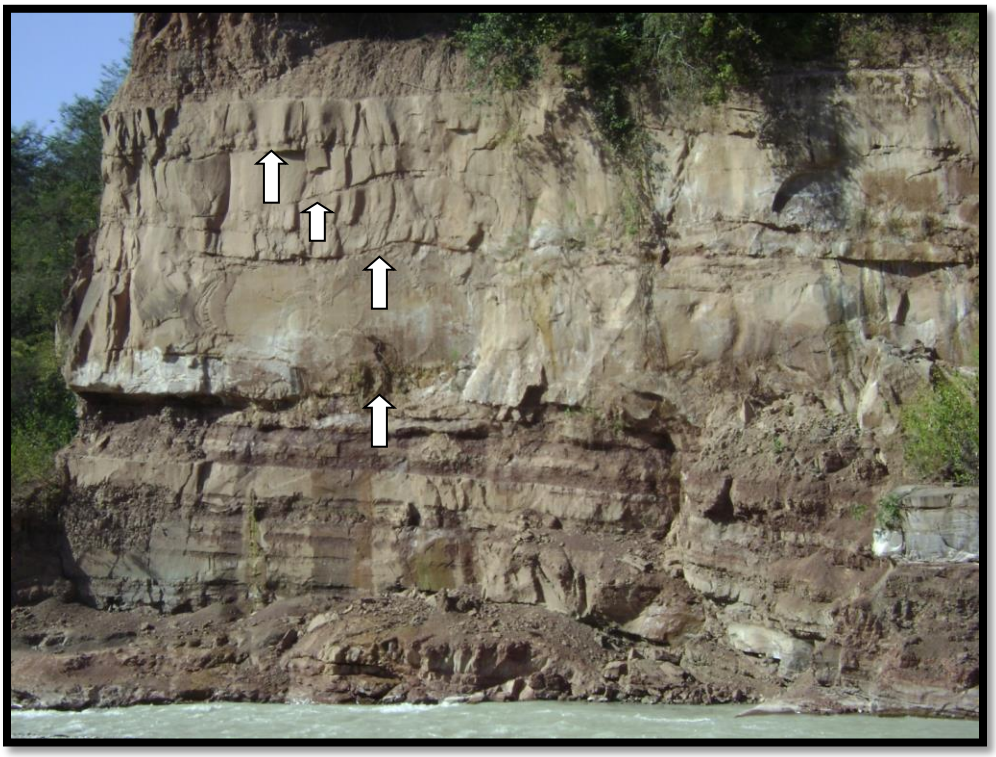

B

Figure 17: Second Progradational Cycle Stream Channels and Conglomeratic Sandstones
(A) Arrows point to scour surfaces, (B) pebble layer in sandstone.


A

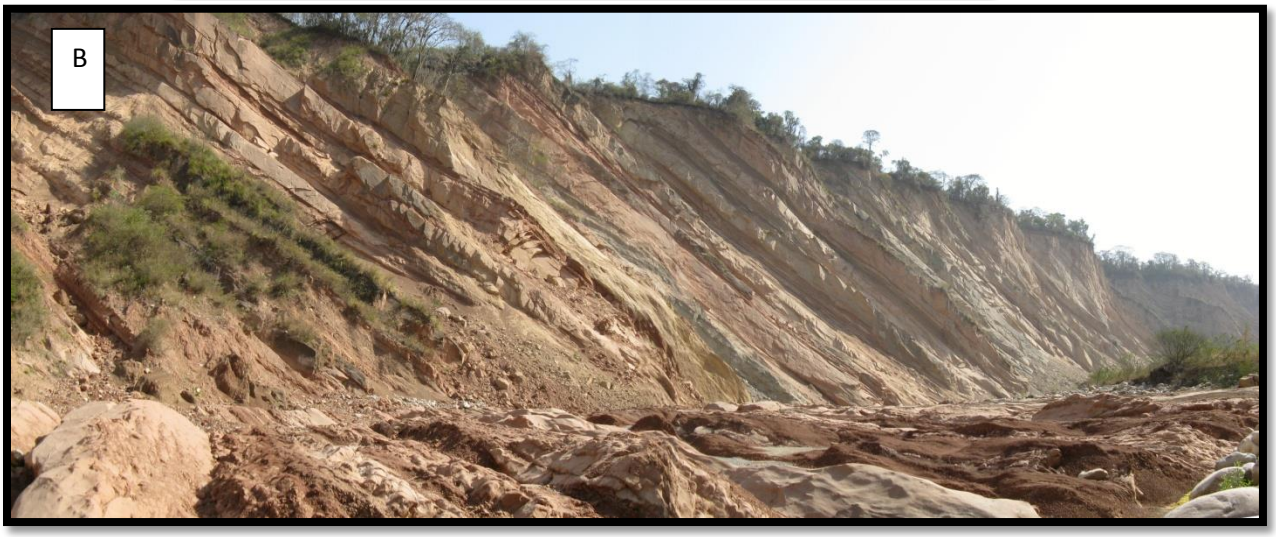
B

Figure 18: Upper stratigraphic section of Iruya
(A) Lowest conglomerate at Iruya River. The white bar is a meter in thickness. (B) Sandstone-dominate stratigraphy representative of the top of the Second Progradational Cycle.

Interpretation of Iruya Lithology (Sedimentary Environment)

The base of the stratigraphic column, the Tranquitas Formation (TF) in the facies Tq, is the fluvial system described by Hernández et al. (1996) and Reynolds et al. (2000). This unit is also known in the literature as the Areniscas Superiores (Superior Sandstones) a name proposed by Stark and Vergani (2001). Even though TF has been recorded in the literature as fluvial deposits with high incident of paleosols, no paleosols were identified in TF at the Iruya stratigraphic section. This could be the result of a higher sedimentation rate when compared with P. Colorada and La Porcelana sections (Echevarría et al. 2003), or on the contrary, the result of intense erosion of this formation that occurred between the last deposits for TF and the First Progradational Cycle.

The unconformable boundary between the Tranquitas Formation and the First Progradational Cycle described by Echevarría et al. (2003) corresponds to a hiatus of one to two million years (Figure 4). The poorly exposed First Progradational Cycle is characterized by alternations between sandstones and mudstone strata that represent a set of sedimentary environments found on floodplains and in channels. The combination of this sedimentary sequence corresponds to the discharge of sediment into the floodplain formed by the tabular to linguoid sandstones (ST) interpreted as crevasse splays. The thickness of the sandstones versus the mudstone strata represents the proximity of the site of deposition to the channels: the thinner sandstones with thicker mudstones represent more distant channels in comparison with the thinner or sand-laminated mudstones and thicker sandstone sections, which represent a closer proximity to the fluvial channels. Thicker mudstones tend to be more weathered as well promoting the development of soils that are going to be subsequently buried with the next flood event or the deposition of a new crevasse splay. The continuity of this system is interrupted by the inaccessibility of the data until up to the 1700 meters of the stratigraphic column.

The chronostratigraphy (Figure 4) implies that there exists a hiatus of roughly one million years between the top of First Progradational Cycle and the base of the Second Progradational Cycle, and the basal part of the Second Progradational Cycle is no longer exposed along the Iruya River. The Second Progradational Cycle presents changes, beginning with an upward coarsening system. The presence of facies Sch, Scch, and SCGL in the sandstones reveals a closer proximity to the mountain front than was recognized in the exposed sector of the First Progradational Cycle. The frequent concave geometry accompanied by scours, suggests deposits by crevasse splay channels. However, the stratified sand over a pebble bed suggests meandering deposits, but these are infrequent. Instead, the dominant sandstone faces (Sch, Scch, and SCGL) are interpreted to have been produced by channels that are part of a braided system. The second package of sediments within the Second Progradational Cycle, with facies ST and Scch that are truncated by facies Flc, suggests possible lateral accretion architecture. That facies association is followed by an upward coarsening sedimentary sequence that continues to the base of the Third Progradational Cycle. I interpret that this sub-cyle corresponds to the lateral migration of a DFS system.

There is no known hiatus between the Second and Third Progradational sequences, but instead an increase in grain size to the base of the Third Progradational Cycle. The interpretation of Hernández et al. (1996) is that the base of the Third Progradational Cycle represents a reduced distance from the mountain front to the Iruya depositional site, and therefore a tectonic event. The new environmental interpretation is consistent with that view. The Third Progradational Cycle levels studied in this project are composed of Flc, Ss, ST, and GCGL facies, which represent the most proximal sediments. The thick non-laminated mudstones capped by thick sandstone beds suggest the product of extended times of mud deposition, probably as the result of a more channelized river system. The gravel deposits indicate not only the proximity of the main channel,

but the proximity to the mountain front with a more restricted flow path producing enough energy to carry out coarser sediments. The superposition of facies Ss over GCGL suggests flashflood deposits that overlie the floodplains, and this input of coarse sands allowed more permeable floodplain drainage. That adjustment of the floodplain drainage may be the reason why calcium carbonate accumulated in a well-defined horizon. The PS facies constitute paleosols, which are the most well developed examples in the Iruya stratigraphic column. These results support the theory between paleosol development with the proximity or accessibility to the river channels (Kraus 1997).

In the Iruya River section, the First Progradational Sequence accumulated at a rate about 500 m/my, whereas the Second Progradational Sequence accumulated at a rate of approximately 1000 m/my. Overall, the sedimentary record preserved in the Iruya River coarsens upward, but the constituent lithologies and sedimentary architecture change little from the base to the top of the section, with consistent sedimentary facies that represent a braided river system. The sandstones of the Iruya River are tabular sand sheets with scour surfaces at their bases as well as some scour surfaces within sandstone sheets. Diversity within the sandstone lithology derives primarily from variability in the grain size. Variations among the many mudstones result from the variability of sand grain sizes within dominant mud-sized particles, and from the variable thickness of inter-layered sandstone lamina to beds among mud-dominated beds. Even though these two basic lithologies persist throughout the Iruya column and present no remarkable changes in geometries or internal structures of the beds, the frequency of alternation between sandstones and mudstones, as well as the thickness of bed sets of the two lithologies change upward in the column. Because of this lithology, the Iruya River lithology is separated into 4 different sections, including one that pre-dated the local thrust deformation within the Subandean Belt. Right now, the arrangement of

the Middle Miocene and Early Pliocene facies along with their lithology suggest a sedimentary record of a proximal distributary fluvial system (Weismann et al, 2010), or a Mega-Fan as described by DeCelles and Horton (2003a).

Peña Colorada

General characteristics

This stratigraphic column represents a location in the Subandean-Chaco basin that is about 25 km northeast of the Iruya River study site (Fig. 1). This column exceeds 3000 m in thickness, dominated throughout by mudstones and sandstones (Hernández et al., 1996). The section coarsens upward but alternations between the fine and coarse sediments persist throughout the column. This study described and analyzed the lowest 2560 m thickness, which are analogous in time (Middle Miocene to Early Pliocene) with the section studied at the Iruya River (Figure 19).

The Peña Colorado strata correspond to a position within today's thrust fold belt that is east of the Pintascayo Range and west of the Baja Oran Range (Echevarría et al., 2003). Until roughly 7 Ma, all of the thrust deformation occurred west of or within the Pintascayo Range, placing the Peña Colorado location in the foredeep (Hernández and Echevarría, 2009). However, the thrust-fold belt migrated eastward across Peña Colorada between 7 Ma and 6.5 Ma (Hernández et al., 2002; Hernández and Echevarría, 2009), shifting this location into a wedge-top basin position. This study documents the sedimentary evolution during this basin-scale transition, and the transition may be expressed by lithology, facies, and architecture of these Neogene sediments. Though correlative in time with the Iruya River section, the strata are formed by mudstones and sandstones with no conglomerates observed at this location. The intercalated sandstones and mudstones are described in the following sections of this paper. Like the Iruya section, an upward

coarsening sequence is observed, that progresses upward from fine sandstone to coarse sandstones. The Tranquitas Formation forms the base of this stratigraphic column, representing the initial Middle Miocene environmental conditions.

Tranquitas Formation

The lowermost ~130 m of strata in the Peña Colorada River section corresponds to the Tranquitas Formation (or Areniscas Superiores [Upper Sandstones]), which starts with a set of reddish to yellowish coarse sandstones that, similar to the Iruya section, are arranged in several sand packages bounded and subdivided by erosional surfaces. The erosional surfaces scour significantly into the underlying bed, with angles sometimes up to 45° on a concave contour (Fig 20.). Amalgamated sets of sandstones are also present at this location of the Tranquitas Formation (facies Tq). No calcium carbonate concretions were observed in the sandstones. In comparison with the Iruya Section, the sandstones at Peña Colorada present a different hue with a gray color on many of the sandstone strata. The reason for this is the presence of hydrocarbons in the pore space at this location (Echevarría et al., 2003). Each sandstone stratum is 2–20 m thick, followed by a mudstone stratum of about 1 m or less in thickness, which present little to no paleosol development. However, the presence of hydrocarbons in these strata might have altered diagnostic paleosol features in this deposit, making it impossible to observe such characteristics. The sandstones with hydrocarbon content extend up to 50 m in the stratigraphic column, then the sandstones exhibit a more reddish coloration for another 80 m in the stratigraphic column. An important feature of the Tranquitas Formation at this location is the absence of paleosol development. Besides a few mudstones of about 20 cm thickness that interrupt a few of the sandstones (Fig. 19), Peña Colorada section represents the stratigraphic column with the least

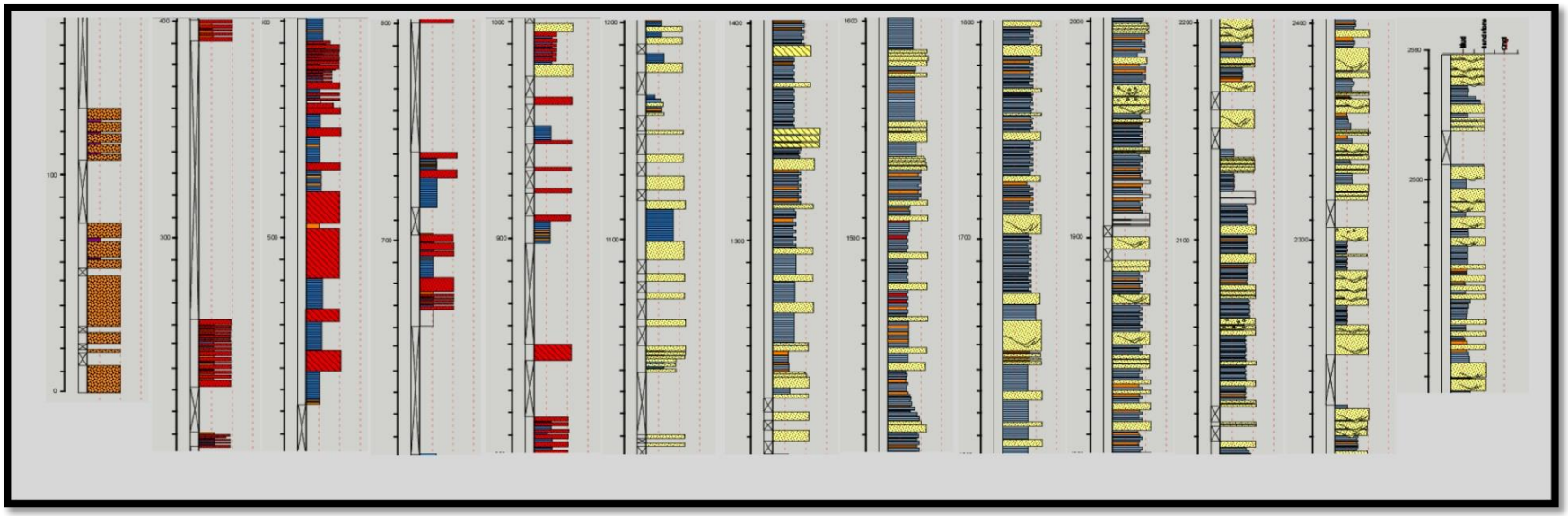

Figure 19: Peña Colorada Stratigraphic Column
Grain size is indicated by the width of the column (maximum particle size corresponds to greatest width) and symbols illustrate the sedimentary structures. Symbols of sedimentary structures and lithologies are presented in Figure 13.

amount of mudstone in Tranquitas. Following these deposits, the section is covered; the estimated thickness of covered strata is 70 m. Above the covered zone crops out the First Progradational Cycle.

First Progradational Cycle (Echevarría et al. 2003)

The lower 290 m of the First Progradational cycle (130–420 m in the stratigraphic column; Figure 19) crops out very poorly. A series of strata exposed between the 200 m and 210 m levels in the column reveal intercalations of sandstones and mudstones. Here the sandstone beds have a thickness of a meter with mudstone beds no thicker than 40 cm. The sandstones and mudstones both have a red coloration, 10R 4/4 on the soil color Munsell Chart. The sandstones exhibit a fine- to medium-sand grain size, with well-rounded grains, and can be also described as greywackes, with mud-sized particles responsible for the coloration that is similar to the mudstones. On top of these 10 m of outcrop is a poorly developed paleosol grains. These sandstones correspond to Scch facies. All the paleosols recorded in this stratigraphic section are described in the previous chapter. The facies and intercalations between sandstones, mudstones, and paleosols from 200-210 m in the column is basically repeated up to the top of the First Progradational Cycle at 850 m.

The subsequent deposits in the First Progradational Cycle differ mainly in grain size and in the thickness of the strata. For example, the next exposure of the strata, between stratigraphic levels 230 m and ~260 m (Figure 19) displays a pattern of repetitions between sandstones (Scch) and mudstones (Fln) like those described immediately above, with poorly developed paleosols. The lateral geometry of these deposits is almost impossible to define due to the lack of lateral exposure because of vegetation. In fact, the next outcrop is located at 390 m in the column (Figure

A

B

C

D

Figure 20: Peña Colorada Sedimentary Deposits
(A) Tranquitas Formation at Peña Colorada: The arrow indicates the direction to younger deposits and the length of the arrow is about 10 meters long. (B) First Progradational Cycle: The arrow is about 30 meters in length and points in the direction toward younger deposits. This corresponds to the deposits at the base of the First Progradational Cycle. It is possible to notice the intercalations between sandstones and mudstones, each with thickness not greater than 1 meter with the exception of the sandstones located at the bottom (left side of the picture) of 10 meters in thickness. (C) This is a sandstone located at 440 meters in the stratigraphic section. The hammer is presented in the figure for scale. Here it is possible to observe the low angle concave geometry of the sandstone bed that is capped by another sandstone bed. This sandstone terminates with a low angle into another sandstone. This is interpreted as an Scch sedimentary facies. (D) Geometries of sandstone beds such as presented here, exhibiting a convex-up geometry indicative of erosion, are a criteria for the Scch facies. Here a later sand deposit accumulated, creating a multi-storey sandstone. This sandstone is 80 cms at the thickest point, located in the middle of the picture.

19), exposing 10 meters of thin sandstones of no more than a meter in thickness and mudstones of 40 cm, similar to the underlying exposed sections.

Between 420 m and 600 m in the column (Figure 19), both mudstones and sandstones are well exposed and, despite the vegetation, geometries of the strata are more visible. The mudstones do not present internal structure; these deposits are classified as Fln. The sandstones correspond to the Scch and ST facies, based in their internal structure and the texture. However, where thicker sandstones are exposed, concave-up geometries as well as convex-up geometries occur, some examples terminating with a wedge shape against an adjacent sandstone bed (Figure 20 C and D). Figure 20D shows an example of a flat-based sandstone bed with convex-up top surface. In general, horizontal sand beds with a flat, non-erosional contact at the bottom and the top are classified as ST sedimentary facies. Despite the curved upper surface, the internal laminations in the Figure 20D example are planar and parallel the general bedding surfaces, not conforming to the convex shape of the bed boundary. This suggests that the sandstone should be considered to be of the ST facies, but it was eroded and later capped by another sandstone to form a multistorey sandstone body. The tabular sandstone beds fluctuate between 0.50 to 2 m in thickness, and are separated by 10-m-thick intervals of mudstone. Laminations of fine sand are conserved within these mudstones, which leads to designation as Fll facies. However, the sand lamina reduce in thickness where the interbedding is thinner, with mudstone beds <20 cm and sandstone beds <0.50 m (Figure 19; ~520–560 m in column). This zone of continuous outcrop ends upward with a 30-m-thick sandstone sequence that is capped by a series of mudstones. Between 670 m and 740 m in the stratigraphic column (Fig. 19) thin sandstones and mudstones display similar facies and the same sedimentary pattern of repetition as those below. The uppermost exposed strata in the First Progradational Cycle (~840–850 m in the column) are multistorey sandstones of medium to coarse

sand grain size. This sandstone deposit presents dominantly parallel internal laminations, which intersect at the erosional surface boundaries, and local cross lamination. However, as mentioned earlier, the limited exposure of these deposits allows only classification as the Sch facies.

Overall, the sedimentary sequence represented at this part of the stratigraphic column is built of facies Fln, Fll, Scch, and ST. Moving upward, these are arrayed in the following vertical sequence on a 10's of meters scale: Fln→ST→Fln→Scch→ST→Fln→Fll.

Second Progradational Cycle (Echevarría et al. 2003)

The lower 50 m of what Echevarría et al. (2003) interpreted to be the basal Second Progradational Cycle are covered, with the lowest beds exposed at the 900 m level in the column. The Second Progradational Cycle is initiated with a sequence of mudstones followed by a discontinuous series of medium-grained sandstone beds (Fig. 19, levels 910 m to 970 m). These sandstone strata are no more than a meter in thickness, with flat, smooth contacts at the bottoms and tops of the beds. Nearing the 1000-m-level, a lighter color and thicker sandstone occurs, in the color spectrum around 10R 5/2 of the Munsell Color chart. These sandstones are medium sand size and better sorted than those below, which probably explains why the coloration of these deposits changed. Between the 1000 m and 1230 m levels in the column, the repetitious intercalation of sandstones and mudstones remains the defining characteristic of these deposits. Tabular sandstones (ST) are the main sedimentary facies with their thickness fluctuating between 0.5 m up to almost 10 m in thickness. Mudstones present constant properties with no laminations, to be denominated as Fln. However, the record of mudstones is much less complete than for the sandstones, for the lack of exposure until above the 1200 m level in the column.

From 1200–1800 m in the stratigraphic column, the vertical spacing between sandstone and mudstone remains quite constant, with the main variations presented in the sandstones (Figure 19 and 20). The texture of the sandstone beds varies from medium to medium-coarse sand size. Scoured surfaces within the sandstones lead to their classification as Sch facies. The thickness of the beds varies between 1 m to 10 m, with exception of a thicker sandstone bed, almost 20 m, at around the 1650 m level (Figure 19). This bed of 20 m in thickness marks a point of turn-around in a series of systematic changes in bed thickness and texture. After gradually increasing in thickness and coarsening upward toward this level in the stratigraphic column, the beds above become progressively thinner upward as well as finer-grained. A change in the sandstone facies also occurs: sandstones below the 1650 m level change upward from ST to Sch, to Scch, and above that level they change back to ST again. This succession of sandstones is repeated with another point of turn-around in the sedimentary deposits at about the 1970 m level in the column followed by a progressive thinning and fining to the top of the Second Progradational Cycle at 2200 m. The most noteworthy difference between the second center-of-cycle thick sandstone (15 m thick, at the 1970 m level) and the one at the 1650 m level is the presence of calcium carbonate concretions in the upper one. These thick sandstone deposits also exhibit scoured internal surfaces, and therefore these are identified as multistorey sandstone packages.

The comparatively good exposure through the Second Progradational Cycle facilitates recognition of a trend that is also true of the First and Third Progradational Cycles, that the progradational cycles can be recognized through progressive changes in the texture of the mudstone. The mudstones, that represent the intercalated and more poorly exposed sediments throughout this stratigraphic column, present a gradual but persistent increase in their grain size.

A

B

Figure 21: Peña Colorada Section Mudstones and Sandstones
(A) 1230-1259 meters above the base of the stratigraphic section. Alternating mudstones and sandstones; arrow head points toward the younger beds. Sandstones are overlying and underlying the mudstone package. This arrangement of facies repeats through the whole stratigraphic column. The sandstone where one of the field members is located is about 2 meters in thickness. The whole section is almost 20 meters in thickness. (B) This deposit represents the position 2330 to 2350 above the base of the stratigraphic column. The arrows point toward younger deposits. The center sandstone is about one meter in thickness.

Progressing upward, more sand is incorporated into the mudstones, and yet their coloration shows almost no change and remains close to a color around 10R 4/4. In addition, the abundance of sand laminations within every mudstone package increases upward.

The facies sequence of about 50 m throughout this Second Progradational Cycle follows the pattern of Fln→ST→Scch→Sch→ST→Fln. This sequence terminates with a series of sandstones with erosional surfaces, sometimes separated by thin layers of mudstones, or even a thin clay lamina. Echevarría et al. (2003) placed the top of the second sequence around 2190 m in the stratigraphic record.

Third Progradational Cycle (Echevarría et al. 2003)

Only the 360 m thick basal part of the last sequence in this Peña Colorada stratigraphic section was analyzed, from 2190 m to 2560 m height in the column (Fig. 19 and 21). Although lateral exposures are still limited by vegetation, the lateral extent of sandstone bodies is better exposed than in the lower two Progradational Cycles.

Even though an alternation between sandstones and mudstones is consistent with the pattern in the Second Progradational Cycle, the vertical distances between sandstones and mudstones differs in the Third Cycle. In this Progradational Cycle, sandstones are of greater thickness than in the older cycles of the column. Sandstones are formed by coarse sand with medium sorting, lacking mud-sized detritus within the sandstone. Sandstones are dominated by Sch and Scch sedimentary facies. Although the ST facies is present, it is of diminished importance. The typical sandstone facies order of upward succession is ST→Scch→Sch→Scch→ST throughout the Third Cycle. Several of the sandstone bodies are multistorey, with Scch on top of

either Sch or ST facies with prominent scour surfaces as the contact between strata. Because of their multistorey nature, the thickness of sandstone bodies varies from 1 m to 20 m.

Overall within the Third Progradational Cycle, the most noticeable sedimentological upward trends are an increase in the scours within sandstone bodies, an increase in particle size in the sandstone, and a change upward in the mudstone texture. The most noticeable change that reflects the long-term dynamics of the depositional system is the decreased vertical separation between the sandstone bed-sets and mudstone bed-sets, compared to the underlying cycles.

Interpretation of Peña Colorada sedimentary environment

The sandstones of the Tranquitas Formation formed in a fluvial environment. Although the sparse outcrops suggest similar river-related depositional conditions for the sandstones at Peña Colorada as at locations that are widely spread across northwestern Argentina, the lack of well-preserved paleosols distinguishes this location. According with Hernández et al. (1996), the contact between Tranquitas Fm and the base of the First Progradational Cycle is characterize by an unconformity, which make a variable contact between these two stratigraphic units from place to place.

The stratigraphic shift in the progradational cycles between Hernández et al. (1996) and this study (Figure 12) was based on the fact that I described the cycles in accord with their lithology rather than using depositional age as the criteria. From here, the oldest deposits in the succession of progradational cycles in the Peña Colorada section correspond to a fluvial system highly influenced by fine sediments, which suggests a low energy environment. This environmental setting might have been part of the northern sector of the same mega-fan responsible for the Iruya River deposits. If so, the long distance from the fluvial channel near Iruya to this location required

that the coarser and well sorted sediments of the First Cycle at Peña Colorada were delivered only by the highest energy flood events. The sands were deposited as the result of crevasse splay events, and thereafter these remote parts of the mega-fan were subjected most often to flood waters that carried only the finest sediments (mainly clay). However, an alternative interpretation for the high silt content in the sandstones should be considered. The mega-fan environment might also possess some wind-transported materials which, after bioturbation in the well vegetated landscape, would be integrated with the water-borne sediments. Iriondo (1996) demonstrated that eolian deposits are present in part of every modern Distributary Fluvial System (mega-fan) in northwest Argentina and southwest Bolivia. Although eolian dunes have never been recorded in the area of this study for the Neogene strata, this additional sediment delivery system and its possible influence during times of low precipitation in the past cannot be disregarded. The upward coarsening of this stratigraphic sequence implies that the position of the central axis of the mega-fan shifted somewhat northward through time.

The Second Progradational Cycle in the Peña Colorada stratigraphic column is represented by coarser sediment texture in the sandstones as well as in the mudstones. It is possible to observe a rhythm of long-lived progressive change of the environment just by observing the sediment texture in the mudstones, which progresses upward from mudstones with fine sand to mudstones with medium-coarse sand. This mudstone textural trend parallels the upward progression in sandstones from facies ST→Scch→ST through this sequence. Overall, the order of facies for this stratigraphic sequence is Fll→ST→Fll→ST→Scch→Sch→Scch→ST→Fll. I interpret this as changes in position of the fluvial system produced by the lateral migration of the mega-fan, first an approach of the mega-fan axis toward Peña Colorada, and then an increase in distance to the mega-fan axis.

Sandstones of this second progradational sequence contain calcite, and in the upper part of the sequence the abundance of calcite reaches the point of forming cemented concretions in coarser sandstones. There appears to have been a correlation between grain size and calcium carbonate precipitation in the mega-fan environment. This observation is very important, because it is the opposite of the trend of calcite abundance in the paleosols. At Peña Colorada there is less calcium carbonate in the paleosols than in the paleosols at Iruya, where calcium carbonate concretions were also found in sandstones deposits.

Only the first stages of this column's uppermost progradational cycle are documented here. Echevarría et al (2003) described the continuity of this sequence for another 600 m more above the top level that I studied. Nevertheless, the progradational cycle can be recognized within the 360 m of this sequence described here, expressed by a coarsening in the texture of the sandstones accompanied by a decrease in the particle size of the mudstones. In addition, there is a progressive upward decrease in the frequency of mudstone intervals in comparison with the sandstones. This sequence at the scale of tens of meters differs from the rest of the Peña Colorada column in its facies order (Fll→ST→Sch→ST→Fll), that produces thicker sandstone intervals and significantly less mudstone volume.

Peña Colorada stratigraphy corresponds to a distal environment of deposition when compared with the Iruya River section. The environment of deposition represents a comparatively lower energy regime, expressed in the ratio between sandstones and mudstones and in the lack of ripples or cross-bed deposits. In this case, "distal" refers either to proximity to the mega-fan head region or to proximity to the mega-fan axis. If the Mio-Pliocene mega-fans were as elongate as is the modern Bermejo DFS (Fig 8 of Chapter 1), the Peña Colorado location could have been only

25 km north of the Iruya region, but subjected to relatively distal water and sediment transport conditions.

According to Echevarría et al. (2003) the Baja Oran fault immediately east of the Peña Colorada section began movement at 7 Ma (Figure 2). This event corresponded in time with the upper sector of the second progradational sequence. The strata demonstrate a subtle change in facies expressed by a coarser grain size and greater erosional scour that is suggestive of channels, as well as an increase in thickness of the beds.

La Porcelana

General characteristics

La Porcelana stratigraphy records the sedimentary environments 15 km to the east of Peña Colorada and 35 km NE of the Río Iruya study site (Figure 1). Considering thrust shortening since the time of deposition, La Porcelana was located roughly 45 km distal of the Río Iruya site during the Late Miocene (Echevarría et al., 2003). This location completes the surface transect of the distribution of sedimentary facies across the Miocene-Early Pliocene mega-fan. Reynolds et al. (2001) illustrated the general lithologic trends of this 4600-m-thick section. For this study, only the lower part of the La Porcelana column is studied, composed of 1960 m of sandstones and mudstones. No record of pebbles or conglomerates were recognized in this interval of strata (Figure 22). This portion of the La Porcelana section represents the analogous interval of time as described for the Iruya and Peña Colorada columns (Middle Miocene to Early Pliocene). This stratigraphic column represents less thickness of sediments accumulated compared with the previous stratigraphic columns of this study during the same interval of time. This section, found between Baja de Orán and Sierra de San Antonio Ranges, was within the foredeep throughout the

Late Miocene and Early Pliocene. It became part of a wedge-top basin within the thrust-fold belt approximately 4.5–4 Ma (Echevarría et al., 2003), younger than the interval studied here. The facies analysis is conducted in the framework of the multiple progradational cycles described by Echevarría et al. (2003), which differ from those illustrated by Reynolds et al. (2001).

Tranquitas Formation

The base of La Porcelana section is also formed by the Tranquitas Formation or Tq sedimentary facies of this study. An important outcome of the geochronology investigation described above was the analysis of a highly weathered volcanic ash, identified as a bentonite deposit in the field. This thin layer of clayey material was analyzed for zircons, giving the oldest age for the Tranquitas. This confirms the appropriateness of identification of these strata as the Tranquitas Formation. Hydrocarbon residues also occur in these exposed strata.

Mudstone and sandstone interbeds form these deposits. The sandstones are reddish to yellow in color, and fine to medium sand texture. Pedogenic development occurs in several of the mudstones, which react weakly with dilute HCl. Root casts were found in some of the mudstones, which is further evidence for soil development at the time of deposition (Figure 23). The sandstones present high redox features including areas with red coloration and grey-green mottling or even reduced clay laminations 10 mm thick. Sandstones are amalgamated similar to the Iruya River section, and the sandstones are arranged in multistorey packages with erosional surfaces as the contacts. Each sandstone stratum varies between 20 cm to a meter in thickness. The thickest mudstone strata are no more than 40 cm thick. Some of the mudstone beds are truncated into the sandstones as presented on Figure 23. The whole exposed formation is a little more than 30 m thick in this area, although Reynolds et al. (2001) estimated the formation thickness to be 100 m.

The top of the exposed formation consists of a set of mudstones before vegetation and a local landslide obscure the contact with the overlying unit.

First Progradational Cycle (Echevarría et al. 2003)

The first outcrop that represents the First Progradational Cycle described by Echevarría et al (2003) appears above a 30-m-thick covered zone which hides the contact with the Tranquitas Formation. The basal outcrop is composed of a series of red sandstones similar to the ones described at Peña Colorada. These sandstones have a fine-to-medium sand grain texture, with contact geometries that go from flat to concave downward (Figure 24A). Mudstones present no laminations, and pedogenic development can be observed in many forms including clay cutan deposits (Figure 24 A and B). The contacts between sandstone bodies are erosional and are truncated into series of sandstone beds which truncate laterally in some cases against mudstones and in other cases against other sandstone bodies producing onlap sandstones over an underlying relief. Beds composed of sedimentary facies Scch are overlain by a variety of other facies, inclusive of Fln, ST, or PS. The sedimentary architecture of this progradational cycle follows a systematic upward sequence at scales of 30 m between facies Fln→ST→Scch→ST→Fln, and sometimes facies Fln→ST→ Fln→ST, repeating cyclically for nearly 200 m in the stratigraphic column. However, a decrease in the mudstone thickness juxtaposed with an increase in the sandstone strata thickness is observed up to the 330 m level, to end up with two thick sandstone beds, each almost 5 m thick that are separated by a mudstone of less than a meter in thickness. The change upward at ~330 m from these thick sandstone beds to a sequence of mudstone beds marks the top of the First Progradational Cycle and the base of the Second Cycle.

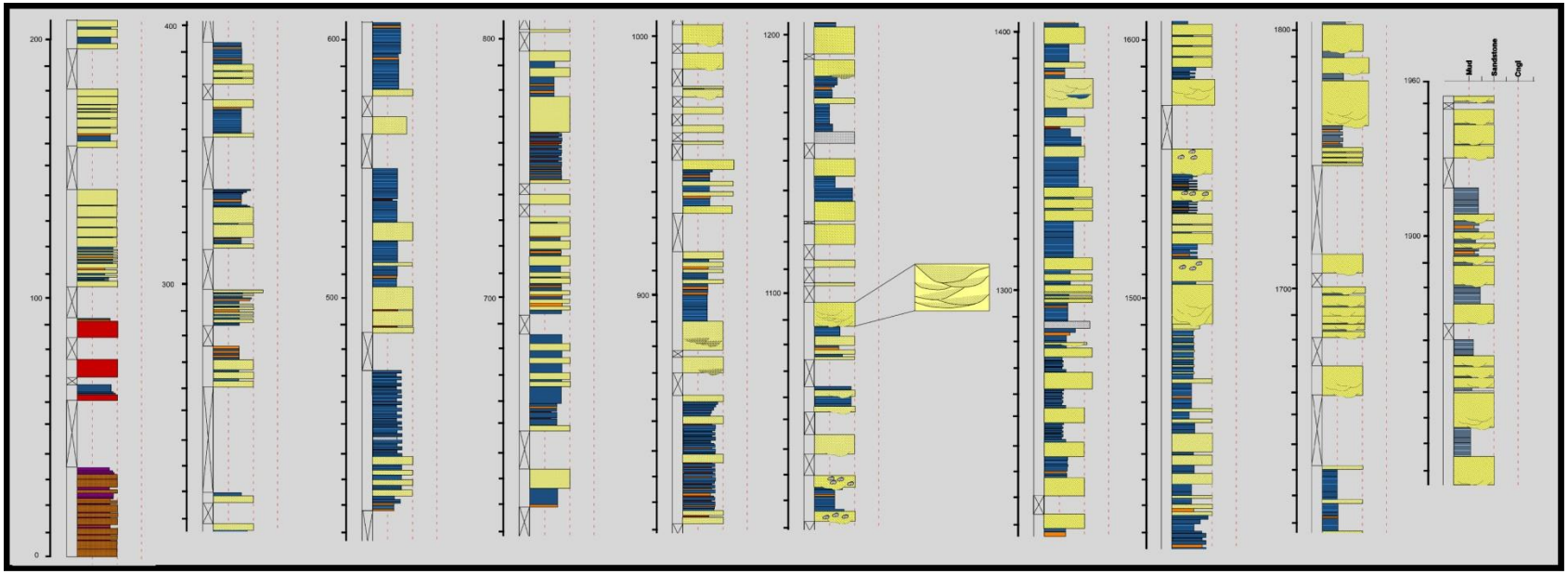
200
100
0
400
300
600
500
800
700
1000
900
1200
1100
1400
1300
1600
1500
1800
1700
1960
1900
Mud
Sandstone
Cngl

Figure 22: La Porcelana River Stratigraphic Column
Grain size is indicated by the width of the column (maximum particle size corresponds to greatest width) and symbols illustrate the sedimentary structures Symbols of sedimentary structures and

A

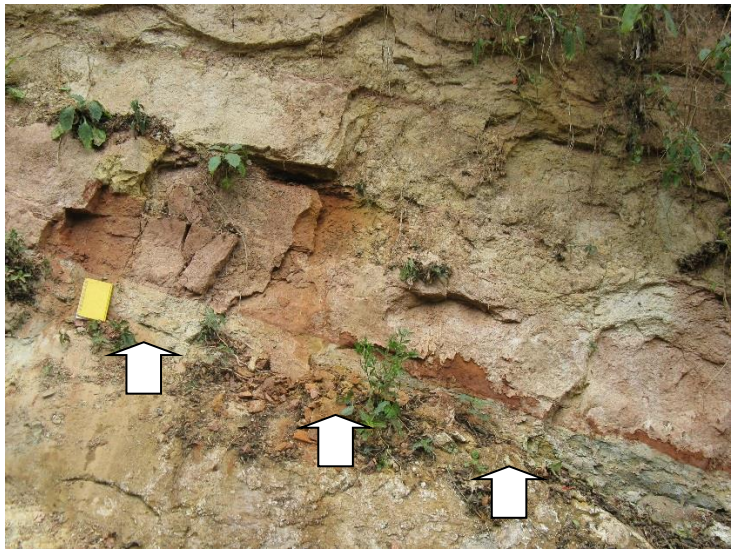

B

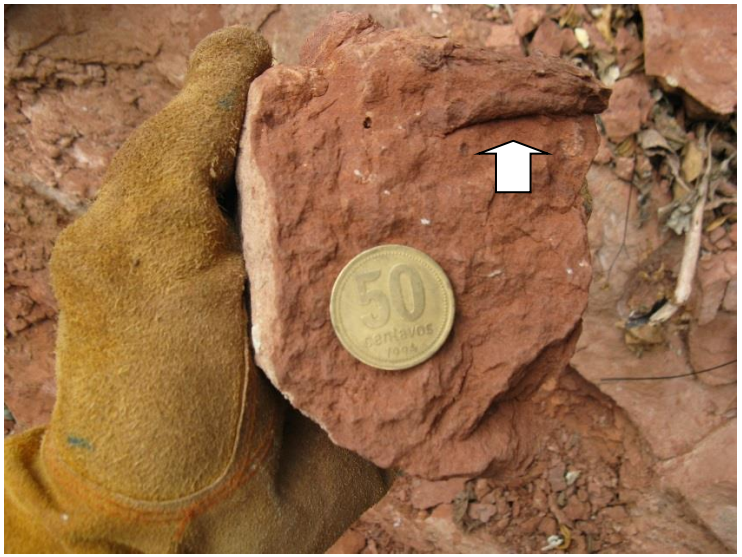

C

Figure 23: Tranquitas Formation at La Porcelana Stratigraphic Section
(A) Common features of the Tranquitas Formation include sandstone beds interlayered with truncated mudstones. (B) The arrows point to a bentonite deposit with a smooth-flat contact at the top and the botton (notebook for scale). (C) This is a sandy mudstone deposit with pedogenic development. This picture shows mottling as well as a root cast marked by the arrow.

Second Progradational Cycle (Echevarría et al. 2003)

Mudstones are thicker and more frequent within the deposits that represent the second progradational sequence of fluvial deposits described by Hernández et al. (1996) and Echevarría et al. (2003). Several of these mudstones exhibit clay cutans, root casts, redoxomorphic features, and a blocky texture, all indicators of pedogenesis. This facies of mudstones were classified as PS facies, and they intercalate between mudstones without pedogenic features and sandstones, similar to in the Iruya and Peña Colorada river sections. The thickest sections of mudstones reach 30 m, within which there are thin sandstone beds or sandstone laminations. At this location, these intercalated mudstones with fine sandstone laminations are described as Fll facies. La Porcelana represents the section with the most continuity between mudstones when compared with the previously described stratigraphic columns to the west. The vertically measured (in a stratigraphic sense) sandstone: mudstone ratio for the lower 700 m of the Second Cycle (spanning 330–1000 m) is on the order of 3:5 (Figure 22).

La Porcelana exhibits the same problem of vegetation cover and several landslides as at Peña Colorada. I make the assumption that sandstones are better exposed due to their greater resistance to weathering compared with the mudstones, and construct the stratigraphic column based on this assumption.

Sandstones tend to be tabular, with smooth flat boundaries; the vegetation cover prevents examination of their lateral continuity beyond distances of several tens of meters. The contacts tend to be flat on both tops and bases of beds, with the exceptions of the concave base sandstones interpreted as Scch facies. The sand grains are rounded and well-sorted; medium grain size dominates.

A

B

C

Figure 24: La Porcelana Sandstones and Mudstones Described at the First Progradational Cycle

(A) These are sandstones with a middle sandstone bed (handle of hammer on the middle sandstone) with a concave and irregular base that implies an erosional surface interpreted to represent a crevasse splay channel. This channel deposit is capped by 30 cm of mudstones followed by another sandstone. These will be categorized as Scch and ST respectively, with an Fln mudstone. Hammer for scale, with hammer head pointing to the younger deposits. (B) Mudstone with no laminations. (C) Clay cutans can be observed in this mudstone. Some of the cutans are the product of clay translocation suggesting pedogenesis of these deposits.

The frequency of sandstone increases around the 1000 m level in the column (Figure 22). Near that level in zones where outcrops are well exposed and it is easy to observe the vertical arrangement in the lithologic packages, the ratio between sandstones: mudstones is close to 1:1. Also near the 1000 m level, sandstone deposits start to present thicker beds, up to 10 m in some cases, with concave bed geometries, multistorey sandstone packages, and calcium carbonate concretions similar to the stratigraphic columns studied to the west (Figure 22).

Facies sequences presented here overlap with the range of mudstone and sandstone facies mentioned for the Peña Colorada section. A noteworthy difference is the addition of Fll facies, which first appears at 400 m and continues to be one of the facies present up to about the 1600 m level in the stratigraphic column (Fig. 22). Acknowledging that there is variability in the facies arrangement through this progradational cycle, the tendency of the sequence at the scale of 50 m is mainly dictated by upward successions of Fln→Fll→ST→Scch→Sch→ST→Fll→Fln. This facies sequence is very similar to the First Progradational Cycle at this location, and to the Second Progradational Cycle at the Peña Colorada section. This cycle terminates in a series of Scch and Sch facies where calcium carbonate concretions are present, followed by a series of ST deposits (Figure 23). The described section culminates with Scch facies at approximately 1710 m height in the column.

Third Progradational Cycle (Echevarría et al. 2003)

Limited by the poor exposure, the examined sedimentary deposits of the third cycle start with a series of sandstones. The lowest exposed sandstones are tabular, but change rapidly upward, such that above the 1760 m level the facies are Scch and Sch. These new sandstone facies are multistorey in nature. Even at a finer scale within a single bed, the sandstone is divided by thin

mudstones which drape erosionally scoured surfaces overlying sand beds. The series of Scch and Sch sandstones persists to the top of the studied stratigraphic column at 1950 m, changing only the thickness of the strata. The sediment texture exhibits medium-grained, rounded, and well sorted sandstone. Mudstones in the lower part of this cycle are fine sand, silt, and clay texture, which becomes progressively sandier as one moves up in the column. The mudstone facies are Fln to Fll, including some PS facies. This series of sandstones and mudstones represents an upward coarsening sequence similar to the previous two progradational cycles Fln→Fll→ST→Sch→ST→Fll→Fln. The result is an even finer grained set of sediments than in the third cycle found in Peña Colorada due to the addition of facies Fln.

Interpretation of La Porcelana sedimentary environment

The progradational cycles described by Echevarría et al. (2003) have been identified in this detailed study. If these progradational cycles represent stratigraphic sequences in a formal sense, conventional reasoning implies that there should be unconformities separating the sequences (e.g., Posamentier et al., 1993; Posamentier and Allen, 1999). No obvious unconformities were observed in the field. Nevertheless, the preferred correlation of the magnetic stratigraphy to the global magnetic polarity time scale (Figure 12) reveals that one or more unconformities occur near the 1000 m level in the column at the middle of the second progradational cycle, which together produce a 1-million-year duration hiatus. A second major unconformity occurs between 250–300 m level, in the middle of the First Progradational Cycle (Figure 12).

These progradational cycles can be described by the sequences of 100 to 200 meters thick in which there are lithologic changes such as Fln→ST→ Fln→ST for the first, Fln→Fll→ST→Scch→Sch→ST→Fll→Fln for the second, and

Fln→Fll→ST→Sch→ST→Fll→Fln for the third and last one. Within these progradational cycles, major changes are found in the distribution of the sedimentary facies. I interpret the succession or arrangement of the sedimentary facies correlated to the north-south migration of the megafan, which develop the patterns of the sub-cycles facies nested within the progradational cycles. These features indicate a history of a dynamic fluvial system with a sedimentary evolution in the east-west and north-south axes during crustal shortening and the accommodation space available in the foreland basin.

Interpretation of NWA Geochronology and Sedimentary Environment

The modern depositional systems of the Chaco Basin foredeep provide an analogy for use in considering the possible physical relationships between the three Upper Miocene columns studied. Figure 25 illustrates the scale and spatial relationships that likely existed between the three columns during the Late Miocene, as the strata of the First and Second Progradational Cycles accumulated. On the premise that the modern north-trending orientations of the major Subandean thrust faults were expressed during the Late Miocene as north-trending topographic constraints on the basin margin that was cut by east-trending river valleys that drained into the basin, the La Porcelana section seems likely to have been located comparatively distal to both the Iruya and Peña Colorada locations whereas the Peña Colorada section was located along-strike relative to the Iruya location. One hypothesis is that, over long periods of time, a set of megafans fed from major catchment basins might remain relatively stationary, filling the available accommodation space through frequent shifts in the locus of deposition that sweep the entire fan surface. An alternative hypothesis is that the long-term history of a megafan might involve persistence over hundreds of thousands of years in consistent locations, starving some parts of the basin, followed

by significant and long-lived shifts in the axis of deposition to in-fill the parts of the basin that had previously received little sediment. In theory, the correlations among the three columns deposited in the foredeep basin might either reflect relatively complete and consistent deposition throughout the space they represent, reflective of the first hypothesis for long-term megafan behavior, or might display spatially variable correlations with substantial incompleteness of the record, reflective of the second hypothetical mode. The character of the correlations among the columns provides insight to which of these styles of megafan dynamics occurred.

Figures 4 and 12 display the three columns in a spatial relationship to one another that approximates their arrangement in a mega-fan geometry (Figure 25). All three locations can be correlated to the Magnetic Polarity Time Scale such that the base of the First Progradational Cycle is progressively younger with increasing distance from the presumed position of the megafan: ~11.5 Ma at the Iruya River, ~11.1 Ma at Peña Colorada, and 9.5 Ma at La Porcelana. According to the best chosen correlations of the Peña Colorada and La Porcelana sections (Figure 12), the contact between the First and Second Progradational Cycles at all three sites was an unconformity, with a hiatus of 0.5 to ~1 million years duration. While the Iruya and La Porcelana hiatuses can be simultaneous, the plausible correlation at Peña Colorada indicates that its sequence boundary is not simultaneous. Instead, the sequence boundary at Iruya and La Porcelana seems to be nearly a million years younger than the sequentially similar sequence boundary at Peña Colorada. The conformable base of the Third Progradational Sequence is approximately correlative at all three locations. This could mean that the sediment deposition of the megafan move toward the north direction during the Second Progradational Cycle producing starvation at the Iruya and La Porcelana sections and later the megafan was displaced southward producing an unconformity later in time.

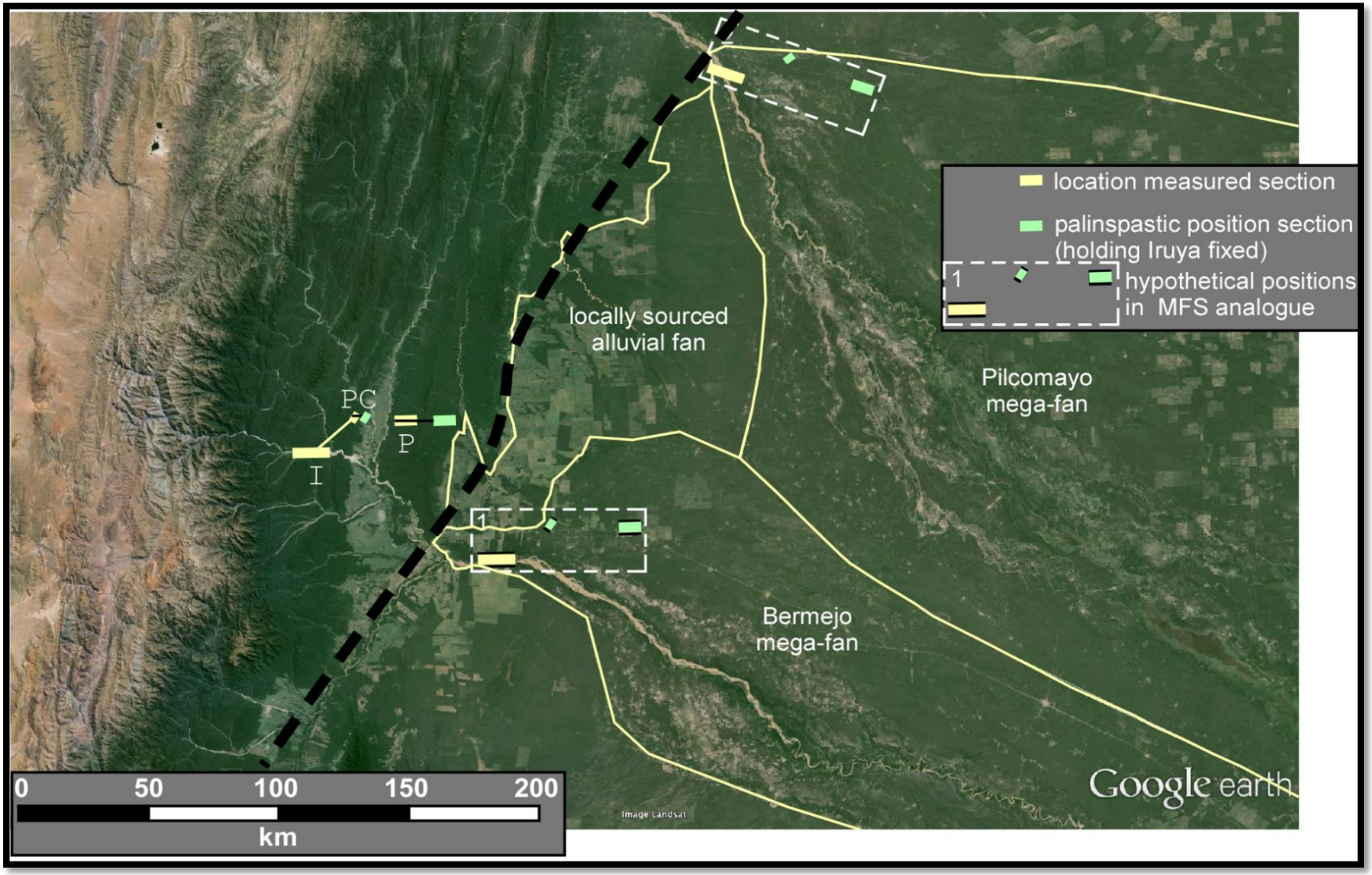
location measured section
palinspastic position section (holding Iruya fixed)
1
hypothetical positions in MFS analogue
locally sourced alluvial fan
Pilcomayo mega-fan
Bermejo mega-fan
PC
P
I
1
0
50
100
150
200
km
Image Landsat
Google earth

Figure 25: Palinspastic Analysis
Left of black dashed line, map indicates the modern locations of three studied section in the Subandean thrust belt (I, Iruya; PC, Peña Colorada; P, La Porcelana). Right of dashed black line, the boundaries are mapped between two megafans that are produced by two major river catchments, the Bermejo and Pilcomayo River, and smaller alluvial systems fed from local drainage basins. On the modern fans, two options are shown for the palinspastically restored relative positions of the three sections at the time of deposition in a megafan environment. Numerous other options can be imagined that conserve the true spatial relationships between the three Miocene locations.

The eastward advance of the megafan is recorded by the three progradational cycles explained here and by Echevarría et al (2003) and Hernández et al. (1996). The sedimentary record is similar to the sequences of facies described by Hartley and Weissmann (2010) for the modern DFS at Bermejo River. Uba et al (2005) findings at the Pilcomayo sedimentary record are also analogous to the modern DFS that corresponds to the southern Bolivian river. Both if these modern systems are also explained by Hartley and Weissmann (2010), which explains how the Bermejo DFS consists from a braided river system at the basin section closest to the mountain front, and turning into a meandering system over 100 km eastward. This is consistent with the findings at the sections studied here, where the three of them present a braided river system and other modern DFS described by Shukla (2009), or Shukla and Singh (2004). However the main differences in our interpretations rely on their description of a classical fluvial system from mountain front alluvial fans to lowland deposits described as playa-lake. In contrast, the new descriptions lead to the interpretation of a Distributary Fluvial System that still persist today as the Bermejo megafan.

Seismic Stratigraphy: DFS Sedimentary Environment

Seismic stratigraphic analysis of the foreland basin fill within the study area is designed to illuminate the architecture of the sedimentary package at a larger spatial scale than visible with the lithostratigraphic columns developed during field work. The larger scale provides the opportunity for insights closer to the tectonic scale, such as subsidence and geometries of sequence boundaries. Seismic Line 27202 (Figure 26) crosses near the upper limit of the stratigraphic column studied along the Iruya River. A 10-km-long segment of the line represents a South-North profile (Figure 27).

In accord with the geometries developed by the strong reflections, three seismic stratal sequences were identified. The First one located around 5000 m is planar with parallel internal reflections. The second one is located around 4500 m in depth and even though seems planar as the previous section mentioned above, this one contain no clear internal structure or a lack of any strong reflection. The last sequence above 4500 m is formed by a series of truncations and onlaps with reflections dipping north.

The lower sector of the seismic profile presents a series of strong reflections (depths approximately 5000–5500 m) comprised of three to four reflections. The middle ones have defined lateral continuity, though the uppermost and lowermost ones grade laterally to zones with little reflectivity (Figure 27). The next overlying zone (approximately 4200-5000 m depth) is characterized by a series of "fuzzy" or weak reflections. Above the 4000 meter level, there follows a set of seismic reflections of intermediate strength that are laterally discontinuous, in which truncations and onlap can be observed.

Figure 27 shows the mapped terminations of reflections. Below 4000 m these erosional truncations and onlaps define three sequence boundaries. Above 4000 m, there are numerous truncations and onlaps that do not occur near horizons that extend across the 10 km line distance. The lowest sequence boundary, below 5000 m, separates reflections that are moderately incline and truncate upward, from laterally extensive reflections above. The next higher sequence boundary, which is near 4700 m depth along the left side of Figure 27, separates two nearly parallel bodies of reflections and is identified primarily on the base of subtle truncations near the south side of this segment of the seismic profile. The third sequence boundary, highlighted particularly by a pair of onlap terminations, intersects the left side of Figure 27 near 4200 m depth. The truncations and


N
64°30'0"W
Bolivia
22°30'0"S
Argentina
22°30'0"S
La
Porcelana
Peña
Colorada
Pescado River
27202
Iruya River
Iruya
23°0'0"S
23°0'0"S
64°30'0"W
9 4.5 0 9 Kilometers

Figure 26: Seismic Line 27202 Location Map
The seismic line section studied for this research is about 22 km in length of an almostv 50 km seismic line. The section studied at Figure 27 is presented in the small box at the left of Iruya River study.

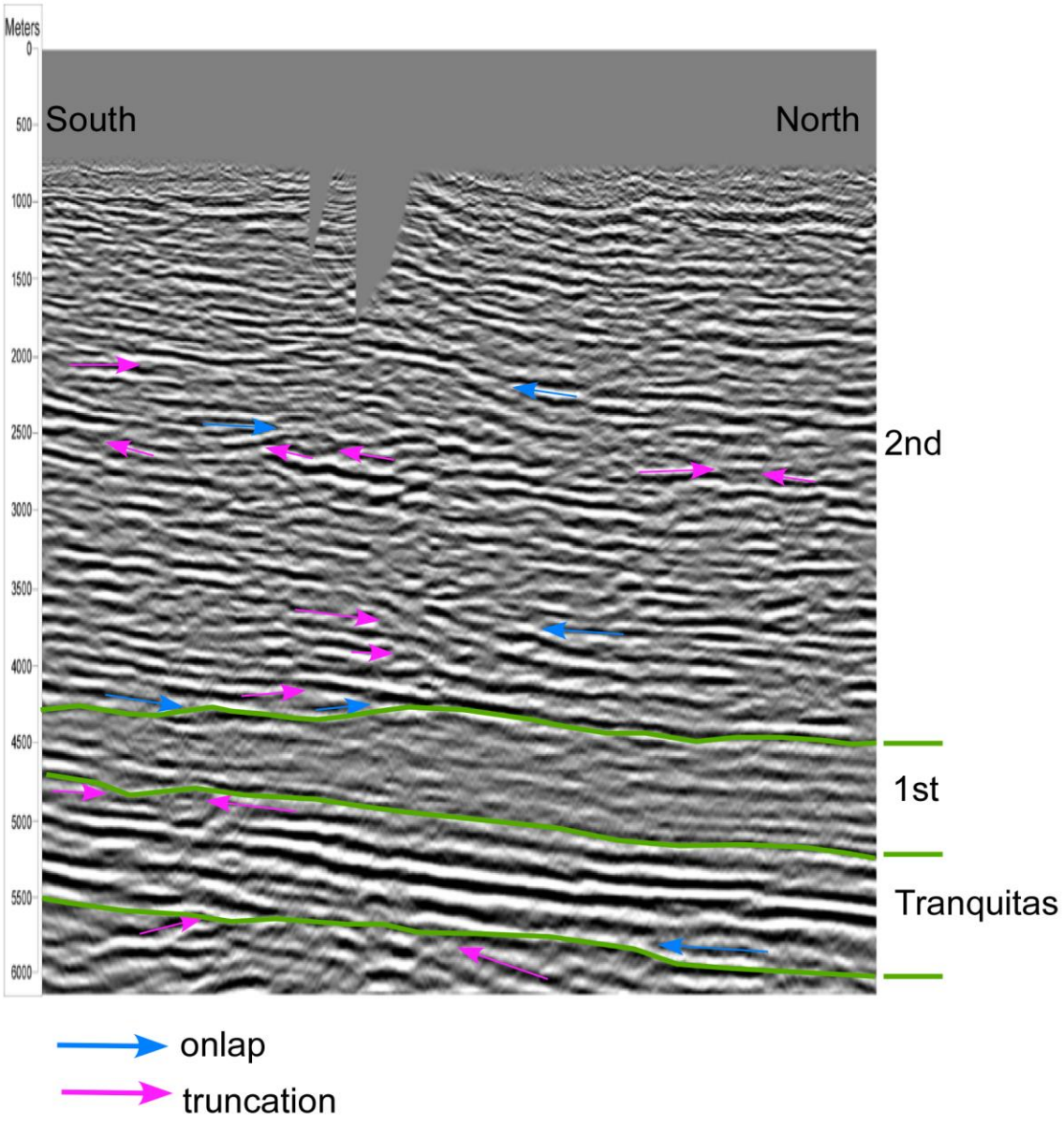
Meters
0
500
1000
1500
2000
2500
3000
3500
4000
4500
5000
5500
6000
South
North
2nd
1st
Tranquitas
onlap
truncation

Figure 27: Depth-converted Seismic Line 27202
This figure presents the seismic geometries and their correlation between Tranquitas, the First, and Second Progradational Cycles.

onlaps above 4000 m are suggestive of a body of rock composed of a set of small scale channel systems, which could be utilized to define parasequences.

Between the two lowest sequence sequence boundaries, the reflections (orange lines, Figure 28A) (5000–5500 m) are strong and laterally continuous. This sequence of reflection is about 500-600 m in thickness. Between the second and third sequence boundaries, the body of rock displays very weak reflections, for which only the base and top reflections are strong enough to readily traced laterally (green lines).

The reflections above the third sequence boundary, near 4000 m depth, highlighted by purple-blue lines (Figure 28) are discontinuous laterally, arranged in packages of either strong or weak reflectivity. Only the lowest set of reflections above the base of this upper sequence has good lateral continuity. Near the mid-point of the seismic line between 3500–4000 m depth, reflection truncations and onlaps patterns in combination with gently inclined reflections suggest a channel form several kilometers wide. Above that level there is less lateral continuity of any of the reflection, and several additional cases of inclined reflections suggest channel forms. In accord with the observations and characterization of the seismic reflectivity, three seismic facies domains were identified (Figure 28B).

The depth section to the stratigraphic column is compared to the stratigraphic column, adjusted in height for the location where the seismic profile crosses the river profile (Figure 28). In general, the short section of uppermost Tranquitas Formation measured in the Iruya River column appears to coincide with the sequence dominated by strong and laterally continuous reflections. The First Progradational Cycle and Second Progradational Cycle generally coincide with the two overlying seismic stratigraphic sequences. As described above, a revised correlation of the Iruya magnetic polarity zones to the global time scale means suggests about 500 m of strata

in the Second Progradational Cycle may be repeated by faulting (Figure 4) and that the stratigraphic section in an unfaulted location is thinner than measured in the field. For that revision of the column thickness, the interpretation for the correspondence of the stratigraphic column to the seismic profile is shown in Figure 29 (left column).

Interpretations

The lowest sequence boundary separates deformed strata from near horizontal reflectors, and therefore likely corresponds to the base of the Tranquitas Formation. With that as a starting horizon, the three seismic sequences identified for seismic profile of Line 27202 correspond to the (I) Tranquitas Fm, (II) First Progradational Cycle, and (III) Second Progradational Cycle (Figure 12 and 29). Tranquitas Formation is characterized by sandstones with paleosols, where paleosols tend to be identified commonly as unconformities in seismic profiles (Ruskin, 2007). However, even though Tranquitas Formation is known for exhibit paleosols, seismic reflections of Line 27202 do not represent clearly any evidence of internal truncation. Nevertheless, the top of Tranquitas Formation can be easily identified by a well-defined reflection dividing Tranquitas Formation from the base of the First Progradational Cycle. This reflection if observed as an unconformity in the field as the result of the difference in time between the Salta and Oran Group sedimentary deposition. This will be represented by the first seismic facies domain presented by the orange lines and Roman Numeral I. The thickness of that sequence is compatible with the literature, which presents Tranquitas Fm with thickness up to 600 m. The second seismic sequence, corresponding to the First Progradational Cycle, lacks reflection, probably as the result of the homogeneity of the strata formed mainly by mudstones. The uppermost seismic sequence represents the thickest section, about 2500 m thick. The seismic facies suggests lateral

discontinuities of sediment delivery systems. Geometries include mound-like morphologies that can be correlated with fluvial ridges, broad concave-up reflections that appear to be channels, and the onlap of short segments of the reflections suggesting lateral displacement of the fluvial system. This set of reflection and termination geometries could result from the focusing of deposition within a megafan around the major distributary channels, and movement laterally of those channel locations through time to develop a three-dimensional Distributary Fluvial System.

The differences in seismic reflectivity between the First Progradational Cycle and the Second Progradational Cycle presented as a homogeneous sequence and a heterogeneous sequence respectively, could be due to the sedimentary facies representing proximal versus distal deposits. The distal deposits represented by the First Progradational Cycle are formed by mudstones and sandstones alternations with mudstones been deposited continuous and the most dominant deposit. On the other hand, the Second Progradational Cycle consists on a combination between mudstones and sandstones, but sandstones at this stratigraphic section are formed by channels deposits where the erosion and cannibalization of the floodplains not only promote erosional surfaces but a discontinuity of the stratigraphic sequence and timeline.

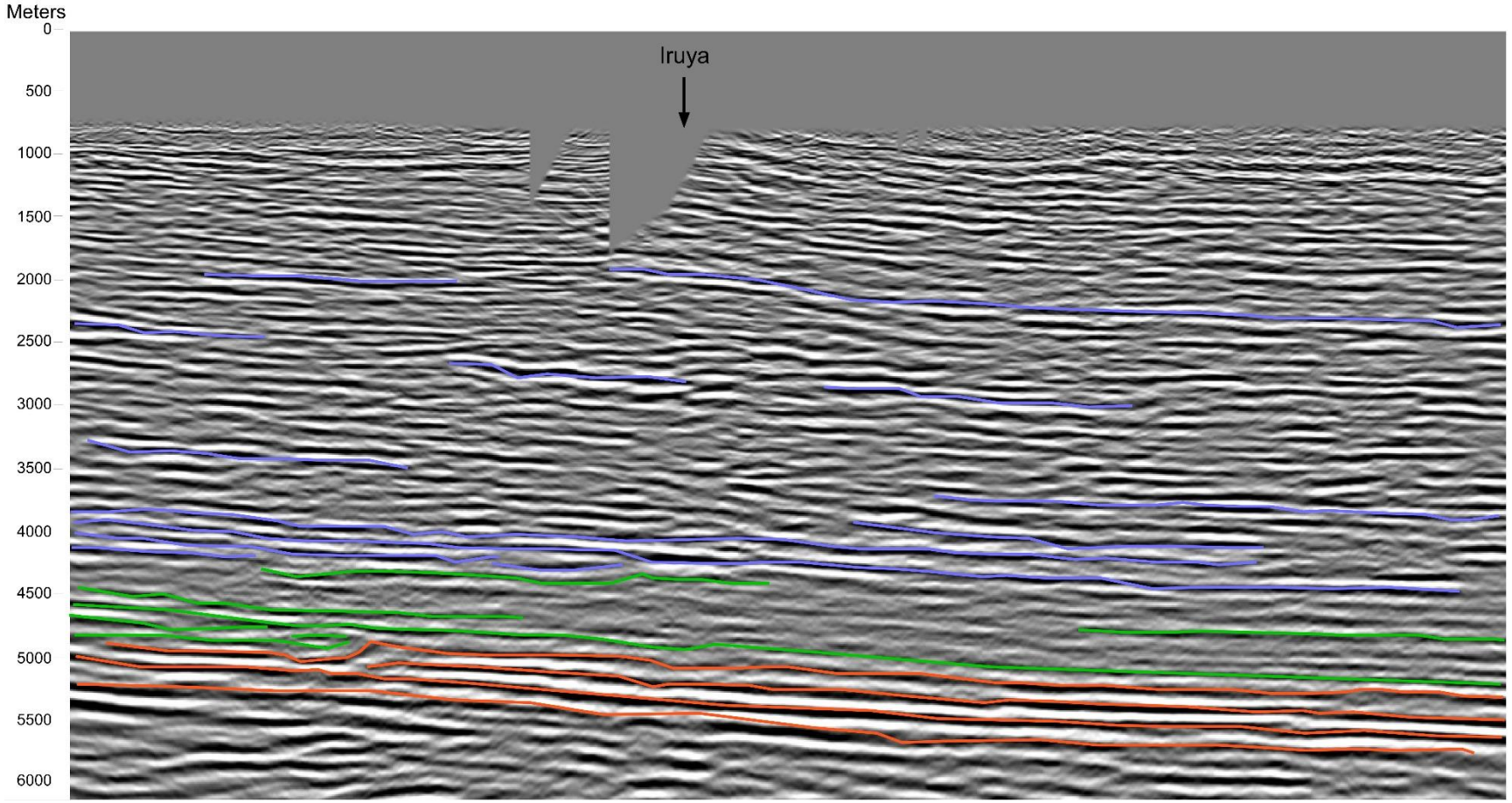
Meters
0
500
1000
1500
2000
2500
3000
3500
4000
4500
5000
5500
6000
Iruya

Figure 28: Seismic Facies and Unconformity Interpretation of Depth-Converted Seismic Line 27202, With The Location of the Iruya River Marked
Coloured lines represent strong seismic reflections with a nticieable lateral continuity. The Orange lines al reflections inbterpreted as Tranquitas Formation sequences, green lines are interpreted as the First Progradational Cycle, and blue lines as the Second Progradational Cycle.

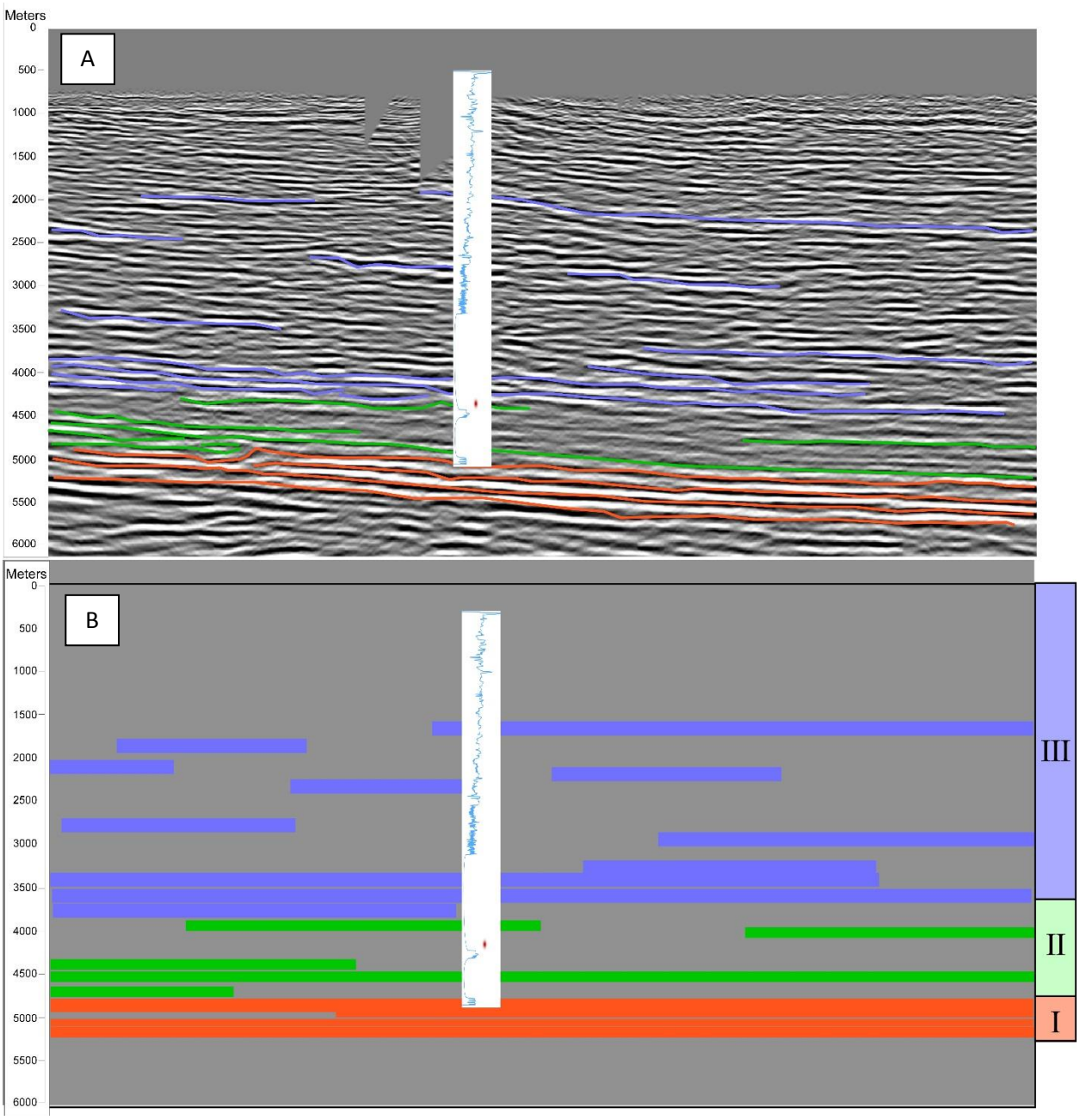
Meters
0
500
1000
1500
2000
2500
3000
3500
4000
4500
5000
5500
6000
A
Meters
B
III
II
I

Figure 29: Seismic Facies and Wheeler Diagram
A) Seismic facies and unconformity interpretation of depth-converted seismic Line 27202, with the location of the Iruya River marked and the Iruya stratigraphic column superimposed based on position that the seismic line crosses the outcrop belt and on comparison of the estimated seismic depth to the column thickness. Lines represent the contonuity opf seismic reflections, and the colors are the reflections for three stratrigraphic sequence domains (Roman numbers), and the colors orange, green, and blue are the sedimentary interpretation for Tranquitas Formation, First, and Second Progradational Cycles respectively. B) It is a Wheeler Diagram for the seismic reflections in Figure A.

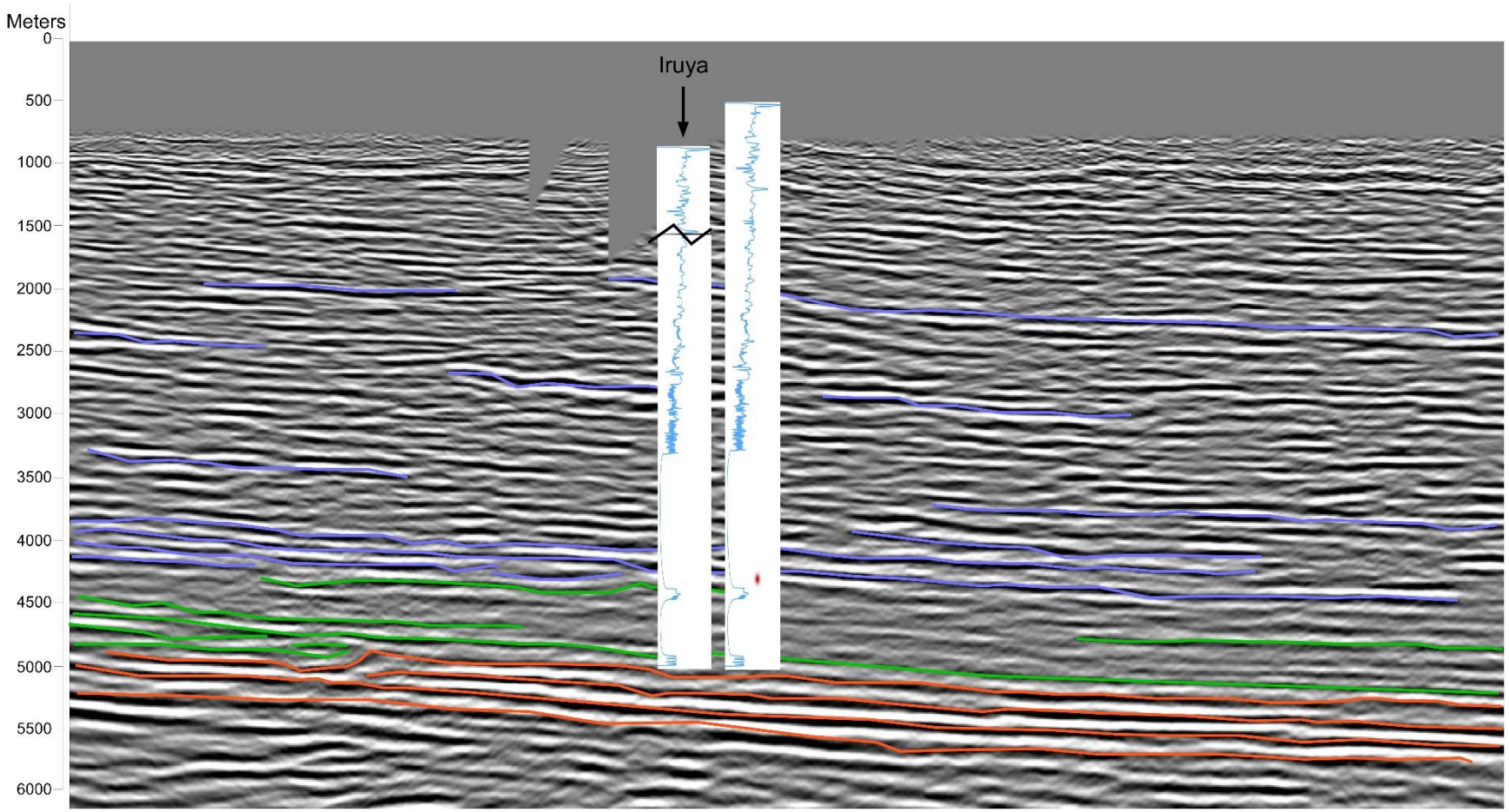
Meters
0
500
1000
1500
2000
2500
3000
3500
4000
4500
5000
5500
6000
Iruya

Figure 30: Seismic Profile and Possible Stratigraphic Repetition by Faulting Correlation
A) Depth-converted seismic Line 27202, with the location of the Iruya River marked and the Iruya stratigraphic column superimposed based on position that the seismic line crosses the outcrop belt. Two alternative correlations are shown, reflecting (right) the reported thicknesses (Hernández et al 1996) compared to column (left) if the ~500 m fault repetition inferred from the magnetostratigraphic correlation is removed from the column.

Conclusions

The vertical and lateral distributions of sedimentary facies in the First, Second and lowermost Third Progradational Cycles represent a Distributary Fluvial System, and the spatial relations are compatible with all three locations receiving sediment from a single shared megafan whose position was somewhere near the Río Iruya. The division of the strata into three cycles implies that the megafan migrated along an axis that changed position three times.

The largest scale control on changes in the stratigraphic record corresponds to the progradational cycles described by Starck and Schultz (1996); Hernández et al. (1996), and Echevarría et al (2003). This produced an end result of the three stacked coarsening upward sequences. I accept those authors' interpretation that these cycles were caused by unsteady eastward steps in the basin-margin faults or folds that controlled the position of the megafan head.

The second order of sedimentary control was the subsidence in the synclinal divisions of the foreland that formed in the wedge-top zone, which increased the accommodation space of the Iruya and Peña Colorada zones allowing the high preservation of strata, but not at La Porcelana (Echevarría et al., 2003). This control is registered by the especially thick section at the Iruya River, as well as the difference in sedimentary facies where floodplains and channel deposits are more abundant and better preserved.

The third order of sedimentary control is the dynamics of the megafan or DFS. For the geographic relations of the study area, the lateral displacement of the megafan represents a north-south migration of the system. This can be observed in the seismic profile in the Second Progradational Cycle, or uppermost seismic sequence, where lateral displacement of the sedimentary environment is represented by truncations and onlap.

This set of analyses implies that the Distributary Fluvial System environment has dominated the foreland basin for at least 14 million years. The First and Second Progradational Cycles are interpreted to be tectonically driven by pulses of accommodation space and movement of the topographic front. The sub-cycles are interpreted to result from the autogenic lateral migration of the DFS. Neither tectonic activity nor climate change are needed to explain those lateral shifts. The facies of the first two progradational cycles are repetitive which implies that there was no major climate change between 12 Ma and 5 Ma.

References

Adams, C. J., et al. The Puncoviscana Formation of northwest Argentina: U-Pb geochronology of detrital zircons and Rb-Sr metamorphic ages and their bearing on its stratigraphic age, sediment provenance and tectonic setting. *Neues Jahrbuch für Geologie und Paläontologie-Abhandlungen* 247.3 (2008): 341-352.

Allmendinger, R. W., and Gubbels, T., 1996, Pure and simple shear plateau uplift, Altiplano-Puna, Argentina and Bolivia: Tectonophysics, v. 259, no. 1-3, p. 1-13.

Allmendinger, R. W., Jordan, T. E., Kay, S. M., and Isacks, B. L., 1997, The evolution of the Altiplano-Puna plateau of the Central Andes: Annual Review of Earth and Planetary Sciences, v. 25, p. 139-174.

Amidon, W.H., Luna, L.V., Fisher, G.B., Burbank, D.W., Kylander-Clark, A.R.C. & Alonso, R., 2015: Provenance and tectonic implications of Orán Group foreland basin sediments, Río Iruya canyon, NW Argentina (23°S). Basin Research, 10.1111/bre.12139

Augustsson, C., Rüsing, T., Adams, C. J., Zimmermann, U., Chmiel, HKocabayoglu, M., Büld, M., Berndt, J. & Kooijman, E., 2011: Detrital quartz and zircon combined: the production of mature sand with short transportation paths along the Cambrian west Gondwana margin, NW Argentina, Journal of Sedimentary Research 81, 284-298

Augustsson, C. & Bahlburg, H., 2008: Provenance of late Palaeozoic metasediments of the Patagonian proto-Pacific margin (southernmost Chile and Argentina), International Journal of Earth Sciences 97, 71-88.

Augustsson, C., Münker, C., Bahlburg, H. & Fanning, C. M., 2006: Provenance of late Palaeozoic metasediments of the SW South American Gondwana margin: a combined U-Pb and Hf-isotope study of single detrital zircons, Journal of the Geological Society 163, 1-13.

Augustsson, C. & Bahlburg, H., 2003: Cathodoluminescence spectra of detrital quartz as provenance indicators for Paleozoic metasediments in southern Andean Patagonia, Journal of South American Earth Sciences 16:1, 15-26.

Baby, P., Herail, G., Lopez, J. M., Lopez, O., Oller, J., Pareja, J., Sempere, T., and Tufino, D., 1989, Structure of The Subandean Belt of Bolivia - Influence of The Pre-Orogenic Sedimentary Pile Geometry on Thrust Propagation: Comptes Rendus De L Academie Des Sciences Serie Ii, v. 309, no. 17, p. 1717-1722.

Barbeau, D. L., Gombosi, D. J., Zahid, K. M., Bizimis, M., Swanson-Hysell, N., Valencia, V., and Gehrels, G. E., 2009, U-Pb zircon constraints on the age and provenance of the Rocas Verdes basin fill, Tierra del Fuego, Argentina: Geochemistry Geophysics Geosystems, v. 10.

Bennett, G. L., Weissmann, G. S., Bakeo, G. S., and Hyndman, D. W., 2006, Regional-scale assessment of a sequence-bounding paleosol on fluvial fans using ground-penetrating radar, eastern San Joaquin Valley, California: Geological Society of America Bulletin, v. 118, no. 5-6, p. 724-732.

Ingersoll, RV and Busby, CJ, 1995, Tectonics of sedimentary basins: In, CJ Busby and RV Ingersoll (Eds.), Tectonics of Sedimentary Basins, Blackwell Science, p. 1-52

Cardozo, N., and Jordan, T., 2001, Causes of spatially variable tectonic subsidence in the Miocene Bermejo Foreland Basin, Argentina: Basin Research, v. 13, no. 3, p. 335-357.

Carrapa, B., Bywater-Reyes, S., DeCelles, P.G., Mortimer, E., and Gerhels, G. (2012), Cenozoic synorogenic basin evolution in the Eastern Cordillera of northwestern Argentina (25°-26°S): Regional implications for Andean orogenic wedge development, Basin Research,

v. 23, 1– 20
Carrapa, B., and DeCelles, P. G., 2008, Eocene exhumation and basin development in the Puna of northwestern Argentina: Tectonics, v. 27, no. 1.
Collo, G., Astini, R.A., Cawood, P.A., Buchan, C., and Pimentel, M., 2008, U–Pb detrital zircon ages and Sm–Nd isotopic features in low-grade metasedimentary rocks of the Famatina belt: implications for late Neoproterozoic–early Palaeozoic evolution of the proto-Andean margin of GondwanaJournal of the Geological Society, v. 166:303-319
Davila, F. M., Astini, R. A., Jordan, T. E., Gehrels, G., and Ezpeleta, M., 2007, Miocene forebulge development previous to broken foreland partitioning in the southern Central Andes, west-central Argentina: Tectonics, v. 26, no. 5.
DeCelles, P. G., Carrapa, B., and Gehrels, G. E., 2007, Detrital zircon U-Pb ages provide provenance and chronostratigraphic information from Eocene synorogenic deposits in northwestern Argentina: Geology, v. 35, no. 4, p. 323-326.
DeCelles, P. G., Carrapa, B., Horton, B. K., and Gehrels, G. E., 2011, Cenozoic foreland basin system in the central Andes of northwestern Argentina: Implications for Andean geodynamics and modes of deformation: Tectonics, v. 30.
DeCelles, P. G., and Cavazza, W., 1999, A comparison of fluvial megafans in the Cordilleran (Upper Cretaceous) and modern Himalayan foreland basin systems: Geological Society of America Bulletin, v. 111, no. 9, p. 1315-1334.
DeCelles, P. G., and Horton, B. K., 2003a, Early to middle Tertiary foreland basin development and the history of Andean crustal shortening in Bolivia: Geological Society of America Bulletin, v. 115, no. 1, p. 58-77.
-, 2003b, Early to middle Tertiary foreland basin development and the history of Andean crustal shortening in Bolivia: Geological Society of America Bulletin, v. 115, no. 1, p. 58-77.
Echevarría, L., Hernandez, R., Allmendinger, R., and Reynolds, J., 2003, Subandean thrust and fold belt of northwestem Argentina: Geometry and timing of the Andean evolution: Aapg Bulletin, v. 87, no. 6, p. 965-985.
Flemings, P. B., and Jordan, T. E., 1989, A synthetic stratigraphic model of foreland basin development: Journal of Geophysical Research-Solid Earth and Planets, v. 94, no. B4, p. 3851-3866.
-, 1990, Stratigraphic Modeling of Foreland Basins - Interpreting Thrust Deformation and Lithosphere Rheology: Geology, v. 18, no. 5, p. 430-434.
Flemings, P. B., Jordan, T. E., and Reynolds, S., 1986, FLEXURAL ANALYSIS OF 2 BROKEN FORELAND BASINS - LATE CENOZOIC BERMEJO BASIN AND EARLY CENOZOIC GREEN RIVER BASIN: Aapg Bulletin-American Association of Petroleum Geologists, v. 70, no. 5, p. 591-591.
Folguera, A., Bottesi, G., Duddy, I., Martín-González, F., Orts, D., Sagripanti, L., Vera, E.R., and Ramos, V.A., 2015, Exhumation of the Neuquén Basin in the southern Central Andes (Malargüe fold and thrust belt) from field data and low-temperature thermochronology: Journal of South American Earth Sciences, v. 64, p. 381–398
Galli, C.I., and Hernandez, R.M., 1999, Evolucion de la Cuenca de Antepais dese la zona de la Cumbre Calchaqui hasta la Sierra de Santa Barbara, Eoceno inferior - Mioceno medio, provincia de Salta, Argentina:Acta Geologica Hispanica, v. 34, no. 2-3, p. 167-184.
Galewsky, J., 2009: Orographic precipitation isotope ratios in stratified atmospheric flows: Implications for paleoelevation studies, Geology, v37, pp. 791-794
Garreaud, R. D., Molina, A., and Farias, M., 2010, Andean uplift, ocean cooling and Atacama

hyperaridity: A climate modeling perspective: Earth and Planetary Science Letters, v. 292, no. 1-2, p. 39-50.
Garreaud, R. D., Vuille, M., Compagnucci, R., and Marengo, J., 2009, Present-day South American climate: Palaeogeography Palaeoclimatology Palaeoecology, v. 281, no. 3-4, p. 180-195.
Garreaud, R., Vuille, M., and Clement, A. C., 2003, The climate of the Altiplano: observed current conditions and mechanisms of past changes: Palaeogeography Palaeoclimatology Palaeoecology, v. 194, no. 1-3, p. 5-22.
Garzione, C.N., Auerbach, D.J., Smith, J.J.S., Rosario, J.J., Passey, B.H., Jordan, T.E., Eiler, J.M., 2014. Clumped isotope evidence for diachronous surface cooling of the Altiplano and pulsed surface uplift of the Central Andes. Earth Planet. Sci. Lett. 393, 173–181
Gebhard, J., 1974, Estudios geologicos en el area comprendida entre el Rio Santa Maria y de Las Piedras, Prov. De Salta Y Jujuy. YPF. Informe Inedito
Gehrels, G., Kapp, P., DeCelles, P., Pullen, A., Blakey, R., Weislogel, A., Ding, L., Guynn, J., Martin, A., McQuarrie, N., and Yin, A., 2011, Detrital zircon geochronology of pre-Tertiary strata in the Tibetan-Himalayan orogen: Tectonics, v. 30.
Gehrels, G., V. Valencia, and A. Pullen (2006), Detrital zircon geochronology by Laser-Ablation Multicollector ICPMS at the Arizona LaserChron Center, in *Geochronology: Emerging Opportunities Pap. 12*, edited by T. Loszewski, and W. Huff, pp. 67–76, Paleontol. Soc., Washington, D. C.
Gubbels, T. L., Isacks, B. L., and Farrar, E., 1993, High-Level Surfaces, Plateau Uplift, And Foreland Development, Bolivian Central Andes: Geology, v. 21, no. 8, p. 695-698.
Hartley, A. J., Weissmann, G. S., Nichols, G. J., and Warwick, G. L., 2010, Large distributive fluvial systems: characteristics, distribution, and controls on development: Journal of Sedimentary Research, v. 80, no. 1-2, p. 167-183.
Hernández, R. M., and L. Echavarria (2009), Faja plegada y corrida Subandina del noroeste Argentina: Estratigrafía, geometría y cronología de la deformación, Asoc. Geol. Argent. Rev., 65, 68–80.
Hernández, R. M., J. Reynolds, and A. Di Salvo, 1996, Análisis tectosedimentario y ubicación geocronológica del Grupo Oraán en el río Iruya: Boletín de Informaciones Petroleras, Tercera Epoca, v. 45, p. 80–93.
Hernandez, R.M., Jordan, T.E., Dalenz Farjat, A., Echevarria, L., Idleman, B.D., Reynolds, J.H., 2005, Age, Distribution, Tectonics, and eustatic controls of the Paranense and Caribbean marine transgressions in southern Bolivia and Argentina: Journal of South American Earth Sciences, v. 19, p. 495-512.
Horton, B. K., Constenius, K. N., and DeCelles, P. G., 2004, Tectonic control on coarse-grained foreland-basin sequences: An example from the Cordilleran foreland basin, Utah: Geology, v. 32, no. 7, p. 637-640.
Horton, B.K., 1998, Sediment accumulation on top of the Andean orogenic wedge: Oligocene to late Miocene basins of the Eastern Cordillera, southern Bolivia: Geological Society of America Bulletin, v. 110, p. 1174–1192.
Horton, B. K., and DeCelles, P. G., 1997, The modern foreland basin system adjacent to the Central Andes: Geology, v. 25, no. 10, p. 895-898.
-, 2001, Modern and ancient fluvial megafans in the foreland basin system of the central Andes, southern Bolivia: implications for drainage network evolution in fold-thrust belts: Basin Research, v. 13, no. 1, p. 43-63.

Husson, L., and Moretti, I., 2002, Thermal regime of fold and thrust belts - an application to the Bolivian sub Andean zone: Tectonophysics, v. 345, no. 1-4, p. 253-280.
Isacks, B. L., 1988, Uplift of the Central Andean Plateau and bending of the Bolivian Orocline: Journal of Geophysical Research-Solid Earth and Planets, v. 93, no. B4, p. 3211-3231.
Johnston, S., Gehrels, G., Val;encia, V., Ruiz, J., 2009, Small volume U-Pb geochronology by laser ablation multicollector ICP-MS. Chemical Geology, v. 259, iss. 3-4, p. 218-229
Jordan, T. E., Schlunegger, F., and Cardozo, N., 2001, Unsteady and spatially variable evolution of the Neogene Andean Bermejo foreland basin, Argentina: Journal of South American Earth Sciences, v. 14, no. 7, p. 775-798.
Jordan, T.E., 1995, Retroarc Foreland and Related Basins, chapter in C. Busby and R. Ingersoll, eds., Tectonics of Sedimentary Basins: Blackwell Scientific Publications, p. 331-362.
Jordan, T.E., Flemings, P.B., and Beer, J.A., 1988, Dating thrust fault activity by use of foreland basin strata, in New Perspectives in Basin Analysis, Kleinspehn, K., and Paolo, C., editors: Springer-Verlag, p. 307-330.
Judge, P. A., and Allmendinger, R. W., 2011, Assessing uncertainties in balanced cross sections: Journal of Structural Geology, v. 33, no. 4, p. 458-467.
Kraus, M.J, 1992, Alluvial Response to Differential Subsidence - Sedimentological Analysis Aided by Remote-Sensing, Willwood Formation (Eocene), Bighorn Basin, Wyoming, USA: Sedimentology, v. 39, no. 3, p. 455-470.
Kraus, M.J., 1997, Lower Eocene alluvial paleosols: Pedogenic development, stratigraphic relationships, and paleosol/landscape associations: Palaeogeography Palaeoclimatology Palaeoecology, v. 129, no. 3-4, p. 387-406
Laffa, D.N., Sabat, F., Bello, D., Ferrer, O., Mon, R., Gutierrez, 2011. Tectonic inversion in a segmented foreland basin from extensional to piggy back settings: The Tucumán basin in NW Argentina. Journal of South American Earth Sciences, v. 31, p. 457-474
Lawrence, R. L., R. Cox, R. W. Mapes, and D. S. Coleman (2010), Hydrodynamic fractionation of zircon age populations, *Geol. Soc. Am. Bull.*, **123**, 295–305
Leier, A. L., DeCelles, P. G., and Pelletier, J. D., 2005, Mountains, monsoons, and megafans: Geology, v. 33, no. 4, p. 289-292.
Ludwig, K.R., 2003, Isoplot/EX version 3.0, A geochronological toolkit for Microsoft Excel: Berkeley Geochronology Center Special Publication.
Mack, G.; James, W.; Monger, H. Classification of paleosols. Geological Society of America Bulletin, v. 105, p. 129-136, 1993.
Martinod, J., Regard, V., LetourmyY., Henry, H., Hassani, R., Baratchart, S., Carretier, S., 2016. How do subduction processes contribute to forearc Andean uplift? Insights from numerical models. Journal of Geodynamics, v. 96, p. 6-18
Masek, J. G., Isacks, B. L., Gubbels, T. L., and Fielding, E. J., 1994, Erosion and Tectonics at The Margins of Continental Plateaus: Journal of Geophysical Research-Solid Earth, v. 99, no. B7, p. 13941-13956.
McQuarrie, N., and DeCelles, P., 2001, Geometry and structural evolution of the central Andean backthrust belt, Bolivia: Tectonics, v. 20, no. 5, p. 669-692.
McQuarrie, N., Horton, B. K., Zandt, G., Beck, S., and DeCelles, P. G., 2005, Lithospheric evolution of the Andean fold-thrust belt, Bolivia, and the origin of the central Andean plateau: Tectonophysics, v. 399, no. 1-4, p. 15-37.
Miall, A.D., 1996. The Geology of Fluvial Deposits. Springer-Verlag, New York
Mingram, A., y Russo, A., 1972, Sierras Subandinas y Chaco Salteno. En Leanza (ed.). Geologia

Regional Argentina. Acadf. Nac. Cs. Cba 185-221
Mortimer, E.J., Patom, D.A., Scholz, C.A., Styrecker, M.R., 2016. Implications of structural inheritance in oblique rift zones for basin compartmentalization: Nkhata Basin, Malawi Rift (EARS). Marine and Petroleum Geology, v. 72, p. 110-121

Mulch, A., Uba, C. E., Strecker, M. R., Schoenberg, R., and Chamberlain, C. P., 2010, Late Miocene climate variability and surface elevation in the central Andes: Earth and Planetary Science Letters, v. 290, no. 1-2, p. 173-182.
Posamentier, H. W., Allen, G. P., 1999, Siliciclastic sequence stratigraphy: concepts and applications. SEPM Concepts in Sedimentology and Paleontology no. 7, 210 pp.
Posamentier, H. W., Allen, G. P., James, D. P., 1992, High resolution sequence stratigraphy – the East Coulee Delta, Alberta. Journal of Sedimentary Petrology 62,2, 310– 317.
Rech, J. A., Currie, B. S., Michalski, G., and Cowan, A. M., 2006, Neogene climate change and uplift in the Atacama Desert, Chile: Geology, v. 34, no. 9, p. 761-764.
Reynolds, J. H., Damanti, J. F., and Jordan, T. E., 1991, Magnetostratigraphic constraints on the development of paired fold-thrust belts foreland basins in the Argentine Andes: Aapg Bulletin-American Association of Petroleum Geologists, v. 75, no. 3, p. 660-661.
Reynolds, J.H., Idleman, B. D., Hernandez, R. M., and Naeser, C. W., 1994, Preliminary chronostratigraphy constratints on Neogene tectonic activity in the Eastern Cordillera and Santa Barbara System, Salta Province, NW Argentina: Geological Societu of America Abstracts with Programs, v. 26, no. 7, p. A-503.
Reynolds, J. H., Galli, C. I., Hernandez, R. M., Idleman, B. D., Kotila, J. M., Hilliard, R. V., and Naeser, C. W., 2000, Middle Miocene tectonic development of the Transition Zone, Salta Province, northwest Argentina: Magnetic stratigraphy from the Metan Subgroup, Sierra de Gonzalez: Geological Society of America Bulletin, v. 112, no. 11, p. 1736-1751.

Rosario, J. J., Hernández, J., Hernández, R., and Jordan, T. (2008), Evolución tectono-sedimentaria durante el Terciario en la Provincia de Jujuy, Argentina (Tectonosedimentary evolution during the Tertiary in the Jujuy Province, Argentina) Geología y Recursos Naturales de la Provincia de Jujuy (B. Coira, ed.): XVII Congreso Geológico Argentino, IIF Ciclo Ándico - Etapa compresional (Paleógeno-Holoceno) - Geología, Relatorio, p. 263-285.
Ruskin, B. G., Davila, F. M., Hoke, G. D., Jordan, T. E., Astini, R. A., and Alonso, R., 2011, Stable isotope composition of middle Miocene carbonates of the Frontal Cordillera and Sierras Pampeanas: Did the Paranaense seaway flood western and central Argentina?: Palaeogeography Palaeoclimatology Palaeoecology, v. 308, no. 3-4, p. 293-303.
Ruskin, B. G., 2007, Sequence stratigraphy and paleopedology of nonmarine foreland basins: Iglesia Basin, Argentina and Axhandle Basin, Utah. Doctoral Thesis, Cprnell University, University, p. 1489-214, 2007-11-12T19:43:42Z
Russo, A., 1972, La Estratigrafia Terciaria en el Noroeste Argenino. V Congr. Geol. Argentino, Actas, J, 14.
Russo, A, y Serraiotto, A., 1978, Contribucion al conocimiento de la estratigrafia terciaria en el noroeste argemntino. VII Congreso Geologico Argentino, Neuquen, actas, 1, 715-730
Salvany, J. M., Larrasoana, J. C., Mediavilla, C., and Rebollo, A., 2011, Chronology and tectono-sedimentary evolution of the Upper Pliocene to Quaternary deposits of the lower Guadalquivir foreland basin, SW Spain: Sedimentary Geology, v. 241, no. 1-4, p. 22-39.

Shukla, U. K., 2009, Sedimentation model of gravel-dominated alluvial piedmont fan, Ganga Plain, India: International Journal of Earth Sciences, v. 98, no. 2, p. 443-459.
Shukla, U. K., and Singh, I. B., 2004, Signatures of palaeofloods in sandbar-levee deposits, Ganga Plain, India: Journal of the Geological Society of India, v. 64, no. 4, p. 455-460.
Shukla, U. K., Singh, I. B., Sharma, M., and Sharma, S., 2001, A model of alluvial megafan sedimentation: Ganga Megafan: Sedimentary Geology, v. 144, no. 3-4, p. 243-262.
Soman, A., Geisler, T., Tomaschek, F., Grange, M., Berndt, J., 2010: Alteration of crystalline zircon solid solutions: a case study on zircon from an alkaline pegmatite from Zomba–Malosa, Malawi. Contributions to Mineralogy and Petrology, v. 160, iss. 6, p. 909-930
Starck, D., and A. Schulz, 1996, La configuracio´n estructural del lı´mite entre Cordillera Oriental y Sierras Subandinas en el extremo norte de la Republica Argentina: Boletı´n de Informaciones Petroleras, Tercera Epoca, v. 52, p. 39–46.
Starck, D., Vergani, G., 1996, Desarrollo Tectosedimentario del Cenozoico en el sur de la provinvia de Salta, Argentina: XIII Congr. Geol. Arg. Y III Congr. Exploracion de Hidrocarburos, Actas I, p. 433-452.
Uba, C. E., Heubeck, C., and Hulka, C., 2005, Facies analysis and basin architecture of the Neogene Subandean synorogenic wedge, southern Bolivia: Sedimentary Geology, v. 180, no. 3-4, p. 91-123.
-, 2006, Evolution of the late Cenozoic Chaco foreland basin, Southern Bolivia: Basin Research, v. 18, no. 2, p. 145-170.
Uba, C. E., Strecker, M. R., and Schmitt, A. K., 2007, Increased sediment accumulation rates and climatic forcing in the central Andes during the late Miocene: Geology, v. 35, no. 11, p. 979-982.
Uba, C.E., Kley, J., Strecker, M. R., and Schmitt, A. K., 2009, Unsteady evolution of the Bolivian Subandean thrust belt: The role of enhanced erosion and clastic wedge progradation: Earth and Planetary Science Letters 281 (2009) 134–146
Weissmann, G. S., Hartley, A. J., Nichols, G. J., Scuderi, L. A., Olson, M., Buehler, H., and Banteah, R., 2010, Fluvial form in modern continental sedimentary basins: Distributive fluvial systems: Geology, v. 38, no. 1, p. 39-42.

CHAPTER 3
PALEOCLIMATE HISTORY DURING THE EVOLUTION OF THE SUBANDEAN BELT BY USING OXYGEN, CARBON, AND CLUMPED ISOTOPES OF CARBONATES, NORTHWESTERN ARGENTINA

Abstract

Continental climate change history proves to be specific by region and established by the physical, chemical, and biological controls constrained in the area. This paper provides insights to the climate history and its variability on west-central South America during the Middle Miocene through the Early Pliocene, based on ancient soils, specifically carbonate nodule stable isotope geochemistry ($\delta^{18}O$, $\delta^{13}C$, Δ_{47}) and paleosol characterization. The strata containing the paleosols are exposed in the Subandean foothills, primarily along the Iruya River. Over thousands of meters of stratigraphic thickness spanning 14–5 Ma, the paleosols changed little, typified by the accumulation of allogenic clays and the precipitation of pedogenic calcium carbonate, in immature soil profiles whose most prominent horizon sequences are AC, BC, Bt, Bw, and Bk. The monotony of pedogenic development and compositions and microstructures of the paleosols suggest static climatic conditions, characterized by strong seasonality, throughout the time from the late Middle Miocene to the Pliocene. For paleosols formed between 8 Ma to 5 Ma, soil carbonate oxygen isotopes present values in the range between -10.5‰ to -4.5‰ (VPDB), and carbon isotopes with values between -12‰ to approximately -8‰ (VPDB). Oxygen isotopes represent stable climate conditions and no systematic variation through time, yet they reveal that climate or vegetation conditions produced soil carbonate that was consistently slightly more depleted than modern precipitation in the region. The carbon isotopes present a C3 plant dominance with a tendency toward slightly increased abundance of C4 plants after 7 Ma until 5 Ma. The soil carbonate Δ_{47} measurements imply paleotemperatures in the range between 28 to 44 ^{o}C. If the higher apparent paleotemperatures have not been diagenetically reset, they are suggestive of warm summers with values similar to modern summer temperatures. The middle Miocene to early Pliocene climate in Northwestern Argentina is interpreted to have been similar to modern climate with a minor increase in C4 plants around 6 Ma comparable to the global history of vegetation during this time.

It is concluded that the orographic barrier produced by the Central Andes created a stable climate for the Subandean Region that was established by the Middle Miocene.

Introduction

The topographic uplift of the Central Andes Mountains likely caused significant changes in the climate of west-central South America (e.g., Alpers and Brimhall, 1988; Sillitoe and McKee, 1996; Rech et al., 2006), causing strong differentiation of rainfall patterns on the eastern and western flanks of the highlands (Figure 1). Today at 21°S latitude, the west side of the Andes is the Atacama Desert and the east-side counterpart is the subtropical Subandean Belt and the Chaco Basin (Figure 1A). Alpers and Brimhall (1988) and Rech et al. (2006) interpreted that the climate in the Atacama Desert changed from semi-arid to hyperarid during the Middle Miocene due to uplift of the Central Andes, which enhanced the rain-shadow effect (Figure 1B). Subsequent studies have debated the timing of onset of hyperaridity as well as the importance of an Andean rain-shadow (Alpers and Brimhall, 1988; Sillitoe and McKee, 1996; Rech et al., 2006, Figure 1A and 1B). That set of studies raises the question of whether an increase in precipitation was registered on the opposite side of the Andes, the Subandean Belt (Figure 1B and 1C), during the same period of time. If it is correct that the growth of elevation of the Andes Mountains caused drying on the lee side, then enhanced orographic rise of air masses ought to have caused greater rain-out on the eastern side and more vigorous hydrological activity (Kleinert and Strecker, 2001; Garzione et al.; 2008; Ehlers and Poulsen, 2009; Mulch et al, 2010). If this coupled change in precipitation did not occur, then it is likely that an onset of hyperaridity in the Atacama Desert was due to causes other than the uplift of the Andes.

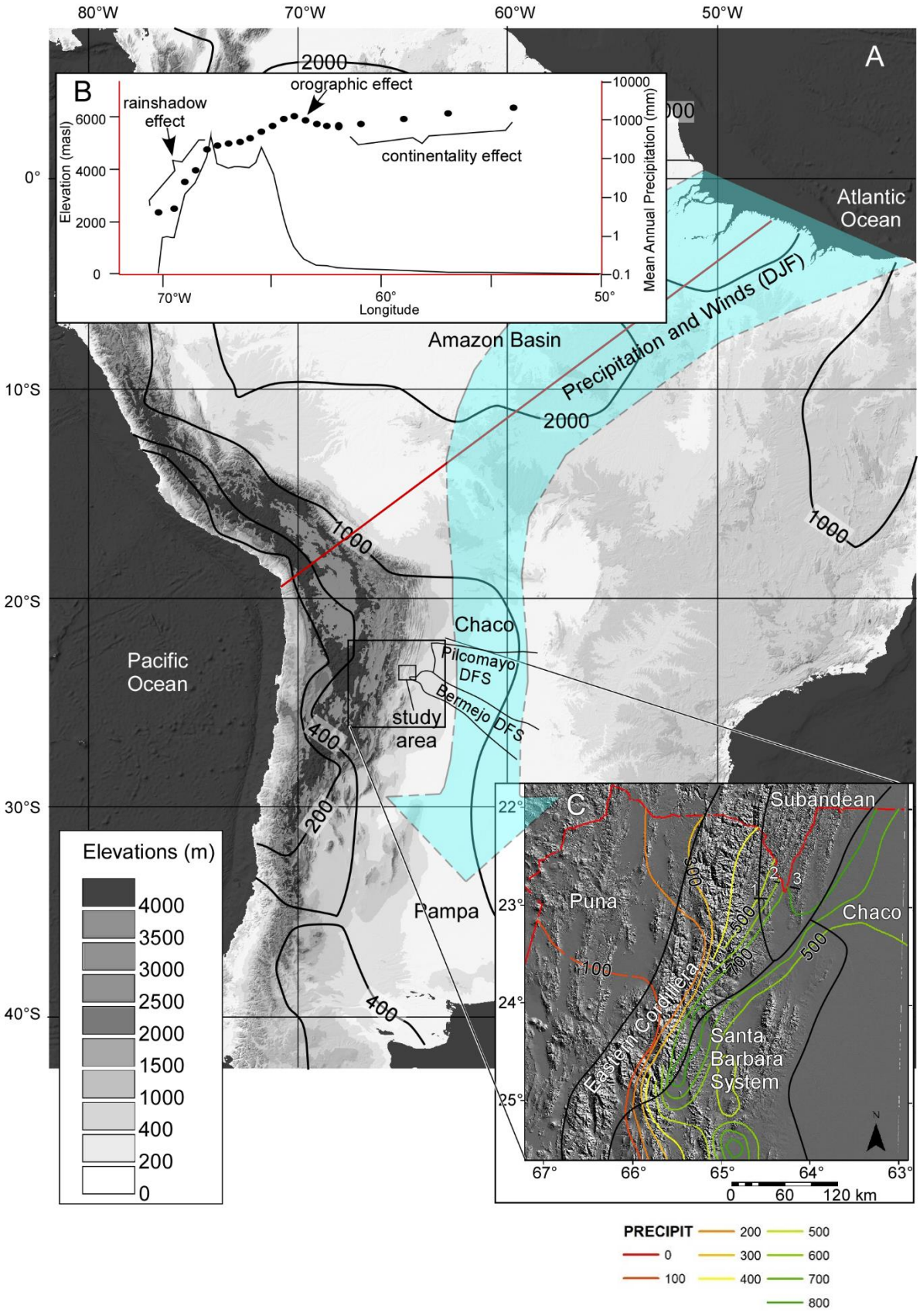
80°W
70°W
60°W
50°W
0°
10°S
20°S
30°S
40°S
A
B
C
2000
orographic effect
rainshadow effect
continentality effect
Elevation (masl)
Mean Annual Precipitation (mm)
70°W
60°
50°
Longitude
Atlantic Ocean
Amazon Basin
Precipitation and Winds (DJF)
2000
1000
1000
Chaco
Pilcomayo DFS
Bermejo DFS
study area
Pacific Ocean
400
200
Pampa
400
Elevations (m)
4000
3500
3000
2500
2000
1500
1000
400
200
0
22°
23°
24°
25°
Subandean
Puna
Chaco
Eastern Cordillera
Santa Barbara System
300
100
500
700
500
1
2
3
67°
66°
65°
64°
63°
0
60
120 km
N
PRECIPIT
0
100
200
300
400
500
600
700
800

Figure 1: **Area of Study Map and Oxygen Isotopes and Rainfall Measurements**
A) Observed annual total precipitation in South America (contours in mm), 1976-2009 (data provided by the NOAA/OAR/ESRL PSD, Boulder, Colorado, USA, http://www.esrl.noaa.gov/psd/data/gridded/data.south_america_precip.html; Liebmann and Allured, 2005). The light blue arrow shows the principal water vapor supply path across the continent to the study area. Red line is the line of cross section in B. Large box is the area shown in C. Small box is the study area. B) Cross section of land surface altitude and mean annual precipitation (Houston and Hartley [2003]). C) Mean annual precipitation across the eastern flank of the Andes and westernmost Chaco Plain in northwestern Argentina and southernmost Bolivia (national border in red). Precipitation contour lines are part of the *Instituto Nacional de Tecnología Agropecuaria* (INTA) database in Argentina. The locations of stratigraphic sections reported in this study are marked 1, 2, and 3. Section 1, Iruya River section, is the source of the isotopic data.

For the modern Andes, the elevation threshold condition for orographic precipitation occurs at 1000 m to 1500 m above sea level, for topographic obstacles of at least 3 km radius or lateral extent (Bookhagen and Strecker, 2008). In the Central Andes, where the easterly wind direction and south-flowing South American Jet carry the moisture from the Amazonian Forest to the mountain belt, this elevation threshold is exceeded locally within the Subandean Belt and regionally at the boundary between the Subandean ranges and the Eastern Cordillera (Masek et al., 1994, Figure 1). We studied the sedimentary record of the basin along the eastern flank of the Eastern Cordillera that would mark when the orographic effect caused by tectonic uplift of the Central Andes was enhanced. Paleoclimate history thus becomes a clue to regional-scale tectonic history.

The main purpose of this paper is to obtain insights to the climatic conditions during the Middle Miocene to the Early Pliocene of the lowlands immediately east of the Andes. Observations focus on paleosols, which function as paleo-precipitation gauges, both using profiles of weathering and pedogenesis and using oxygen and carbon isotopic data. These methods constitute the groundwork for treatment of theories and conceptual modeling of the regional climate history of the Central Andes during the Miocene. For this study, we focused on the Miocene-Pliocene strata of the Subandean Belt due to their proximity to the 4000–5000 m high Eastern Cordillera (Figure 1), and because today's Subandean Belt was the lowland Chaco foreland basin at the flank of the Andes during the Miocene. New information constraining the paleo-rainfall regime in the Subandean Belt of extreme northern Argentina near 21°S can be compared with results of previous paleoclimate studies for southern Bolivia in the Pilcomayo River region (Figure 1A; Uba et al, 2005, Uba et al, 2009; Mulch et al, 2010). This study takes advantage of the available high resolution geochronology provided by Hernández et al. (1996) and Echevarría et al (2003) (chapter

2), which is valuable because it enables comparisons to time-correlative isotopic data sets elsewhere the Andes.

Paleosol-based Isotopic Climate Proxies

The study of climatic patterns through the geologic record by the use of geochemical proxies has been one of the main focuses during the last decades for paleoclimatologists (Rozanski et al., 1993; Grootes, 1993; Ghosh et al., 2006; Eiler, 2011; Suarez et al., 2011, Rohrmann et al., 2014). Proxies based on paleosol properties including isotopic values are possible because soils and paleosols represent their average climatic conditions during their development, adjusted to precipitation, temperature, and vegetation (Figure 1 and Figure 2). The time scale resolution for paleosols is on the order of 10^3 to 10^4 years depending on the environmental factors of preservation and erosion (Krauss, 1997; Sheldon and Tabor, 2009; Tabor and Myers, 2015). A major thrust has been the use of oxygen ($\delta^{18}O$) and carbon ($\delta^{13}C$) isotopes, and carbon-oxygen co-occurrence (Δ_{47}) for calcium carbonate nodules developed in paleosols. Independent of the stable isotope properties of paleosols, the physical and chemical attributes of the ancient soils themselves are valuable clues to climate conditions (Rozanski et al., 1993; Grootes, 1993; Ghosh et al., 2006; Eiler, 2011; Suarez et al., 2011).

Among the different methods of investigation to study earth-atmosphere interactions discussed by Roe (2005), this paper pursues field-based observations combined with geochemical analyses of stable isotopes. Grootes (1993) and Rozanski et al (1993) have shown that analyses of oxygen isotopes illuminate relationships between changes in water sources and rain amount through geologic history. Changes in values of isotopic ratios occur by fractionation of the isotopic masses when moving from one physical state to another (e.g. liquid→gas).

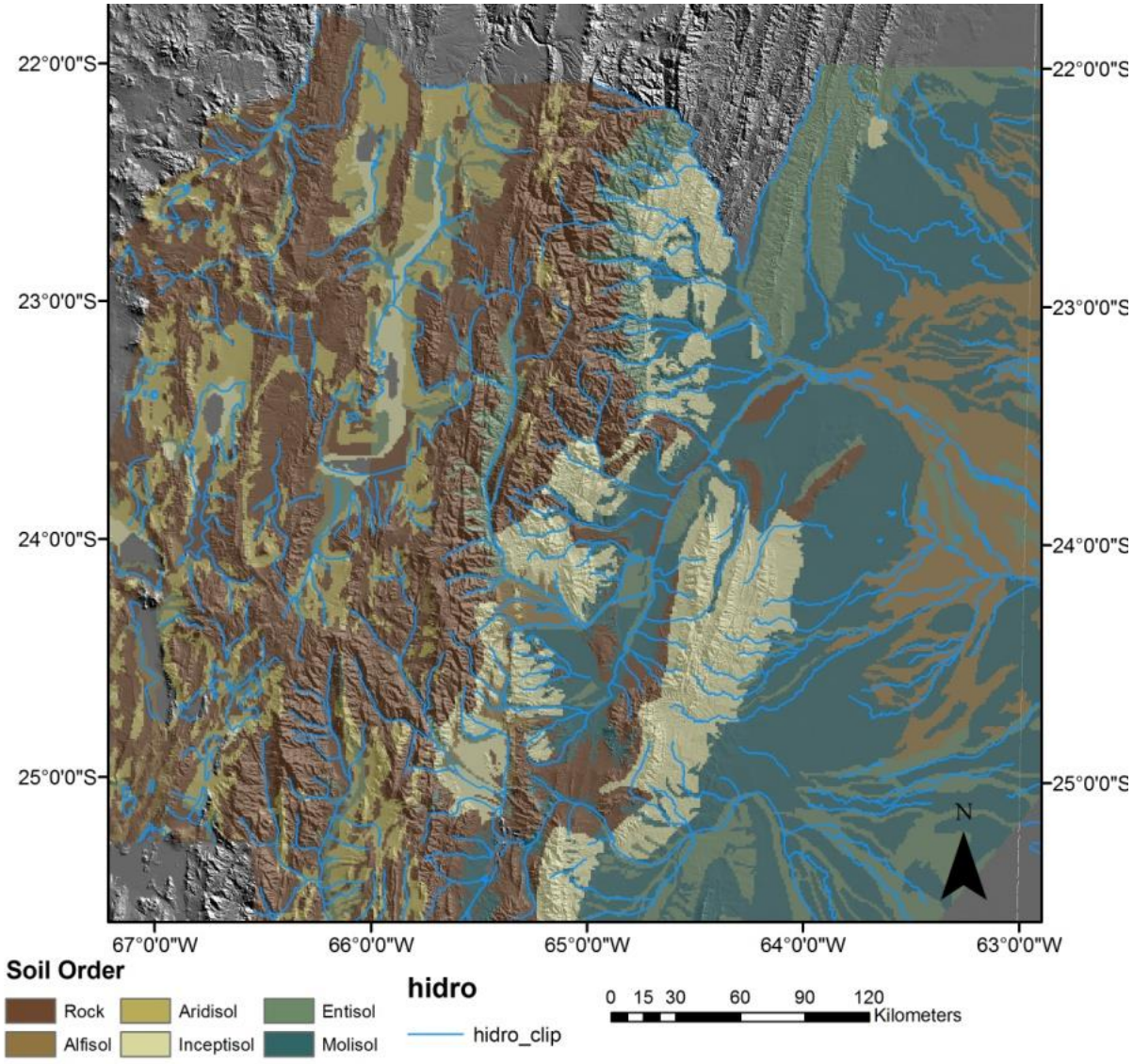
22°0'0"S
23°0'0"S
24°0'0"S
25°0'0"S
67°0'0"W
66°0'0"W
65°0'0"W
64°0'0"W
63°0'0"W
N
Soil Order
Rock
Alfisol
Aridisol
Inceptisol
Entisol
Molisol
hidro
hidro_clip
0 15 30 60 90 120
Kilometers

Figure 2: Soil and Hydrology Map
Map of soil orders and major streams superimposed over a DEM map of central Andes (Atlas de suelos de la República Argentina [CD-ROM], *Instituto Nacional de Tecnología Agropecuaria* [INTA]).

For this study with the published hypothesis that uplift of the Andes would lead to enhanced rainout from air masses that passed over the study area, a stratigraphic sequence of paleosol oxygen isotopes is anticipated to show a change in rain amount (Sheldon et al., 2002; Uba et al, 2005; Insel et al., 2012, 2013). Modern precipitation enters the region near the eastern Andes with an annual mean $\delta^{18}O$ value of -3.9‰, and monthly values as heavy as 1.25‰ (winter) and as light as -11.3 (summer) (Gonfiantini et al., 2001; 1982–1985 GNIP data). Modern precipitation becomes progressively depleted of the heavy ^{18}O isotope for catchments that span the eastern flank of the Andes near the study area (Figure 1 and Figure 2). The published rainfall transect closest to the study area, 20.6–21.2°S, demonstrates that the mean $\delta^{18}O$ of three years of monthly data ranges from -4.4‰ in some low elevations (<1 km) catchments to -13.4‰ for high elevation catchments (>4 km) (Fiorella et al., 2015). By analogy, enhanced rain out through the time span sampled by the Subandean foreland basin strata would be anticipated to have caused rain water to progress from early $\delta^{18}O$ mean annual values no more negative than -4‰ to later $\delta^{18}O$ values that are several per mil more negative.

The ratios between the stable isotopes of carbon, ^{13}C and ^{12}C, in paleosol calcium carbonates are derived from the interactions of plants with soils. With the carbon isotopes, a fingerprint is left of C3, C4, and Cam plants (Cerling and Quade, 1993; Rozanski et al, 1993; Cotton et al., 2014). It is possible to observe subtle and gradual changes in vegetation from the Subandean Belt Ranges until the end of the Bermejo megafan following the river flow direction. The vegetation changes from evergreen forest to shrubs, to grasses where mollisols are developed, and ending in a swamp vegetation. On the premise that there would have been an east-west gradient in precipitation and soil moisture across the Miocene-Pliocene foreland basin, perhaps accentuated in close proximity to the Andes and perhaps tightly coupled to the stream channel system, changes

in carbon isotopic ratios both laterally and through geological time likely occurred. To observe patterns of the changes in rain fall and vegetation across the Miocene landscape, $\delta^{13}C$ values were obtained in a stratigraphic column.

Paleo-temperatures at which soil carbonates form can be estimated using the Δ_{47} method, which measures the abundance of a particular isotopologue in a carbonate mineral and relates the relative abundance of that isotopologue to temperature of formation. As explained by Eiler (2007), there exist in nature two or more variants of molecules whose difference is the isotope of the constituent atoms, and these different molecules are referred to as isotopologues. Carbonates are one category of material that has multiple constituents, e.g., oxygen and carbon, and combinations of the isotopes of these elements comprise the isotopologues. The term "clump" is used to refer to the set of possible isotopic combinations in these multiply-substituted materials like carbonate. Although there may be a stochastic distribution of all the stable isotopes in a given population of molecules among all possible isotopologues, for the case of interest Eiler (2007) showed that the clumped isotopes formed by the combinations between the isotopologues of CO_2 exhibit a strong correlation with the temperatures present when these isotopes combined (Figure 3). The temperature measures are based on the abundance on ^{13}C-^{18}O bonds in the calcium carbonate crystal (Ghosh et al., 2006; Eiler et al., 2007). The abundance of the $^{13}C^{18}O^{16}O$ isotopologue in a given sample is expressed with the parameter Δ_{47}, which is the difference in per mil between the masses 47/44 ratio in the sample and the masses 47/44 ratio expected in a random distribution all the C and O isotopes among all the possible CO_2 isotopologues. The significance of this parameter to paleotemperature studies is that it has a one-to-one relationship with the temperatures at which CaCO3 samples of both calcite and aragonite are known to have been deposited, where that relationship is given by:

$$\Delta_{47} = \frac{0.0592}{(10^6 \text{ x } T^2 - 0.02)} \qquad \text{(T in Kelvins)}$$

and gives the graphic relationship presented in Figure 3. If the isotopes were combined during pedogenesis to form a carbonate nodule, then the isotopologue would reflect the temperature of the soil. For carbonate, the isotopologue of central interest is the one whose mass sums to 47, primarily $^{13}C^{18}O^{16}O$. Its abundance relative to a stochastic mean is expressed as:

$$\Delta_{47} = \left(\frac{R_{measured}}{R_{stochastic}} - 1 \right) \times 1000$$

The values of $R_{measured}$ represent the ratio of the sample (unknown) to be analyzed, $R_{stochastic}$ represents the ratio of the calculated values (expected) from laboratory experiments. However, according to Quade et al. (2013) the resetting of paleotemperatures given by C-O clumped isotopes can occur when strata experienced burial history deeper than ~2.5 km. This theory is based on the observations of a change in temperatures from calcium carbonate nodules from the Siwalik sections in Pakistan. Nevertheless, Quade et al. (2013) points out that this "*inference should be tested through detailed studies of the fabrics and trace element geochemistry of partially reset, deeply buried soil carbonates"*. This insight does not eliminate the results obtained from strata that experience burial depth deeper than 2.5 km, but diagenetic temperature resetting is a possibility that needs to be taken in consideration.

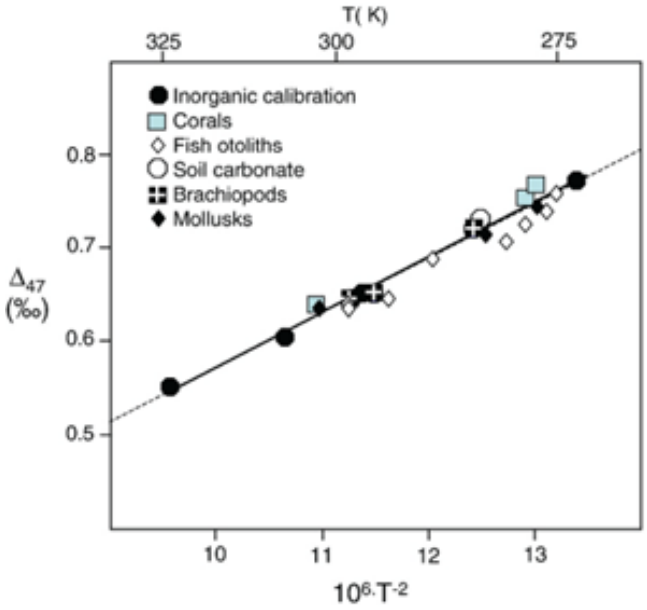
T(K)
325
300
275
Inorganic calibration
Corals
Fish otoliths
Soil carbonate
Brachiopods
Mollusks
0.8
0.7
0.6
0.5
Δ47
(‰)
10
11
12
13
10⁶·T⁻²

A

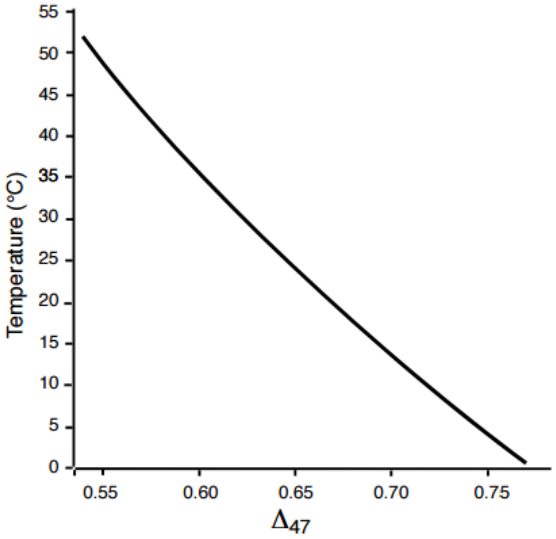
55
50
45
40
35
30
25
20
15
10
5
0
Temperature (°C)
0.55
0.60
0.65
0.70
0.75
Δ47

B

Figure 3: Correlation Between Δ_{47} Values and Temperature in Calcium Carbonates
Figure A shows the distribution of calcium carbonate systems and their correlation with Δ_{47} and temperature (from Eiler et al. [2007]). Figure B it is a graph that present a similar set of Δ_{47} values with temperature in ^{o}C.

Methods

In the field, paleosols were identified and located relative to the stratigraphic column previously measured and described by Hernández et al. (1996) (Figure 4; see also Chapter 2). Individual paleosol profiles were studied, focusing on texture, horizonation, and color referenced to a Munsell Color Chart, and classified by their stage of pedogenesis (Chapter 1). Carbonate nodules were examined for evidence of recrystallization or carbonate overgrowths, and larger calcium carbonate nodules were dismissed as likely products of groundwater flow. Samples of about 500 grams were collected of calcium carbonate from nodules, root casts, or rizoliths for laboratory analyses. The age of each paleosol was determined using the correlation of the stratigraphic column to the geological time scale detailed in Chapter 2.

Several paleosol thin sections were studied with a petrographic microscope. One of the main purposes for paleosol thin sections was to look at carbonate nodules and root tubules for evidence of recrystallization in the samples, to use as a criterion that diagenetic alteration likely occurred and thereby to identify samples not appropriate for the analysis of stable isotopes. Samples found to be suitable for isotopic study were milled with a dental drill to target primary micrite and avoid spar.

Samples were prepared for isotopic analyses by crushing to 250 μm size. Milled samples were then washed with a strong base, around 30% concentration, in order to remove any organic material from the calcium carbonate sample. The pedogenic carbonate $^{18}O/^{16}O$ and $^{13}C/^{12}C$ ratios were analyzed at the University of Rochester SIREAL laboratory (Stable Isotope Ratios in the Environment, Analytical Laboratory) using an automated carbonate preparation device (Gasbench II) coupled to a Thermo Electron Delta Plus XL continuous flow instrument. The data were normalized to the PDB scale by fitting the sample data to a linear correction curve based on

SIREAL internal standards and reference materials. Values reported for soil and paleosol carbonates are presented using VPDB, and meteoric water oxygen isotopes is presented using the VSMOW standard.

To obtain Δ_{47} values, sample preparation begins like that for the carbonate analyses. Thereafter the samples were reacted in ≥100% H3PO4 at 90°C in a common acid bath device. The evolved CO_2 was purified by passage through multiple dry ice/ethanol traps (~-75°C) and a Porapak-Q gas chromatography column held at -10°C. A Thermo-Finnigan MAT 253 gas source stable isotope ratio mass Spectrometer at Caltech provided isotopologue ratios of purified CO_2. All reported Δ_{47} values were normalized relative to high-temperature equilibrium gases (Huntington et al., 2009) and calibrated relative to the Caltech intralab reference frame of Huntington et al. (2009). Analytical errors are determined from the standard deviation of carbonate standards analyzed multiple times during the run sessions. For two analytical sessions, the 2% error of standards was 0.038‰, slightly worse than the long-term laboratory average 2% of 0.027‰. Generic 95% confidence intervals for Δ_{47} were computed from the 1% precision of standards and the number of samples N (95% CI = 1.96 x 1x $(N)^{-0.5}$.

Results

Paleosols where recognized throughout the whole stratigraphic section of the Iruya River with variabilities in their frequency as well as their stage of development (Chapter 1). The lower 4420 m of the Iruya River stratigraphic column presents at least 70 paleosols (Figure 4), including the ones categorized as poorly developed or stage I of pedogenic development (Table 1, Chapter 1). The complementary sections at La Porcelana and Peña Colorada exhibit over 200 paleosols all together; however, these paleosols lack deposition of calcium carbonate. In the

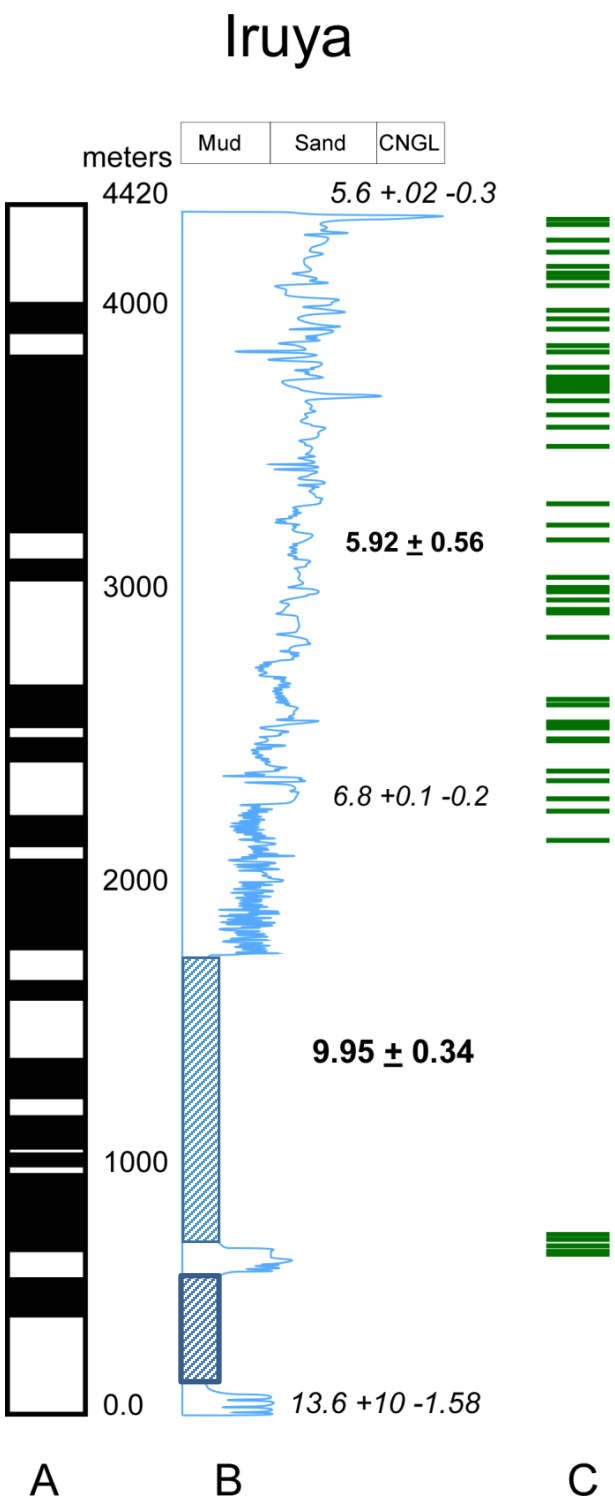
Iruya
Mud
Sand
CNGL
meters
4420
4000
3000
2000
1000
0.0
5.6 +.02 -0.3
5.92 ± 0.56
6.8 +0.1 -0.2
9.95 ± 0.34
13.6 +10 -1.58
A
B
C

Figure 4: Iruya Sedimentary Column
(A) This is the paleomagnetic data presented by Echevarría et al., 2003. (B) Iruya River stratigraphic column summary displayed in the form of grain size distribution along the sedimentary record. Conglomerates are expressed by deviations of the blue line to the far right; mudstone is represented by the most leftward positions of the line (Chapter 2). Two covered intervals are represented by boxes in with diagonal lines. (C) The position of paleosols found in the stratigraphic record (Chapter 1).

absence of calcium carbonate, the selected stable isotope methods were not viable. For this reason, for Peña Colorada and La Porcelana only the soil characteristics provide environmental history (Chapter 1).

Over 30 paleosols from the Iruya River section were selected to be analyzed for O and C stable isotopes. The stratigraphically lowest paleosol (RI 1) was omitted because this paleosol, despite an immature degree of pedogenic development, contains large calcium carbonate nodules with coarsely crystallized zones, for which diagenesis or groundwater influences are suspected. Therefore, the dataset starts at 300 m above the base of the stratigraphic column, with a major gap until more carbonate-nodule bearing paleosol horizons are exposed at 1320 meters (Figure 4). Above another long gap, the subsequent set of paleosols starts at 2100 meters and continues until 4420 m above the base of the Neogene strata.

Paleosols

Iruya River paleosols are equally dispersed along the stratigraphic column, with a few zones of more abundant paleosol horizons (Figure 4). The dominant texture of these paleosols is a blocky structure; the remaining paleosols have a nodular and granular texture. The chroma and hue range for these paleosols go from 5 yr 4/3 (yellowish) to 10 yr 5/3 (reddish). Paleosols in the Miocene-Pliocene strata at Iruya River are mainly represented by B and C horizons capped by thin A horizon. Nevertheless, close to one-third of the strata were recognized to be paleosols formed by AC horizons. Paleosols occur repeatedly in the Iruya River stratigraphic section and are consistently poorly developed BC and/or AC horizons; both of those two categories can be observed in all parts of the column. It is important to mention that paleosols with BC horizonation may be the result of the erosion of the upper horizon, with the outcome of the loss of the A horizon.

All the details about the frequency, structure, texture, and pedogenic development categories are described in detail in chapter 1 of this study. The dominant structures of the carbonate nodules and root-casts are the zonation of calcium carbonate, micrite mixed with calcium carbonate, and mottling of oxides at microscopic level (Chapter 1, Figure 15). These features are expected of primary soil nodules and are the basis for confidence about the quality of the samples for paleoenvironmental analysis.

Oxygen Isotopes

Calcium carbonate nodules developed in the paleosols of Iruya River stratigraphic section are present in almost all the paleosols. Table 1 shows that the highest and lowest $\delta^{18}O$ values are 25.8‰ and 19.8‰ (VSMOW) respectively, which covers a range of nearly 6.0‰. The oldest sample at Iruya River (RI 1) The stratigraphically oldest paleosol (RI 1) was omitted as explained above in order to maintain the purity of these analyzes avoiding resetting and overprinting of the isotopic signature by recrystallization.

These values are displayed relative to the stratigraphic position of the paleosols (Figure 5A) as well as relative to the age (Figure 5B) for comparison with the geological history of the Andes. There is no consistent long-term trend in values for the oxygen isotopes. The oldest (~ 12.5 and ~ 8.9 Ma) values tend to be quite negative, yet the most negative values occur between 6.05 and 5.9 Ma. The youngest values are consistently less depleted, with a mean $\delta^{18}O$ value of -8.1‰ between 5.3 – 5.1 Ma (Table 1, Figure 5B).

Carbon Isotopes

There is a more consistent trend of $\delta^{13}C$ values in calcium carbonate soil nodules. The lowest value is -13.3‰ and the highest value of -8.9‰ to give a range of values of only 4.4‰ (VPDB). Carbon isotope data start with a relatively positive value for the oldest result at 12.5 Ma (Figure 6). Horizons dated 9 Ma to 6.5 Ma have $\delta^{13}C$ that fluctuates between -11.8 and -10.7‰ making this a very constant set of values for $\delta^{13}C$, until the horizons corresponding to 6.5 Ma, where a subtle but consistent tendency toward heavier values begins. Figure 8 compares the carbonate $\delta^{13}C$ values to charcoal $\delta^{13}C$, for deposits at 3300 m height in the section, or 6 Ma. The values for the charcoal are -27.57‰ and -27.06‰, displaced about 17‰ more negative than the carbonates (Figure 7). These results fall into the values presented in the literature for both, plant material as well as for the calcium carbonate values found in soils and paleosols.

Δ_{47} Paleotemperatures

The eight paleosols analyzed for clumped isotope Δ_{47} paleothermometry are well distributed through the stratigraphic column (Figure 8; Table 1). The lowest Δ_{47} value is 0.567 given by the oldest paleosol in this analysis, and the highest value is 0.632 given by the second youngest paleosol in this dataset. From those Δ_{47} data, the corresponding paleotemperatures are, in principle, measures of the environmental condition under which each calcium carbonate nodules precipitated. The range of temperatures goes from 44 to 28 ^{o}C, with apparent paleotemperatures remaining around 42 ^{o}C until 5.85 Ma. For younger samples there is a drastic shift by 16 ^{o}C to colder temperatures of 28 °C and 30 ^{o}C for the youngest two samples. Table 1 present the clumped isotope values in light grey and the carbon isotope values in darker grey.

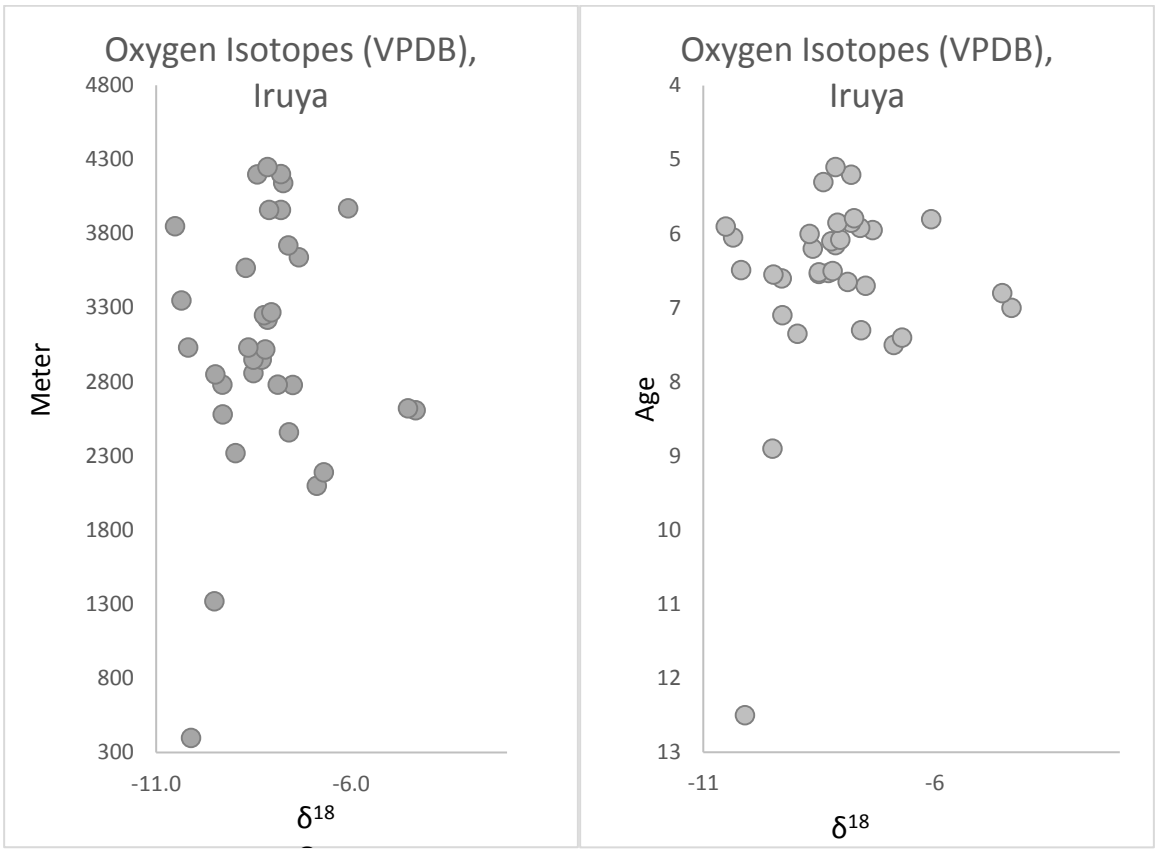
Oxygen Isotopes (VPDB), Iruya
Meter
4800
4300
3800
3300
2800
2300
1800
1300
800
300
-11.0
-6.0
δ18
Oxygen Isotopes (VPDB), Iruya
Age
4
5
6
7
8
9
10
11
12
13
-11
-6
δ18

A B

Figure 5: Iruya River Oxygen Stable Isotope ($\delta^{18}O$)
Figure 5A shows the stable isotope results in accord with the paleosols position in the stratigraphic column. Figure 5B shows oxygen stable isotopes in time.

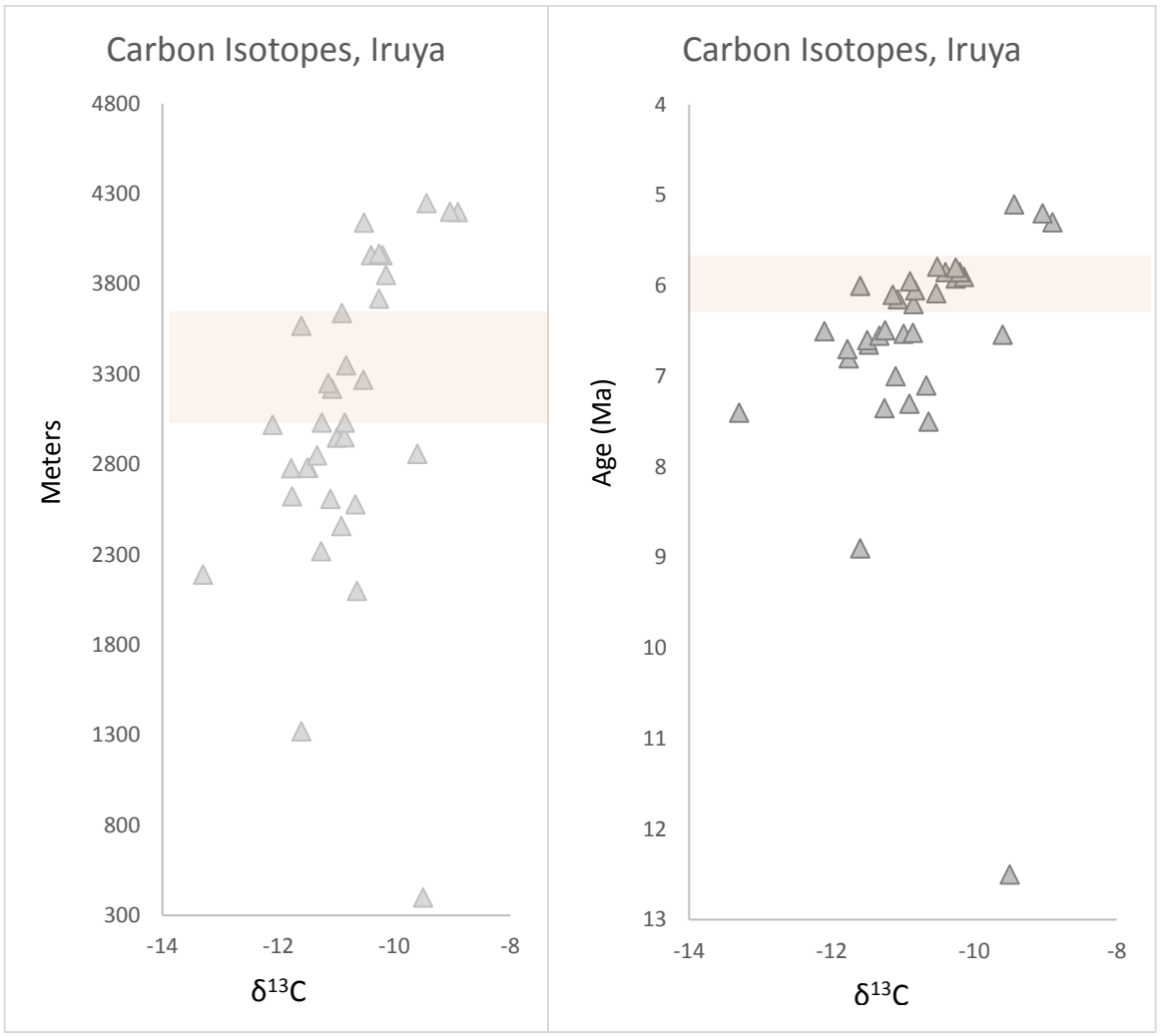
Carbon Isotopes, Iruya
Meters
4800
4300
3800
3300
2800
2300
1800
1300
800
300
-14
-12
-10
-8
δ13C
Carbon Isotopes, Iruya
Age (Ma)
4
5
6
7
8
9
10
11
12
13
-14
-12
-10
-8
δ13C

A B

Figure 6: Iruya River Carbon Stable Isotope ($\delta^{13}C$)
Figure A shows the stable isotope results in accord with the paleosols position in the stratigraphic column. Figure B shows carbon stable isotopes in time. Shaded area represents the stratigraphic interval with possible repetition by faulting.

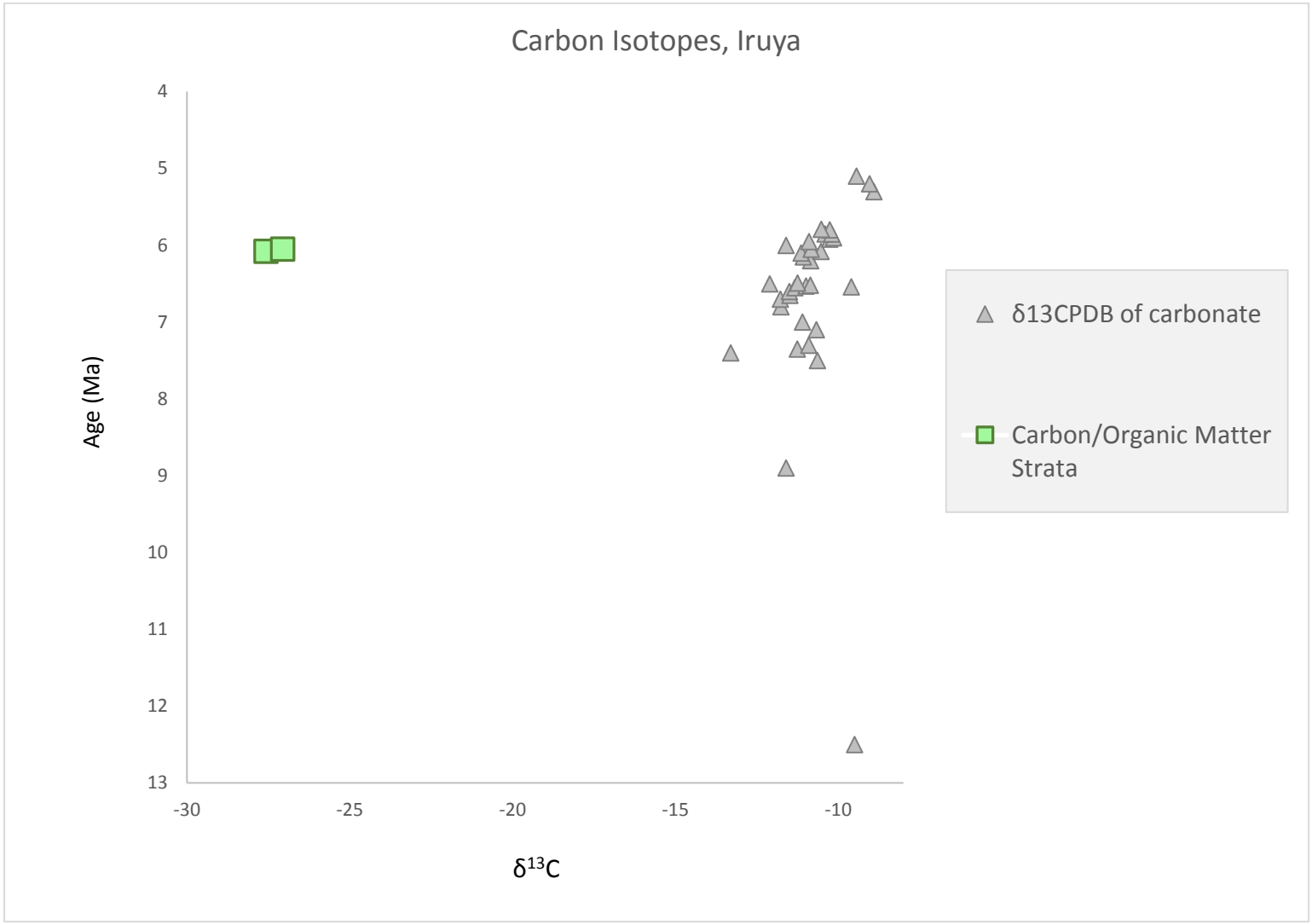
Carbon Isotopes, Iruya
Age (Ma)
4
5
6
7
8
9
10
11
12
13
-30
-25
-20
-15
-10
δ13C
δ13CPDB of carbonate
Carbon/Organic Matter Strata

Figure 7: Iruya River Carbon Stable Isotopes from Paleosols and Charcoal
It is possible to see the difference in values from the carbon from calcium carbonate in paleosols (triangles) and the carbon from the organic matter from charcoal (squares). This goes in accord with the expected shift in values due to the $\delta^{13}C$ enrichment with the heavier isotopes.

Sample ID	Mean Delta 13C OfAnalyses (VPDB)	MeanDelta 18O OfAnalyses (VSMOW)	Location in the Stratigraphic Column (m)	Age	Δ_{47} of extracted CO_2	Temperature (^{0}C)
RI 1	-15.42	-5.7	90	13.4	/	/
RI 08 (8)	-9.5	-10.1	400	12.5	0.567	44
P.S. 4 (7)	-11.6	-9.5	1320	8.9	0.581	41
RI 2	-10.64	-6.9	2100	7.5	/	/
RI 3	-13.3	-6.7	2190	7.4	0.578	41
RI 4	-11.26	-9.0	2320	7.35	/	/
RI 5	-10.91	-7.6	2460	7.3	/	/
RI 6	-10.67	-9.3	2580	7.1	/	/
RI 7	-11.1	-4.3	2610	7	/	/
Sample # 9	-11.76	-4.5	2623	6.8	/	/
RI 8	-11.78	-7.5	2780	6.7	/	/
RI 9	-11.48	-7.9	2781	6.65	/	/
RI 10	-11.5	-9.3	2782	6.6	/	/
RI 11	-11.33	-9.5	2850	6.55	/	/
P.S. 26 (07)	-9.6	-8.5	2860	6.54	0.587	39
RI 12	-10.99	-8.3	2950	6.53	/	/
RI 14	-10.86	-8.5	2951	6.52	/	/
RI 15	*-12.1*	*-8.2*	*3020*	*6.5*	*0.579*	*41*
RI 16	*-11.25*	*-10.2*	*3032*	*6.49*	/	/
RI 17	*-10.85*	*-8.6*	*3033*	*6.2*	/	/
RI 19	*-11.07*	*-8.1*	*3220*	*6.15*	/	/
RI 20	*-11.14*	*-8.2*	*3250*	*6.1*	/	/
RI 21	*-10.53*	*-8.0*	*3270*	*6.08*	/	/
RI 22	*-10.83*	*-10.4*	*3350*	*6.05*	/	/
RI 23	*-11.6*	*-8.7*	*3570*	*6*	*0.571*	*44*
RI 24	*-10.9*	*-7.3*	*3640*	*5.95*	/	/
RI 25	*-10.26*	*-7.6*	*3720*	*5.92*	/	/
RI 26	-10.14	-10.5	3850	5.9	/	/
RI 27-A	-10.4	-7.8	3960	5.85	/	/
RI 27B	-10.2	-8.1	3960	5.85	0.632	28
RI 28 sample 2	-10.26	-6.1	3970	5.8	/	/
Laminated Strat. Nodules	-10.52	-7.7	4141	5.79	/	/
RI 29-2	-8.9	-8.4	4200	5.3	0.622	30
RI 29 (1)	-9.04	-7.8	4201	5.2	/	/
RI 30	-9.44	-8.1	4250	5.1	/	/
Coal 1	-27.57	/	/	6.08	/	/
Coal 2	-27.06	/	/	6.05	/	/

Table 1: Stable Isotope Data with Respective Stratigraphic Positions

Oxygen and Carbon isotope data from paleosols at Iruya River, with their respective stratigraphic location (height above base of column), age (Ma), and isotopic values. Charcoal carbon isotopes data are also included. Highlighted are the 8 paleosols for which clumped isotope data for paleosol carbonates (delta-47) were also obtained. Oxygen and carbon isotope values in italics represent the stratigraphic section where possible repetition by faulting is present.

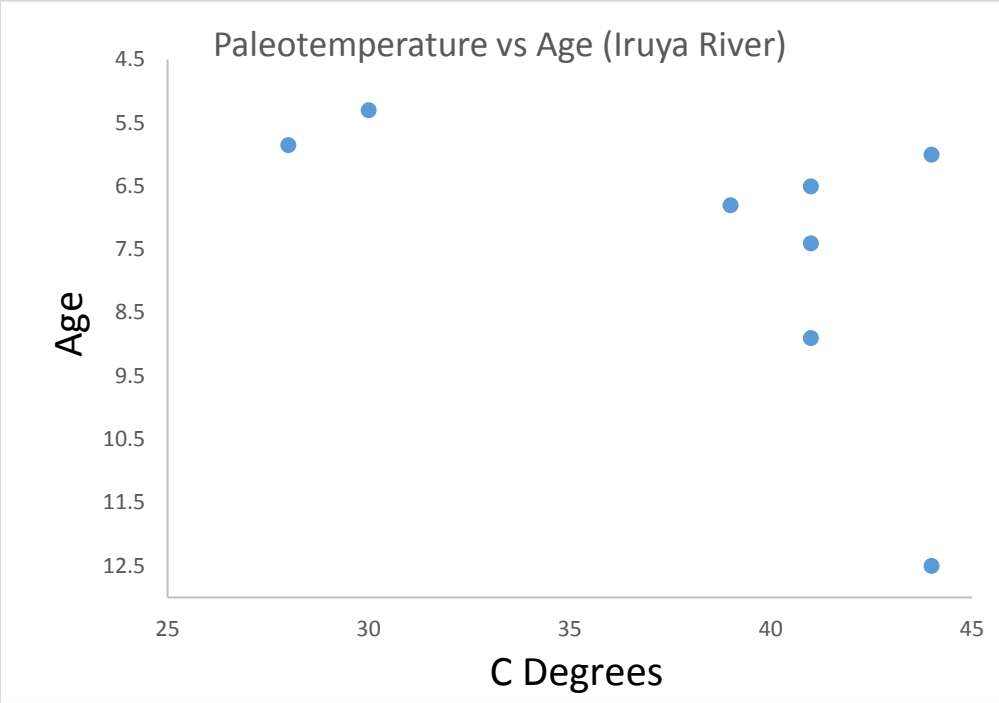
Paleotemperature vs Age (Iruya River)
Age
4.5
5.5
6.5
7.5
8.5
9.5
10.5
11.5
12.5
25
30
35
40
45
C Degrees

Figure 8: Temperatures as the result of Δ_{47} from Clumped isotopes at Iruya River
The age of deposition (Y axis) versus apparent temperature (X axis) from Δ_{47} data. The results are strongly bimodal. Paleosol carbonate from positions below 3600 m height in the column and at the right of the figure yield apparent temperatures, suggesting very warm temperatures prior to 6 Ma. Paleosol carbonates from shallower positions, at the left, suggest that the environmental conditions at Iruya River were much cooler than before, and intermediate between today's mean annual temperature and mean maximum temperature. For more details refer to table 1.

Discussion

Paleosols provide information about conditions spanning ~12 Ma to 5 Ma. Nevertheless, 32 of the 35 horizons whose paleosols provided isotopic data occur in horizons whose ages are between 8 Ma and 5 Ma. Thus most of the discussion focuses on that time interval, within the Late Miocene and earliest Pliocene.

All of the insight gained from paleosols and their isotopic values depends on preservation of surface materials, which depends on basin dynamics. The sedimentation rate of five locations in the foreland basin of northwestern Argentina was determined by Echevarría et al (2003), who demonstrated that for the Iruya section between 12–8.5 Ma the rate of accumulation was relatively slow and unsteady, whereas from 8.5–5 Ma the rate was the highest of any part of the basin system (1.01 mm/yr). That high rate suggests that there was a persistent abundance of accommodation space during the 3 million years in which most of the studied paleosols formed and allowing their preservation. While accommodation space is necessary in order for sediment to accumulate and become sedimentary rock, accommodation space can be inherited from previous tectonic subsidence events (Flemings and Jordan, 1990) and need not form at the time of sediment accumulation. In contrast, Blaine and Terence (1994) explain that the driving force for sediment transportation must be contemporaneous with the depositional age of strata. For the Andean foreland basin, the driving forces for sediment transportation are derived from potential energy produced by the elevation of the Andes and from the kinetic energy encompassed in the river hydrology.

Paleosols

Paleosols throughout the Iruya River section display weak differentiation of horizons, with evidence of illuviation of clays, accumulation of calcium carbonate, and evidence of roots and other forms of bioturbations. Their continuous distribution and constant properties suggest persistent environmental and climatic conditions through the late Middle, Late Miocene and earliest Pliocene. Likewise, the texture of paleosols as well as their bounding strata also suggest that sediment supply and accumulation was stable through the 7 myr interval.

The observed repetitive physical properties of the strata in which the paleosols are embedded and the texture and thickness of the paleosols indicate that stream hydrology must have been constant throughout the nearly three-million-year history best documented in the Iruya River section. If surface water hydrology was essentially constant, then it is anticipated that the climate of the headwaters region as well as of the megafan depositional system changed little through time. As explained in chapters 1 and 2, the differences among paleosols that have been documented are best explained to be the result of the proximity to the stream channel as well as their location in the sedimentary basin. It is important to point out a possibility of stratigraphic repetition by faulting, which is explained in Chapter 2. However, from previous sections/chapters, these paleosol stratigraphic clusters are the results of the Distributary Fluvial System (DFS) dynamics and the accommodation space in the basin, and not the result on different periods of climatic conditions during their development.

For paleosols throughout the studied column, from 12-5 Ma, the accumulation of pedogenic calcium carbonate as well as the illuviation of clays both suggest that the basic climate regime changed little through time. That climate was characterized by strong seasonality between warm and wet summers and cold and dry winters (see Chapter 1). In order for calcium carbonate

to accumulate and be preserved, the soil must have consistent physical parameters such as soil texture and drainage. This requirement provides some qualitative insight into climate variability at the interannual to centennial scale, suggesting that although the climate was strongly seasonal the multi-annual changes in precipitation were modest.

Oxygen Isotopes

The non-diagenetic carbonate reflects paleo-environmental conditions (Sheldon and Tabor, 2009). The oxygen isotopes varying between -10.5‰ to -4.3‰ (VPDB), and express no clear long-term pattern or trend. The small range in these isotope values, only ~6‰, denotes little change related to even short-lived climate changes.

The oxygen isotopic values recorded in the Iruya column in the Miocene South American interior lowland Andean foreland basin creates a baseline for oxygen isotopes used as proxies for rain fall amount and the elevation of the lowland of the Andes. Such data for a position that was approximately 30 km to the east of the Late Miocene topographic front of the Eastern Cordillera are crucial to correct interpretation of data sets like those of Garzione et al (2006; 2008; 2014) and Ghosh et al. (2006).

Modern soils in northwestern Argentina receive rain water whose $\delta^{18}O$ is little depleted relative to ocean water in winter (e.g., weighted mean for September of -2‰ (VSMOW; Figure 9), and moderately depleted during the rainier Austral summer (e.g., weighted mean for February -10‰; Figure 9), giving average annual $\delta^{18}O$ values between -6 to -10‰ (VSMOW). It is expected that paleosols in northwestern Argentina in the past that were developed under similar climate conditions would exhibit oxygen isotopic values similarly depleted relative to the contemporaneous ocean. Because Late Miocene subtropical Atlantic surface water differed from

Weighted Annual $\delta^{18}O$

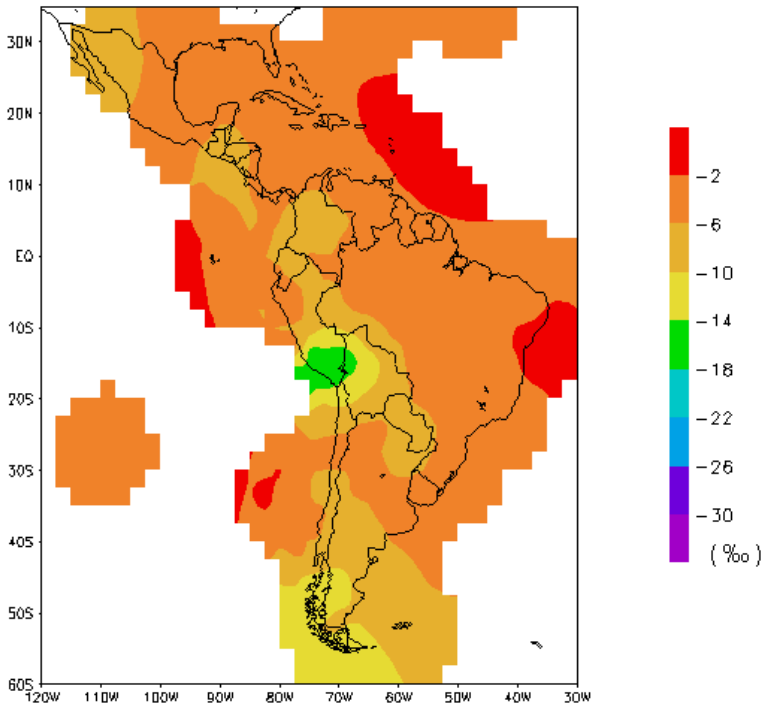

Weighted Feb. $\delta^{18}O$

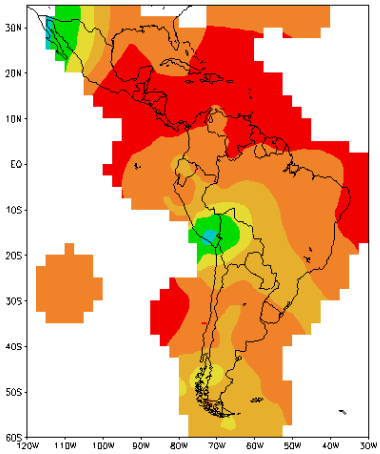

Weighted Sep. $\delta^{18}O$

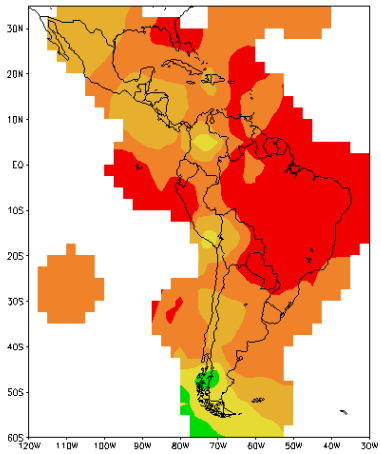

Figure 9: Modern Oxygen Isotope Data
GNIP oxygen isotope data summary from 1961 to 1999.
(http://www-naweb.iaea.org/napc/ih/documents/userupdate/Waterloo/)

modern $\delta^{18}O$ at the same location by only about 1‰ (Savin et al., 1985), one expects the soil carbonates formed in the Miocene and today to have similar ^{18}O fractionation. The northwestern Argentina paleosol carbonate $\delta^{18}O$ isotopic range of values actually fall within modern precipitation isotopic measurements (modern precipitation measured in relation with VSMOW, and soil carbonates in relation with VPDB).

Isotopic data for modern precipitation in the Chaco lowlands from the Global Network of Isotopes in Precipitation (GNIP) range between -2‰ SMOW in the center of the Amazon basin to about -6‰ SMOW in the Chaco basin (Figure 9). Based on Cerling and Quade's (1993) 2–5‰ shift toward less negative values on transformation of meteoric water to carbonate, were soil carbonate to form in modern soils we expect they would have values of about 0‰ to -5‰ PDB in the Amazon and Chaco, respectively. These anticipated modern soil carbonate values are 0 to 5‰ lighter than values found in the Subandean Belt Miocene records (-10.5‰ to -4.3‰ VPDBD). This suggests that the oxygen isotopes during the Miocene presents $\delta^{18}O$ values that fall into the range of isotope values predicted from modern low elevation rain out (-4‰ to -11.3‰), without exceeding negative values that are correlated with higher elevations (> -13‰) when compared with modern precipitation.

The stable isotope results from this study follow the rationale from Lenters and Cook (1997), Garreaud (1999) and Insel et al. (2009) that describe the atmospheric dynamics by which moist air from the Amazon basin today is advected southward in the foreland basin adjacent to the Andes, and then part of that air-mass is lifted up the Andean front by the easterly component of air flow. During southern hemisphere summer season there is enhanced easterly flow of wet air masses from the low elevation foreland basin region toward the eastern flank of the Andes. Insel et al. (2009) show that an Andes region that is even half of the height of today's Andes would

produce this general regional atmospheric circulation pattern. As Elger et al. (2005), Horton (2005, 2012), Rech et al. (2006, 2010), DeCelles et al. (2011) and others have demonstrated, a large fraction of the Andean highlands had been generated by the Middle Miocene, before the foreland basin strata studied here began to accumulate.

The lack of a long-term pattern of shift in the Subandean $\delta^{18}O$ is consistent with those interpretations that the Andes rose to a height sufficient to set up the modern atmospheric circulation system prior to 12.5 Ma. These new results add further credibility to the assumption that the basic modern air and moisture circulation patterns (Figure 1) operated throughout the late Middle Miocene, Late Miocene, and earliest Pliocene time span of interest even though boundary conditions like sea surface temperature and absolute height of the Andes almost certainly changed progressively over millions of years. Short-term fluctuations in climate would have been superimposed on the million-year-scale trends as well (Rohrmann et al., 2016).

Values of rainfall $\delta^{18}O$ on transects across the Andean highland (Figure 10) grow steadily more negative with increasing elevation, with the sharpest gradient where the Andes surpass 2000 m. The Iruya River paleosol carbonates isotopes measured (approximately -10 to -4‰), corresponding to approximately -6 to -15‰ precipitation (Cerling and Quade, 1993) fall among the more negative modern values recorded at stations located at less than 2000 m altitude (Figures 1 and 10). For the modern environment, those more negative values correspond to the summer season precipitation when rainout is more intense (Gonfiantini et al. 2001; Fiorella et al., 2015). Because the Iruya section within today's Subandean Belt was located on the windward side of the Eastern Cordillera and Altiplano plateau, the Iruya site provides the initial $\delta^{18}O$ values before changes occur across the Andean mountain belt due to rain-out effects (Figure 10). These new results show that the $\delta^{18}O$ values of the air mass that entered the Eastern Cordillera and

Altiplano/Puna plateau during the Late Miocene to earliest Pliocene (8 to 5 Ma) was 4 to 5‰ lighter than in modern air masses. This suggests that there was more fractionation of air masses as they passed over Amazonia than occurs today.

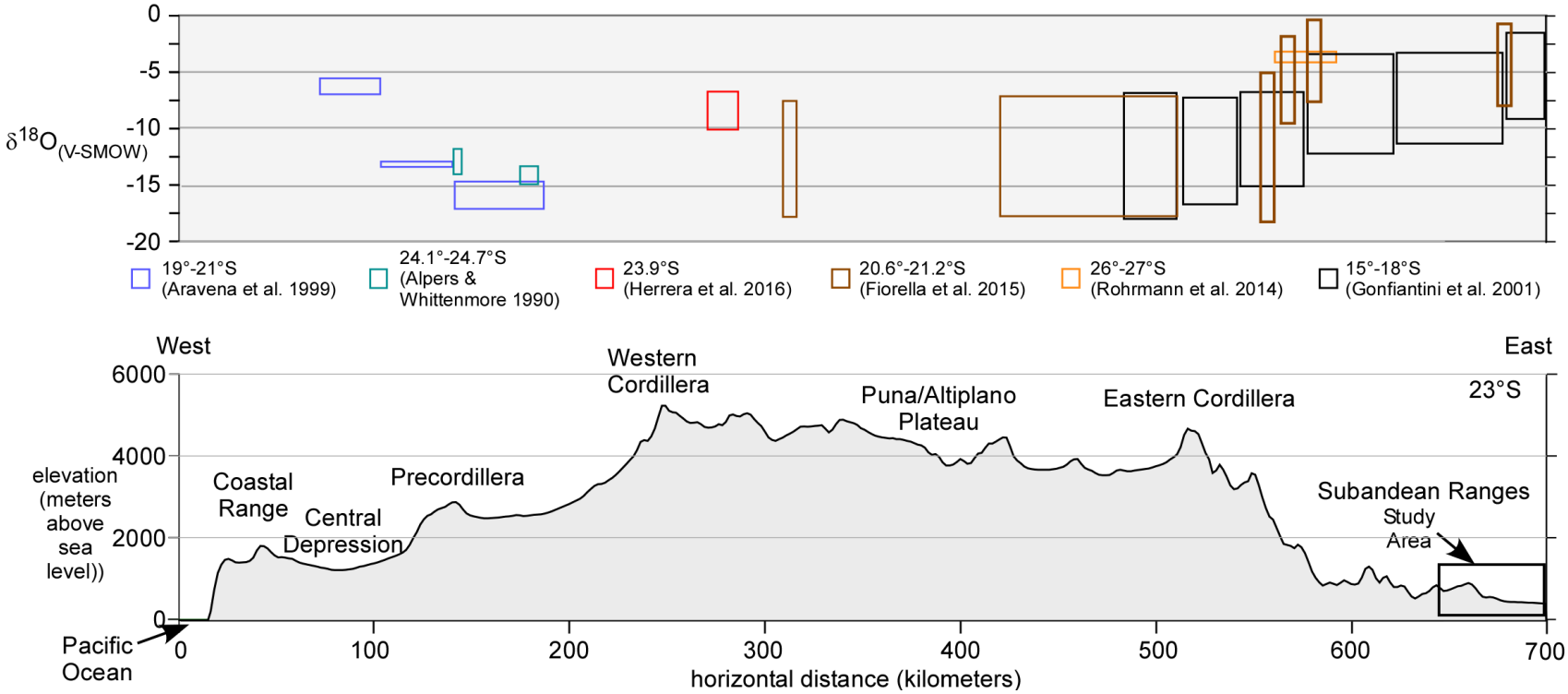
0
-5
-10
-15
-20
δ18O(V-SMOW)
19°-21°S (Aravena et al. 1999)
24.1°-24.7°S (Alpers & Whittenmore 1990)
23.9°S (Herrera et al. 2016)
20.6°-21.2°S (Fiorella et al. 2015)
26°-27°S (Rohrmann et al. 2014)
15°-18°S (Gonfiantini et al. 2001)
West
East
23°S
6000
4000
2000
0
elevation (meters above sea level))
Coastal Range
Central Depression
Precordillera
Western Cordillera
Puna/Altiplano Plateau
Eastern Cordillera
Subandean Ranges
Study Area
Pacific Ocean
0
100
200
300
400
500
600
700
horizontal distance (kilometers)

Figure 10: Andes Cross Section and Oxygen Isotope Data with Respect of Elevation
Topographic section at 23°S (below) and oxygen isotopic composition of precipitation (above) for the Central Andes along a line of cross section passing through the study area. The horizontal lengths of lines or boxes represent positions of bins of sampled locations. Data collected near the 23°S profile are extrapolated to the line of section based on elevation and position relative to the series of topographic barriers on the eastern and western flanks of the Andes: Herrera et al. (2016); Alpers and Whittenmore (1990); Fiorella et al. (2015). For data collected at greater distances from the 23°S profile, data were binned by altitude (usually 1000 m bins) and position of sample locations relative to topographic barriers: Aravena et al. (1999); Gonfiantini et al. (2001); Rohrmann et al. (2014). For all data the box height or vertical line height shows 1 standard deviation above and below the average. For Gonfiantini et al.'s (2001) data, averages are for stations in two transects but standard deviation is for data given for monthly data from a subset of the stations. Modified from a figure in Jordan et al. (in preparation, 2017).

Mulch et al. (2010) showed that oxygen isotopes in pedogenic carbonate in a foreland basin section 200 km to the north at Pilcomayo River, spanning the Tariquia through Guandacay Formations, range between -13.1‰ and -9.8‰ (VPDB), which is more depleted than the Iruya River (Figure 11). The Pilcomayo values vary by 4‰ while those at Iruya vary by 6‰. The greater depletion for Pilcomayo might be the result of differences in air masses that come across the Amazonian Forest (Fiorella et al., 2015; Insel et al., 2013). Considering spatial trends rather than absolute values, a north-south decrease today in the amount of rainfall (Figure 1) raises the possibility that Pilcomayo oxygen values might be more negative that those at Iruya because of a greater rainout effect. Consistent with that reasoning, the spatial trend between the two areas for the modern rainfall oxygen values (Figure 11A) shows the same sense of change as for the results of oxygen isotopes during the Miocene and Pliocene: values are more negative in the Chaco basin near the Pilcomayo area (21°S) than in northernmost Argentina (23°S). Today the Pilcomayo location exhibits more negative summer values with a wider seasonal range, from -14 to -2‰, compared to the Iruya River location, which today varies between season from -10 to -2‰. Consequently, as shown in Figure 9, I interpret that the Pilcomayo River area corresponded to a wetter environment with a higher amount of rainfall than the Iruya River area. The vertical trend of $\delta^{18}O$ that Mulch et al. (2010) determined from Pilcomayo is similar to the trend for Iruya River data, over the same time range – neither varies through time. Both histories are consistent with the hypothesis that the Miocene-Pliocene climate system experienced uniform history over a spatial scale that spanned at least several hundred kilometers distance.

The lack of evidence for a clear long-term oxygen isotopic pattern suggests little or no variability in the climate at the million-year scale. Weather and climate changes over smaller time scales (10^3 to 10^5 years) likely are expressed in the zig zag behaviour of the $\delta^{18}O$ values on a

millennial time scale. The lack of significant change of the $\delta^{18}O$ values is interpreted to mean that there was an absence of stimuli to change the regional scale precipitation pattern.

Carbon Isotopes

A temporal trend of $\delta^{13}C$ values is obvious: values for horizons older than 7 Ma are -10‰ to -11‰ VPDB, but beginning about 6.8 Ma they shift to -11‰ to -12‰, and then at 6 Ma they begin a long progression toward heavier values, to reach close to -8‰ at 5.0 Ma (Figure 6). In the plant-soil system, a fractionation that leads to changes in $\delta^{13}C$ values occurs while the carbon in CO_2 diffuses through the soil, resulting in a ^{13}C enrichment of 12-14‰ in the soil calcium carbonate deposit relative to plants respiring CO_2 (Buotton, 1996, Figure 12). The $\delta^{13}C$ values obtained in the paleosols from the Iruya River stratigraphic section are representative of C3 plants (Buotton, 1996; Figures 6 and 12). This interpretation is supported with the evidence from the charcoal samples from horizons date about 6 Ma (Figure 7). Carbon isotope values of approximately -27‰ for these two samples represent the typical values for C3 vegetation (Cerling and Quade, 1993). Although a change toward heavier values, as occurs from 6–5 Ma, is the trend expected for a shift toward C4 plants (Figure 12), here the magnitude of shift is much less than expected of a change toward the dominance of C4 plants or grasses (Cerling and Quade, 1993; Kelly and Yonker, 1993). For these data, the vegetation will be better described as a mix between C3 and C4 plants, with continued dominance of C3 plants (Cotton et al., 2014). However, the modern environment displays a vegetation arrangement in the NW-SE direction from jungle to grasses and prairies, ending in wetlands and swamps at the international Argentina-Uruguay boundary. The results in changes of C isotopes might been affected by the direction of evolution of the Central Andean Foreland basin into drier and grass vegetation

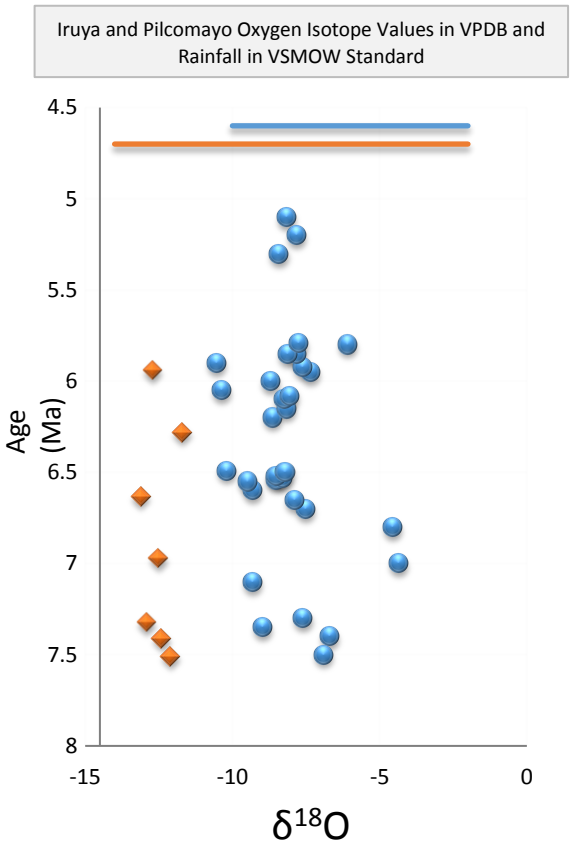
Iruya and Pilcomayo Oxygen Isotope Values in VPDB and Rainfall in VSMOW Standard
4.5
5
5.5
6
6.5
7
7.5
8
Age (Ma)
-15
-10
-5
0
δ18O

A

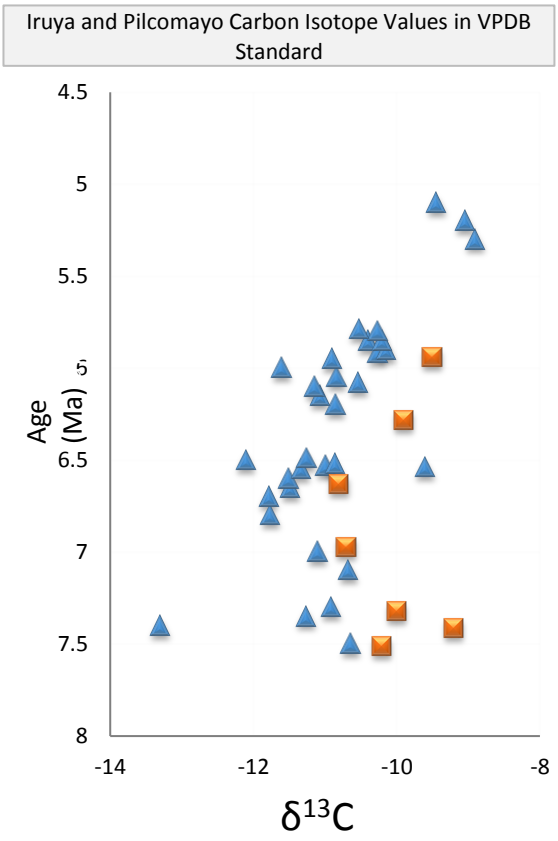
Iruya and Pilcomayo Carbon Isotope Values in VPDB Standard
4.5
5
5.5
6
6.5
7
7.5
8
Age (Ma)
-14
-12
-10
-8
δ13C

B

Figure 11: Iruya River and Pilcomayo Stable Isotope Comparison
Figure A) presents the oxygen isotope values for paleosol carbonates from the Iruya River (blue circles) from Table 1 and averaged bins from the Pilcomayo section (red diamonds), as presented by Mulch et al. (2010) shown relative to depositional ages of the corresponding parent material. The horizontal lines at the top of the graph shows the modern rainfall average oxygen isotope values for each area (red-line for Pilcomayo [-14 to -2‰] and blue-line for Iruya [-10 to -2‰]). Figure B) The stable carbon for paleosol carbonates from Iruya (blue triangles) and Pilcomayo (red squares) Rivers.

zones. This suggests the analyses of calcium carbonate in soils along the W-E megafan axis, as well as the observation of sedimentary facies changes to be compared with the stratigraphic record presented in chapter 2. Nevertheless, the small shift in values could be interpreted as a stable vegetation community during the Late Miocene, which implies a stable climate for this region of the Andean foreland basin.

This result is supported by the carbon isotope data from Mulch et al. (2010; Figure 11B). The binned average $\delta^{13}C$ values from the Pilcomayo River contain a range of values that coincides with the $\delta^{13}C$ results from the Iruya River. Interestingly, a tendency toward more positive values at the Pilcomayo River section occurs over the same geologic time range as for the Iruya River section. This suggests that the climatic and environmental conditions that created the isotopic signature for carbon was not only characteristic of the Iruya River, but exemplify the regional Miocene – earliest Pliocene foreland basin of the Central Andes.

Δ_{47} *Clumped Isotope Paleothermometry*

Clumped isotopes results gave a fairly constant set of values that when transformed into paleotemperatures imply an apparently very warm climate (Table 1; Figure 8). At first impression paleotemperatures about 40 ^{o}C appear to be an overestimation of the temperature. Whether this is truly an overestimation is not straightforward. For example, Passey et al. (2009) explained that calcium carbonate tends to form paleosol nodules under conditions of the average summer maximum high temperatures because of the chemical preference of calcium carbonate to precipitate under the warmer temperatures. These Miocene apparent paleotemperatures compare favorably to local modern average maximum temperatures recorded during the Austral Summer (GeoINTA) in the range of 40-45 ^{o}C (Figure 13) which suggests that these paleotemperature data

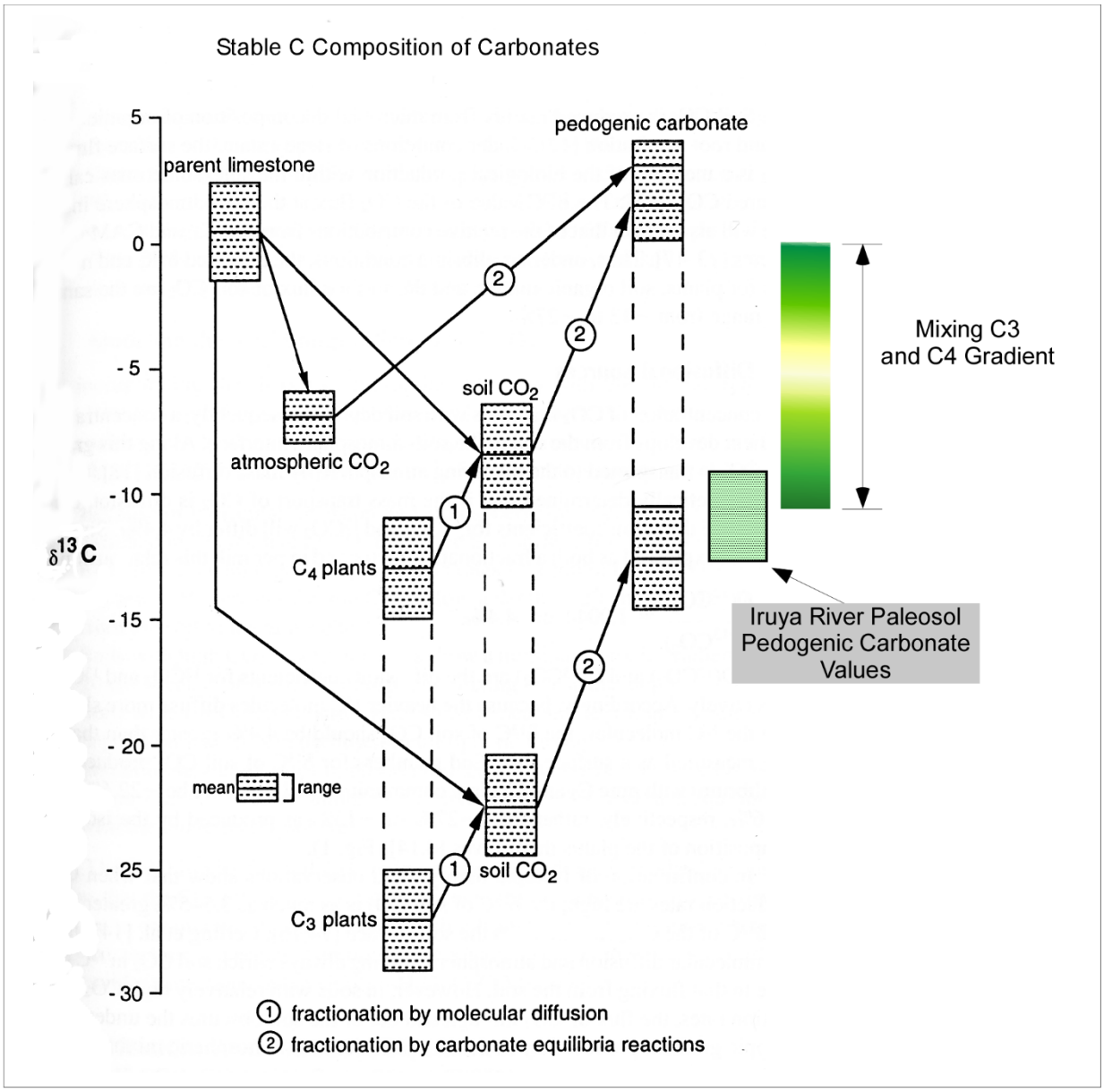
Stable C Composition of Carbonates
5
0
- 5
- 10
- 15
- 20
- 25
- 30
δ13C
parent limestone
pedogenic carbonate
atmospheric CO2
soil CO2
C4 plants
C3 plants
soil CO2
mean
range
Mixing C3
and C4 Gradient
Iruya River Paleosol
Pedogenic Carbonate
Values
① fractionation by molecular diffusion
② fractionation by carbonate equilibria reactions

Figure 12: Stable Carbon Isotopic Composition from carbonates (Modified from Boutton, 1996)
We can observe the different carbon isotopic value domains in accord with each subject studied. Notice the area of mixing C3 and C4 gradient that can be recorded on pedogenic carbonates. More details are presented in the text.

are valuable environmental records. However, Peters et al. (2013) document for a transect across the Andes near 33°S that carbonate clumped isotope paleotemperatures reflect summer season temperatures at high elevation sites but mean annual temperatures at low elevation sites. A comparison of the Passey et al. (2009) and Peters et al. (2013) studies reveal that it is difficult to know which season's temperatures would be captured in a new region. Given the strong seasonality of rain in the Chaco basin and Subandean belt, there exists a reasonable possibility that pedogenic carbonate may best capture the temperature conditions during the interval of drying at the end of the summer monsoonal rains, and not the summer temperatures. However, the range of temperatures between 40^{o}C to 45^{o}C for the austral summer presented in Figure 13, suggests a favorable calcium carbonate precipitation during this season.

Conversely, Quade et al. (2013) present explicitly another problem with clumped isotope-based paleotemperatures above 40 ^{o}C. Those authors explore the possibility that such high temperatures might represent diagenesis produced by the burial history of the strata. They find that pedogenic carbonates in other regions that were buried to a depth of more than 4 km systematically yield diagenetically reset temperatures, which cannot be used as paleoenvironmental indicators. They recommend caution regarding the use of clumped isotope paleothermometry for pedogenic carbonate buried to 2.5-4 km depth, and avoidance for burial depths >4 km.

Consequently, the data at Iruya River are problematic because, of the eight samples analyzed for paleotemperatures, six of them represent a burial history above the 4 km threshold (Figure 4 and Table 1). Only the two youngest samples were buried to roughly 3 km depth (Hernández el al., 1996; Echevarría et al., 2004; Amidon et al., 2015). Interestingly, these two samples that represent ages of 5.85 and 5.3 Ma are the ones with the lowest temperatures, of 28

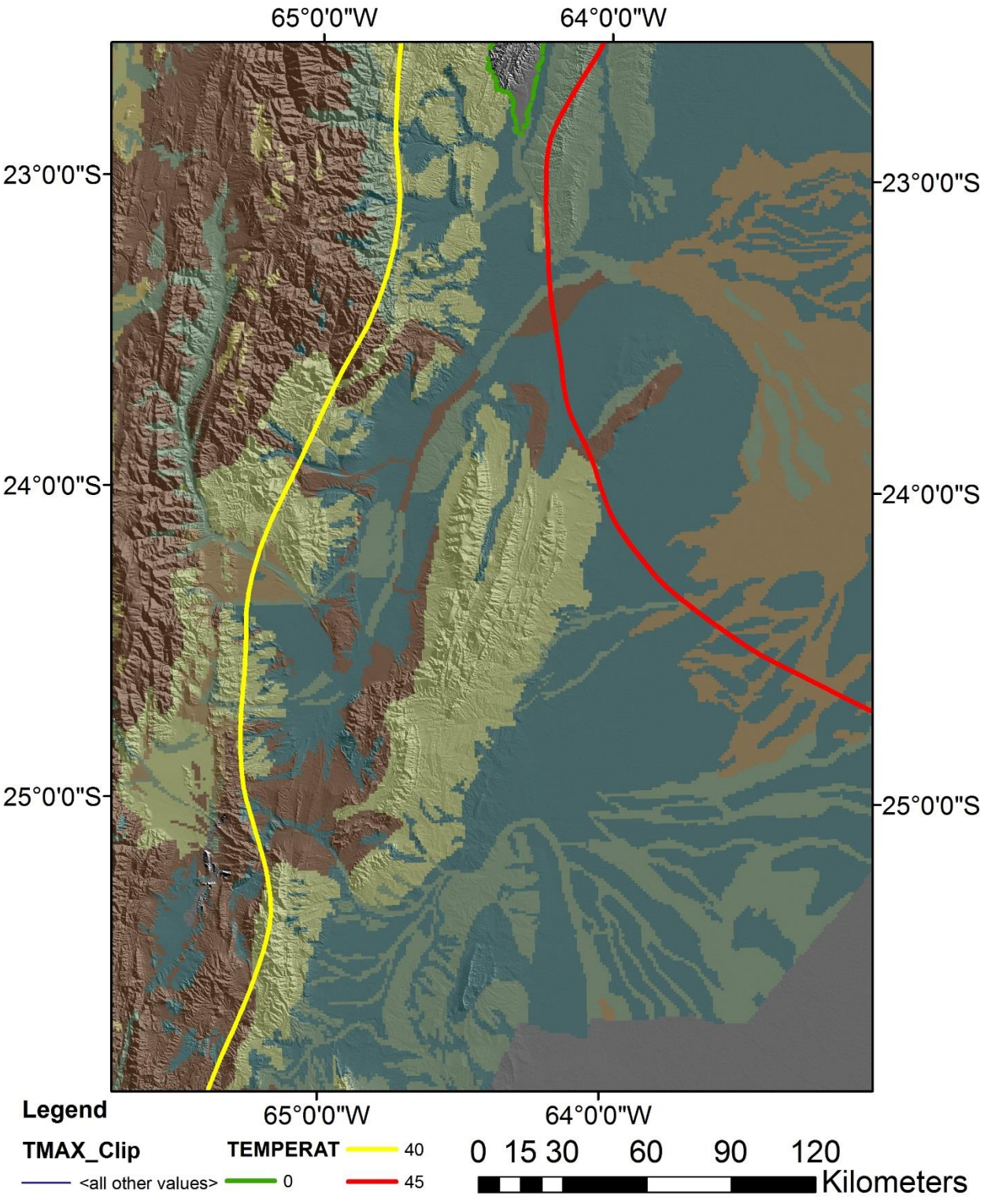
65°0'0"W
64°0'0"W
23°0'0"S
24°0'0"S
25°0'0"S
Legend
TMAX_Clip
<all other values>
TEMPERAT
40
0
45
0 15 30 60 90 120
Kilometers

Figure 13 : Bermejo Megafan Area and Maximum Temperatures
Different colors represent the different soil orders (Chapter 1 for details). Look how it is noticeable how soils are arranged in accord with the megafan geometry at the upper right side of the figure. Temperature units are presented as °C.

°C and 30 ºC, respectively. As anticipated by Quade et al (2013), the burial difference of >4 km compared to 3 km would have resulted in diagenetic resetting of temperatures in the deeply buried samples and explain the difference of 14 ºC between the clumped isotope paleotemperatures.

However, the two shallowest and youngest samples also present an issue when compared with the rest of the paleosols from this stratigraphic column. Most of the paleosol calcium carbonate nodules were sampled between 15 to 20 cm beneath the overlying stratum that capped the palesols. In contrast, the uppermost two paleosols are located in the last floodplain sedimentary facies (Chapter 2). These paleosols formed over the thickest floodplain facies sediments, and were sampled at a depth of 40 cm below the top of the floodplain strata. Based on Quade et al. (2013), this depth below the floodplain surface will produce a more complex interpretation of the data due to the fact that soil temperature decreases exponentially from its atmospheric-soil contact surface. Another reason for skepticism about the interpretation of paleotemperatures from these two samples is that the deeper the calcium carbonate nodule was from the soil surface, the greater the probability that the nodules interacted with shallow groundwater. This concern is especially relevant in the Iruya River section because these paleosols represent well drained soils at the time of development.

Overall, these clumped isotope paleotemperature results and consideration of the process of soil formation, diagenesis, and groundwater interaction lead to three different interpretation scenarios. The first option (i) is to consider the data to be valid as a measure of the average high environmental temperature, comparable to the present summer season. The second option (ii) is to accept only the youngest two data points as valuable for environmental information, and to dismiss the other six due to diagenetic temperature resetting produced by deep burial. The third option (iii) is that all the points are diagenetically altered, though the deeper six are altered by burial and the

youngest two were altered by interaction with groundwater. The main problem is selecting between these three alternatives is the fact that current temperatures are similar to the apparent paleotemperatures of the samples that were buried beyond the depth threshold for diagenetic resetting. This creates the conundrum that even if the results are representative of the real paleotemperature at the time of soil development, it will be basically impossible to know the veracity of these results.

Evolving Environmental Conditions on the Megafan

In this case, climate and climate change history are embedded in the properties of over 7 km thickness of distributary fluvial system strata in a foreland basin. The paleosols on which this study is based and their stable isotope characteristics were shaped by the dynamics of the fluvial sedimentary environment, as well as by the contemporaneous climate state. The isotopic record obtained from ^{13}C isotopes present a constant vegetation, which suggests a constant rain fall and a constant climate. This advocates that other forces controlled the sedimentary record during the time span studied. Irrespective of whether a tectonic event is signaled by the history of climate conditions, an understanding of the climate history is valuable both because of its role in soil development, and also because it is vital to an accurate interpretation of sediment accumulation rates and of erosion models (Mulch et al, 2010).

The study of Middle to earliest Pliocene foreland basin paleosols now found within the Subandean Belt offers information about both the regional and local history of change of climate and surface water hydrology. Regional insight exists because the foreland basin sedimentary environment is likely to be sensitive to climate change and/or to catchment basin changes within the Andes that might be driven by topographic uplift of massive orographic barriers such as the

Andes or the Himalayan Mountain Belt. Because of the interaction of fault-related topographic features and erosion, catchment evolution might either increase or decrease stream discharge to a given megafan, while the partitioning of the orogenic belt by high ridges and valleys might either increase or decrease rainfall within a given catchment (Kleinert and Strecker, 2001; Strecker et al., 2007). Any combination of those factors in the catchment basin will produce changes in sedimentation rates in the corresponding depositional megafan, which would be expressed by both sedimentary facies and by soil properties. Soil structure might change in response to changes in drainage, water supply, and erosion. Thus changes in paleosol physical aspects will indirectly represent distant changes in climatic conditions that influence the catchment area.

Uplift of the Andes might also provoke climate changes that more directly influence the local megafan environment. The Iruya River was about 30 km to the east of the position of a major step in Late Miocene Andean mountain topography at the eastern edge of the Eastern Cordillera (Echevarría et al., 2003). Today, for many sectors of the eastern mountain front of the Central Andes the footprint of orographically formed enhanced precipitation extends somewhat east of the position where the elevation increases (Masek et al., 1994; Bookhagen and Strecker, 2008), to a distance greater than 30 km (Figure 1C). If the Andean topography changed significantly during the 12–5 Ma time span, the Iruya River uppermost Middle Miocene through lowest Pliocene strata may reveal changes in rainfall or other environmental properties that were linked to tectonic rise of the mountain belt (Barnes and Ehlers, 2009). The modern soils of northwestern Argentina reflect regional gradients in environmental conditions (Chapter 1) and offer examples against which to compare the evolution of soil characteristics that might have been driven by precipitation change adjacent to the Andes. The 12.5 to 5 Ma paleosol pedogenic features documented here provide

the opportunity to discover how climatic, hydrological, and vegetation conditions in the lowland basin compared with the current conditions.

Conclusions

Paleosols represent essentially constant pedogenic conditions throughout the 9 Ma to 5 Ma interval studied in detail at the Iruya River site in the Subandean belt of northwestern Argentina. Hence, this study implies that the climatic conditions in the Chaco basin changed little through the geologic record. Trends through time of both $\delta^{18}O$ and $\delta^{13}C$ for pedogenic carbonate are similar to trends revealed by earlier studies in southern Bolivia, which clarifies that the patterns reflect regional properties of the Late Miocene to earliest Pliocene Chaco foreland basin, and not local anomalies.

Oxygen isotopes do not show a clear or preferred pattern through time and display a narrow range of variability compared with today's oxygen isotopic values for the same region. The $\delta^{18}O$ values suggest a very stable water source, even though the atmospheric water pathways may have varied slightly in response to interannual to millennial changes in atmospheric conditions. Iruya River oxygen isotopic values augment analyses of the stable isotopes of carbonates now found in high elevation parts of the Andes Mountains, by showing that the initial isotopic signature of the air masses that supplied moisture to the Altiplano was 4-5‰ lighter prior to rain-out fractionation than is the case today.

Carbon isotopes reveal a subtle shift from C3 toward greater participation by C4 plants, suggestive of a mixture between trees and grasses. However, the $\delta^{13}C$ values remain within the range expected for domination by C3 plants. The subtle shift in vegetation represented by the carbon isotopes is only about 3‰, which is less than the 10‰ shift documented as C4 plants spread

during the Late Miocene in south Asia (Cerling and Quade, 1993) but similar to the shifts documented at other locations in Argentina during the Late Miocene and Pliocene (Latorre et al., 1997; Kleinert and Strecker, 2001).

The Δ_{47} results present values for temperatures around 42 °C that arguably record average maximum summer temperatures, which are very similar to today's temperatures. However, there is a strong possibility that these data are not valid records of paleoenvironmental conditions because these paleosols were buried sufficiently deeply that diagenetic temperature resetting is to be expected (Quade et al., 2013).

In summary, paleoclimate proxies for strata that crop out in the Subandean Belt reveal no significant temporal change in soil development, rainfall, and vegetation within what would have been the westernmost Chaco foreland Basin. Furthermore, excepting the uncertainty on the interpretation of the paleothermometry data, there is also no significant temporal change in summer paleotemperatures. These results suggest overall constant climatic conditions for interior South America spanning the Late Miocene to present time. Once the fundamental circulation patterns on the eastern side of the Andes Mountains were established prior to 9 Ma, the regional climate became remarkably stable.

References

Alpers, C. N., and Brimhall, G. H., 1988, Middle Miocene climatic change in the Atacama Desert, northern Chile: Evidence from supergene mineralization at La

Alpers, C. N., and Whittemore, D. O., 1990, Hydrogeochemistry and stable isotopes of ground and surface waters from two adjacent closed basins, Atacama Desert, northern Chile: Applied Geochemistry, v. 5, no. 5-6, p. 719-734

Amidon, W.H., Luna, L.V., Fisher, G.B., Burbank, D.W., Kylander-Clark, A.R.C., and Alonso, R., 2015. Provenance and tectonic implications of Orán Group foreland basin sediments, Rio Iruya canyon, NW Argentina (23ºS). Basin Research, p. 1-17

Aravena, R., Suzuki, O., Pena, H., Pollastri, A., Fuenzalida, H., and Grilli, A., 1999, Isotopic composition and origin of the precipitation in Northern Chile: Applied Geochemistry, v. 14, no. 4, p. 411-422

Barnes, J.A., Ehlers, T.A., 2009.End member models for Andean plateau uplift. Earth-Sci.Rev.97,105–132.

Blaine, C., Terence, E., 1994. Relative Effects of Tectonism, Eustasy, Paleoclimate, and Paleo-Oceanography on Atlantic Passive-Margin Sedimentation. Predictive Stratigraphic Analysis-Concept and Application, U.S. Geological Survey Bulletin 2110, p. 10-13

Bookhagen, B., and Strecker, M. R., 2008, Orographic barriers, high-resolution TRMM rainfall, and relief variations along the eastern Andes: Geophysical Research Letters, v. 35, no. 6, p. L06403

Buotton, T., and Yamasaki, S., 1996. Mass Spectroscopy of Soils. p. 113-154

Cerling, T. E. and Quade, J., 1993. Stable carbon and oxygen isotopes in soil carbonates. In: Swart, P., McKenzie, J.A., and Lohman, K.C. (eds.): American Geophysical Union Monograph 78: 217- 231.

Coplen, T.B., 1995, Discontinuance of SMOW and PDB: Nature, v. 375, p. 285.

Coplen, T.B., 1996a, New guidelines for the reporting of stable hydrogen, carbon, and oxygen isotope ratio data: Geochimica et Cosmochimica Acta, v. 60, p. 3359.

Coplen, T.B., 1996b, Editorial: More uncertainty than necessary: Paleoceanography, v. 11, no. 4, p. 369-370.

DeCelles, P. G., Carrapa, B., Horton, B. K., and Gehrels, G. E., 2011, Cenozoic foreland basin system in the central Andes of northwestern Argentina: Implications for Andean geodynamics and modes of deformation: Tectonics, v. 30.

Echevarría , L., Hernández, R., Allmendinger, R., and Reynolds, J., 2003, Subandean thrust and fold belt of northwestem Argentina: Geometry and timing of the Andean evolution: AAPG Bulletin, v. 87, no. 6, p. 965-985.

Ehlers, T.A., and Poulsen, C.J., 2009, Influence of Andean uplift on climate and paleoaltimetry estimates: Earth and Planetary Science Letters, v. 281, p. 238–248

Eiler, J. M., 2007, Clumped-isotope" geochemistry—The study of naturally-occurring, multiply-substituted isotopologues: Earth and Planetary Science Letters, v. 262, no. 3, p. 309-327

Eiler, J. M., 2011, Paleoclimate reconstruction using carbonate clumped isotope thermometry: Quaternary Science Reviews, v. 30, no. 25, p. 3575-3588

Escondida: Geological Society of America Bulletin, v. 100, p. 1640-1656.

Fiorella, R. P., Poulsen, C. J., Pillco Zolá, R. S., Barnes, J. B., Tabor, C. R., and Ehlers, T. A.,

2015, Spatiotemporal variability of modern precipitation δ18O in the central Andes and implications for paleoclimate and paleoaltimetry estimates: Journal of Geophysical Research: Atmospheres, v. 120, no. 10, p. 4630-4656

Flemings, P. B., And Jordan, T. E., 1990, Stratigraphic Modeling of Foreland Basins – Interpreting Thrust Deformation and Lithosphere Rheology: Geology, V. 18, No. 5, P. 430-434.

Garreaud, R.D., 1999. Multiscale analysis of the summertime precipitation over the central Andes. Monthly Weather review, v. 127, iss. 5, p. 901-922

Garreaud, R.D., Molina, A., Farías, M., 2010. Andean uplift, ocean cooling and Atacama hyperaridity: a climate modeling perspective. Earth Planet. Sci. Lett. 292, 39–50

Garzione, C.N., Molnar, P., Libarkin, J.C., MacFadden, B., 2006, Rapid late Miocene rise of the Andean plateau: evidence for removal of mantle lithosphere: Earth and Planetary Science Letters, v. 241, p. 543-556.

Garzione, C.N., Hoke, G.D., Libarkin, J.C., Withers, S., MacFadden, B., Eiler, J., Ghosh, P., and Mulch, A., 2008, Rise of the Andes: Science, v. 320, p. 1304–1307

Garzione, C.N., Auerbach, D., Smith, J.-S., Passey, B., Eiler, J., Rosario, J, and Jordan, T., 2014 Clumped isotope evidence for diachronous surface cooling of the Altiplano and pulsed surface uplift of the Central Andes, v. 393, p 173-181.

GeoINTA, Atlas de Suelos de la República Argentina: Buenos Aires: Fundación Argentina: INTA CIRN Instituto de Suelos: Aeroterra S.A., c1995

Gonfiantini, R., Roche, M. -A., Olivry, J. -C., Fontes, J. -C., and Zuppi, G. M., 2001, The altitude effect on the isotopic composition of tropical rains: Chemical Geology, v. 181, no. 1, p. 147-167

Ghosh, P., Adkins, J., Affek, H., Balta, B., Guo, W., Schauble, E. A., Schrag, D., and Eiler, J. M., 2006, 13 C--18 O bonds in carbonate minerals: A new kind of paleothermometer: Geochimica Et Cosmochimica Acta, v. 70, no. 6, p. 1439-1456

Ghosh, P., Eiler, J., Campana, S. E., and Feeney, R. F., 2007, Calibration of the carbon 'clumped isotope' paleothermometer for otoliths: Geochimica Et Cosmochimica Acta, v. 71, no. 11, p. 2736-2744

Grootes, P.M., 1993, Interpreting Continental Oxygen Isotope Records. In Swart, P., McKenzie, J.A., and Lohman, K.C. (eds.): Continental Indicators of Climate. American Geophysical Union Monograph 78, pp. 37-46

Hernández, R. M., J. Reynolds, and A. Di Salvo, 1996, Análisis tectosedimentario y ubicación geocronológica del Grupo Oraán en el río Iruya: Boletín de Informaciones Petroleras, Tercera Epoca, v. 45, p. 80–93.

Herrera, C., Custodio, E., Chong, G., Lambán, L. J., Riquelme, R., Wilke, H., Jódar, J., Urrutia, J., Urqueta, H., and Sarmiento, A., 2016, Groundwater flow in a closed basin with a saline shallow lake in a volcanic area: Laguna Tuyajto, northern Chilean Altiplano of the Andes: Science of The Total Environment, v. 541, p. 303-318

Horton, B. K. (2005), Revised deformation history of the central Andes: Inferences from Cenozoic foredeep and intermontane basins of the Eastern Cordillera, Bolivia, Tectonics, 24

Horton, B.K., 2012, Cenozoic evolution of hinterland basins in the Andes and Tibet. Tectonics of Sedimentary Basins: Recent Advances. Publisher: John Wiley & Sons, Ltd. P. 427-444

Insel, N., C. J. Poulsen, T. A. Ehlers, and C. Sturm (2012), Response of meteoric δ18O to

surface uplift—Implications for Cenozoic Andean Plateau growth, Earth Planet. Sci. Lett., 317-318, 262–272.
Insel, N., C. J. Poulsen, C. Sturm, and T. A. Ehlers (2013), Climate controls on Andean precipitation δ18O interannual variability, J. Geophys. Res. Atmos., 118, 9721–9742
Jordan, T.E., Herrera L., C., Godfrey, L.V., Colucci, S., Gamboa, C., Urrutia, J., and González, G., 2016 in preparation, Precipitation sources and distribution during March 2015 northern Chile extreme precipitation event
Kleinert, K., Strecker, M.R., 2001, Climate change in response to orographic barrier uplift: paleosol and stable isotope evidence from the late Neogene Santa Marín basin, northwestern Argentina. GSA Bulletin, v. 113, no. 6, p. 728-742
Kraus, I.V., Lower Eocene alluvial paleosols: Pedogenic development, stratigraphic relationships, and paleosol/landscape associations: Palaeogeography Palaeoclimatology Palaeoecology, v. 129, no. 3-4, p. 387-406.
Lenters, J.D., and K.H.Cook, 1999: Summertime Precipitation Variability in South America: Role of the Large-scale Circulation. Mon. Wea. Rev., 127, 409- 431.
Masek, J.G., Isaacks, B. L., Gubbels, T.L., and Fielding, E.J., 1994. Erosion and tectonics at the margins of continental plateaus. Journal of Geophysical Research, v. 99, no. B7, p. 13941-13956
Meyer, N.A., Breecker, D.O., Young, M.H., Litvak, M.E., 2014, Simulating the effect of vegetation in formation of pedogenic carbonate. Pedol. Soil Sci. Soc. Am. J., 78 (2014), pp. 914–924
Mulch, A., Uba, C.E., Strecker, M.R., Schoenberg, R., and Chamberlain, C.P., 2010, Late Miocene climate variability and surface elevation in the central Andes: Earth and Planetary Science Letters, v. 290, p. 173–182
Passey, B.H., et al. (2010), High-temperature environments of human evolution in East Africa based on bond ordering in paleosol carbonates. PNAS, 107, 11245–11249
Pingel, H., Mulch, A., Alonso, R.N., Cottle, J., Hynek, S.A., Poletti, J., Rohrmann, A., Schmitt, A.K., Stockli, D.F., Strecker, M.R., 2016. Surface uplift and cinvective rainfall along the southern Central Andes (Angastaco basin, NW Argentina). Earth and Planetary Science Letters 440 (2016) 33–42
Pingel, H., Alonso, R.N., Mulch, A., Rohrmann, A., Sudo, M., and Strecker, M.R., 2014, Pliocene orographic uplift in the southern Central Andes. Geology, v. 42, no.
Quade, J, Eiler, J, Dae¨ron, M, Achyuthan, H., 2013, The clumped isotope geothermometer in soil and paleosol carbonate: Geochimica et Cosmochimica Acta 105 (2013) 92–107
Rech, J. A., Currie, B. S., Michalski, G., and Cowan, A. M., 2006, Neogene climate change and uplift in the Atacama Desert, Chile: Geology, v. 34, no. 9, p. 761-764
Rech, J. A., Currie, B. S., Shullenberger, E. D., Dunagan, S. P., Jordan, T. E., Blanco, N., Tomlinson, A. J., Rowe, H. D., Houston, J., 2010, Evidence for the development of the Andean rain shadow from a Neogene isotopic record in the Atacama Desert, Chile, Earth and Planetary Science Letters 292:371-382.
Retallack, 1994 G.J. Retallack The environmental factor approach to the interpretation of paleosols. R. Amundson, J. Harden, M. Singer (Eds.), Factors of Soil Formation: A Fiftieth Anniversary Retrospective, Soil Science Society of America Special Publication (1994)
Rohrmann, A., Strecker, M. R., Bookhagen, B., Mulch, A., Sachse, D., Pingel, H., Alonso, R. N.,

Schildgen, T. F., and Montero, C., 2014, Can stable isotopes ride out the storms? The role of convection for water isotopes in models, records, and paleoaltimetry studies in the central Andes: Earth and Planetary Science Letters, v. 407, p. 187-195

Rohrmann A., Sasche, D., Mulch, A., Pingel, H., Tofelde., S., Alonso, R.N., and Strecker, M.R., 2016, Miocene orographic uplift forces rapid hydrological change in the southern Central Andes. Nature, Scientific Report 6, no. 35678, DOI: 10.1038/srep35678

Rozanski, K., Aruguas-Araguas, L., and Gonfiantini, R., 1993. Isotopic patterns in modern global precipiation. In Swart, P., McKenzie, J.A., and Lohman, K.C. (eds.): Continental Indicators of Climate. American Geophysical Union Monograph 78, pp. 1-36.

Savin, S. M., Abel, L., Barrera, E., Hodell, D., Kennett, J. P., Murphy, M., Keller, G., Killingley, J., and Vincent, E., 1985, The evolution of Miocene surface and near-surface marine temperatures: oxygen isotopic evidence: Geological Society of America Memoirs, v. 163, p. 49-82.

Sheldon, N.D., Retallack, G.J., and Tanaka, S., 2002. Geochemical Climofunctions from North American Soils and Application to Paleosols across the Eocene-Oligocene Boundary in Oregon. The Journal of Geology, v. 110, p. 687–696

Sheldon, N.D., and tabor, N.J., 2009, Quantitative paleoenvironmental and paleoclimatic reconstruction using paleosols. Earth-Science Reviews, v. 95, iss, 1-2, p. 1-52

Sillitoe, R. H., and McKee, E. H., 1996, Age of supergene oxidation and enrichment in the Chilean porphyry copper province: Economic Geology, v. 91, no. 1, p. 164-179

Strecker, M.R., Alonso, R.N., Bookhagen, B., Carrapa, B., Hilley, G.E., Sobel, E.R., Trauth. M.H., 2007, Tectonics and climate of the southern central Andes. Annu. Rev. Earth Planet. Sci., 35 (2007), pp. 747–787

Suarez, M.B., Passey, B.H., and Kaakineen, A., 2011. Paleosol carbonate multiple isotopologue signature of active East Asian summer monsoons during the late Miocene and Pliocene. Geology, v. 39, no. 12, p. 1151-1154

Tabor, N., and Myers, T., 2015. Paleosols as Indicators of paleoenvironment and paleoclimate. Annual Review of Earth and Planetary Sciences. v. 43, p. 333-361

Uba, C.E., Strecker, M.R., Schmitt, A.K., 2007. Increased sediment accumulation rates and climatic forcing in the central Andes during the late Miocene. Geology 35, 979–982.

Uba, C.E., Kley, J., Strecker, M.R., Schmitt, A.K., 2009, Unsteady evolution of the Bolivian Subandean thrust belt: The role of enhanced erosion and clastic wedge progradation. Earth and Planetary Science Letters 281 (2009) 134–146

Wang, Z., Schauble, E. A., and Eiler, J. M., 2004, Equilibrium thermodynamics of multiply substituted isotopologues of molecular gases: Geochimica Et Cosmochimica Acta, v. 68,